NATIONAL ADVISORY COMMITTEE FOR AERONAUTICS

WARTIME REPORT

ORIGINALLY ISSUED
June 1944 as
Memorandum Report

WIND-TUNNEL TESTS OF THE 1/8-SCALE POWERED MODEL OF THE CURTISS XBTC-2 AIRPLANE

I - PRELIMINARY INVESTIGATION OF LONGITUDINAL STABILITY

By Joseph Weil and Evalyn G. Wells

Langley Memorial Aeronautical Laboratory
Langley Field, Va.

WASHINGTON

NATIONAL ADVISORY COMMITTEE FOR AERONAUTICS

MEMORANDUM REPORT

for the

Bureau of Aeronautics, Navy Department

WIND-TUNNEL TESTS OF THE 1/8-SCALE POWERED MODEL OF THE CURTISS XBTC-2 AIRPLANE

I - PRELIMINARY INVESTIGATION OF LONGITUDINAL STABILITY

By Joseph Weil and Evalyn G. Wells

INTRODUCTION

At the request of the Bureau of Aeronautics, Navy Department a series of wind-tunnel tests was made in the LMAL 7- by 10-foot tunnel of the Curtiss XBTC-2 model (1/8-scale) with power.

The object of these tests was to determine and to improve, as necessary, the complete aerodynamic characteristics of the model.

The present report includes the results of the longitudinal stability investigation of the original model along with results from tests of various modifications. A pressure-distribution survey in the region of the oil-cooler flap location as well as tuft surveys to determine the stalling characteristics for various wing modifications are also presented.

MODEL AND APPARATUS

The model was supplied by the Columbus division of the Curtiss-Wright Corporation. The model was not checked for accuracy. It was equipped with a six-blade dual-rotating propeller which was not to scale; its diameter being 1.813 feet as compared to the scale value of 1.771 feet. A three-view drawing of the model as originally received, is shown in figure 1(a), while a photograph of the original model is presented in figure 1(b).

The cowl flaps shown in these figures were not supplied by the company but were made at LMAL. A drawing of the cowl flaps is shown in figure 2.

The electrical strain gages, used to measure control-surface hinge moments, were supplied with the original model.

The stabilizer angles were set with a vernier inclinometer, while flaps and control surfaces were set with the aid of templets furnished with the model.

Power was obtained from a 50-horsepower three-phase induction motor furnished by the Curtiss Corporation, space for which was provided in the fuselage of the model. The gear box which was used for the dual-rotation propellers was attached to the nose of the model motor. The speed of this motor was first determined by observation of a cathode-ray oscillograph which indicates the output of a small alternator connected to the shaft of the motor. Later it was found to be more practical to use the input frequency to the model motor. The time base for the oscillograph pattern is controlled by an audio-oscillator of the electrically driven tuning-fork type, the frequency of which is known within 0.1 percent.

Pressure measurements were made on the under surface of the fuselage in the region which the oil-cooler flap might occupy. There was no oil-cooler flap on the model. These static pressures were measured about 1/16 inch from the surface of the model using small static pressure tubes. The pressure tubes were alined approximately parallel to the air stream. The points at which the pressures were measured are shown in figure 3.

The leading-edge wing slats, which were of the Handley-Page type, were made in two sections so that two slat spans could be tested (fig. 1(a)).

A revised horizontal tail (horizontal tail 2) was tested when the longitudinal stability of the airplane with the original tail was found to be unsatisfactory. For the revised tail, area was added at the tips giving a larger span and increased aspect ratio (fig. 4). Tests were also made with each tail raised 6.00 inches (model dimensions). For these tests the vertical tail was removed and a streamlined strut used for support (fig. 5).

In order to simulate the flight condition with the pilot's canopy open, the original model canopy was cut and moved back as shown (fig. 6(a) and 6(b)).

Unsatisfactory lateral-stability characteristics also were indicated from early tests. In an attempt to improve the lateral stability, various wing modifications were designed and tested. These modifications are summarized below:

Wing modification		Chief variations from original configuration	Figure
1	Swept-back outer panels	Original outer panel swept back 16.65°; airfoil sections of outer panel skewed by this amount to air stream	7
2	Rectangular outer panels	Wing area = 7.26 sq ft; aspect ratio = 5.38	8(a), 8(b)
3	Upturned wing tips	Γ_{tip} = 35° measured from L.E. chord of outer panel Wing area = 6.46 sq ft; aspect ratio = 6.54; span = 6.5 ft (coefficients based on original model dimensions)	9(a), 9(b)
4	Skewed flaps	Duplex flap pivoted about outboard end so that Λf_o = 0.7°	10

In order to gather data which might be of value in future design work, a rectangular wing was designed and tested. The rectangular wing was composed of a rectangular inner panel built by the Navy, and the rectangular outer panels which had been tested previously. This wing had a mean aerodynamic chord of 12.24 inches (original M.A.C. = 12.26 inches). This discrepancy is considered negligible. The rectangular wing thus had practically the same span, area, and aspect ratio as the original wing and was located so that the mean aerodynamic chord would

coincide with the mean aerodynamic chord of the original wing. A drawing and photograph of the rectangular wing are presented in figures 11(a) and 11(b), respectively. The original center panel had a sharp-edge flap slot entry while the rectangular panel had a smooth flap slot entry (fig. 12). Although flaps on both center panels were about the same area, the chord of the original flaps was about 21 percent of the wing chord, while the chord of the rectangular flaps was about 25.7 percent of the wing chord. The rectangular flaps move back about the same distance in inches as the original flaps, but the original flaps move back about 6.7 percent of the wing chord while the flaps on the rectangular wing move back about 7.9 percent of the wing chord.

TESTS

Test conditions.- The tests were made in the LMAL 7- by 10-foot tunnel at dynamic pressures of 16.37 and 9.21 pounds per square foot, corresponding to airspeeds of about 80 and 60 miles per hour. The test Reynolds numbers were about 746,000 and 560,000 based on the wing mean aerodynamic chord of 12.26 inches. Because of the turbulence factor of 1.6 for the tunnel, effective Reynolds numbers were about 1,192,000 and 896,000.

Coefficients and symbols.- The results of the tests are presented in standard NACA coefficients of forces and moments. Pitching-moment coefficients are given about the center-of-gravity location shown in figure 1(a) (22 percent of the M.A.C. chord of the original wing). The data are referred to a system of axes in which the Z axis is in the plane of symmetry and perpendicular to the relative wind, the X axis is in the plane of symmetry and perpendicular to the Z axis, and the Y axis is perpendicular to the plane of symmetry.

The coefficients and symbols are defined as follows:

C_L lift coefficient (Z/qS)

C_{D_R} resultant-drag coefficient (X/qS)

C_m pitching-moment coefficient (M/qSc)

C_{h_e} elevator hinge-moment coefficient $\left(H_e/qb_e \bar{c}_e^2\right)$

T_c' effective thrust coefficient (T/qS)

V/nD propeller-advance-diameter ratio

P pressure coefficient (p/q)

where the quantities are defined below

X force along X axis

Z force along Z axis

M moment about Y axis

T_e effective thrust

q dynamic pressure $(\frac{1}{2}\rho V^2)$ (16.37 or 9.21 lb/sq ft)

S wing area (6.34 sq ft on original model)

c wing mean aerodynamic chord (M.A.C.) (12.26 in. on original model)

$\bar{c}_e$ root mean square chord of elevator aft of hinge line (original tail) (2.081 in.)

s wing slat (Handley-Page slat)

b_w wing span (6.25 ft on original model)

S_t horizontal tail area

b_e elevator span (original tail) (23.61 in.)

l_t tail length

V air velocity

D propeller diameter (1.813 ft on model)

n revolutions per second

p difference between local static pressure and free-stream static pressure

and

ρ mass density of air

α corrected angle of attack of thrust line, degrees

i_t angle of stabilizer with respect to thrust line, degrees, positive when trailing edge is down

δ control-surface deflection, degrees

β propeller blade angle at 0.75 radius, degrees

ϵ angle of downwash with respect to free stream, degrees

Λ angle of sweep, degrees, positive for sweepback

Γ angle of dihedral, degrees, positive when outboard end is raised

n_p neutral-point location, percent mean aerodynamic chord of original wing (measured from location of leading edge of M.A.C. of original wing)

Subscripts:

e elevator

t tab

f_i inboard flap

f_o outboard flap

c cowl

F front

R rear

i inboard

o outboard

For standard sea-level conditions with the normal wing loading of 39.4 pounds per square foot, the elevator stick force is given by the following relation:

$$F_s = 715 \frac{C_{h_e}}{C_L}$$

Corrections.- All data have been corrected for tares caused by the model support strut. Jet-boundary corrections

have been applied to the angles of attack, the drag coefficients, and the tail-on pitching-moment coefficients. The corrections were computed as follows:

$$\Delta\alpha = 57.3\ \delta_w \frac{S}{C}\ C_L \text{ (degrees)}$$

$$\Delta C_D = \delta_w \frac{S}{C}\ C_L^2$$

$$\Delta C_m = -57.3\ \frac{S}{C}\ \frac{\partial C_m}{\partial i_t}\ C_L \left(\frac{\delta_T}{\sqrt{q_t/q}} - \delta_w \right)$$

where

δ_w jet-boundary correction factor at the wing (0.112)

δ_T total jet-boundary correction at the tail varies between 0.189 and 0.200, depending upon model attitude and flap deflection

S model wing area (6.34 sq ft)

C tunnel cross-sectional area (69.59 sq ft)

$\frac{\partial C_m}{\partial i_t}$ change in pitching-moment coefficient per degree change in stabilizer setting as determined in tests

q_t/q ratio of effective dynamic pressure over the horizontal tail to free-stream dynamic pressure

All corrections were added to the test data.

Test procedure.- The model propeller was calibrated by measuring the resultant drag of a clean model for a range of propeller speeds at $\alpha = 0^\circ$. The thrust coefficients were then computed from the equation

$$T_c' = C_D - C_{D_R}$$

where C_D is the drag of the model with the propeller removed. The results of the calibration are presented in figure 13.

From the data of figure 13, it is only necessary to vary the propeller speed at any particular tunnel speed to obtain any desired thrust coefficient, assuming

that the propeller thrust is independent of the angle of inclination of the propeller (reference 1).

The effective thrust coefficients at which the tests were made are shown in figure 14 as a function of lift coefficient for a simulated constant amount of power with a constant-speed propeller. This chart was supplied by the Curtiss company.

The model with the rectangular outer panels had increased wing area and the coefficients were based on the actual area (7.26 sq ft). Since the relation between T_c' and C_L depend on wing area and wing loading, certain assumptions about airplane weight had to be made. One possibility is to assume that the wing loading remain constant with the corresponding increase in gross airplane weight. Another possibility is that the airplane weight be assumed constant with the corresponding reduction in wing loading. The case of constant airplane weight is called "power A," while that of constant airplane wing loading is called "power B." The simulated engine power is identical for the two cases (3000 horsepower.)

The curves for power B (fig. 14) with the rectangular outer panels were computed at LMAL from the relationship

$$T_c'_2 = T_c'_1 \frac{S_1}{S_2}$$

where

S_1 and S_2 — original wing area and wing area with the rectangular outer panels, respectively

$T_c'_1$ and $T_c'_2$ — values of thrust coefficients based on S_1 and S_2, respectively

Thus, using figures 13 and 14, for a given lift coefficient, the propeller speed necessary to simulate any take-off power flight condition can be determined.

In a previous investigation of the model, the propeller blade angle settings used were $\beta_F = 23\frac{1}{2}^\circ$ and $\beta_R = 22\frac{1}{2}^\circ$ in the landing configuration and $\beta_F = 30\frac{1}{2}^\circ$ and $\beta_R = 29\frac{1}{2}^\circ$ in the cruising configuration. Therefore, all of the initial tests were made with similar settings.

Subsequent tests showed the effect of propeller blade angle on longitudinal stability to be negligible. The remaining tests were therefore all made using $\beta_F = 23\frac{1}{2}^\circ$ and $\beta_R = 22\frac{1}{2}^\circ$. The blade angle used for each test is included in table I.

In the text and on the figures, the model configuration is given as "cruising" or "landing." Unless otherwise noted these conditions are described as follows:

(a) Cruising configuration:

All flaps retracted
Landing gear retracted
Cowl flaps closed
Slats retracted

(b) Landing configuration:

Inboard flaps, $\delta_{f_i} = 50^\circ$
Duplex flaps, $\delta_{f_o} = 50^\circ$
Landing gear extended
Cowl flaps 25°
Outboard slat extended (the 13-inch section shown on figure 1(a))

All tests were run at a tunnel speed of 80 miles per hour with the exception of the power-on tests (landing configuration), which were made at 60 miles per hour. This difference was necessitated because the model motor had insufficient power for the high thrust coefficients required at the high lift coefficients.

A series of stabilizer tests and tail-off pitch tests were made for the model with the original configuration and also with subsequent modifications for both the cruising and landing conditions. Tuft surveys were also run, with the various wing plan forms. Elevator tests were made to determine the elevator effectiveness with windmilling propellers in both the cruising and landing conditions with the original model. Pressure readings were taken in the region of the oil-cooler flap.

Downwash angles and dynamic-pressure ratios at the tail were calculated for the various power conditions, wing modifications and tail locations from stabilizer

and tail-off tests, and represent average values across the span of the tail.

Neutral points that are presented are always given as a distance aft of the leading edge of the original mean aerodynamic chord in percent of the original mean aerodynamic chord.

A complete summary of the figures and test program are presented in table I.

DISCUSSION

Longitudinal Stability

Effect of horizontal tail configuration.- The results of the stabilizer tests made of the original model for several power and model conditions are shown on figures 15 and 16.

The longitudinal stability criterion specified by the Navy for this airplane was that a positive static margin with the center of gravity at its rearmost location exist for all conditions including the landing configuration with take-off power up to a lift coefficient of 2.0.

It may be seen that the airplane with the original tail configuration should be stable in both the cruising and landing conditions with windmilling propellers for all contemplated center-of-gravity locations, throughout the flight range (fig. 17(a) and 17(b)).

With take-off power, however, the original tail is unsatisfactory throughout the speed range for the cruising condition (fig. 18(a)) and unsatisfactory above a lift coefficient of about 1.7 for the landing configuration (fig. 18(b)).

Because the results of the tests with the original horizontal-tail configuration showed it to be unsatisfactory, it was decided to increase the tail effectiveness by increasing both the area and aspect ratio of the tail (fig. 4). In addition, it was felt that the longitudinal stability with power-on might be improved in the landing configuration by raising the tail out of the high slipstream velocity region (fig. 5).

Increasing the size of the horizontal tail (horizontal tail 2) in the original tail location assures satisfactory stability in the cruising condition (fig. 18(a)) and extends the stable speed range in the landing configuration to a lift coefficient of about 2.0 for the most rearward center-of-gravity location with take-off power (which about meets the minimum requirement previously mentioned (fig. 18(b)).

Raising either the original tail or horizontal tail 2 increases the speed range in which the airplane may be expected to be stable as compared to the same tail in the original location (fig. 18(a) and 18(b)).

In an attempt to explain the unusual condition that raising the tail increases the stability for the cruising (flap up) configuration, as well as for the landing (flap down) configuration, the average downwash angles and dynamic pressure ratios at the tail were computed from the data of figures 15 and 16 for all the tail configurations tested. These curves are presented in figures 19 and 20.

It may be seen from figure 20(a) that, with power in the cruising condition, raising the original tail increases the rate of change of q_t/q at the tail with angle of attack, which is unusual, and decreases the rate of change of downwash $(\partial\epsilon/\partial\alpha)$ considerably. Both effects tend to increase the stability of the airplane in the cruising condition where the airplane flies with an up load on the tail for trim. It may be noted that, for the original tail in the original position, the rate of change of downwash $\partial\epsilon/\partial\alpha$ exceeds 1.0 at high angles of attack indicating that the tail contribution to stability is destablizing. This effect may perhaps be traced to the extremely wide center section of the wing which, in conjunction with the slipstream, concentrates much of the lift developed by the wing (and hence a large degree of downwash) in a region which directly influences the horizontal tail. The condition is apparently local, since raising the tail decreases the rate of change of downwash considerably.

With the flaps down, a high rate of change of dynamic pressure for the original tail in the original position is indicated (fig. 20(b)). Such a condition is unfavorable since a download on the tail is required for trim.

Raising the tail decreases $d\frac{\frac{q_t}{q}}{d\alpha}$ and at the same time reduces $\partial\epsilon/\partial\alpha$ slightly. Both of these effects are favorable.

The value of average downwash angle at the tail for the model with the horizontal tail 2 was somewhat larger than that obtained with the original tail. The reason for this is unknown.

Effect of Handley-Page slat configuration.- A series of tests (power-on and power-off) was made to determine the effect of the inboard Handley-Page slat on longitudinal stability and maximum lift. In addition, data were obtained with the slots completely closed. Data are presented for both tail-on and tail-off configurations (figs. 21 and 22).

It appears that the inboard portion of the slot, when open, contributes a destabilizing effect equal to from 1 to 2 percent shift of the neutral point regardless of power (fig. 23). This effect is slight and is approximately within the accuracy of the neutral point calculation. Further, it seems that from the stability standpoint, the absence of all slats would furnish the most desirable configuration. The change in maximum lift coefficient with any slot configuration (tail off) appears to be slight at the very best (figs. 21(b) and 22(b)). However, the slots do have a favorable effect on stalling characteristics as will be shown later.

Effect of propeller blade angle.- The effect of changing the propeller blade angle on the longitudinal stability characteristics is seen to be negligible (fig. 24). Therefore, all of the tests in the latter part of this investigation were made with the same blade-angle setting regardless of model configuration (table I).

Effect of swept-back outboard wing modification.- The outboard wing panel was swept back in order to improve the lateral stability characteristics of the model. It was also decided to determine the longitudinal stability characteristics of the model with this wing revision; therefore, a series of stabilizer tests was made with the swept-back wing using the original horizontal tail. These data, along with the results of tail-off tests for the various model configurations, are presented in figure 25. The neutral point was moved back from 6 to 11

percent of the original mean aerodynamic chord throughout the flight range in the cruising condition (fig. 27(a) and 27(c)), the larger improvement being realized with windmilling propellers. For the landing configuration (fig. 27(b) and 27(d)), the windmilling condition shows an improvement over the original model corresponding to a rearward shift of the neutral point of 9 to 12 percent mean aerodynamic chord. In the landing condition with take-off power and at a lift coefficient 2.0, the airplane with the swept-back wing is neutrally stable at a center-of-gravity location of 25.0 percent mean aerodynamic chord. This characteristic approximately meets the Navy's minimum requirement for this airplane. With the possible exception of take-off power in the cruising configuration at high values of C_L, the airplane appears to have satisfactory longitudinal stability with the swept-back wing using the original horizontal tail configuration.

The principal reason for this increase in longitudinal stability is that the mean aerodynamic center is moved back approximately 10 percent mean aerodynamic chord relative to the original center of gravity through the expedient of sweeping back the wing. Because of a rearward shift of wing weight, the center of gravity will also move back, but to a much lesser extent (about 1 percent mean aerodynamic chord).

Effect of rectangular outboard wing modification.- Another modification, tested primarily to determine its effect on the lateral stability characteristics, is the rectangular outer wing panels. A series of stabilizer tests was made with these rectangular outer panels (fig. 26). A comparison of the neutral points obtained with other outboard plan forms is shown in figure 27.

It appears that the neutral point is shifted from 2 to 5 percent to the rear in the cruising condition (fig. 27(a) and 27(c)), the larger value being obtained with power at low speed. There is a similar change in the landing condition with the propeller windmilling (fig. 27(b)). However, with take-off power in the landing condition at about $C_L = 2.0$, the stability was actually worse with the rectangular panel than with any of the other wing modifications (fig. 27(d)).

It may be noted that the stability with the rectangular outer panels is affected by several factors.

The mean aerodynamic chord is moved back 0.023 of the original mean aerodynamic chord. The center of gravity also moves back about 0.014 of the original mean aerodynamic chord because of redistributed wing weight. Thus, the stability might be expected to be about the same as that obtained on the original model. However, the wing in this instance is of increased area, which decreases the relative tail volume factor, $\frac{S_t l_t}{S\ c}$, tending to decrease the stability. Apparently, in most instances, this is more than compensated by changes in flow at the tail (fig. 28) so that there is an over-all increase in stability.

It would be expected that power A, which represents the lower wing loading, would be more critical than power B. The difference in the neutral points for these two conditions is negligible except at high lift coefficients in the landing condition where power A is appreciably worse.

It should be noted that in the plots of neutral points (fig. 27) similar values of C_L for various configurations of the airplane, only denote the same airplane speed for conditions having the same wing loading.

Effect of rectangular wing.- A rectangular wing was tested not so much for direct application on this model, but rather as a source of general design information. This wing, having a smaller inboard panel, had considerably less area directly affected by the slipstream. The data obtained for the model with the rectangular wing are presented in figure 29. It appears that the longitudinal stability of the model with the rectangular wing is better than that of the model with the original wing, except with take-off power in the landing configurations below a lift coefficient of 1.9 (fig. 30(b)).

The slope of the tail-off pitching-moment curve is not changed by the change of wing plan form for the windmilling condition both in the cruising and landing configurations. Thus it follows that the increase in stability in that condition (figs. 30(a) and 30(b)) must be a function of the flow at the tail. This contention

appears to be borne out by the data of figures 31(a) and 31(b). It appears that $\partial\epsilon/\partial\alpha$ is markedly decreased when the rectangular wing is used. This decrease is especially evident in the cruising condition and may be attributed to a change in the span-load distribution from that of the original wing, with more lift being concentrated on the outboard panels.

The increase in stability for the model with the rectangular wing, in the cruising configuration with take-off power, corresponds to a rearward shift of the neutral point of from 5 to 10 percent mean aerodynamic chord, the larger value being realized at high-lift coefficients. There are several factors which might account for this change. A comparison of tail-off C_m curves for the two wing plan forms (figs. 29(b) and 16(a)) shows that there might be a decrease of $\partial C_m/\partial C_L$ corresponding to from 2 to 3 percent mean aerodynamic chord rearward shift of the mean aerodynamic chord with the rectangular wing for this condition.

A slight decrease in $\partial\epsilon/\partial\alpha$ and an increase in q_t/q at the tail also add to the margin of stability when the rectangular wing is used.

For the model in the landing configuration and with take-off power, the model exhibits more stability at moderate lift with the original wing, while at high values of C_L the model with the rectangular wing is decidedly more stable. A comparison of the tail-off pitching-moment curves for the model with the original and rectangular wings (figs. 16(c) and 29(d)) indicates that the former curve has a much greater stable slope and at the same time gives much larger negative pitching moments to be trimmed by the tail. These differences result from the fact that the original wing has more area affected by the slipstream. These two factors have an opposite effect on the stability of the complete model. That is, the more stable slope tends to increase the stability of the complete model, while the larger negative untrimmed pitching moments tend to reduce the stability of the complete model because of the higher tail downloads for trim. The net effect is a function of the relative magnitude of the individual effects. The difference in slopes of the tail-off curves is greatest at low lift coefficients while the difference in untrimmed pitching moment is greatest at high lift

coefficients. Thus it may be expected that the model with the original wing will be more stable at low lift coefficients and the model with the rectangular wing will be more stable at high lift coefficients.

Effect of opening canopy.- The effect of opening the pilot's canopy on the longitudinal stability characteristics of the model were determined and found to be insignificant for both the windmilling and take-off power conditions in the landing configuration (figs. 32(a) and 32(b)).

Effect of upturned wing tips.- The longitudinal stability appears to be unaffected when the wing tips are upturned (fig. 33). The slight increase in maximum lift with the upturned wing can be almost entirely accounted for by the fact that the original wing area was used in the reduction of the data. The decrease in drag coefficient is probably due in part to a reduction in induced drag.

Effect of skewing flaps.- With propeller windmilling, the maximum lift coefficient is reduced about 0.12 by skewing the outboard flaps from -14.5° to 0.7°; however, this reduction is partly neutralized by a reduction of about 0.1 in the negative pitching-moment coefficient (fig. 34(a)). Correcting for the negative tail load required for trim, the net reduction in maximum lift coefficient would be about 0.09. The slopes of the tail-off pitching-moment curves remained practically unchanged when the outboard flap was skewed. If there is no change in the rate of change of downwash angle at the tail, the longitudinal stability with the propeller windmilling should not be decreased by skewing the flap. It might be expected that the stability with power would be increased because of the smaller negative tail load required for trim. The data of figure 34(b) indicate, however, that the tail load for trim with power will be about the same whether or not the flap is skewed. Consequently, the power-on stability may be expected to be substantially the same.

Effect of elevator and elevator tab deflection.- A series of elevator tests was run with the original horizontal tail in the normal position. These tests were made with the propeller windmilling for both the cruising and landing configuration (fig. 35). A complete discussion of the flying qualities will not be attempted

in this paper since the final airplane is expected to be entirely revised. However, it may be interesting to note that while enough up elevator may be available to make a three-point landing with the original configuration, if the airplane was equipped with the swept-back wing and ground effect were taken into consideration, it is entirely probable that the original elevator would prove inadequate. Using a constant tab effectiveness of $C_{h_{\delta_t}} = -0.0024$ (fig. 36), it appears that an excessive tab deflection would be required to trim in a landing approach attitude (fig. 37).

Effect of wing plan form on maximum lift coefficients.- A comparison of the maximum lift coefficient obtained with the various wing plan forms is presented in the table below. These values of $C_{L_{max}}$ are based on actual wing area and are tail-off values.

Wing	Model configuration	
	Cruising	Landing
Original	1.2	1.9
Swept-back outer panels	1.20	2.0
Rectangular outer panels	1.16	1.9
Rectangular	1.24	2.2

It is interesting to note that in the landing configuration, the rectangular wing produces the greatest lift. This might be due to the use of a smooth flap slot entry as well as several other flap details which have been previously discussed.

Stalling Characteristics

A study of the stalling characteristics of each of the wing modifications tested was made. These surveys were made for various model configurations with and without power. During most of this investigation, sketches were made of the progression of the stall. The flow over the wing was observed by means of silk tufts attached to the wing. Tuft surveys with the rectangular wing, however, were photographed.

Original wing.- Tuft sketches for the model with the original wing without power are presented in figures 38 through 46. These figures show that the stall for most configurations developed first in the vicinity of the

fold line and spread in both directions until the wing was fully stalled. The landing gear, when retracted, delayed the stall over sections of the wing directly behind it (figs. 39, 40). Opening the cowl flaps produced unsteady flow at the wing root causing the wing to stall sooner in that area (figs. 40 and 41). Opening the outboard wing slat appears to reduce the stall on the outboard panel considerably (figs. 41 and 42). The inboard slot does not seem to improve the stall characteristics (figs. 42-45). Because of the difference in scale, the amount of stall indicated at each angle may differ from the full-scale airplane, but the progression of the stall is probably correct.

The tuft pictures of the model with power-on are shown in figures 47 through 52. The effect of power tends to prevent that portion of the wing which is immersed in the slipstream from stalling. The wing stall begins at the trailing edge of the fold line and spreads from there. Power retards the spread toward the fuselage. Opening the cowl flaps tends to produce unsteady flow at the wing-fuselage juncture, but has little effect on the final stall (fig. 48).

Figures 49, 50, and 51, show the effect of opening the wing slots. Opening the outboard slots helps to prevent the wing tips from stalling first. Opening both slots tends to keep a larger portion of the tips unstalled. In general, the duplex flaps were stalled at all angles of attack. There was less tendency for the duplex flaps to be stalled, when the slots were closed. No noticeable effect of retracting the landing gear was observed (figs. 50 and 52).

Swept-back outer panel.- The stall characteristics with the swept-back outer panel are presented in figures 53 through 57. The stall begins at the fold line as it did for the original wing, however, as the stall progresses the movement toward the tips is more rapid than toward the root. This tip stall tendency is greater for the swept-back outer panels than for the original wing. The application of power tends to unstall the root. The outboard slots are fairly successful in maintaining unstalled flow at the tips in the landing configuration (figs. 55, 56). In fact, the stall characteristics may be further improved by extending the slats to the fold line, since most of the stall appears to be confined to the region between the fold line and

the inboard end of the slot. In view of the low test Reynolds number, and the fact that the flaps could not be observed very well, the flap stalls shown cannot be considered very accurate.

Rectangular outer panels.- The stall begins at the trailing edge at the fold line as for the other wings (figs. 58 to 62). The main difference, however, is that the stall does not travel out rapidly to the wing tips. Even when the slots are closed in the landing configuration, the wing tips remain relatively unstalled. Power tends to unstall the root portion of the wing as was true for the other wings.

Rectangular wing.- Photographs of the stall were taken for this wing (fig. 63 to 67). The pictures show that the power-off stalls occur first over the center panel (fig. 63). This condition is characteristic of rectangular wings. In this case, however, center panel stall is made even more pronounced by about 2° washout in the outer panel. The application of power (fig. 64) tends to unstall the wing-fuselage juncture area leaving the most intense stall just inboard of the fold line.

When flaps are deflected, one side stalls before the other (fig. 65, $\alpha = 13.6^\circ$). For the same condition, but with the tip slats open, the asymmetric stall does not occur until $\alpha = 16.6^\circ$ and with less asymmetry. (fig. 66). This difference is unexplained at present since it seems unlikely that the tip slat would have so much effect on the center panel. With power on (fig. 67), the stall is symmetrical with stalled areas centering about the fold line. The flaps are stalled or very unsteady at all deflected conditions.

Pressure Distribution

Oil-cooler survey.- The results of a pressure-distribution survey made in the vicinity of the oil-cooler flap location are presented in figure 68. These results are presented in the form of pressure contours at four angles of attack.

CONCLUSIONS

The Navy's minimum longitudinal stability requirement for this airplane can probably be met by using either:

1. The original wing and horizontal tail 2 in either the raised or normal position.

or

2. The original outer panel swept back in combination with any horizontal tail modification tested.

There is probably insufficient elevator control available to make a three-point landing if the original horizontal tail is used. This is especially true if the swept-back outer panels are incorporated into the final airplane.

The effect of Handley-Page slots, opening the pilot's canopy, or using upturned wing tips on the longitudinal stability is insignificant.

Tuft surveys showed that wing plan form and sweep have a pronounced effect on stalling characteristics. Increasing the tip chord or sweeping the tips forward improved stalling characteristics. Handley-Page tip slots improved the stall characteristics of the wings having poor stalling characteristics.

Langley Memorial Aeronautical Laboratory
National Advisory Committee for Aeronautics
Langley Field, Va., June 1, 1944

REFERENCE

1. Recant, Isidore G., and Swanson, Robert S.: Determination of the Stability and Control Characteristics of Airplanes from Tests of Powered Models. NACA ARR, July 1942.

OUTLINE OF FIGURES ON 1/8-SCALE MODEL OF XBTC-2 AIRPLANE

OUTLINE OF FIGURES ON 1/8-SCALE MODEL OF XBTC-2 AIRPLANE

Concluded

TABLE I - TEST PROGRAM

NATIONAL ADVISORY COMMITTEE FOR AERONAUTICS

Fig.	Title	δf_i, δf_o (deg)	Power	β (deg)	i_t	Wing slots s_i, s_o	Remarks	Test No.
15(a)	Effect of horizontal-tail configuration	0	Windmilling	30	Tail-off	Closed		61
					5°50'		Original tail	66
					1°00'		↓	69 ck.
					5°10'		Original tail raised	171
					0°40'			172
(b)					Tail-off			61
					5°45'		Horizontal tail 2	130
					0°40'			133
					6°00'		Horizontal tail 2 raised	166
					1°00'			165
(c)		50		23	Tail-off	(s_i closed, s_o open)		150
					5°40'		Original tail	213
					0°40'		↓	219
					5°40'		Original tail raised	208
					0°40'			207
(d)					Tail-off			150
					5°45'		Horizontal tail 2	144
					1°05'			145
					6°00'		Horizontal tail 2 raised	154
					1°00'			151
16(a)		0	Take-off	30	Tail-off	Closed		62
					5°25'		Original tail	225
					0°55'		↓	224
					-1°05'			223
					5°10'		Original tail raised	169
					0°40'			174
(b)					Tail-off			62
					5°45'		Horizontal tail 2	132
					0°40'			135
					6°00'		Horizontal tail 2 raised	168
					1°00'			163
16(c)	Effect of horizontal tail configuration	50	Take-off	23	Tail-off	(s_i closed, s_o open)		283-B
					5°00'		Original tail	234
					1°00'		↓	233
					-1°30'			232
					5°45'		Original tail, raised	276
					1°55'		↓	275
					-1°00'			274
(d)					Tail-off			283-B
					5°00'		Horizontal tail 2	279
					2°00'		↓	278
					-1°05'			277
					5°00'		Horizontal tail 2, raised	282
					2°00'		↓	281
					-1°12'			280
21(a)	Effect of Handley Page slat configuration	50	Windmilling	23	6°00'	Open		28
					1°00'	↓		31
					5°35'	Closed		214
					0°40'	↓		217
					5°35'	(s_i closed, s_o open)		213
					0°40'			219
(b)					Tail-off	Open		56
						Closed		222
						(s_i closed, s_o open)		150
22(a)		50	Take-off		5°55'	Open		231
					1°00'	↓		230
					-1°30'			229 ck.
					5°35'	Closed		215
					0°40'	↓		216
					5°00'	(s_i closed, s_o open)		234
					1°00'	↓		233
					1°30'			232
22(b)	Effect of Handley Page slat configuration	50	Take-off	23	Tail-off	Open		57
						Closed		221
						(s_i closed, s_o open)		283-B

TABLE I - Continued

NATIONAL ADVISORY COMMITTEE FOR AERONAUTICS

Fig.	Title	δ_{f_i}, δ_{f_o} (deg)	Power	β (deg)	i_t	Wing slots s_i, s_o	Remarks	Test No.
24	Effect of propeller blade angle	0		30 ↓ 23	5°25' 0°55' -1°5' 5°0' 1°0' -10°30'	Closed		225 224 223 228 227 226
25(a)	Effect of swept-back wing		Windmilling		Tail-off 5°35' -2°55'		Swept-back outer panel	342 347 350
(b)		50			Tail-off 5°0' -2°0'	(s_i closed s_o open)		335 321 324
(c)		0	Take-off		Tail-off 5°35' -2°55'	Closed		341 348 349
(d)		50			Tail-off 5°0' -2°0'	(s_i closed s_o open)		334 322 323
26(a)	Effect of rectangular outer wing panel	0	Windmilling		Tail-off 4°50' -1°12'	Closed	Rectangular outer wing panel	296 284 287
(b)		50			Tail-off 5°0' -1°40'	(s_i closed s_o open)		307 311 314
(c)		0	Take-off (A)		Tail-off 4°50' -1°12'	Closed		297-A 285-A 286-A
(d)			Take-off (B)		Tail-off 4°50' -1°12'			297-B 285-B 286-B
(e)		50	Take-off (A)	23	Tail-off 5°0' -1°40'	(s_i closed s_o open)	Rectangular outer wing panel	308-A 312-A 313-A
(f)			Take-off (B)		Tail-off 5°0' -1°40'			308-B 312-B 313-B
29(a)	Effect of rectangular wing	0	Windmilling		Tail-off 5°15' 2°5' -3°15'	Closed	Rectangular wing	377 365 362 366
(b)		50			Tail-off 5°0' 2°0'	(s_i closed s_o open)		391 392 395
(c)		0	Take-off		Tail-off 5°15' 2°5' -3°15'	Closed		376 364 363 367
(d)		50			Tail-off 5°0' 2°0' -2°20'	(s_i closed s_o open)		390 393 394 397
32(a)	Effect of opening canopy		Windmilling		5°35' 1°5' 5°0' 0°55'		Canopy closed ↓ Canopy open	213 219 235 236-A
32(b)			Take-off		5°0' 1°0' 5°0' 0°55'		Canopy closed ↓ Canopy open	234 233 237 236
33	Effect of upturned wing tips		Windmilling		0°40' 0°55'		Original tips Upturned tips	219 260-A
34(a)	Effect of skewing flaps	50 (δ_{f_i} = 50, δ_{f_o} = 59)	Windmilling		Tail-off	Open	Λ_{f_o} = -14.5 (original) Λ_{f_o} = 0.7	56 187
34(b)	Effect of skewing flaps	50 (δ_{f_i} = 50, δ_{f_o} = 59)	Take-off power	23	Tail-off	Open	Λ_{f_o} = -14.5 (original) Λ_{f_o} = 0.7	57 188

TABLE I - Concluded

NATIONAL ADVISORY COMMITTEE FOR AERONAUTICS

Fig.	Title	δ_{f_i}, δ_{f_o} (deg)	Power	β (deg)	i_t	Wing slots s_i, s_o	Remarks	Test No.
35(a)	Effect of elevator deflection	0	Windmilling	30	1°0'	Closed	δ_e = 5°	72 ck.
							δ_e = 0°	69 ck.
							δ_e = -5°	73
							δ_e = -10°	74
							δ_e = -15°	75
							δ_e = -20°	76
(b)		50		23		Open	δ_e = 0°	31
							δ_e = -15°	34
							δ_e = -25°	35
36	Effect of elevator tab deflection						δ_{e_t} = 10°	127
							δ_{e_t} = 0°	125
							δ_{e_t} = -10°	126

Notes:

Unless otherwise specified:

1. Cowl flaps open and landing gear down for all flap-down tests and cowl flaps closed and landing gear up for all flap-neutral tests.
2. q = 16.37 lb/sq ft. except for take-off power with flaps deflected when q = 9.21 lb/sq ft.
3. Original horizontal tail used ($\delta_e = \delta_t = 0$)

All tests were made through the pitch range at 0° yaw.

The term Handley-Page slats and wing slats are used interchangeably.

Landing gear and L.G. are synonymons.

Only the average blade angles are given; that is, $\beta = 23°$ means $B_F = 23\frac{1}{2}°$, $\beta_R = 22\frac{1}{2}°$.

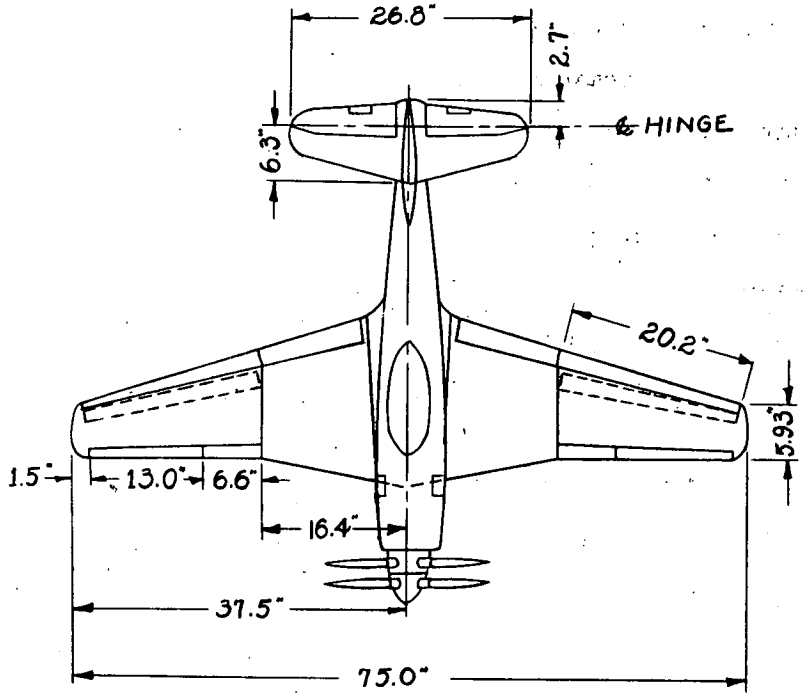

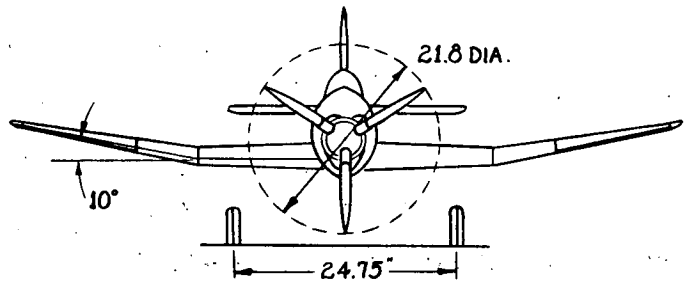

NATIONAL ADVISORY
COMMITTEE FOR AERONAUTICS

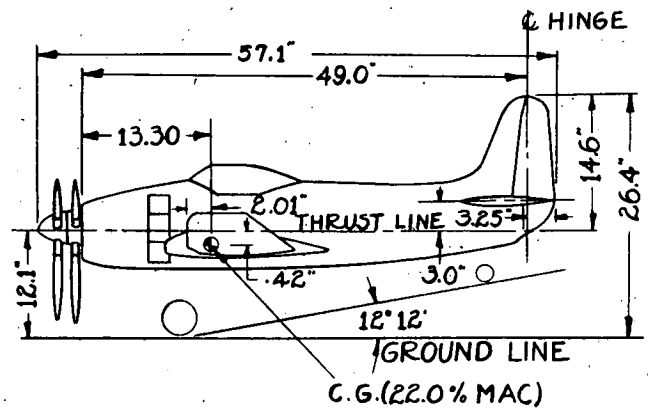

ROOT SECTION NACA 23014.7 (Approx) i_w = 1.5°
BREAK SECTION NACA 23016 i_w = 1.5°
THEO. TIP SECTION NACA 23008 i_w = -0.8°
WING AREA 6.34 SQ. FT, MAC 12.26 IN.

FIGURE 1(a).-THREE VIEW DRAWING OF 1/8-SCALE MODEL OF THE CURTISS XBTC-2 AIRPLANE.
(ORIGINAL MODEL)

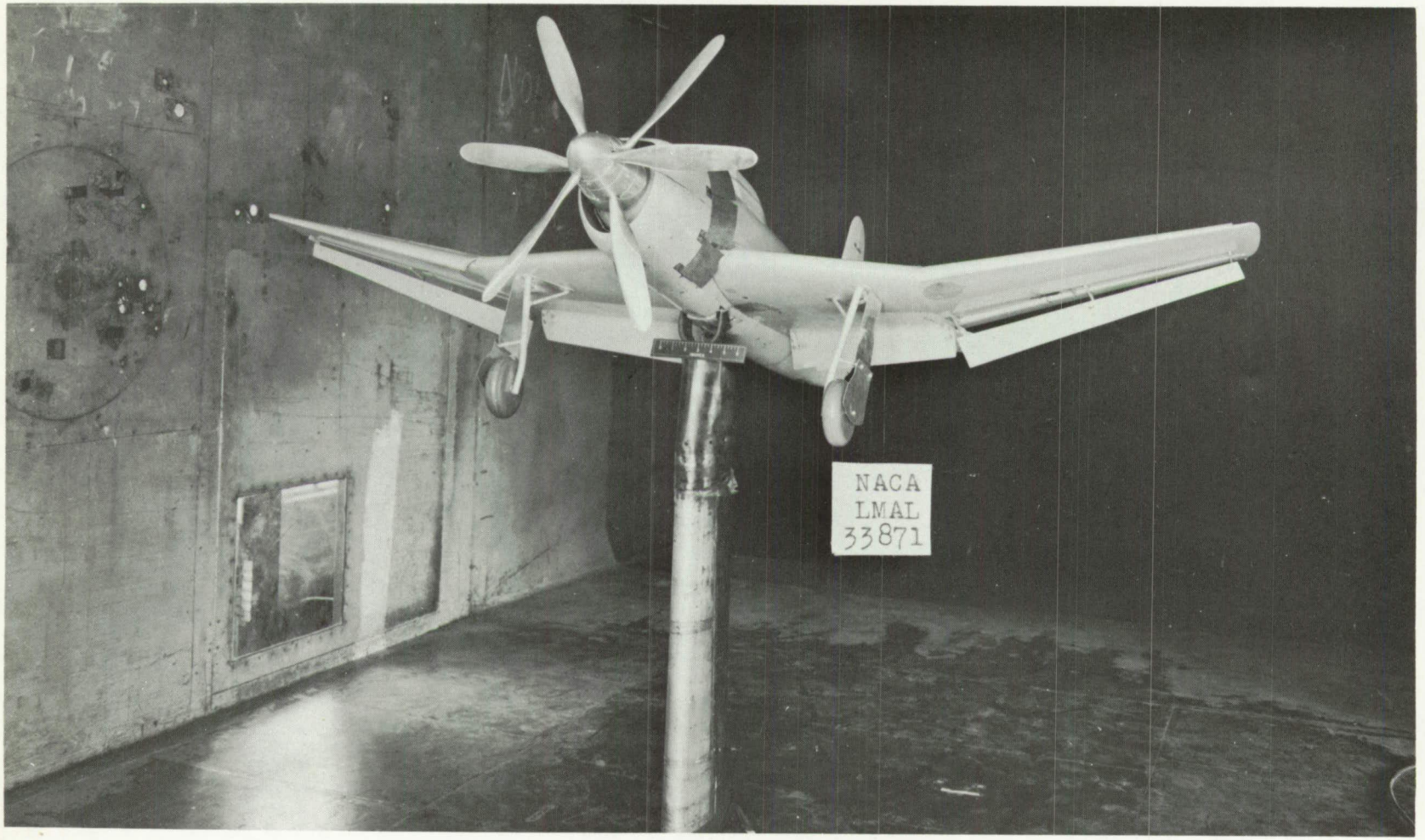

Figure 1(b).- Three-quarter front view of the $\frac{1}{8}$-scale model of the XBTC-2 airplane.

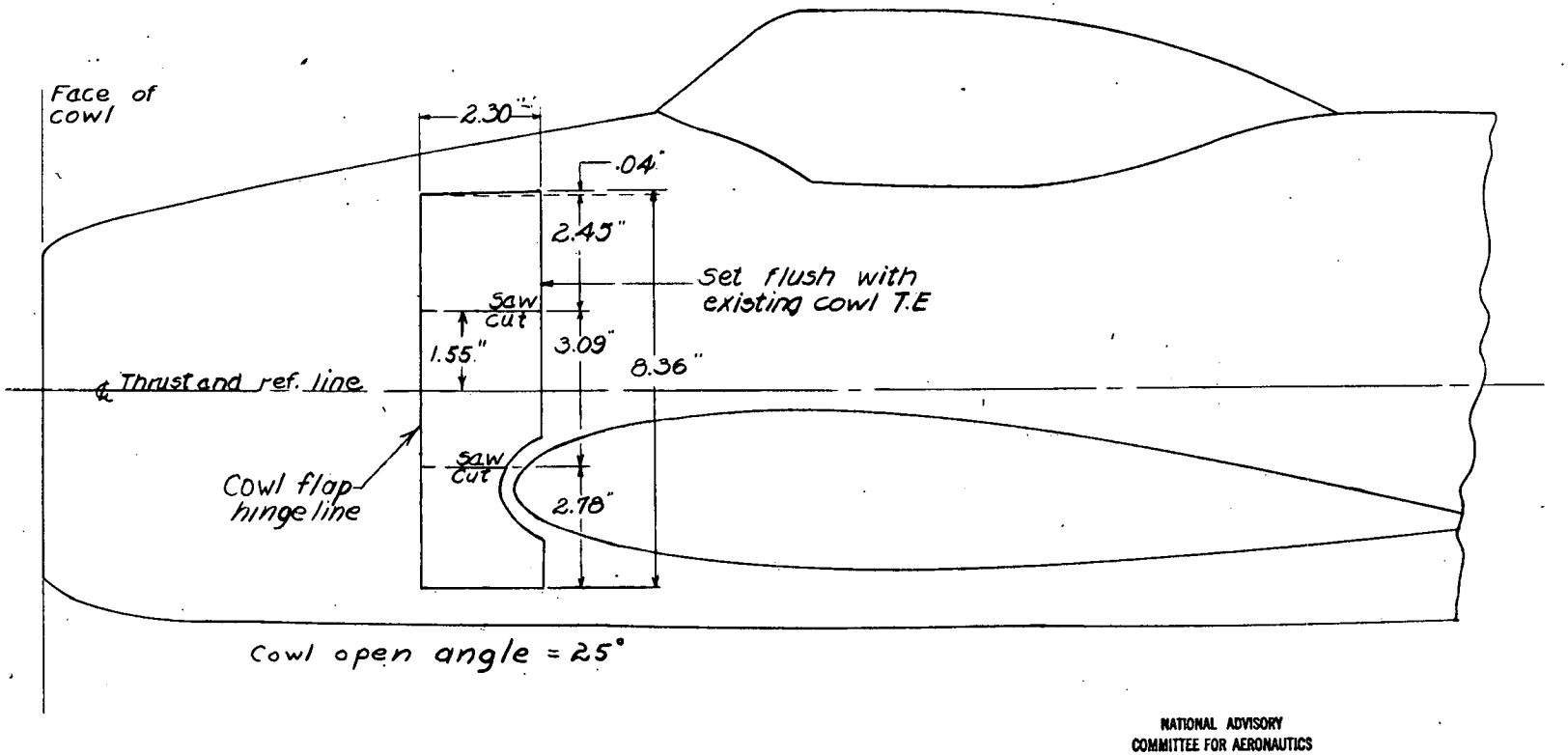

Figure 2 .- Side view of 1/8-scale model of XBTC-2 airplane showing cowl flap details.

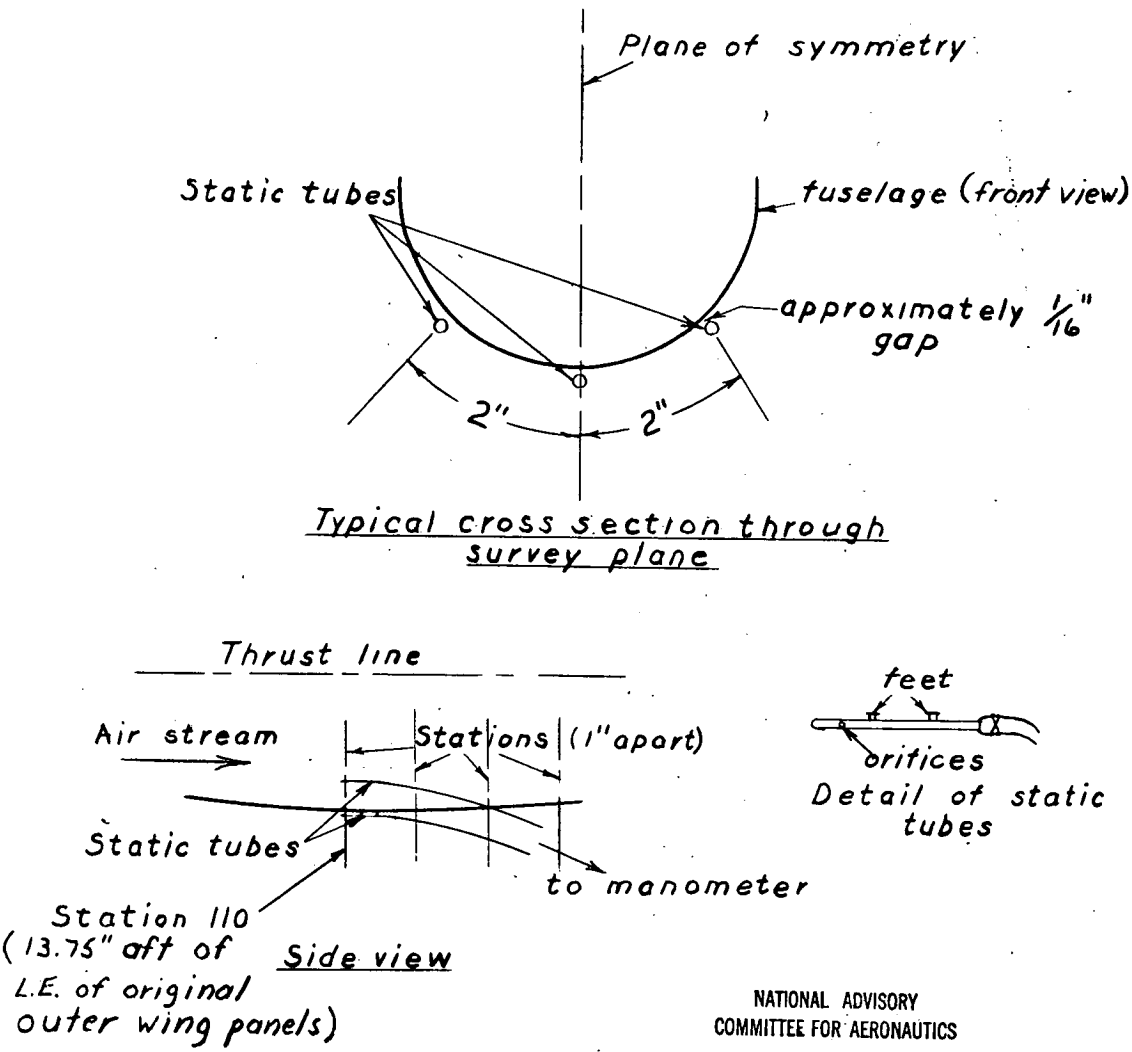

Figure 3 - Location of static tubes for surveying pressures over oil cooler flap location on Curtiss XBTC-2 model (1/8 scale).

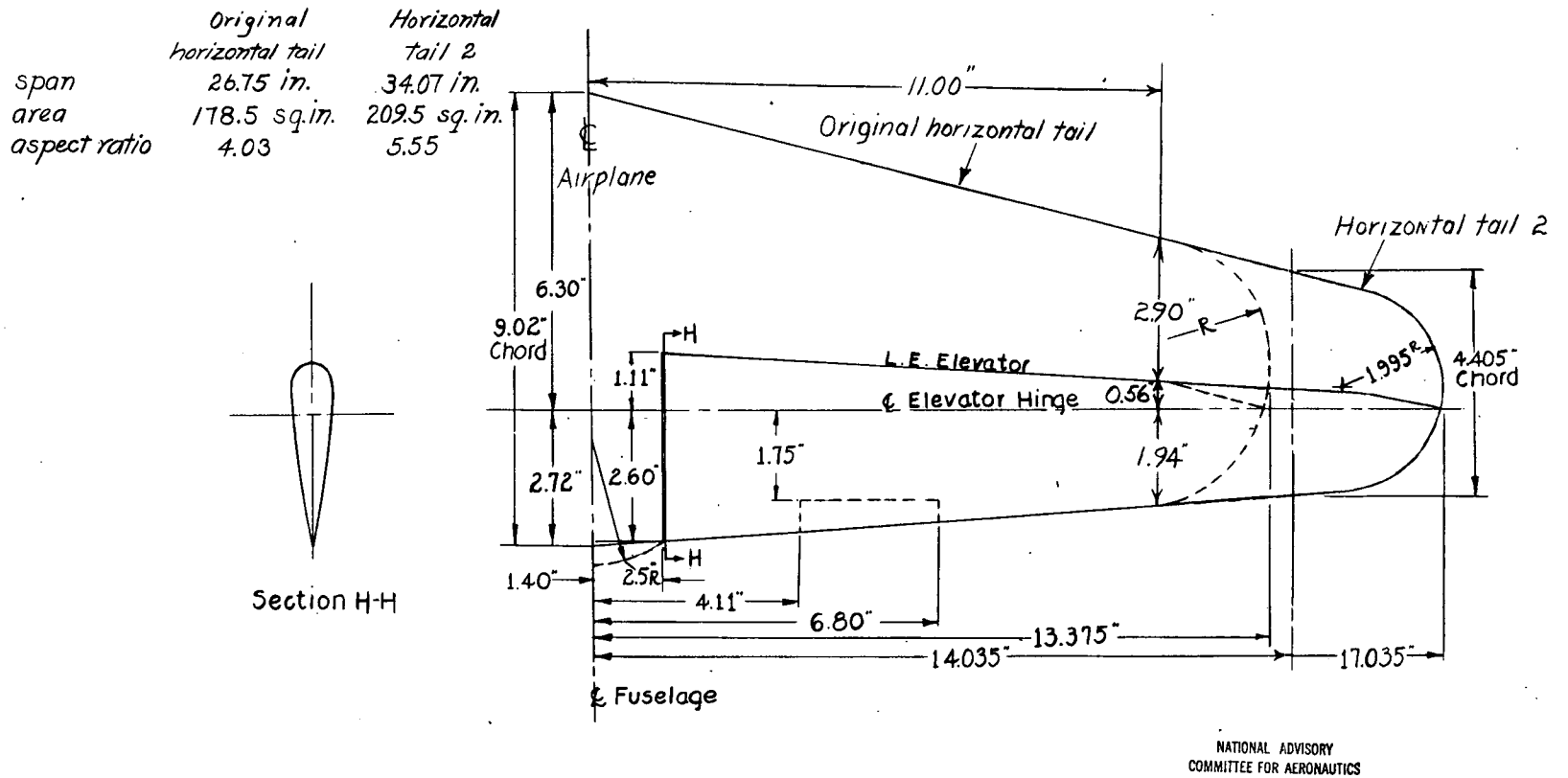

Figure 4.- Comparison of horizontal tails tested on ⅛-scale model of XBTC-2 airplane.

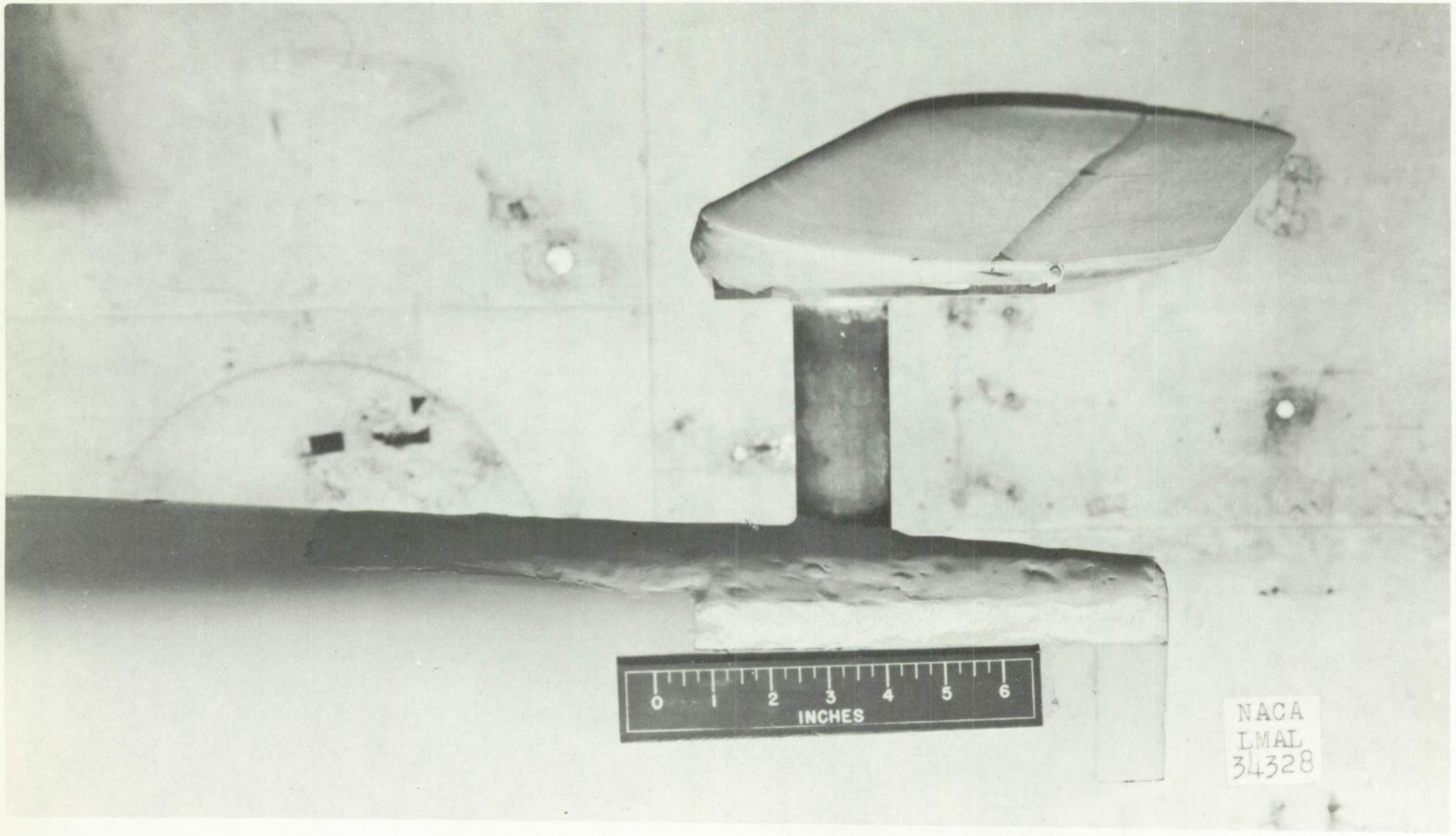

Figure 5.- Side view of $\frac{1}{8}$-scale model of XBTC-2 airplane showing raised horizontal tail location.

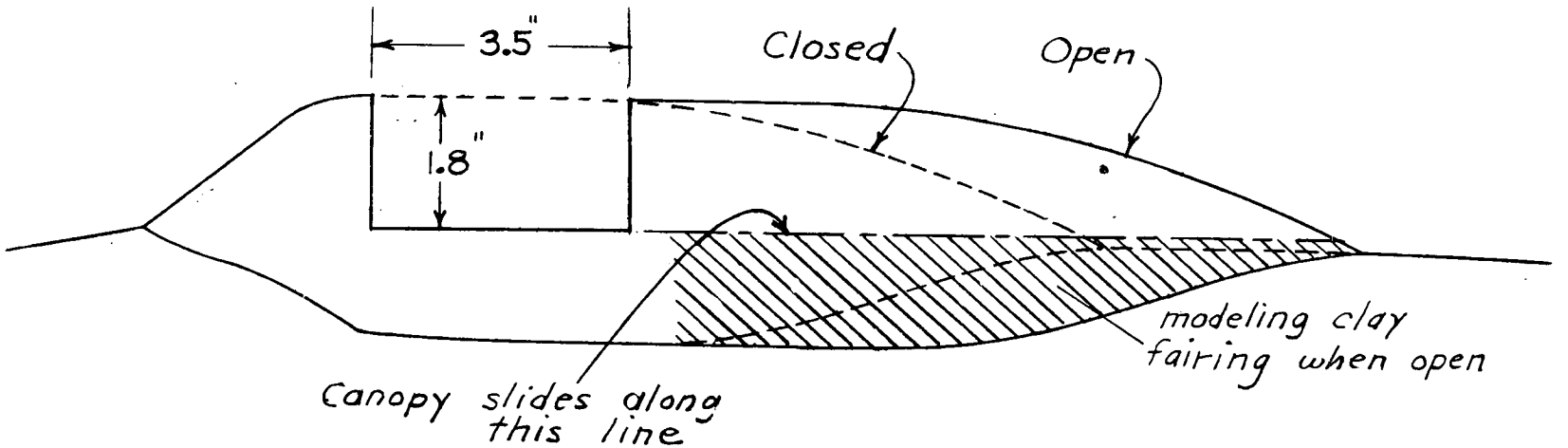

Figure 6(a).- Drawing showing canopy opening on 1/8 scale model of XBTC-2 airplane

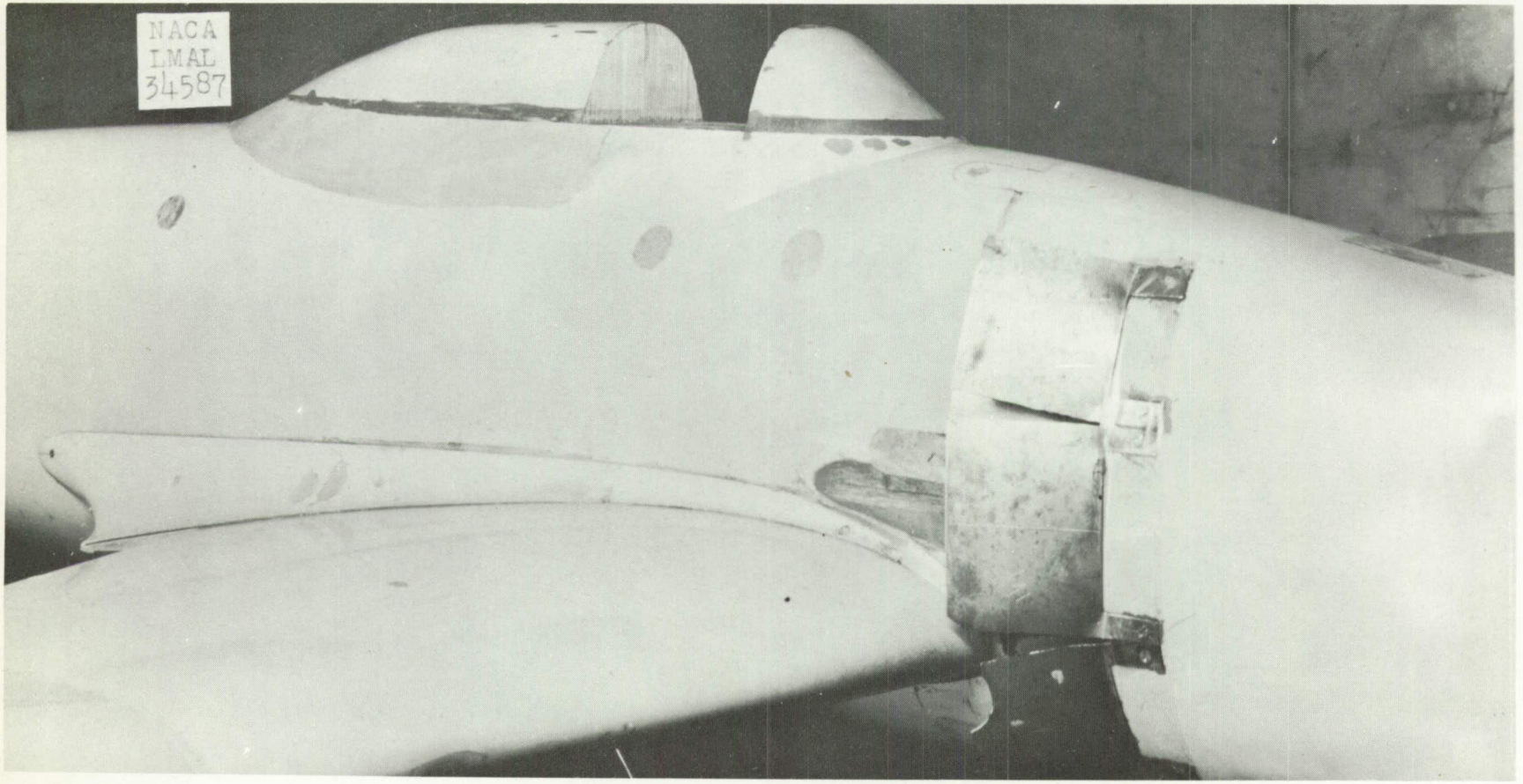

Figure 6(b).- Three-quarter front view of the $\frac{1}{8}$-scale model of the XBTC-2 airplane showing the open canopy.

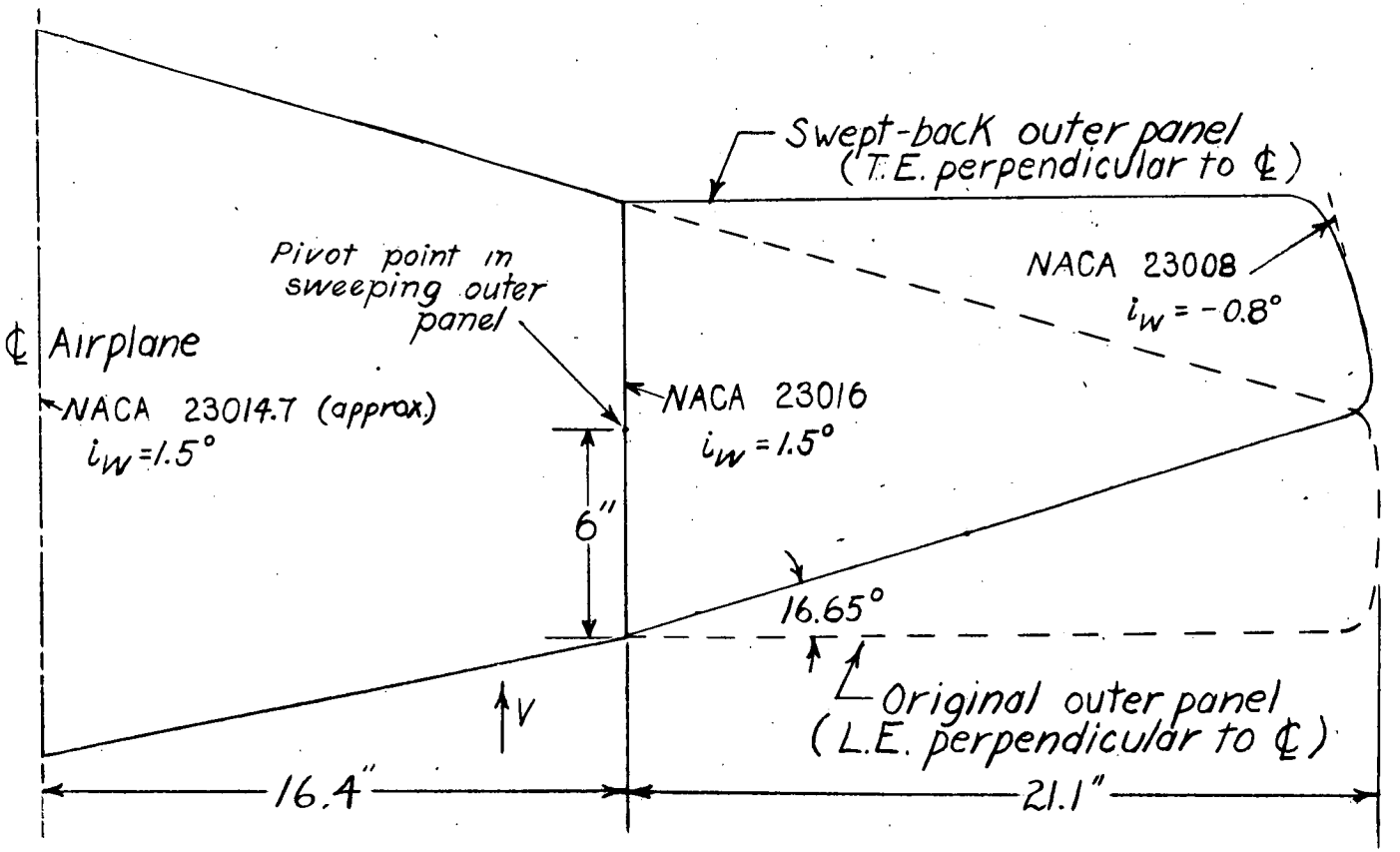

Figure 7.-Left wing panel of 1/8 scale model of XBTC-2 airplane showing swept-back outer panel modification.

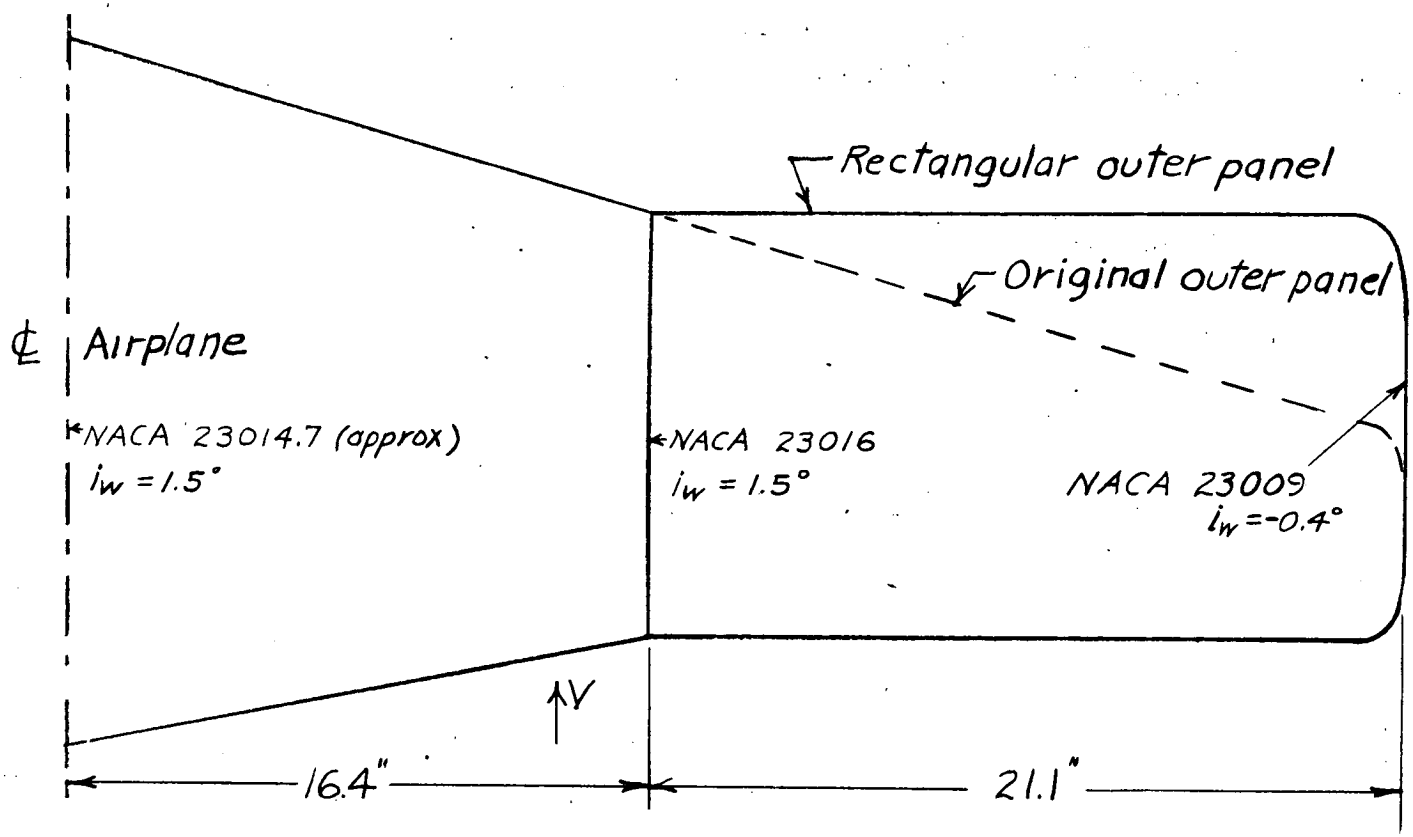

Total original wing area 6.34 sq ft
Total wing area (Rect. outer panels) 7.26 sq ft

NATIONAL ADVISORY
COMMITTEE FOR AERONAUTICS

Figure 8(a) Left wing panel of 1/8 scale model of XBTC-2 airplane showing rectangular outer panel modification

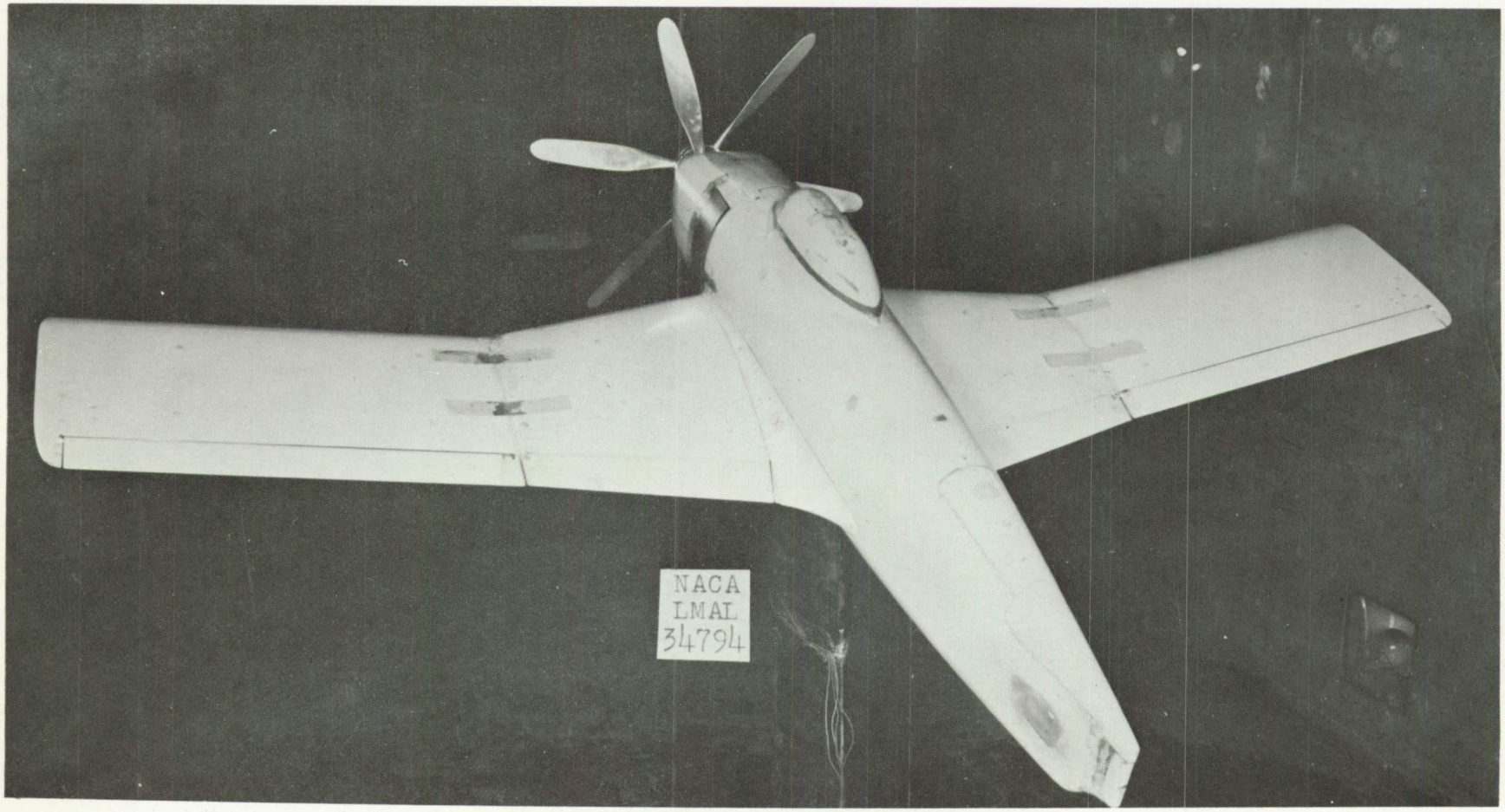

Figure 8(b).- Three-quarter rear view of $\frac{1}{8}$-scale model of XBTC-2 airplane with rectangular outer wing panels.

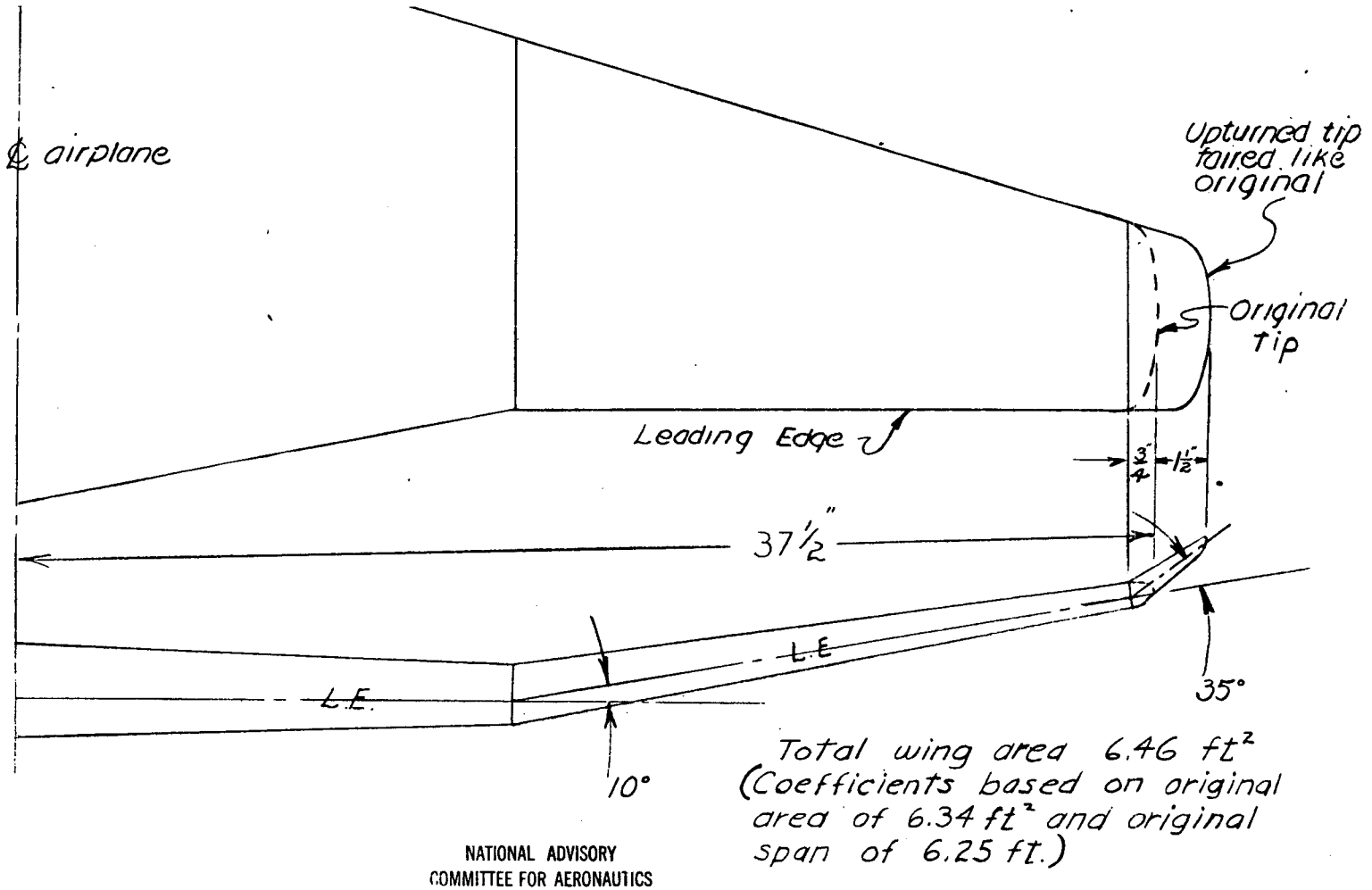

Figure 9(a) - Left wing panel of 1/8-scale model of XBTC-2 airplane showing upturned wing tip.

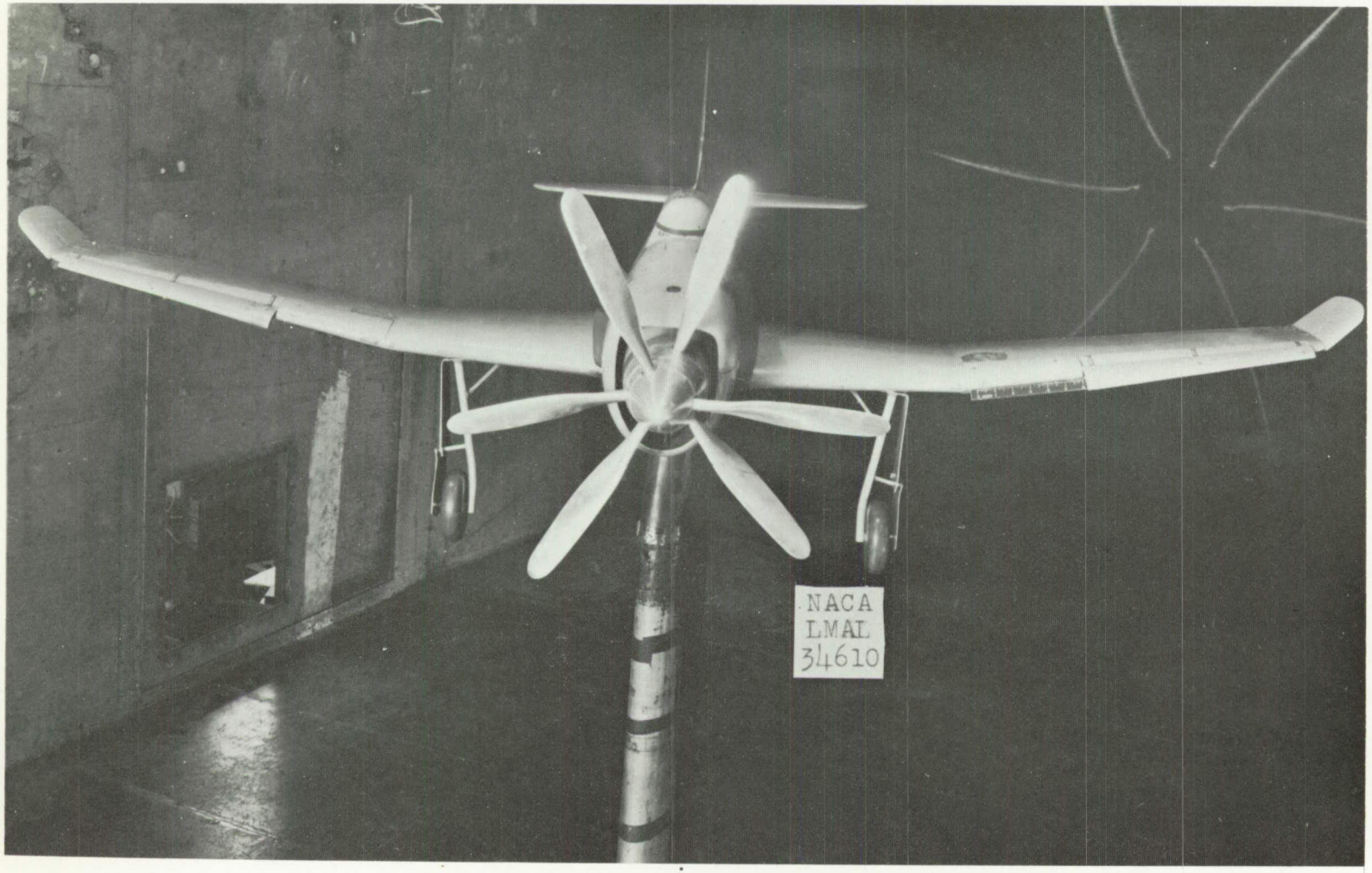

Figure 9(b).- Front view of $\frac{1}{8}$-scale model of XBTC-2 airplane with upturned wing tips.

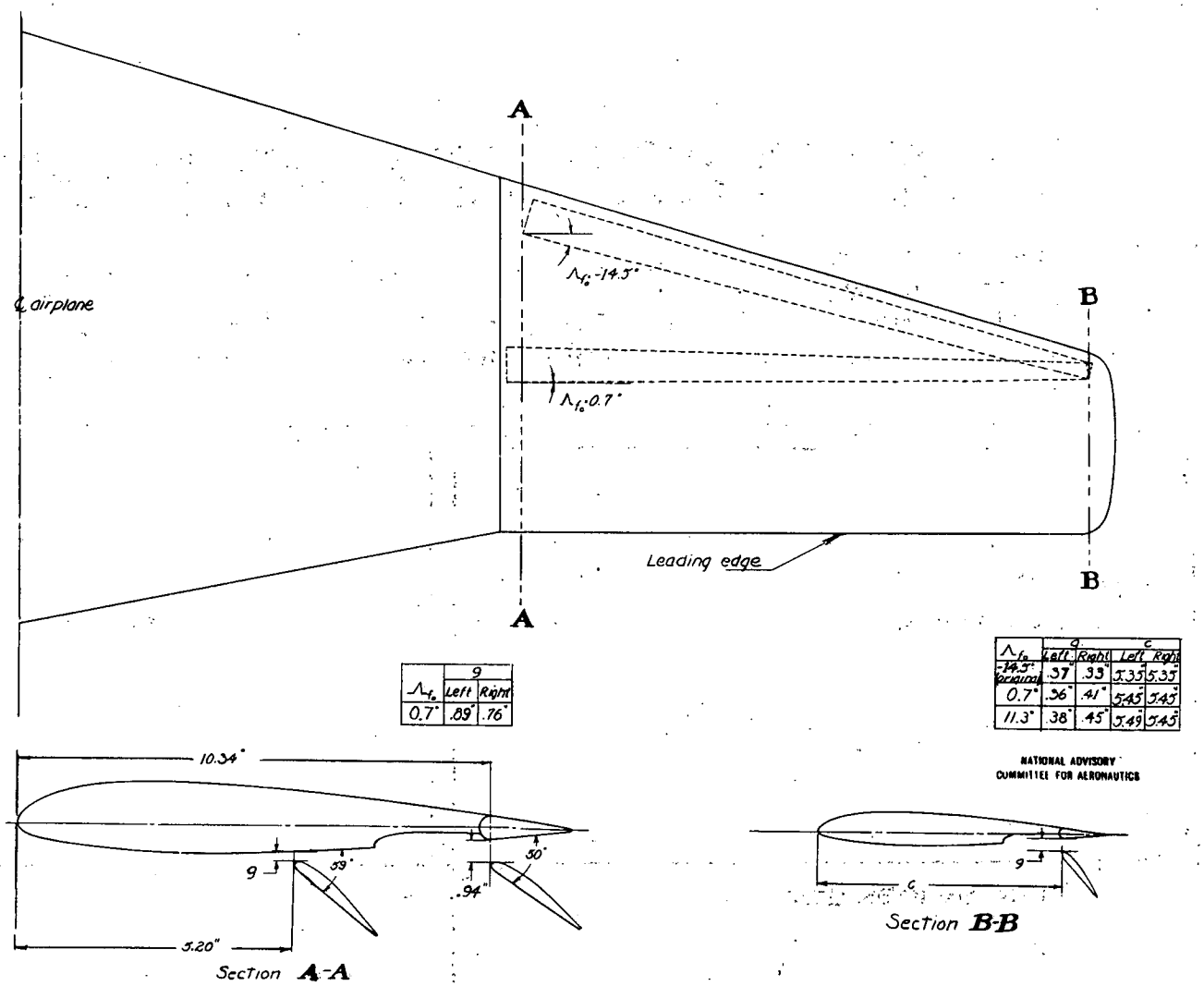

Figure 10.- Left wing panel of 1/6 scale model of XBTC-2 airplane showing outboard flap positions tested.

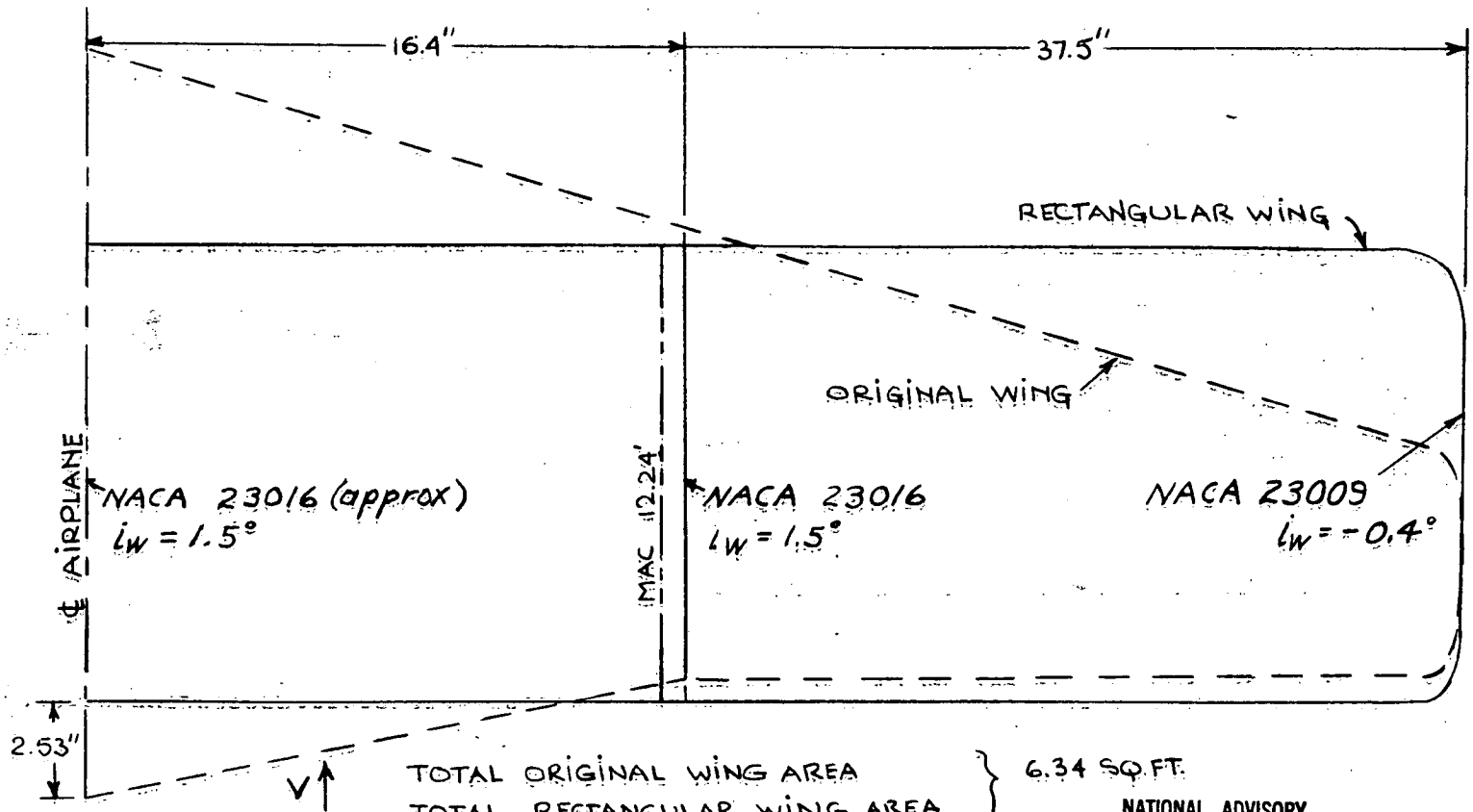

Figure 11a- Left wing panel of 1/8-scale model of XBTC-2 airplane with rectangular planform.

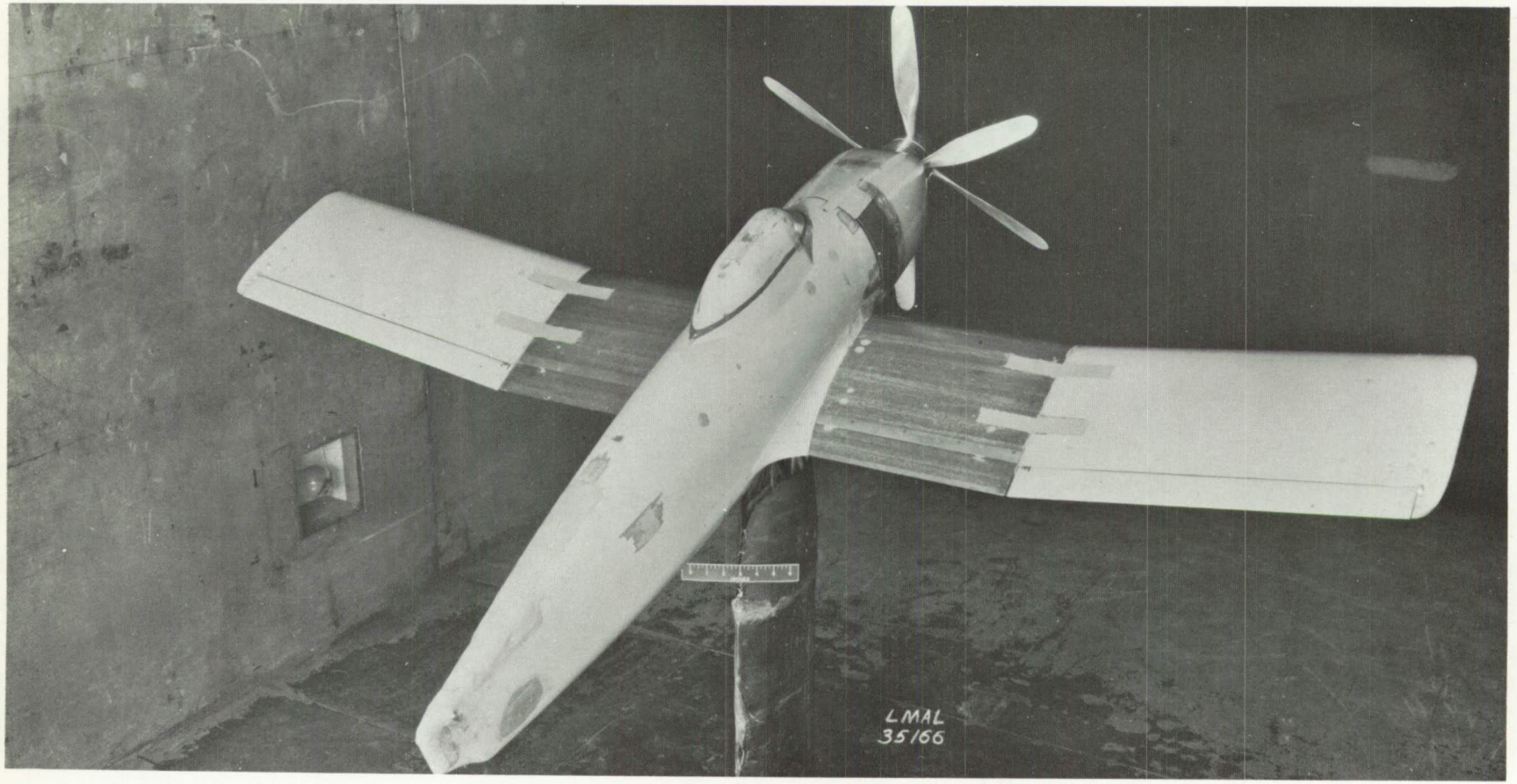

Figure 11(b).- Three-quarter rear view of $\frac{1}{8}$-scale model of the XBTC-2 airplane with rectangular wing.

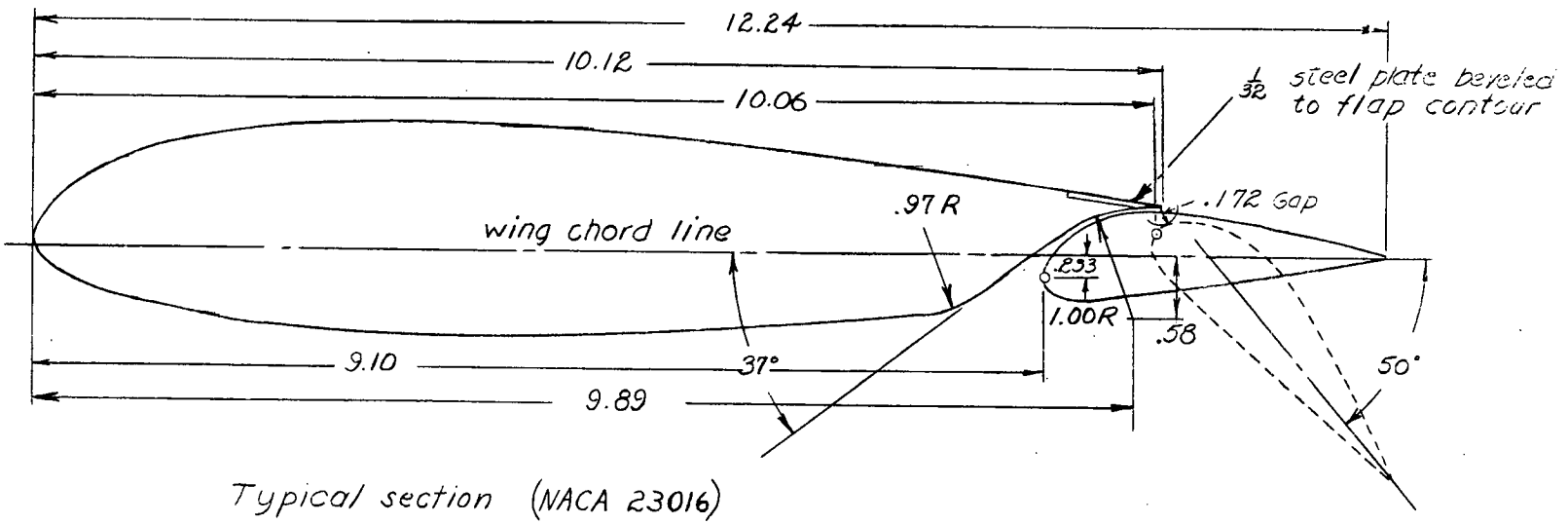

Typical section (NACA 23016)

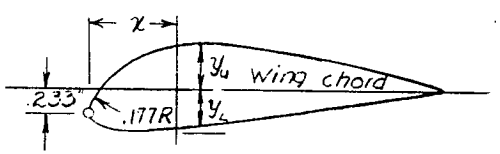

Flap nose section

x	.049	.094	.167	.244	.323	.480	.636	.693	.793	.949	1.105	1.261
y_u	-.073	-.014	.081	.154	.212	.300	.359	—	.401	.417	.409	.388
y_l	.360	.387	.409	.421	.421	—	—	.376	—	—	—	—

All dimensions in inches

NATIONAL ADVISORY COMMITTEE FOR AERONAUTICS

Figure 12 - Details of slotted flap for 1/8 scale model of the XBTC-2 airplane. Rectangular wing

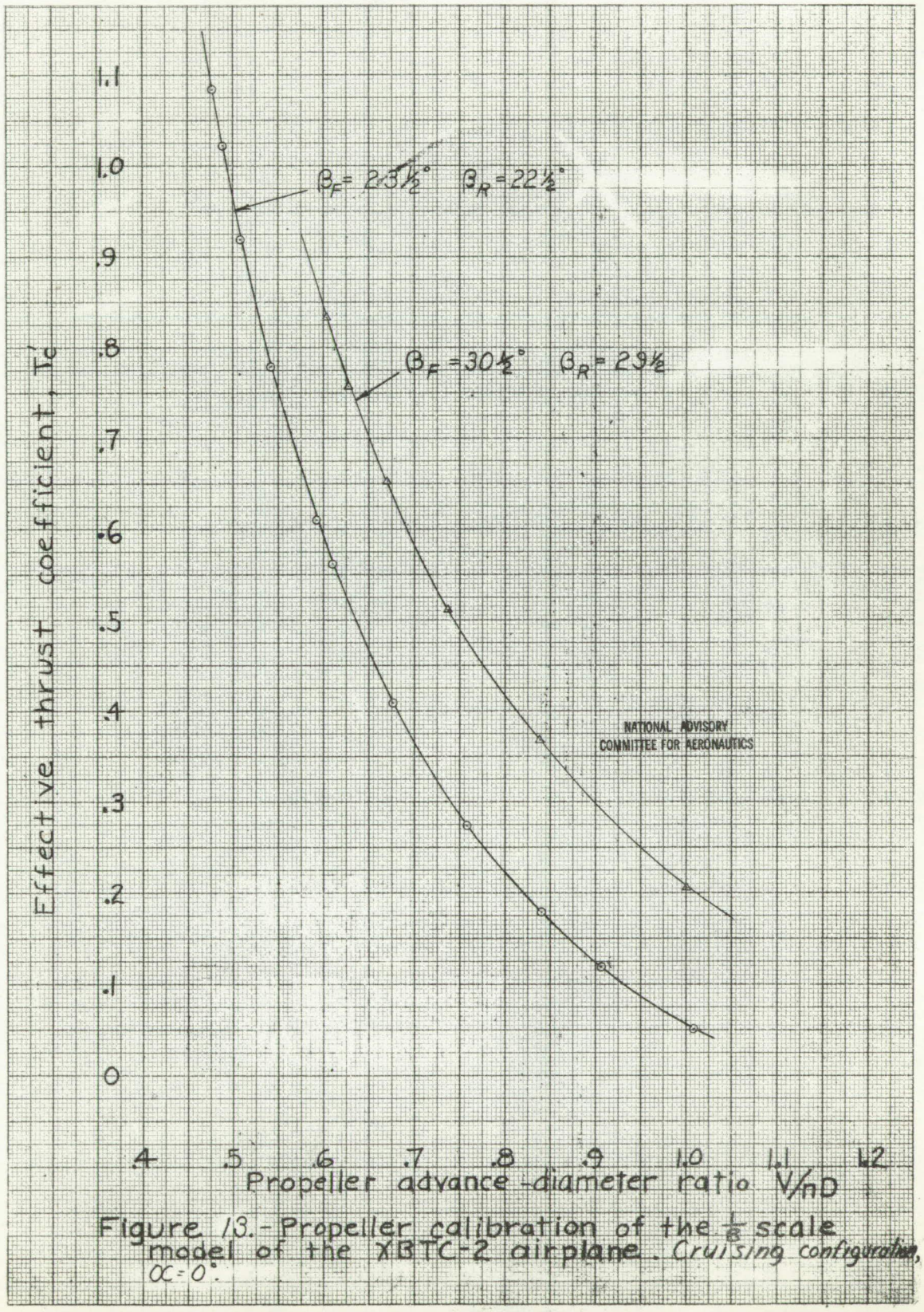

Figure 13.- Propeller calibration of the $\frac{1}{8}$ scale model of the XBTC-2 airplane. Cruising configuration, $\alpha = 0°$.

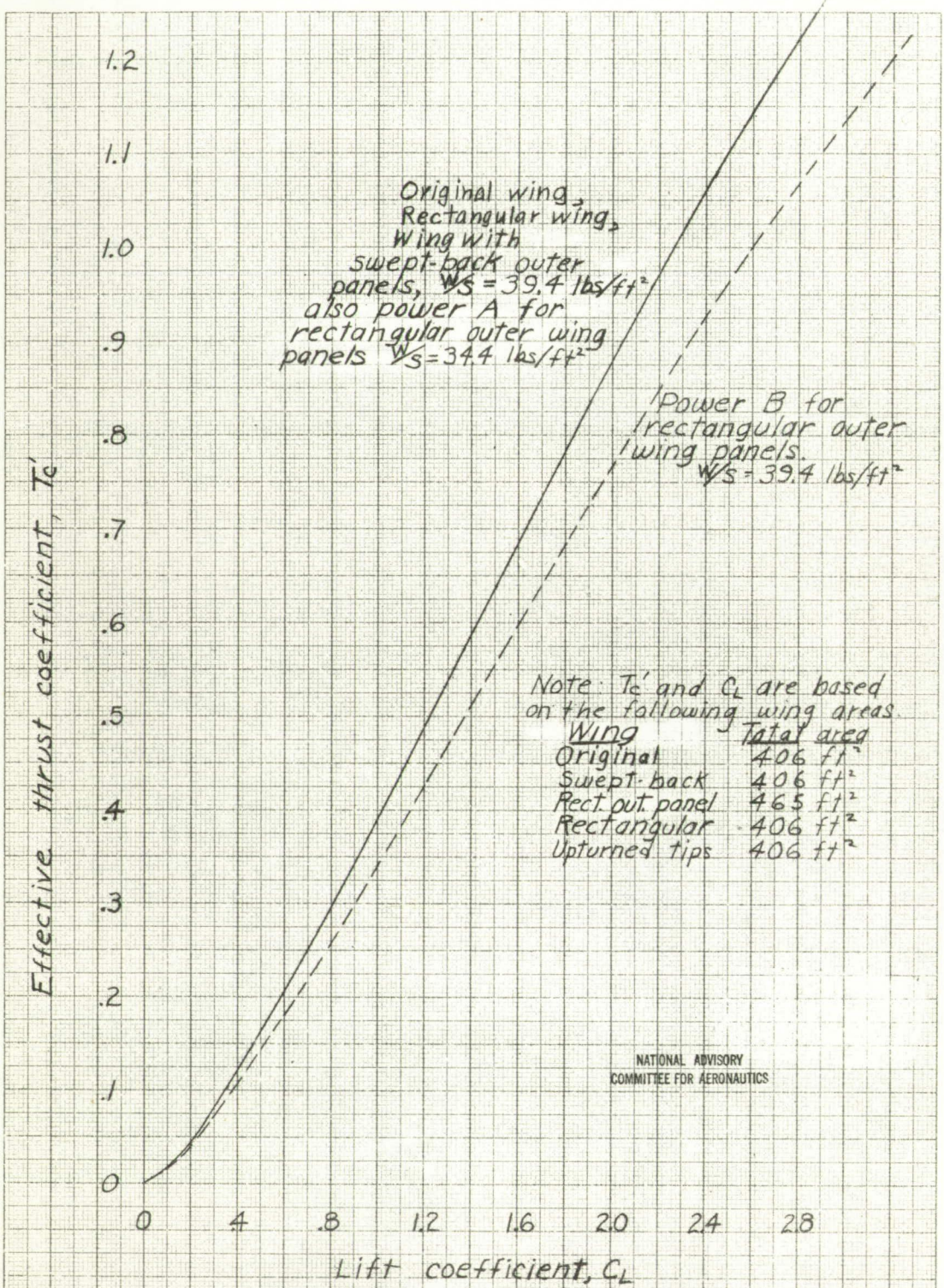

Figure 14.—Variation of effective thrust coefficient with lift coefficient for the XBTC-2 airplane with constant power and a constant speed propeller. Take-off power, 3000 h.p. at 2700 r.p.m. at sea level. Gear ratio 0.39

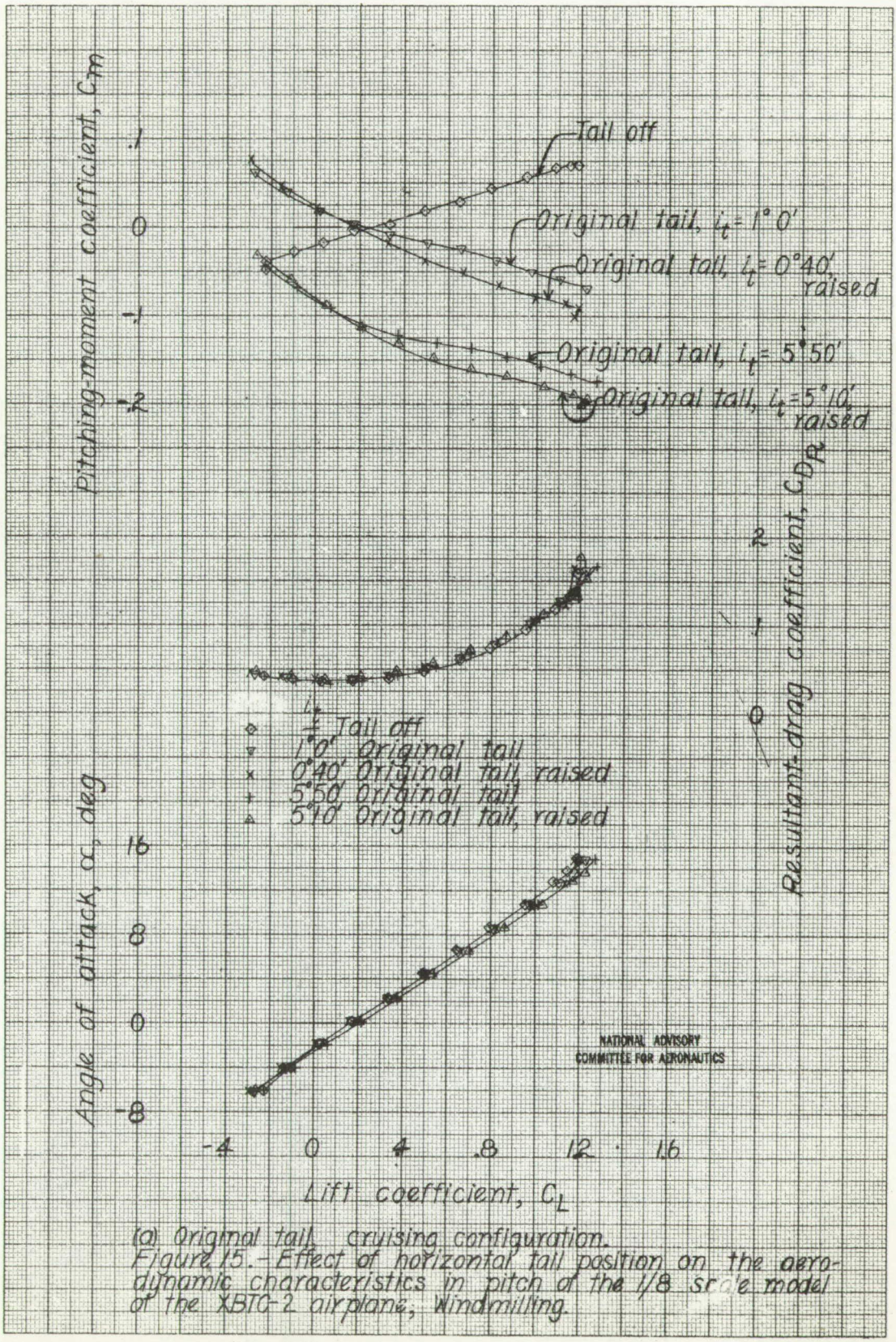

(a) Original tail, cruising configuration.

Figure 15.- Effect of horizontal tail position on the aerodynamic characteristics in pitch of the 1/8 scale model of the XBTC-2 airplane, windmilling.

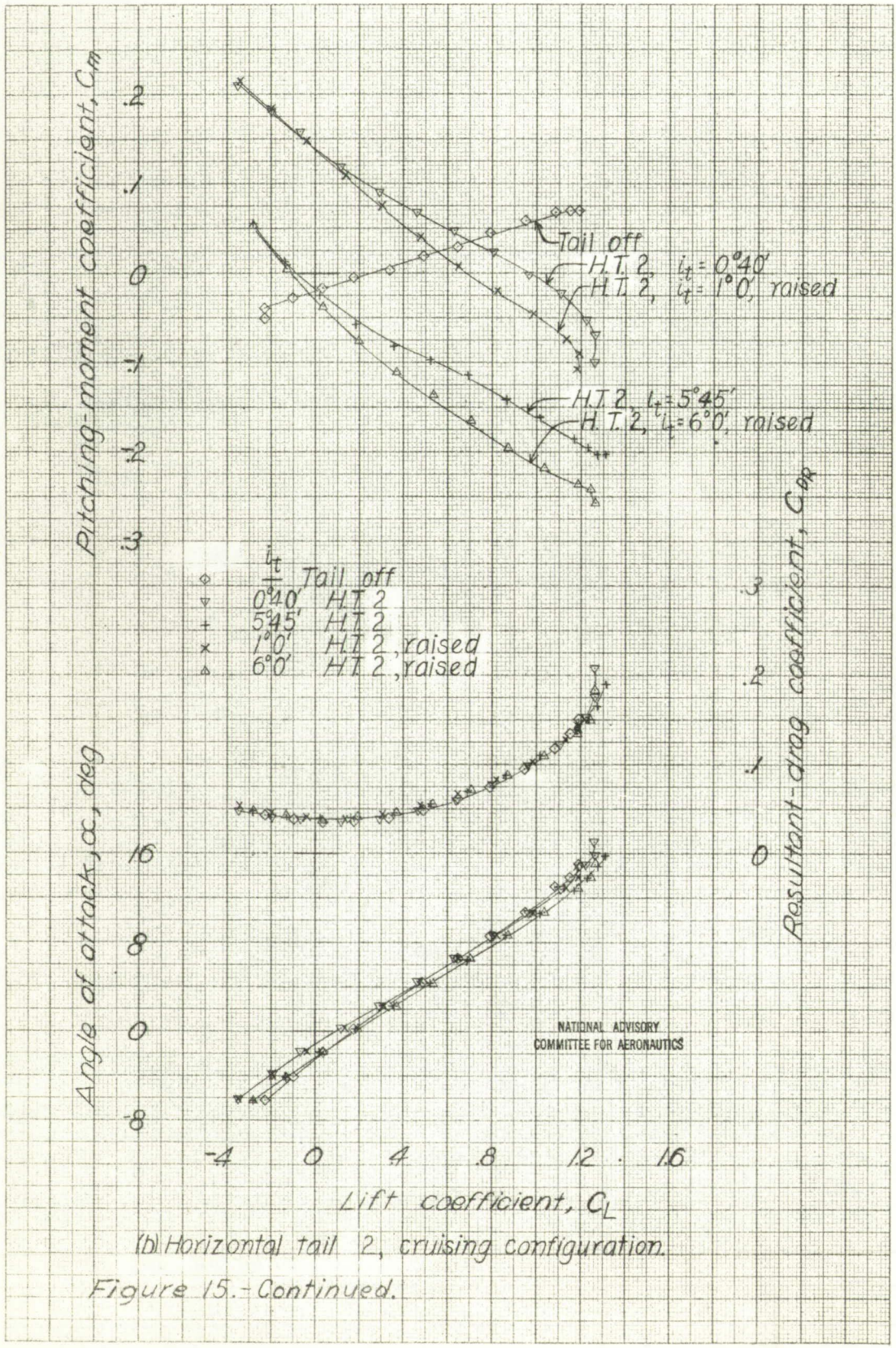

(b) Horizontal tail 2, cruising configuration.

Figure 15.- Continued.

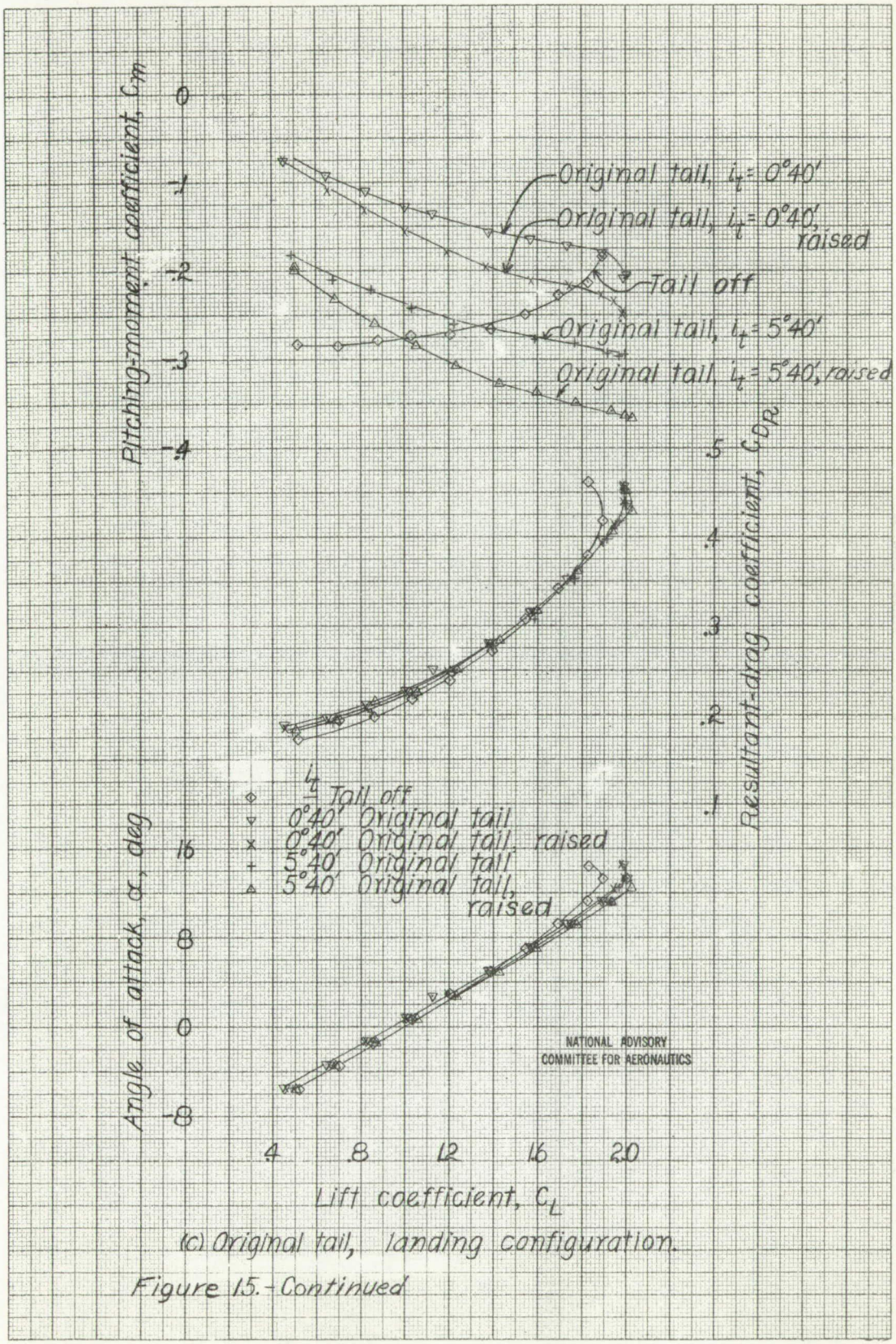

(c) Original tail, landing configuration.

Figure 15.- Continued

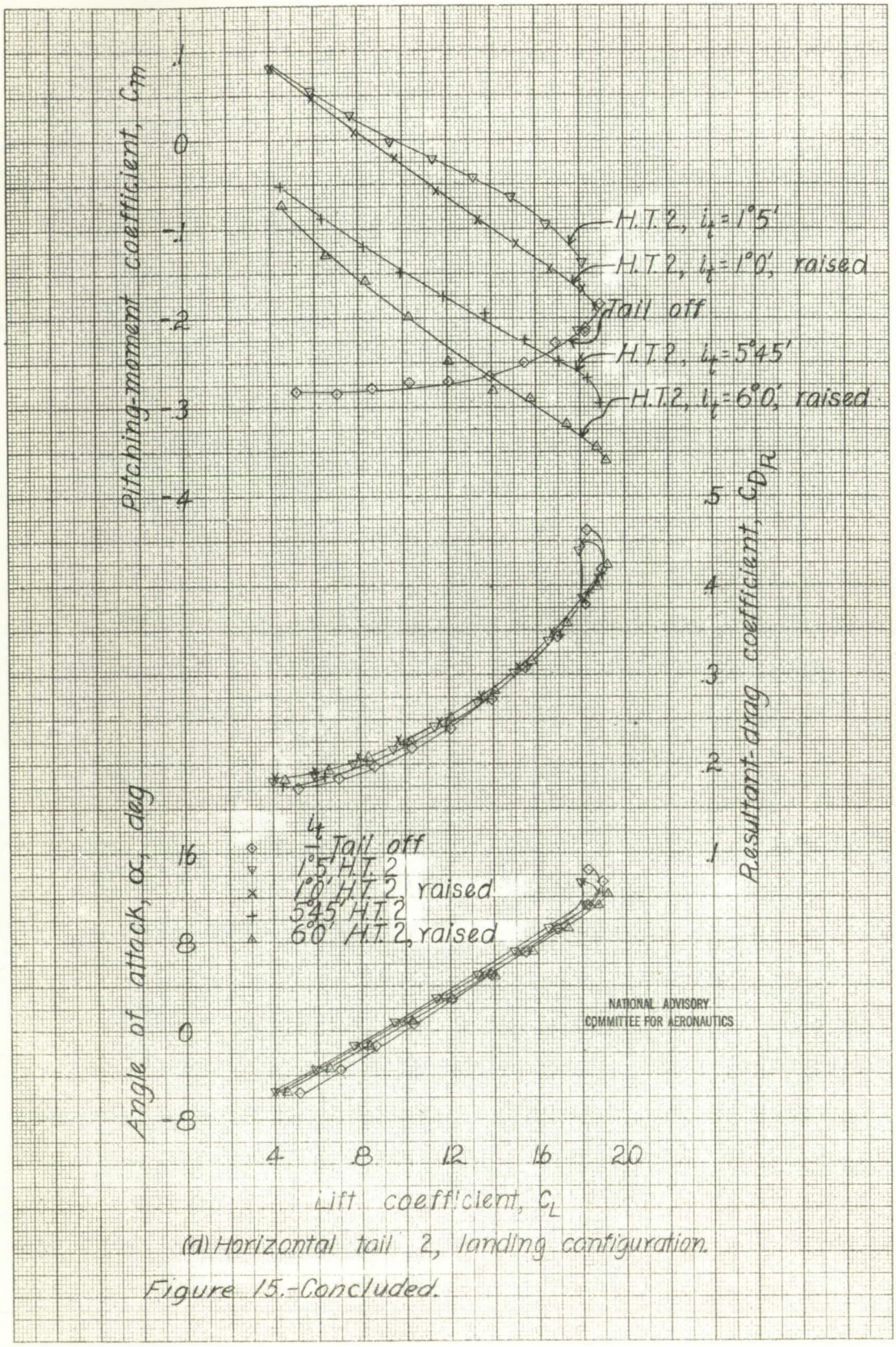

(d) Horizontal tail 2, landing configuration.

Figure 15.-Concluded.

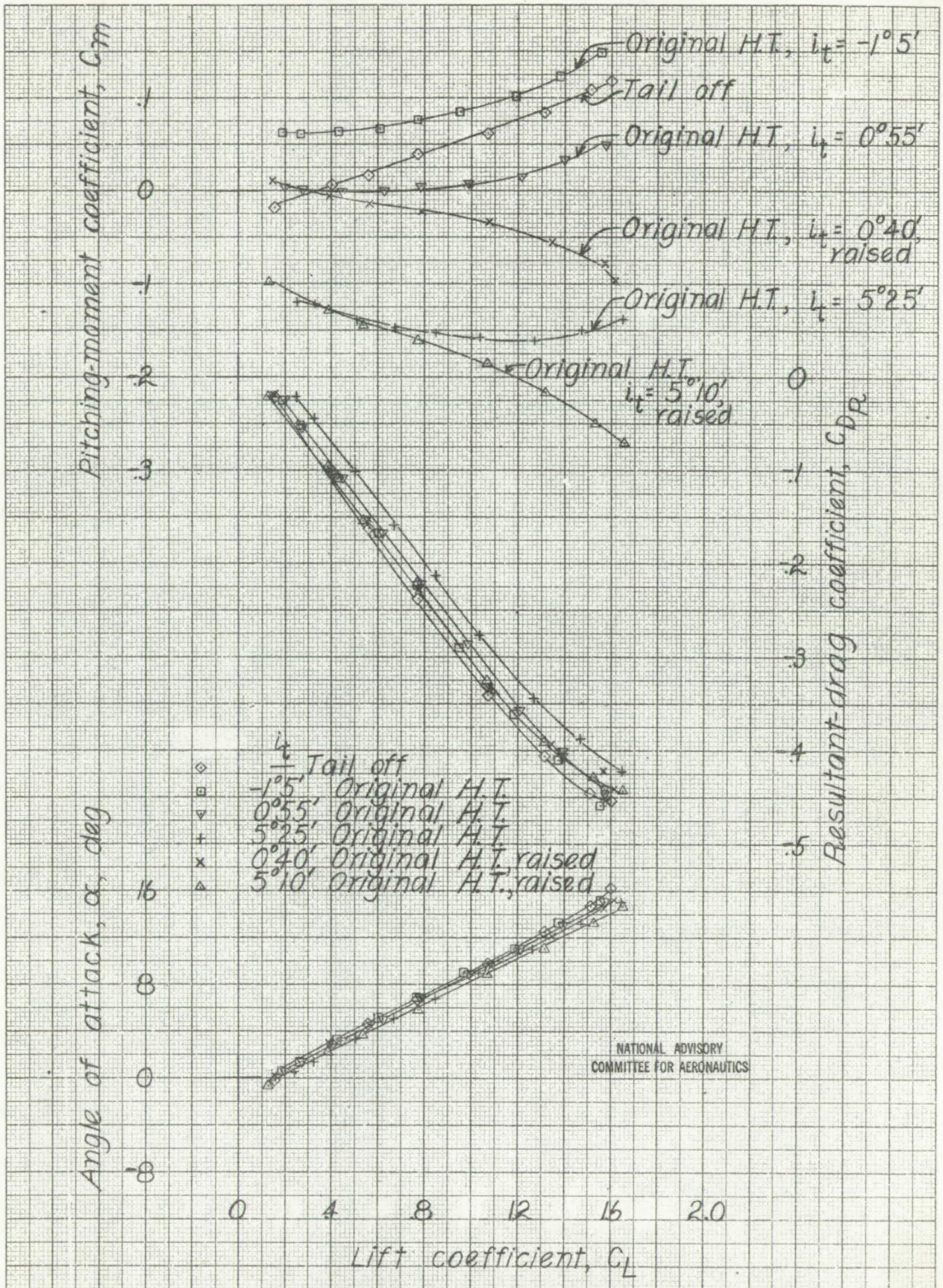

(a) Original tail, cruising configuration.

Figure 16.-Effect of horizontal tail position on the aerodynamic characteristics in pitch of the 1/8 scale model of the XBTC-2 airplane. Take-off power.

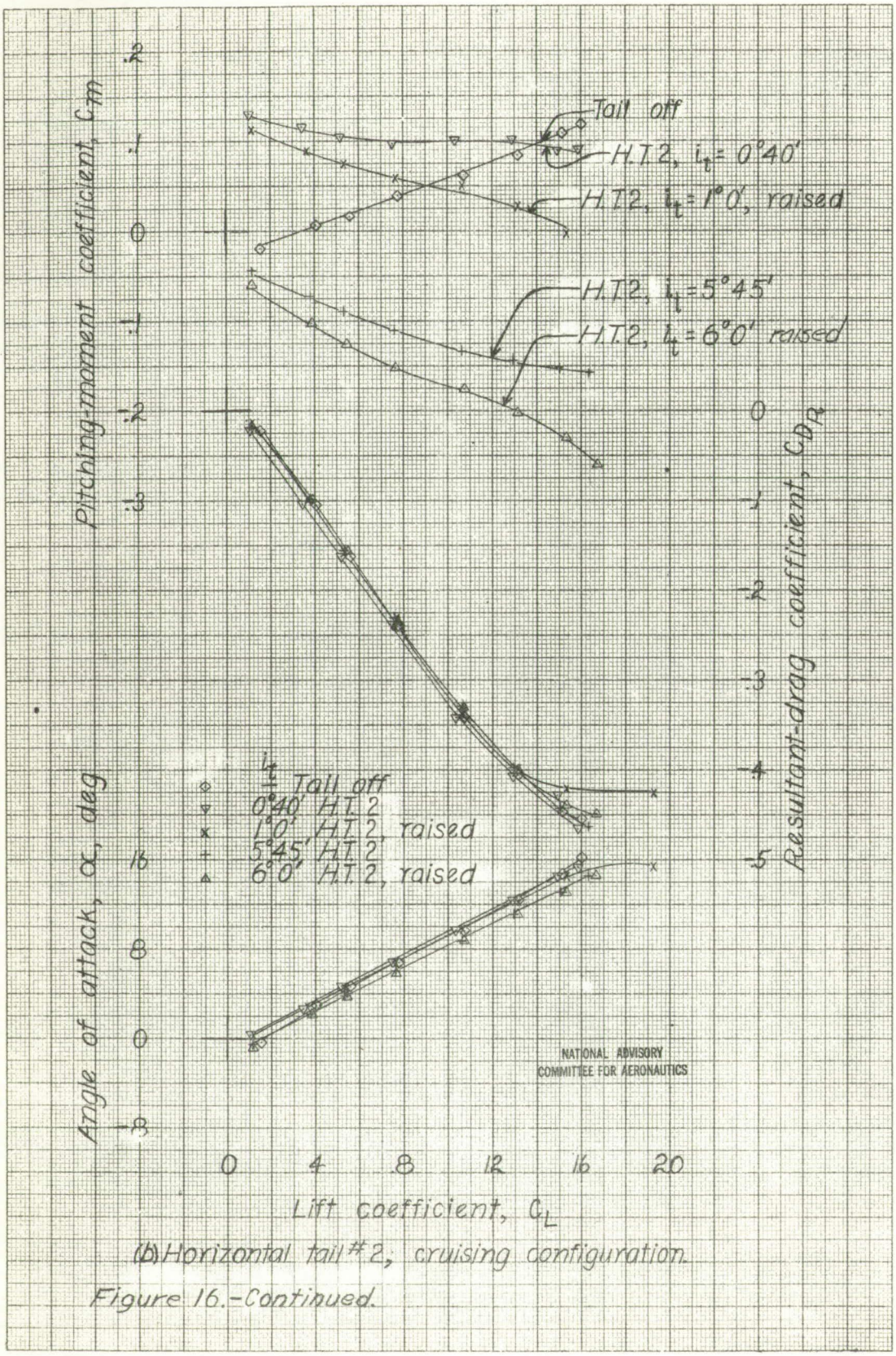

(b) Horizontal tail #2, cruising configuration.

Figure 16.-Continued.

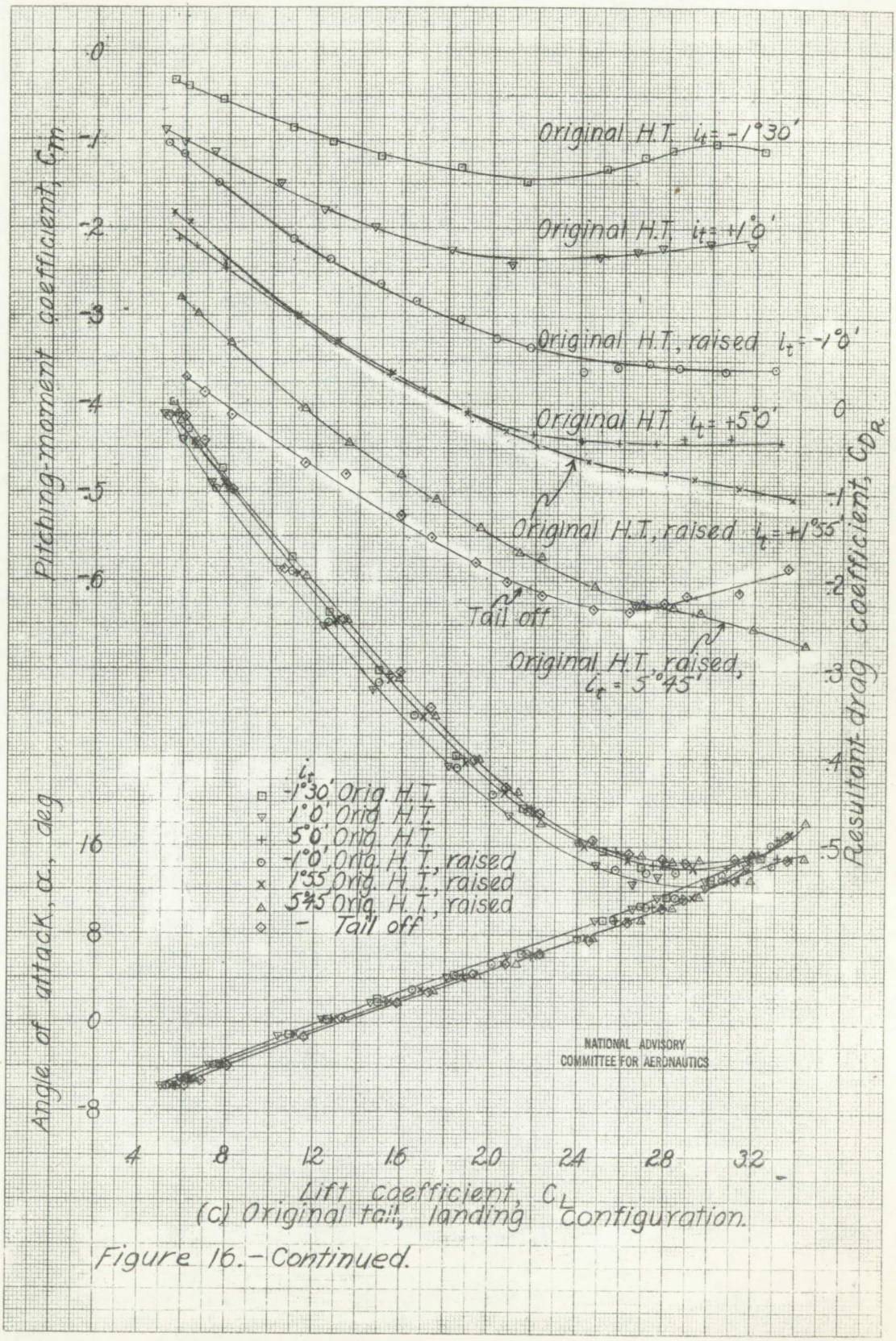

(c) Original tail, landing configuration.

Figure 16.– Continued.

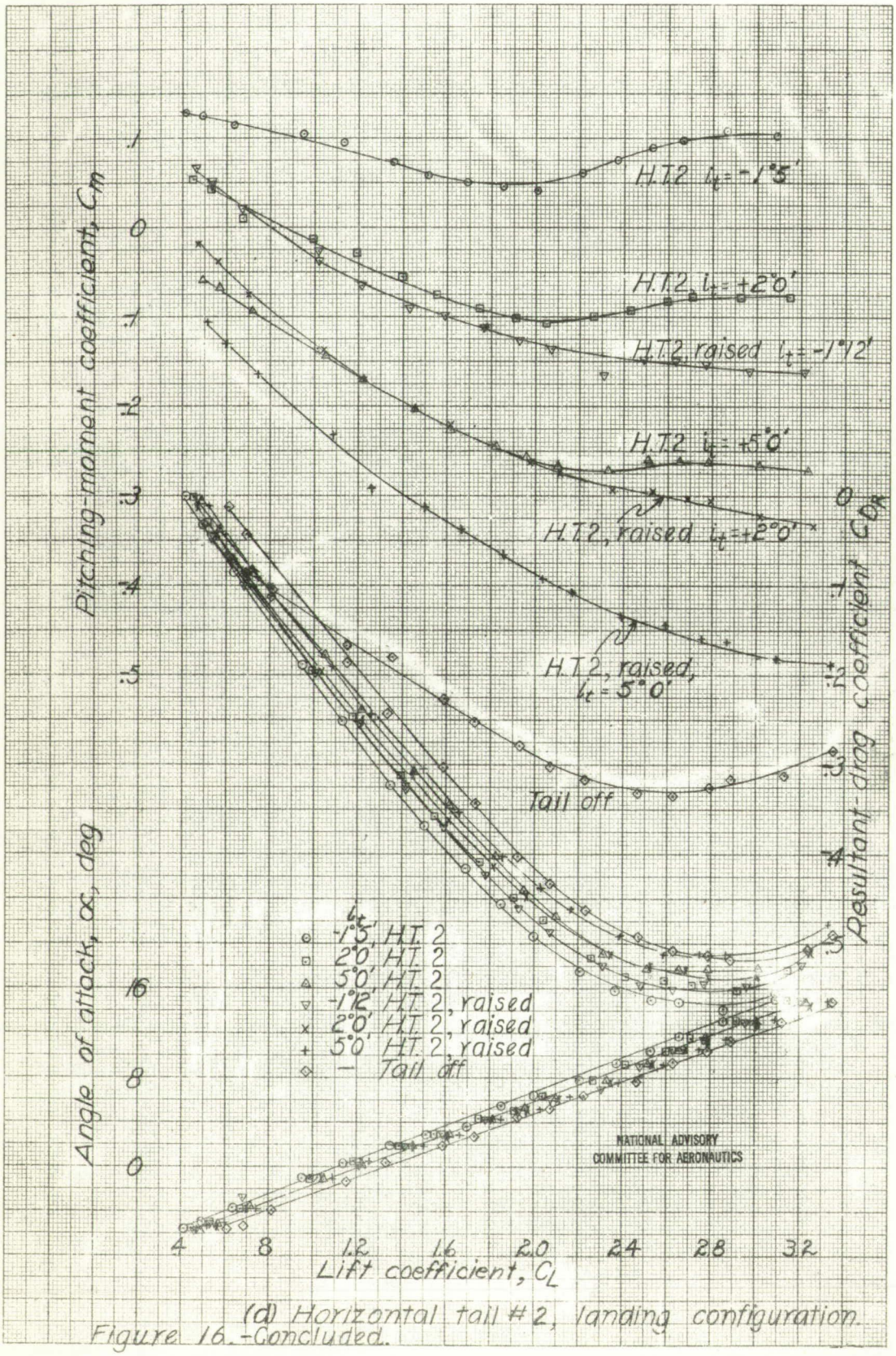

(d) Horizontal tail #2, landing configuration.

Figure 16.-Concluded.

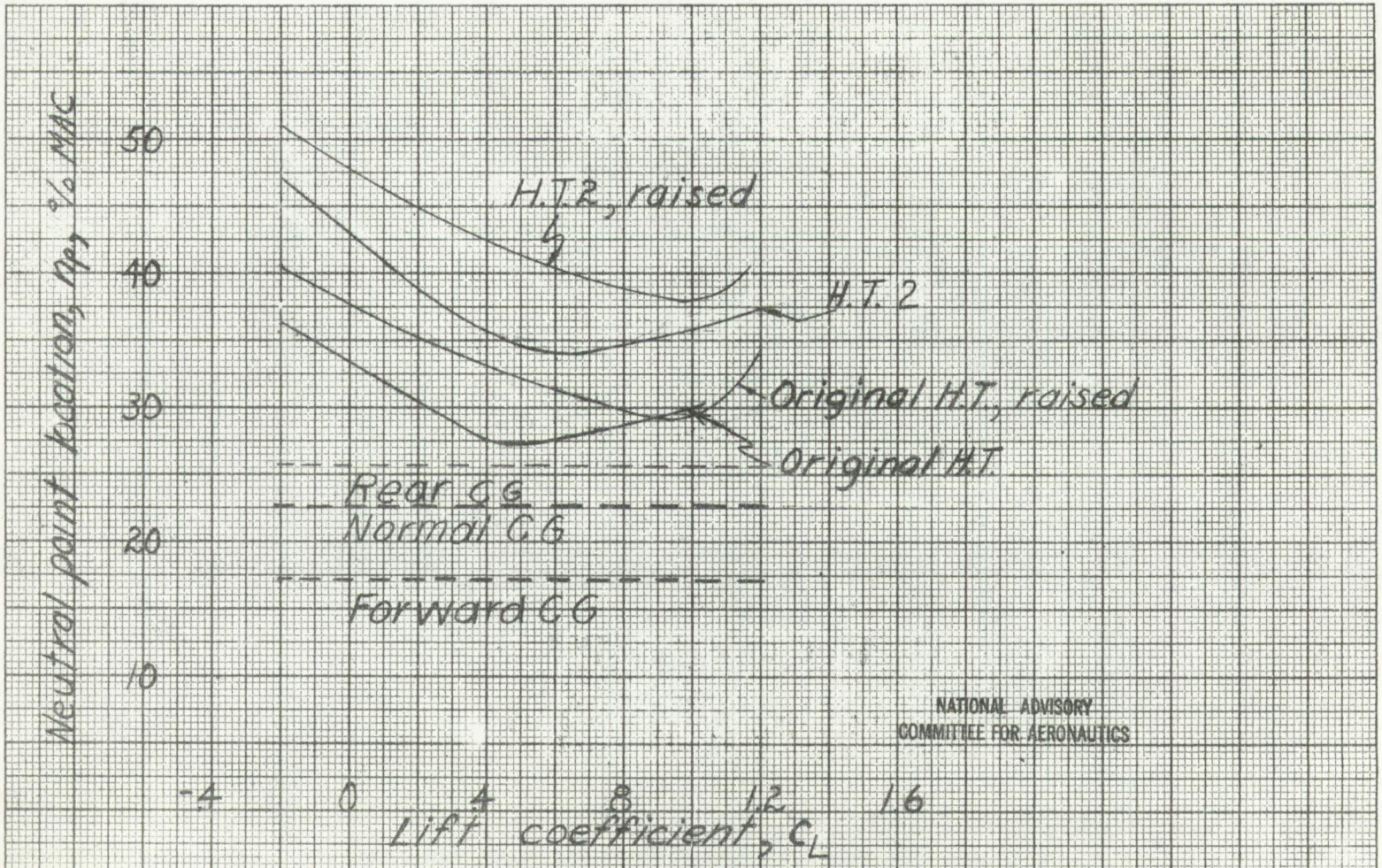

(a) Cruising configuration.

Figure 17.- Effect of horizontal tail configuration on the location of neutral points of the XBTC-2 airplane. Windmilling.

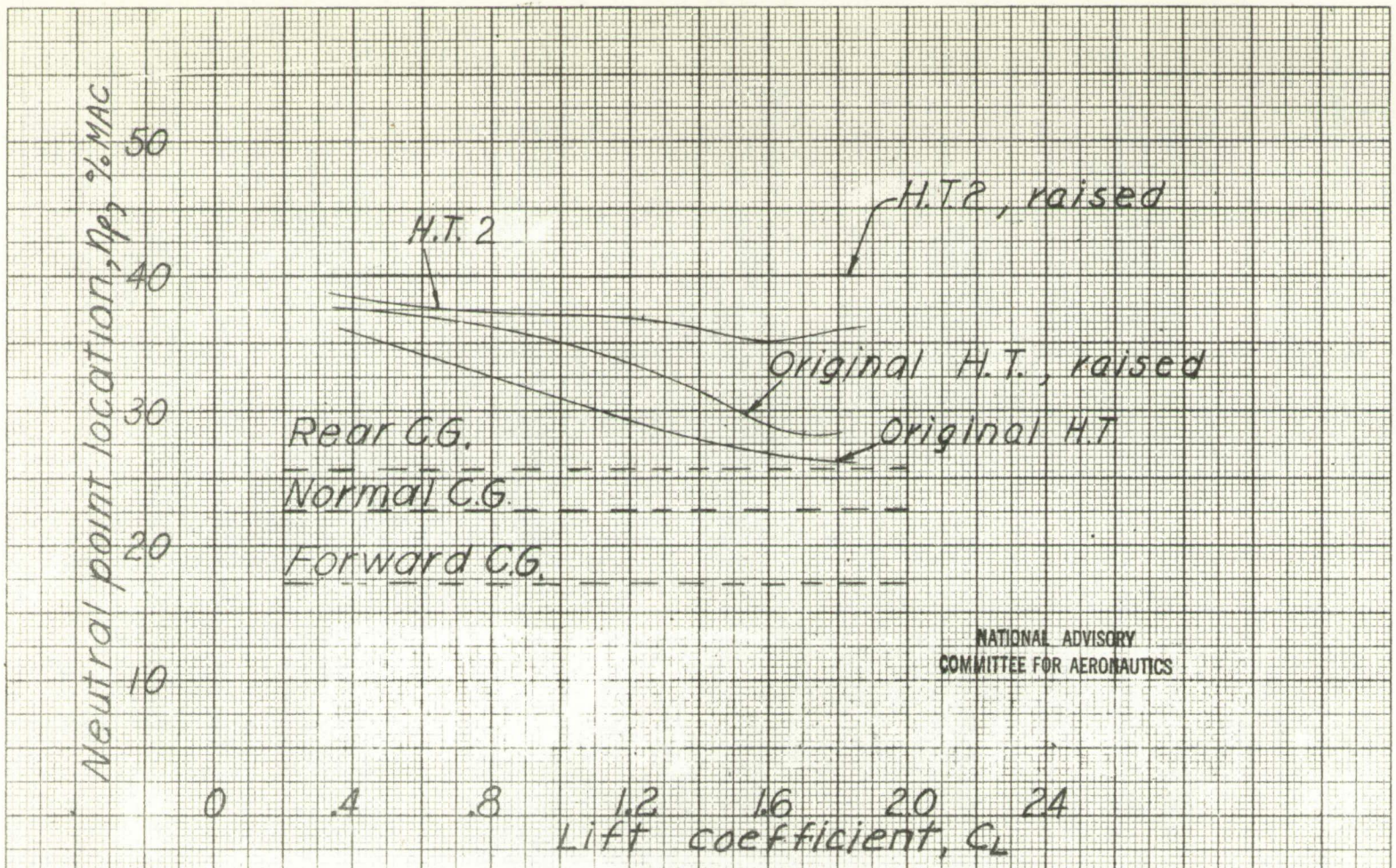

(b) Landing configuration

Figure 17.- Concluded.

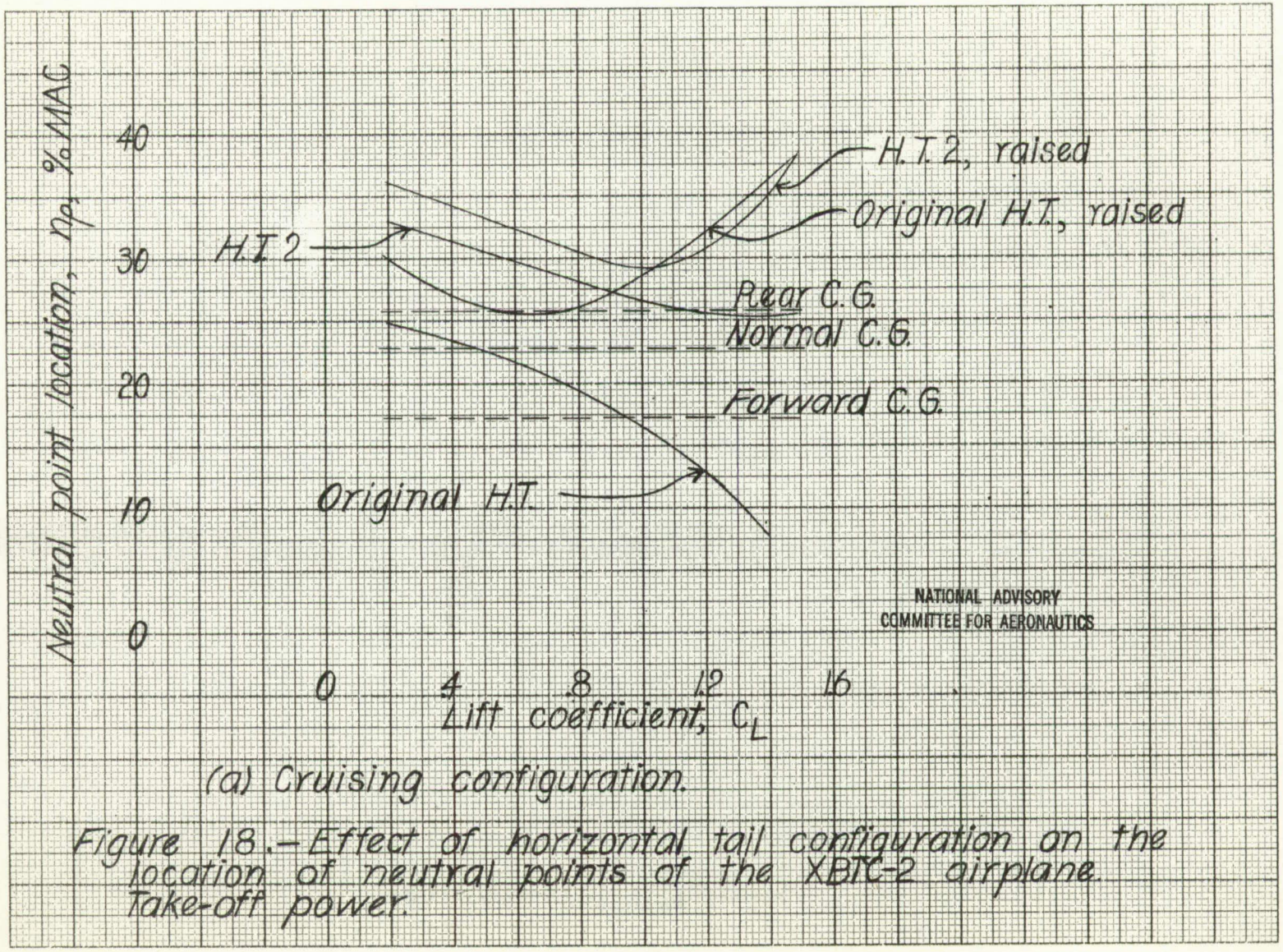

(a) Cruising configuration.

Figure 18.- Effect of horizontal tail configuration on the location of neutral points of the XBTC-2 airplane. Take-off power.

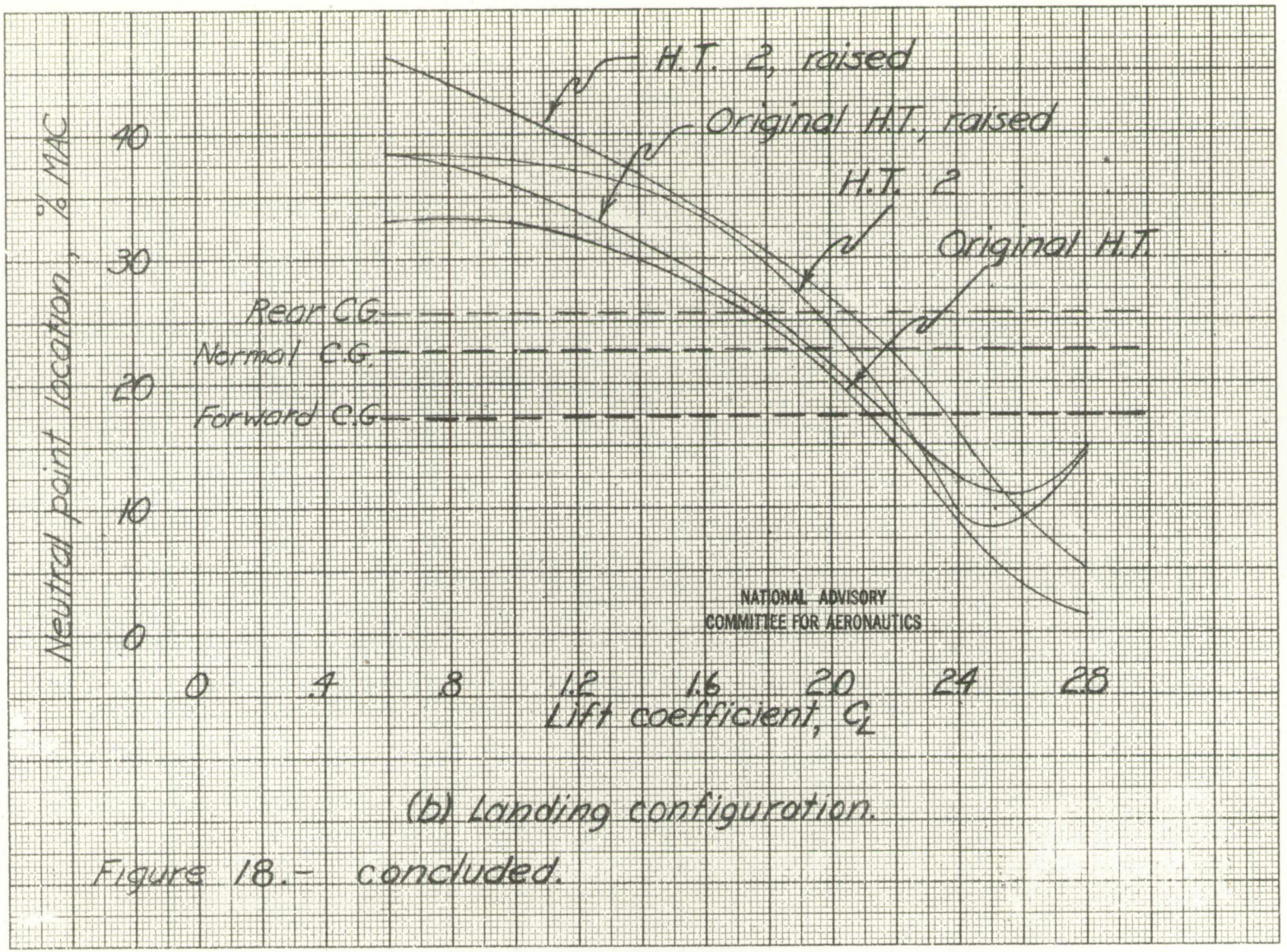

(b) Landing configuration.

Figure 18.- concluded.

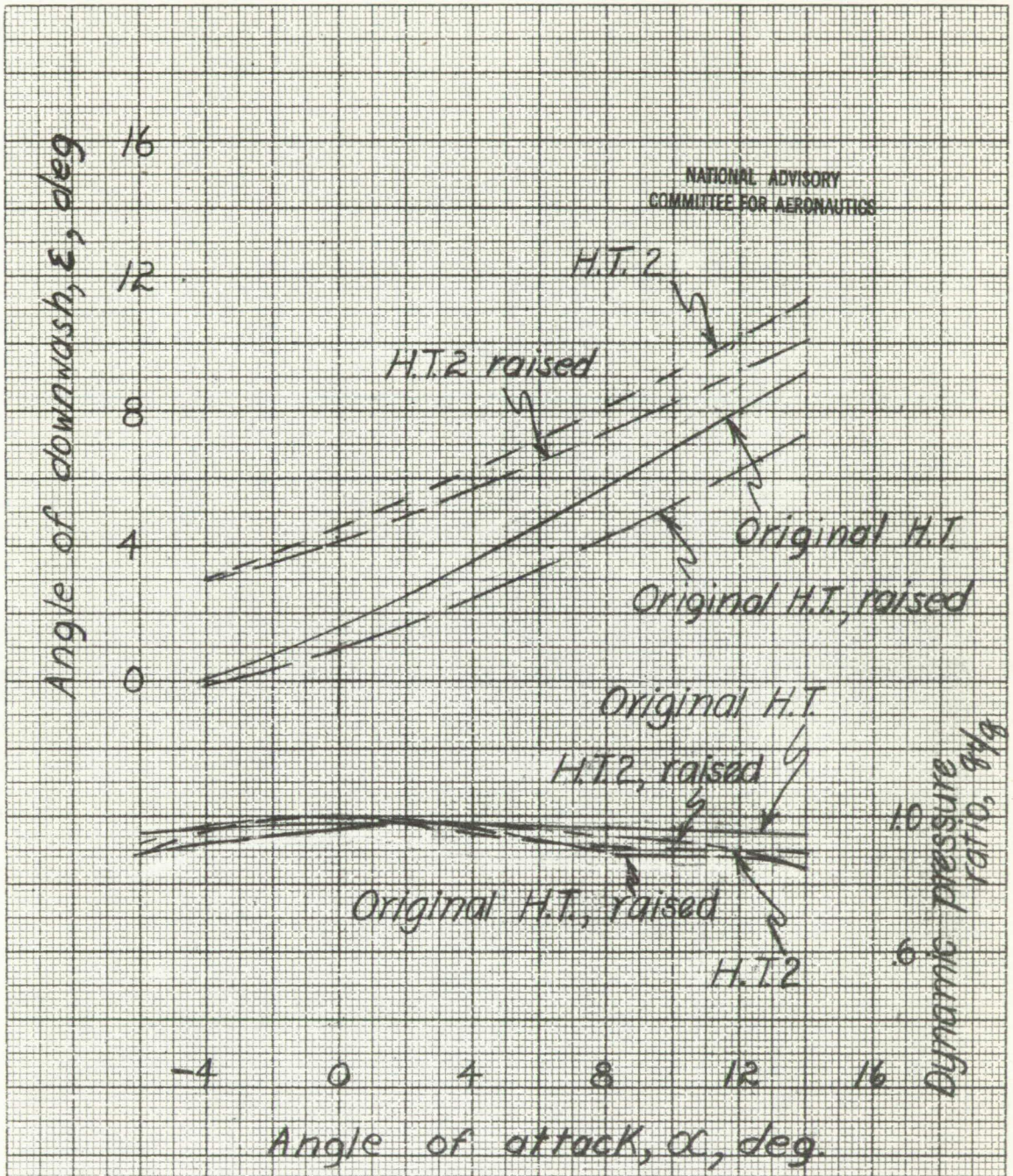

(a) Cruising configuration.

Figure 19.- Effect of horizontal tail configuration on the average downwash angles and dynamic pressure ratios at the tail of the 1/8 scale model of XBTC-2 airplane. Windmilling

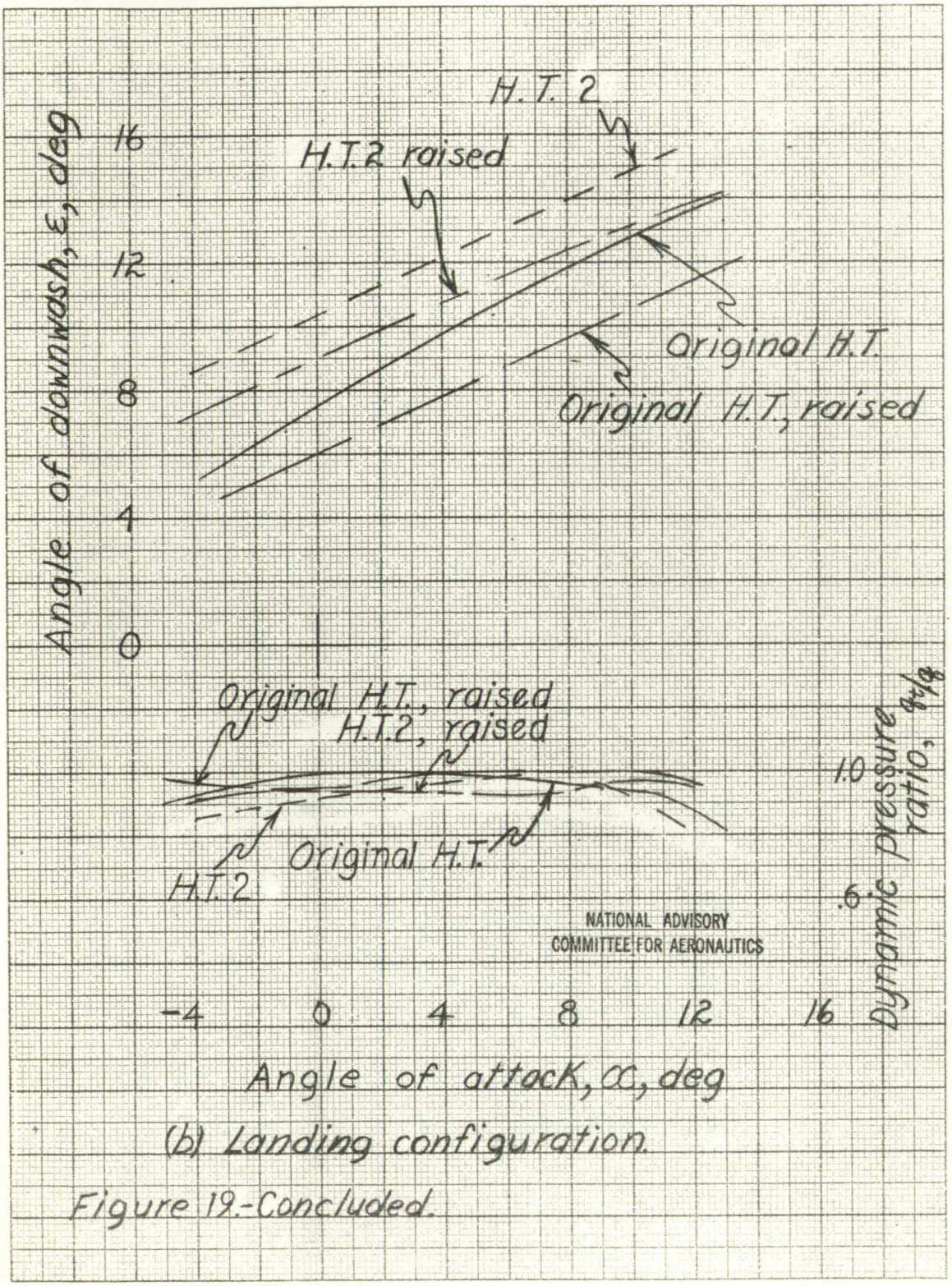

(b) Landing configuration.

Figure 19.-Concluded.

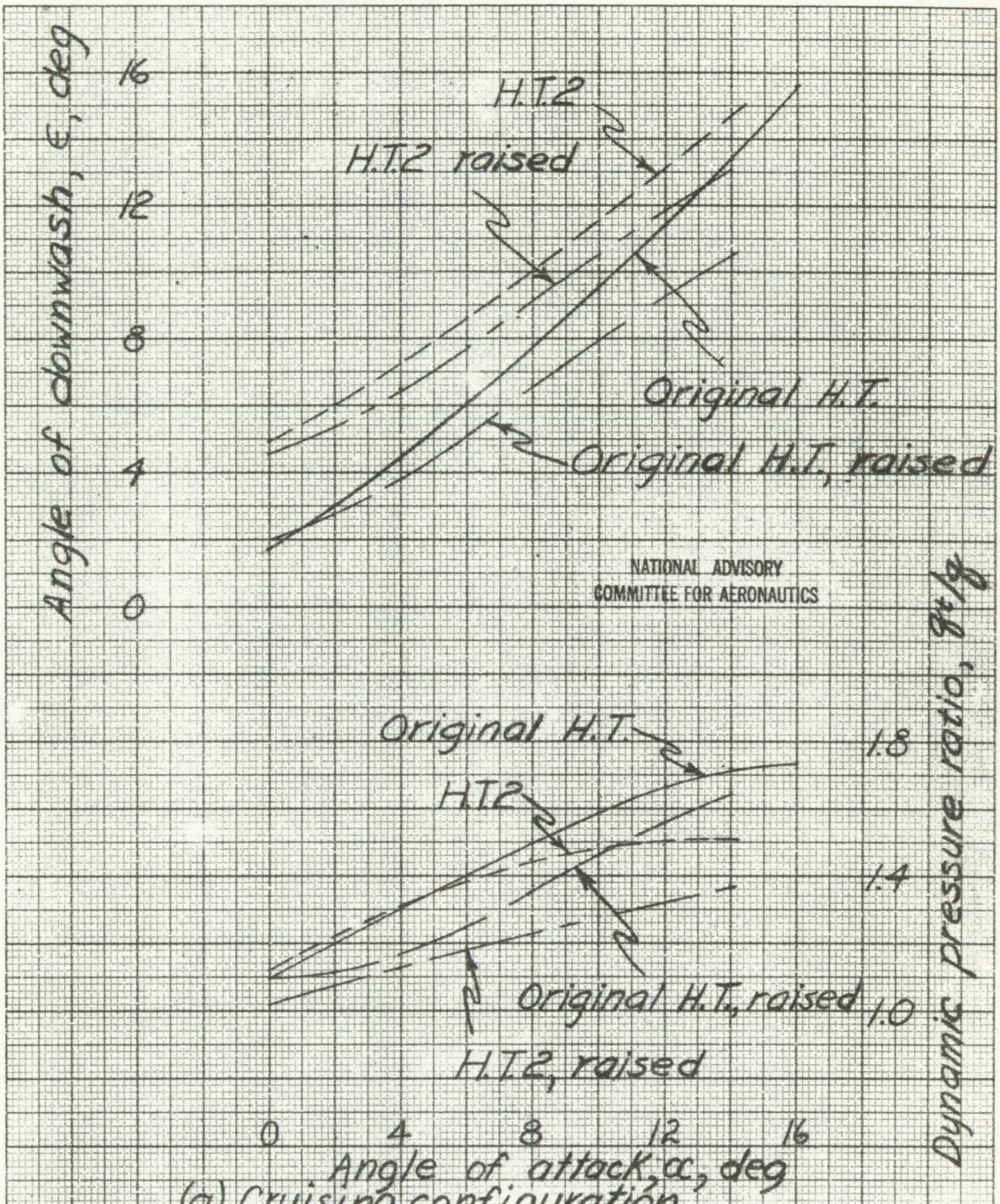

Figure 20.- Effect of horizontal tail configuration on the average downwash angles and dynamic pressure ratios at tail of 1/8 scale model of XBTC-2 airplane. Take-off power.

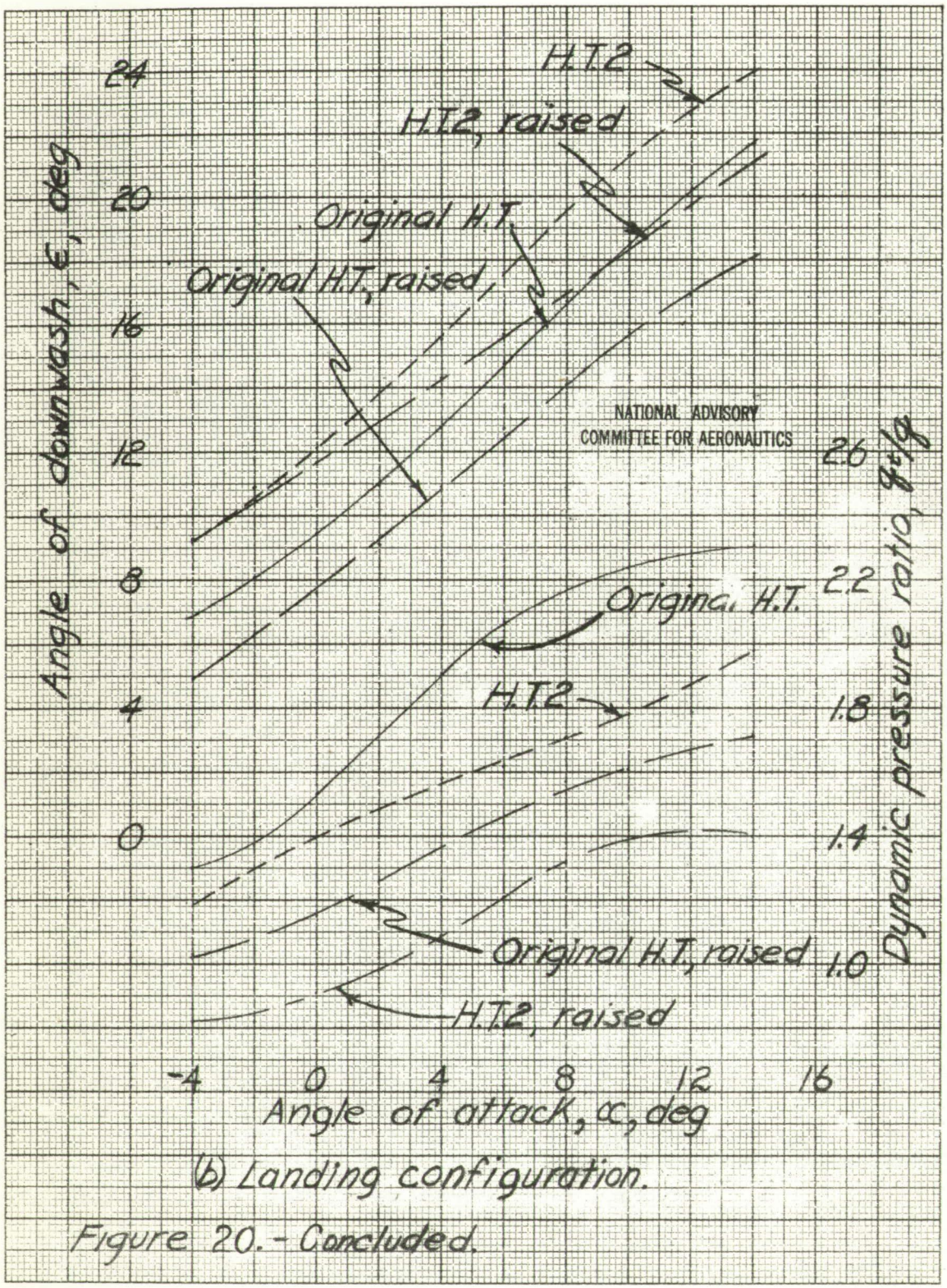

(b) Landing configuration.

Figure 20.- Concluded.

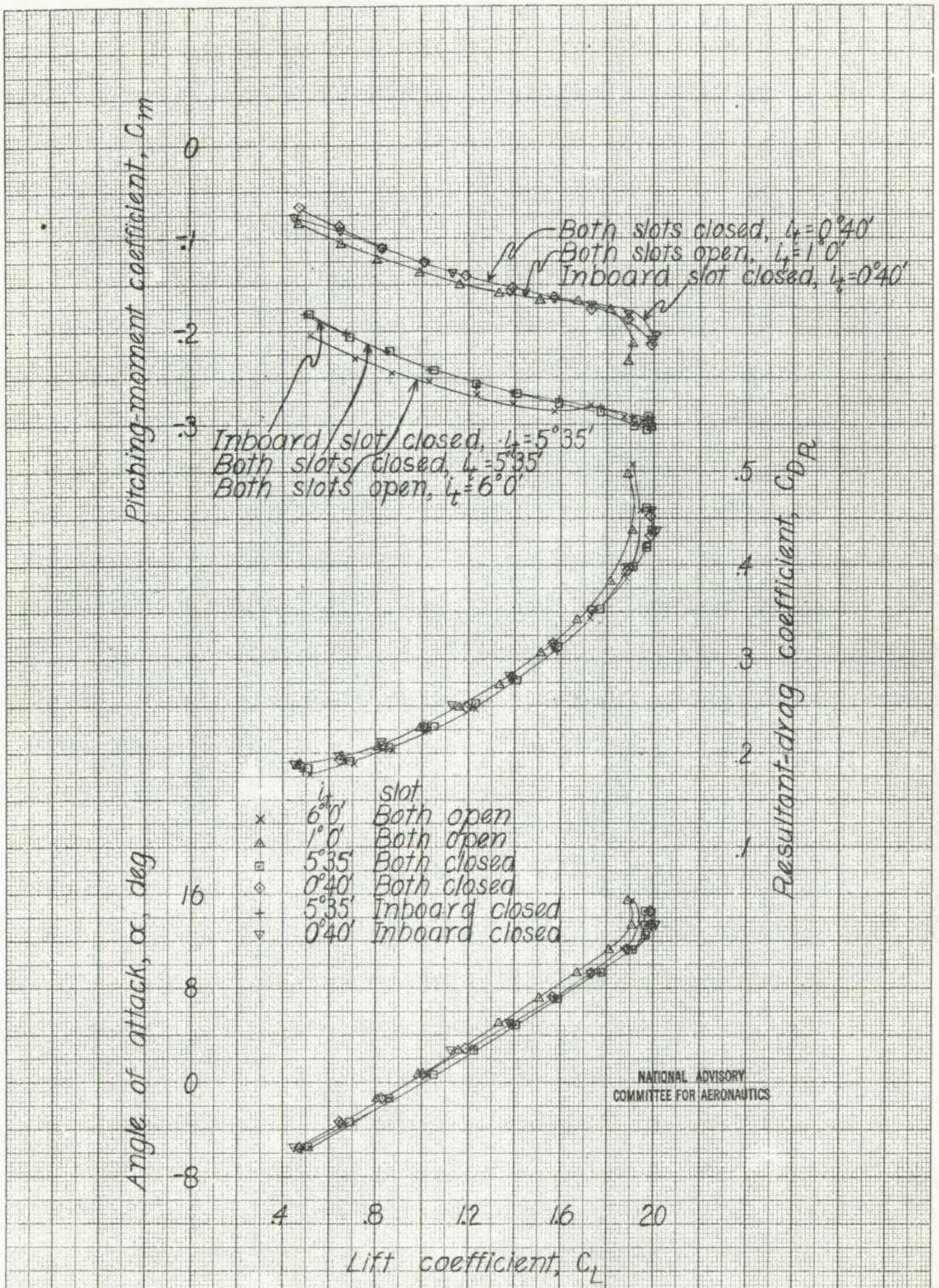

(a) Original tail.

Figure 21.-Effect of Handley-Page slot configuration on the aerodynamic characteristics in pitch of the 1/8 scale model of the XBTC-2 airplane. Landing configuration; windmilling.

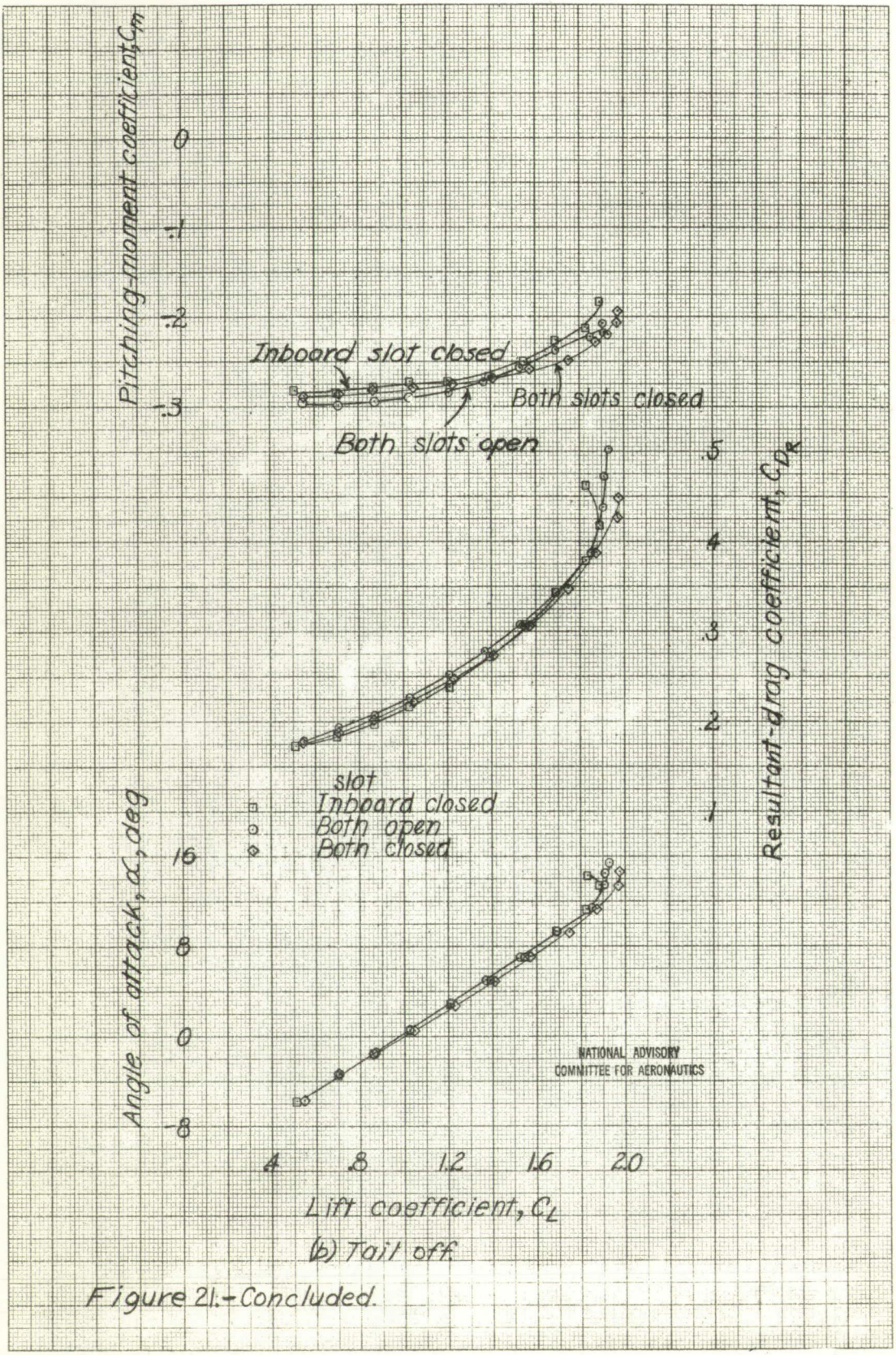

(b) Tail off.

Figure 21.- Concluded.

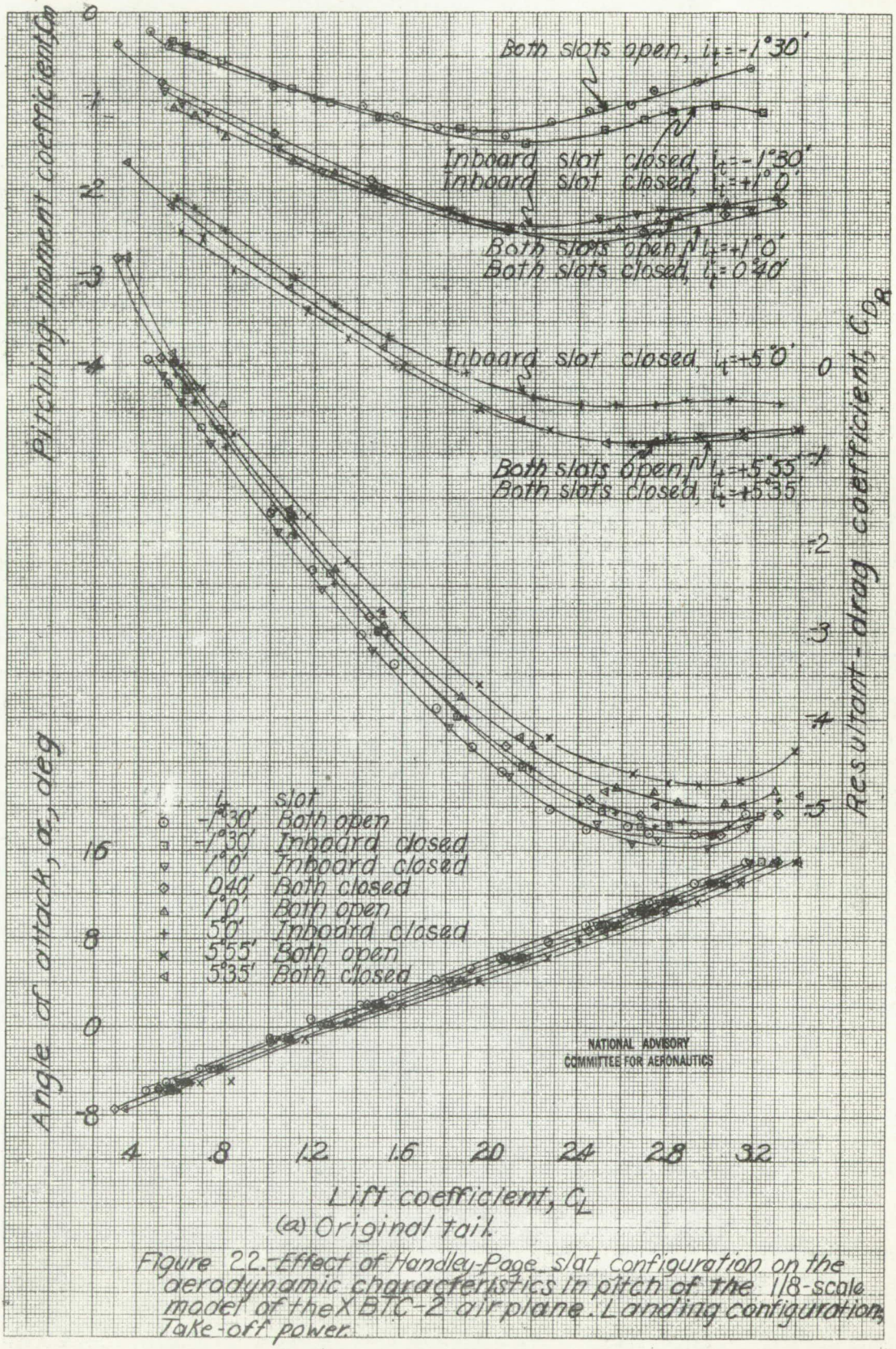

(a) Original tail.

Figure 22.-Effect of Handley-Page slat configuration on the aerodynamic characteristics in pitch of the 1/8-scale model of the XBTC-2 airplane. Landing configuration, Take-off power.

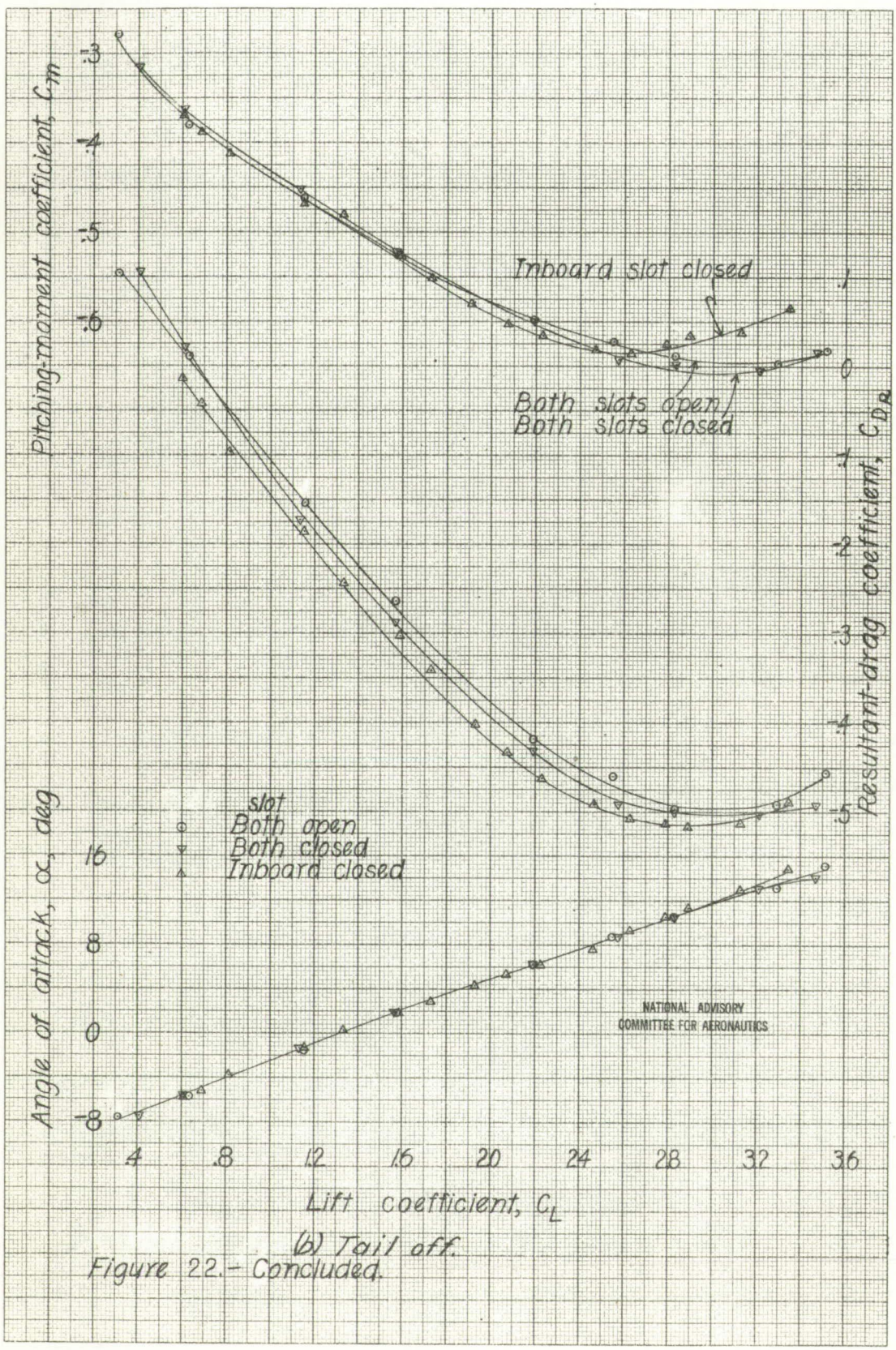

(b) Tail off.

Figure 22.- Concluded.

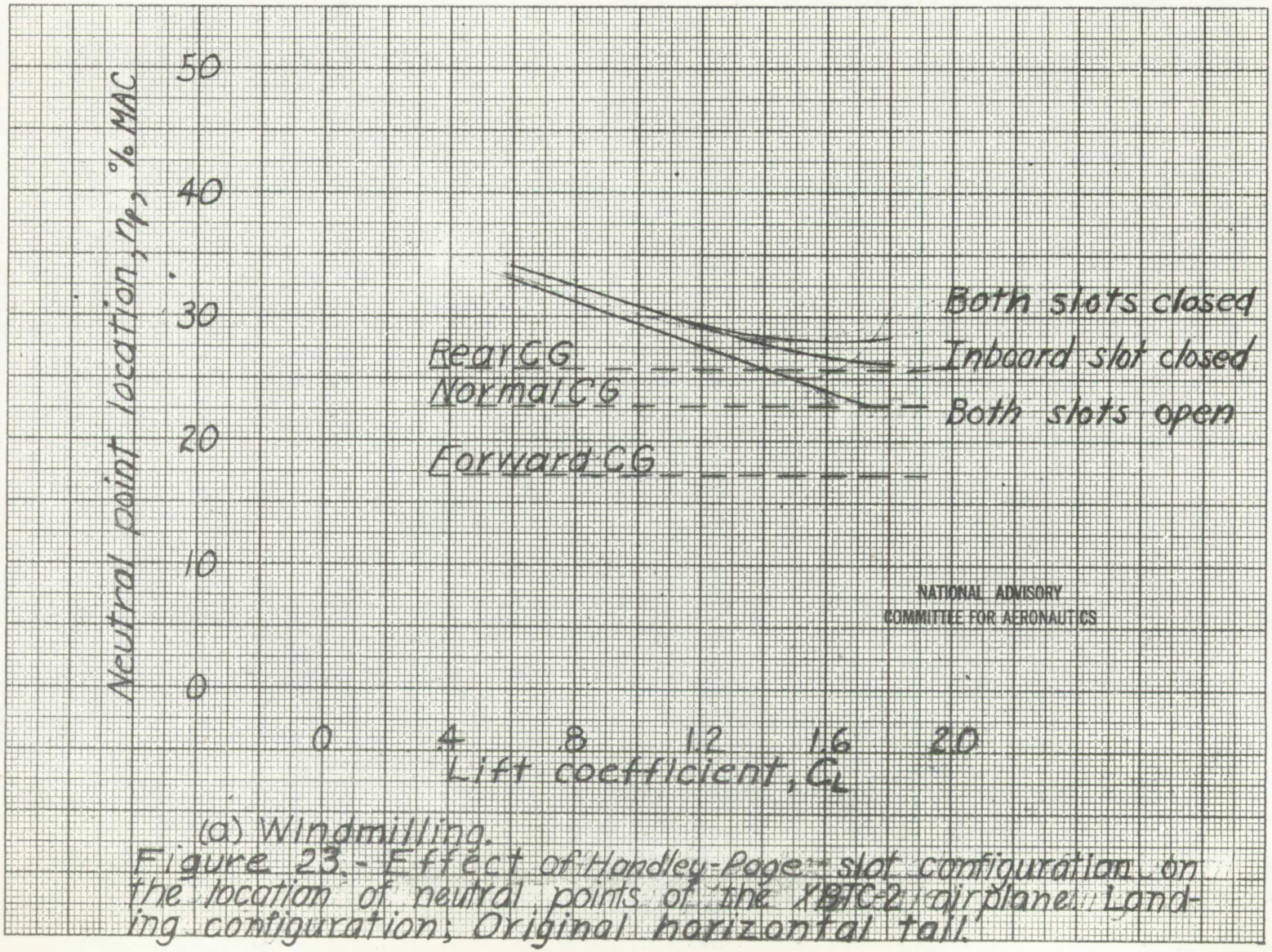

(a) Windmilling.

Figure 23.- Effect of Handley-Page slot configuration on the location of neutral points of the XBTC-2 airplane. Landing configuration; Original horizontal tail.

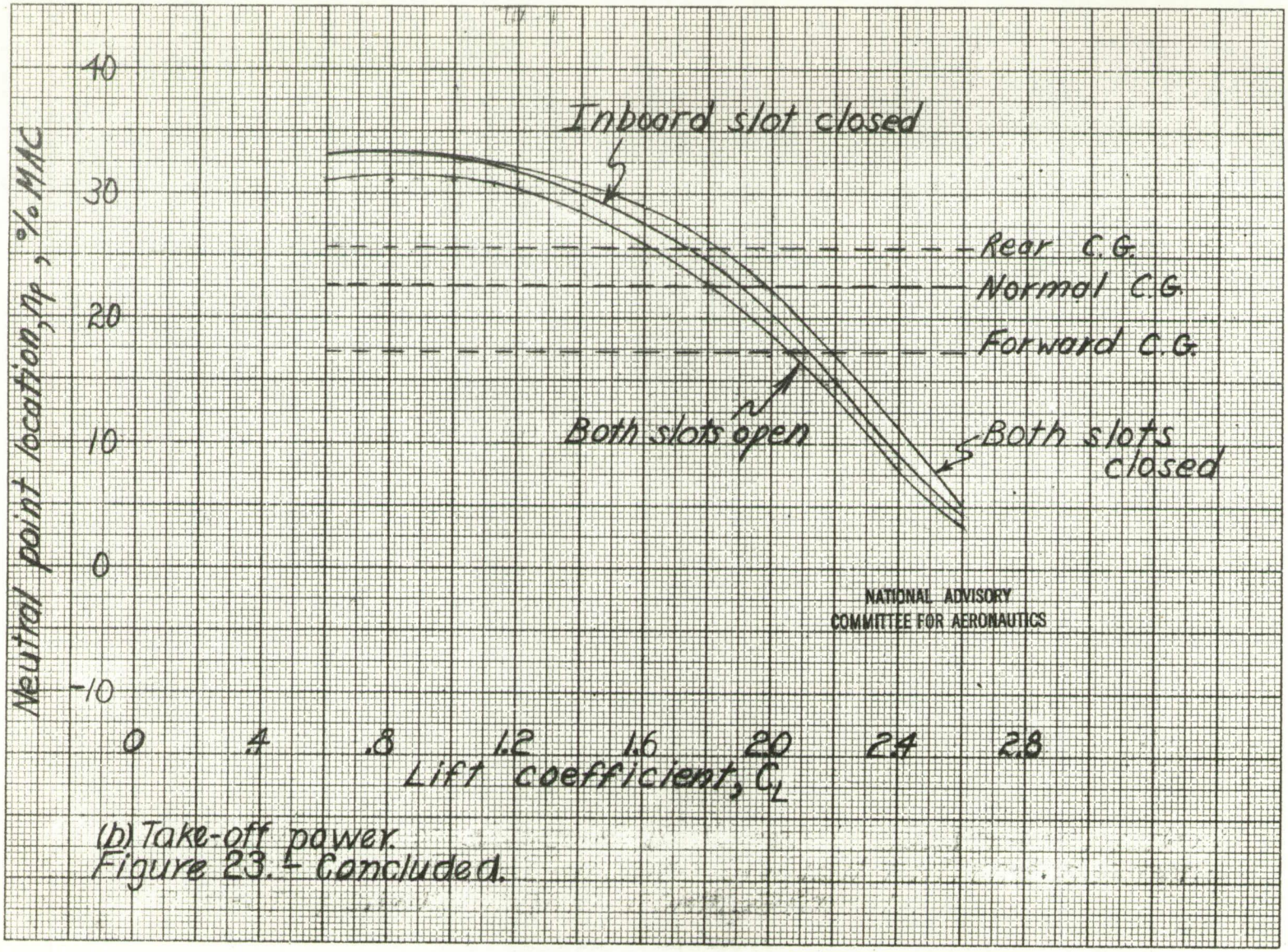

(b) Take-off power.

Figure 23.- Concluded.

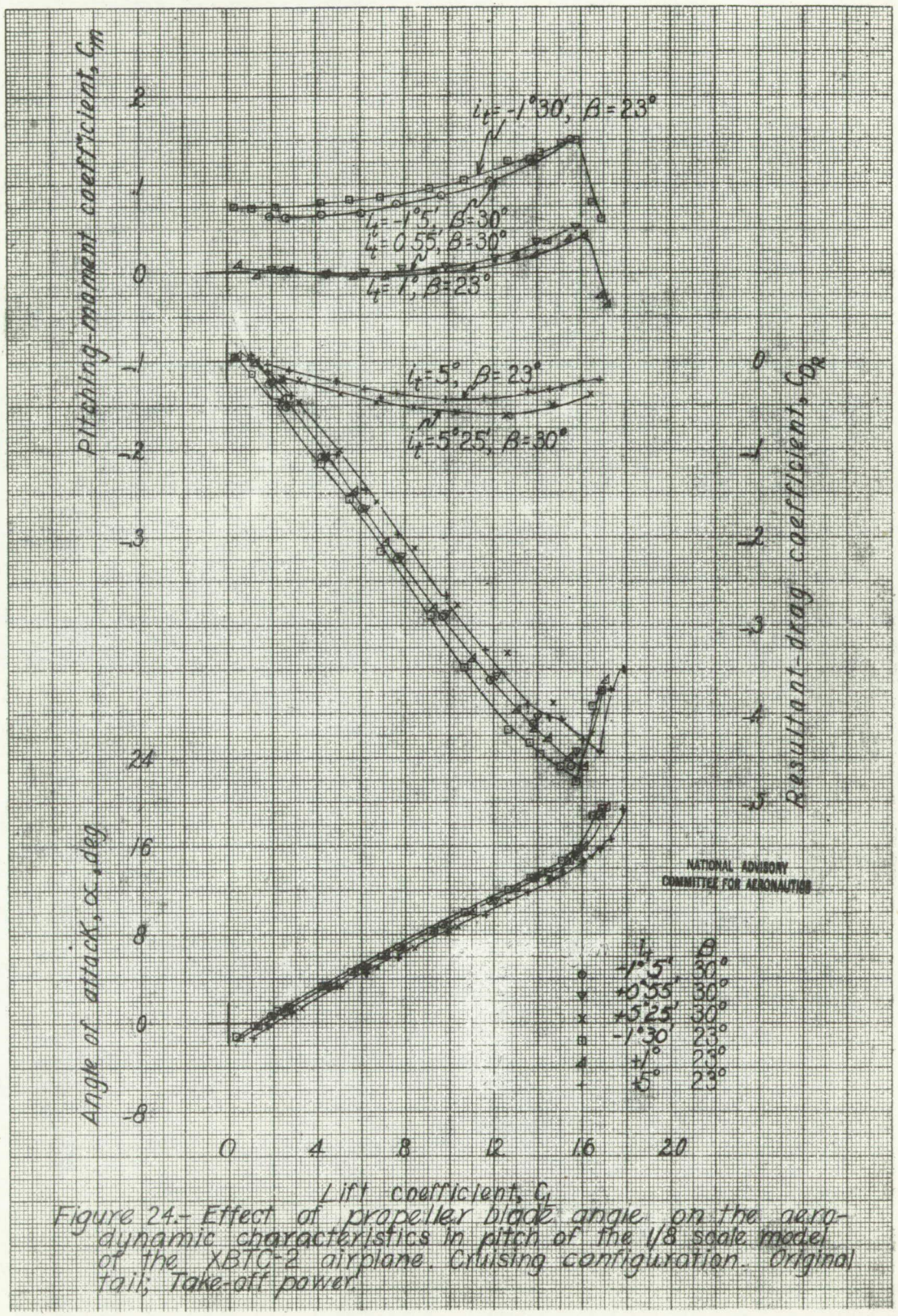

Figure 24.- Effect of propeller blade angle on the aerodynamic characteristics in pitch of the 1/8 scale model of the XBTC-2 airplane. Cruising configuration. Original tail; Take-off power.

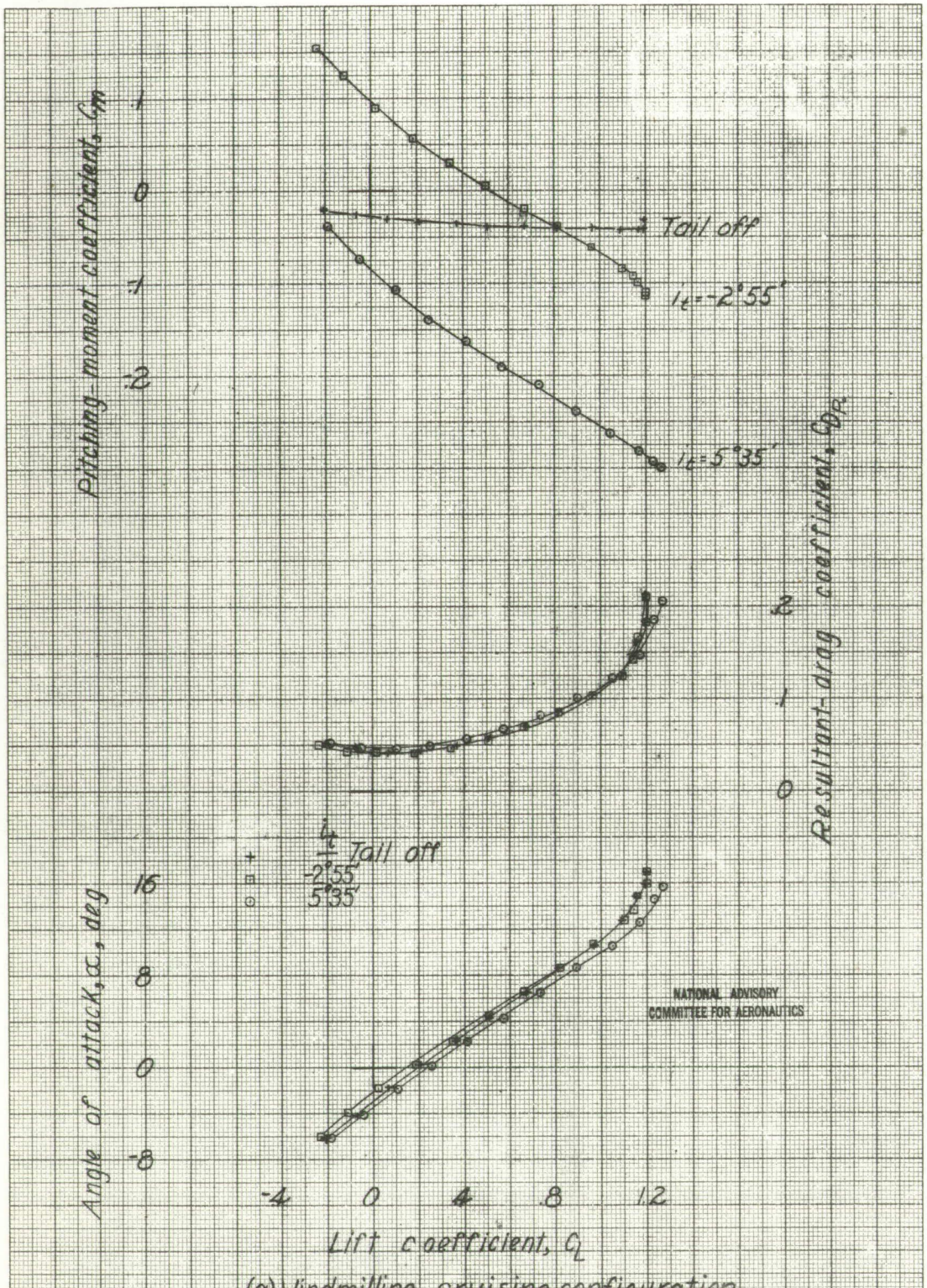

(a) Windmilling, cruising configuration.

Figure 25.-Effect of stabilizer on the aerodynamic characteristics in pitch of the 1/8 scale model of the XBTC-2 airplane. Swept-back outer wing panels; Original horizontal tail.

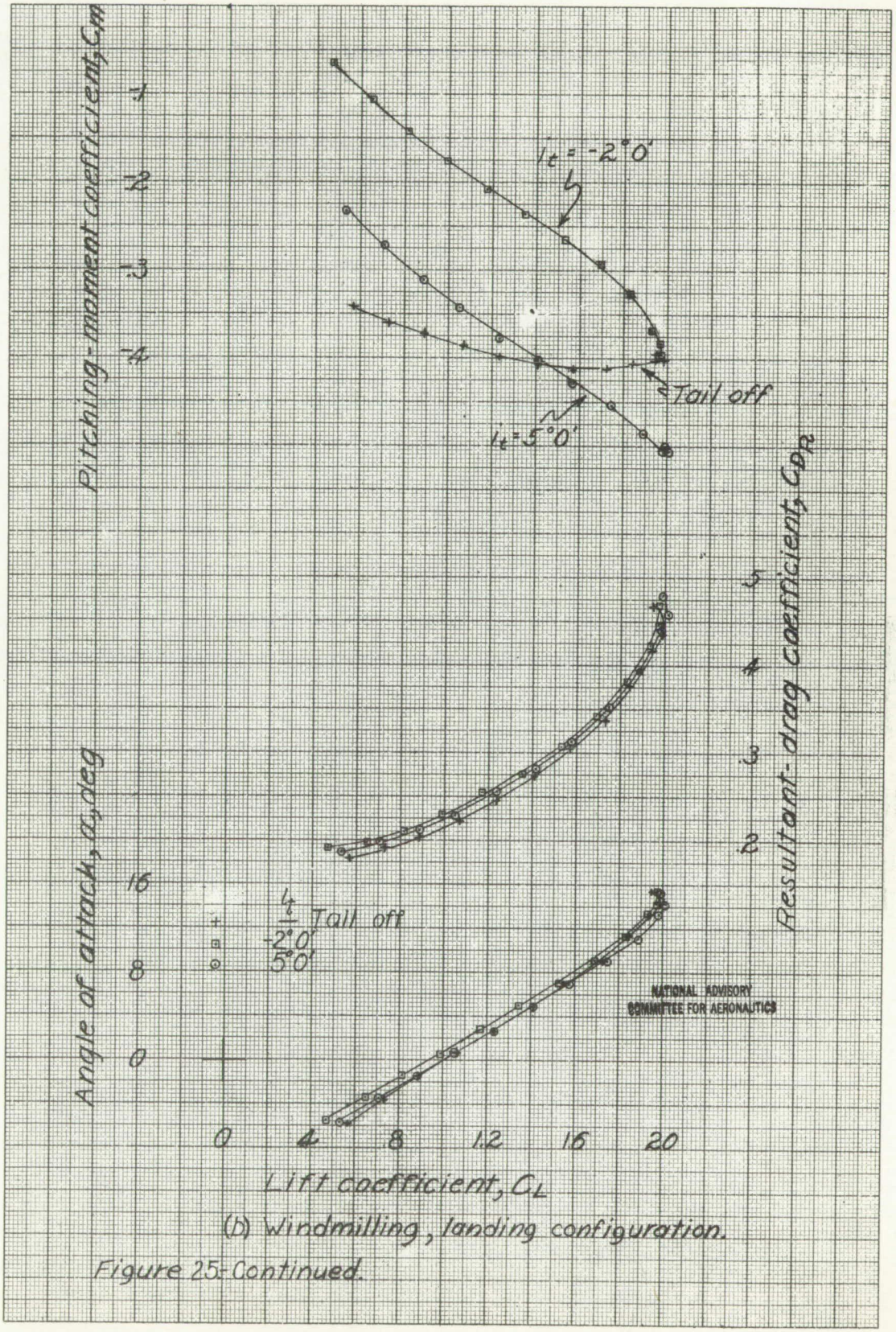

(b) Windmilling, landing configuration.

Figure 25- Continued.

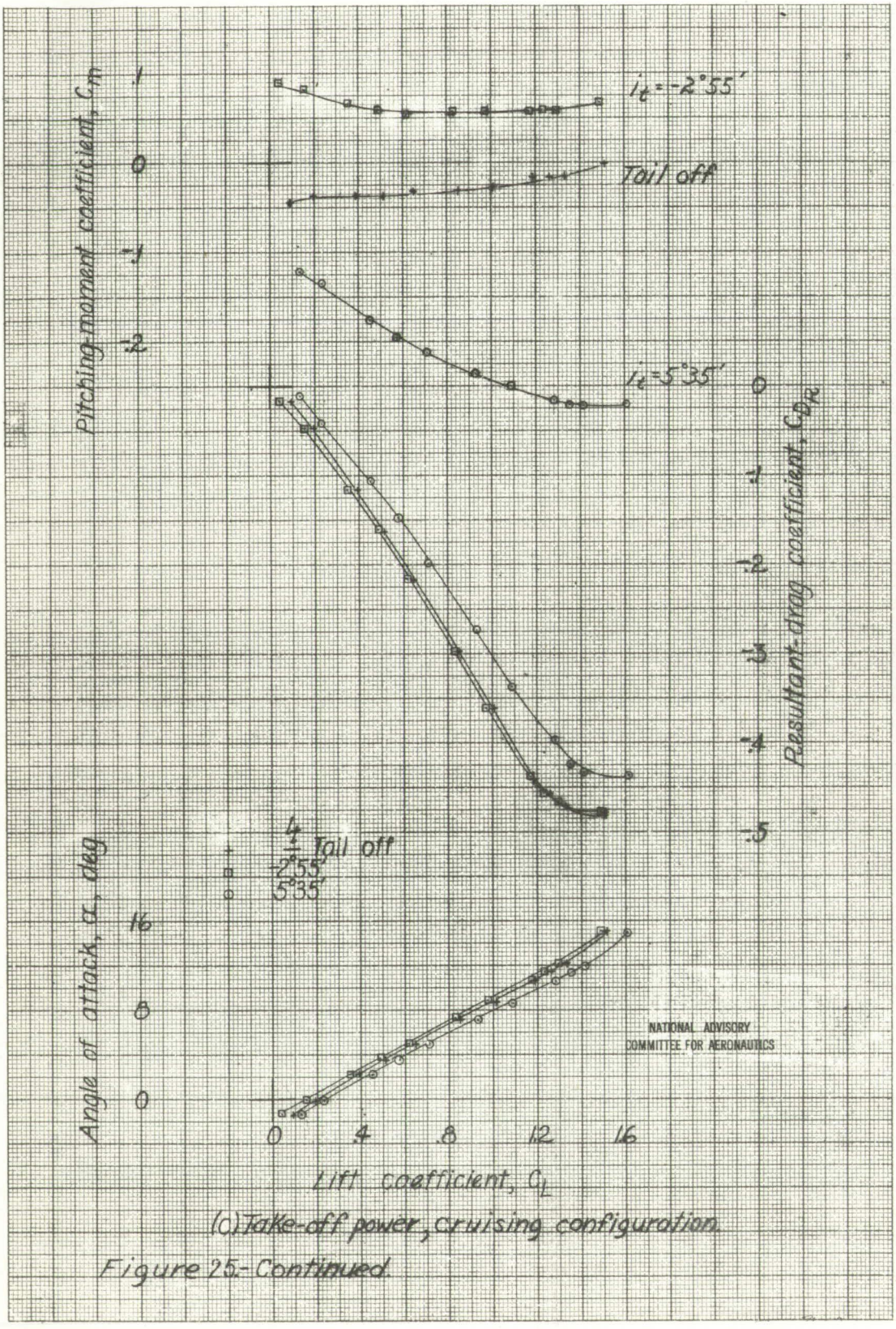

(c) Take-off power, cruising configuration.

Figure 25.- Continued.

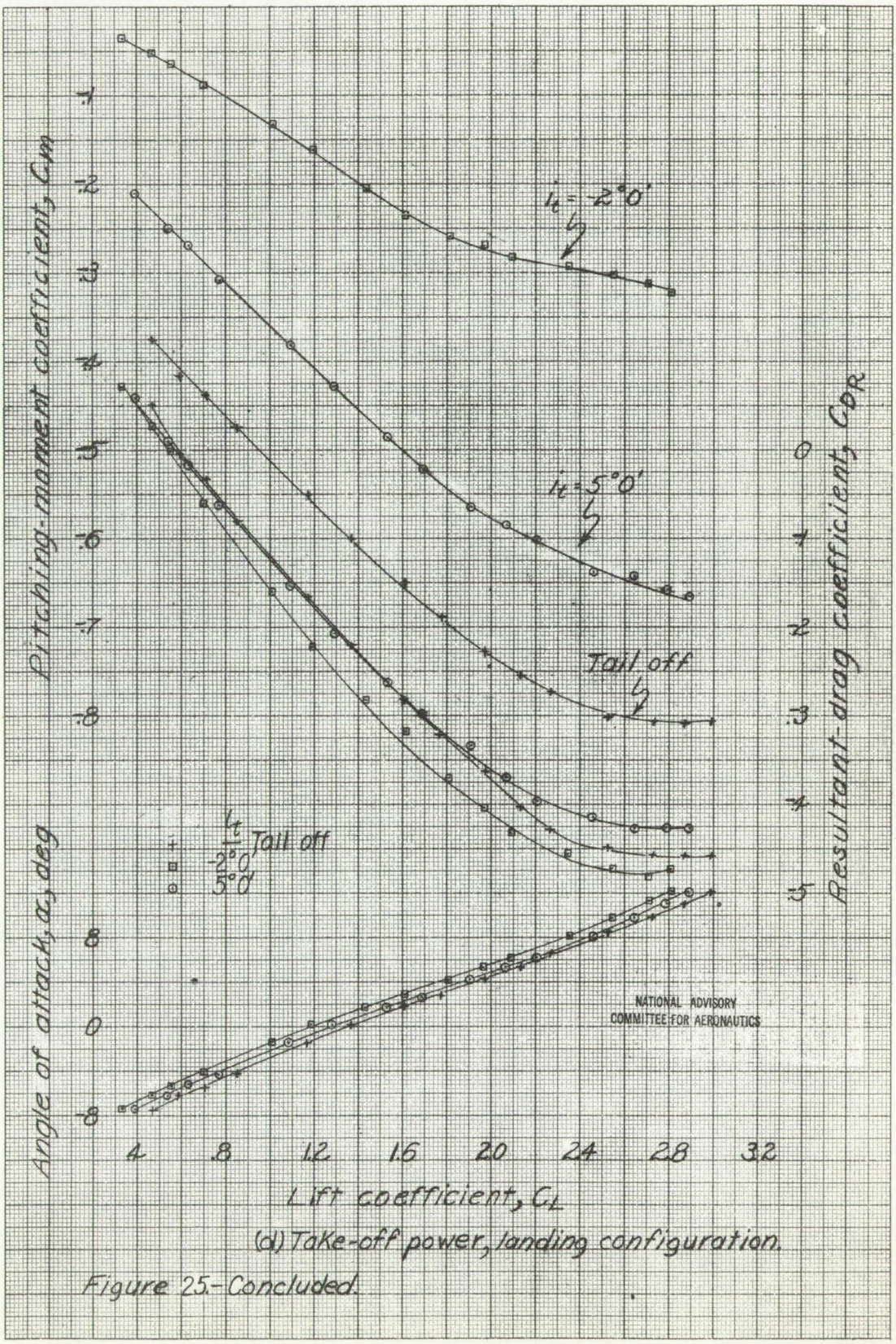

(d) Take-off power, landing configuration.

Figure 25.- Concluded.

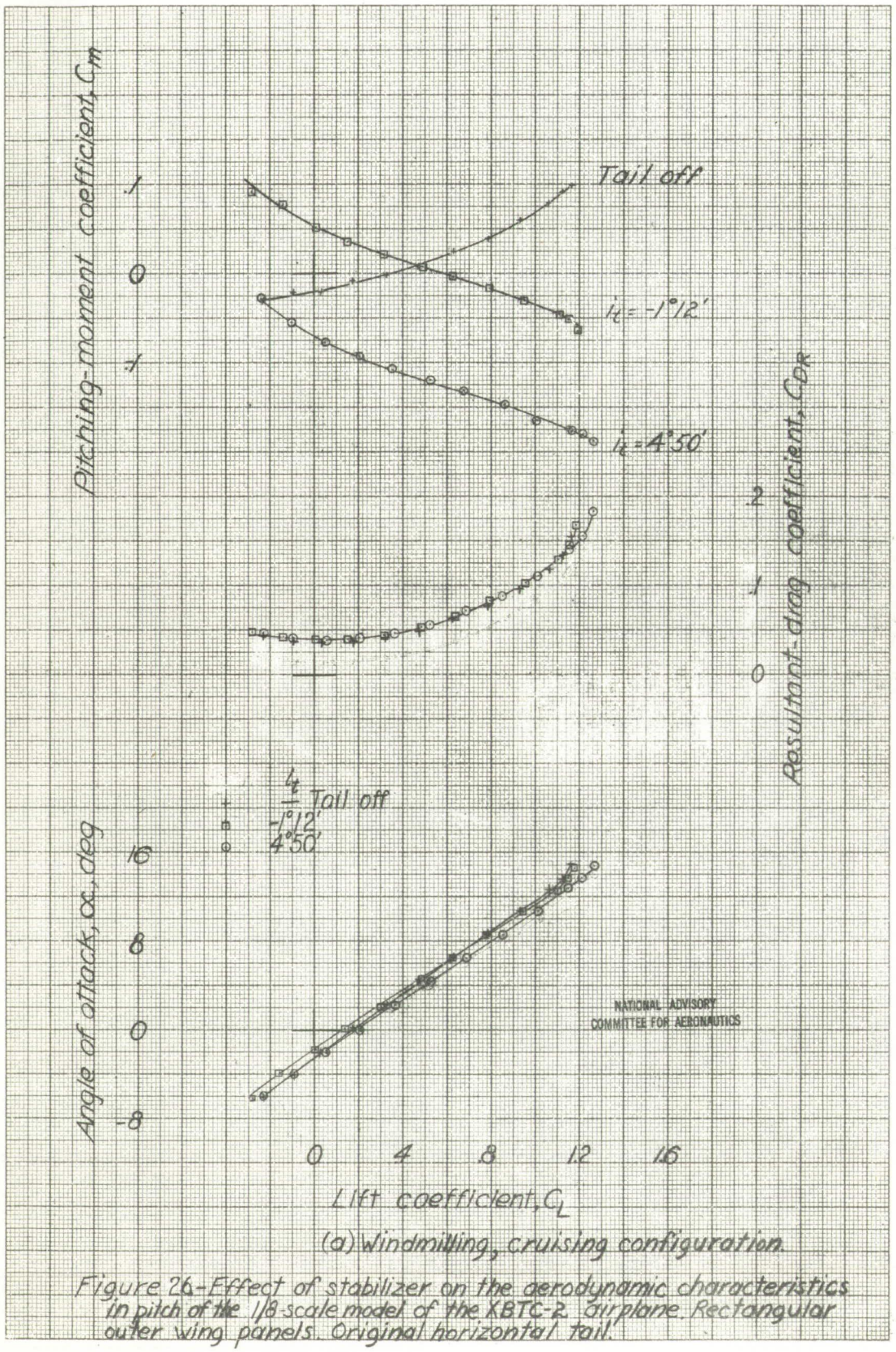

(a) Windmilling, cruising configuration.

Figure 26.- Effect of stabilizer on the aerodynamic characteristics in pitch of the 1/8-scale model of the XBTC-2 airplane. Rectangular outer wing panels. Original horizontal tail.

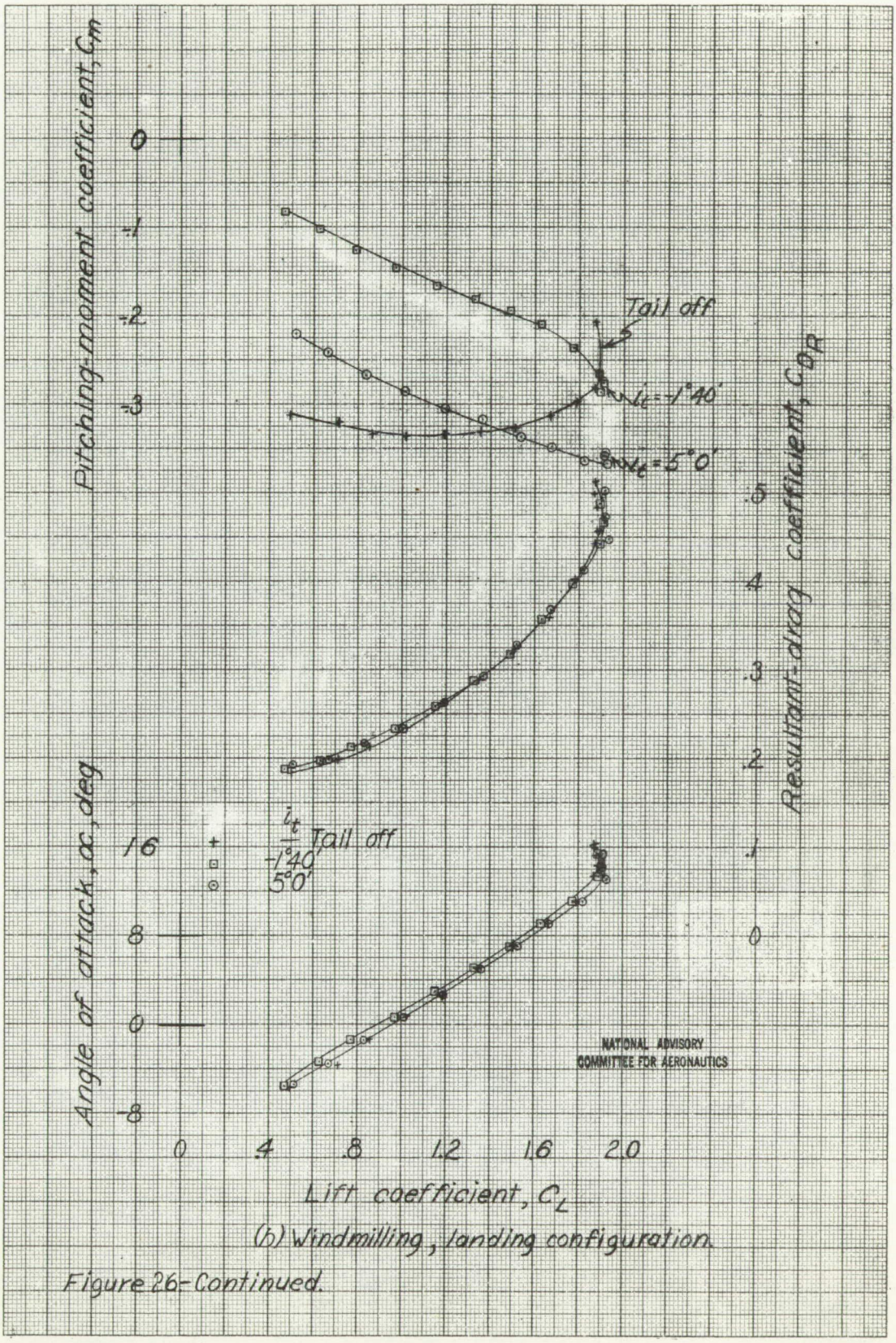

(b) Windmilling, landing configuration.

Figure 26- Continued.

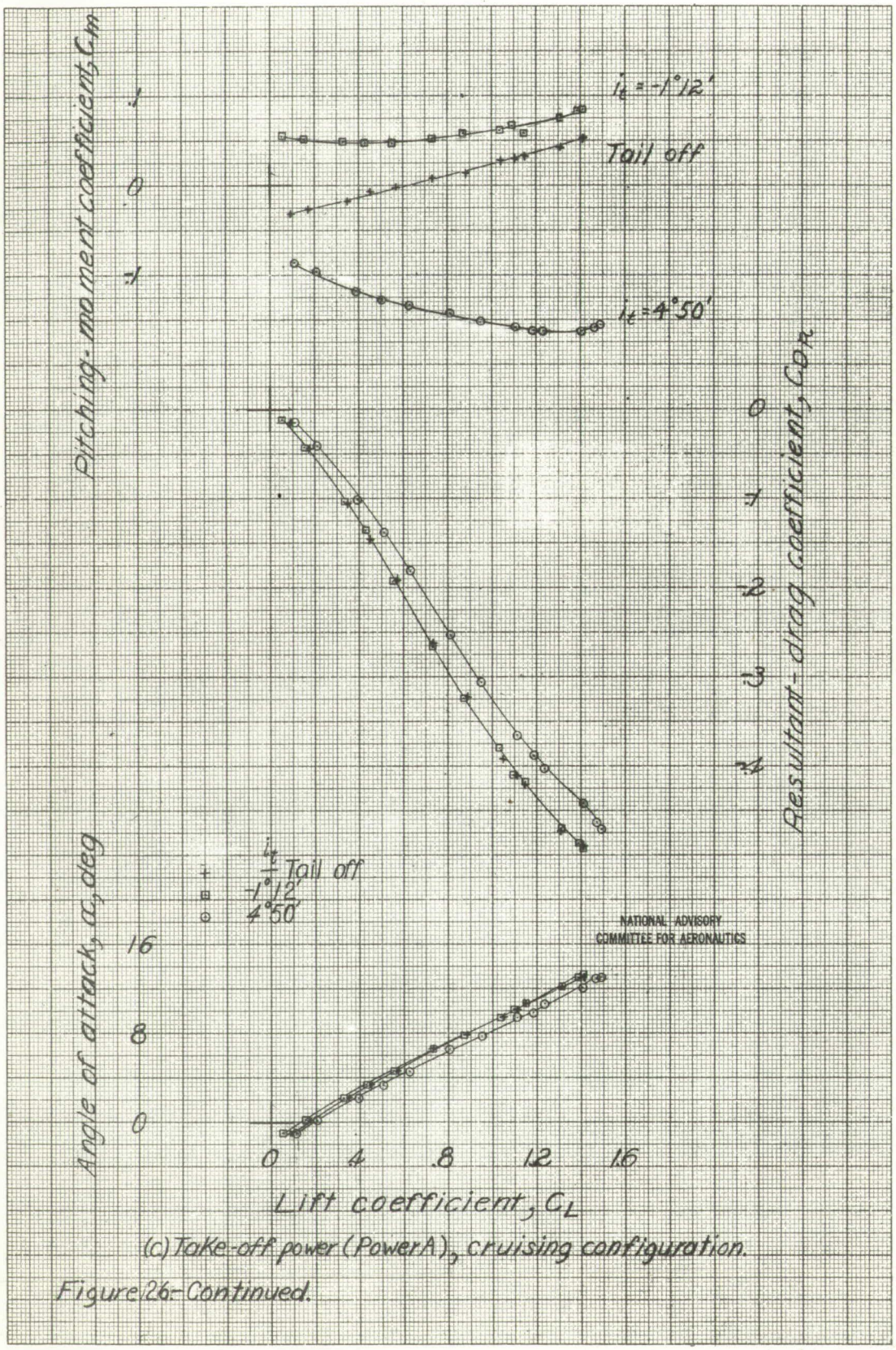

(c) Take-off power (Power A), cruising configuration.

Figure 26.- Continued.

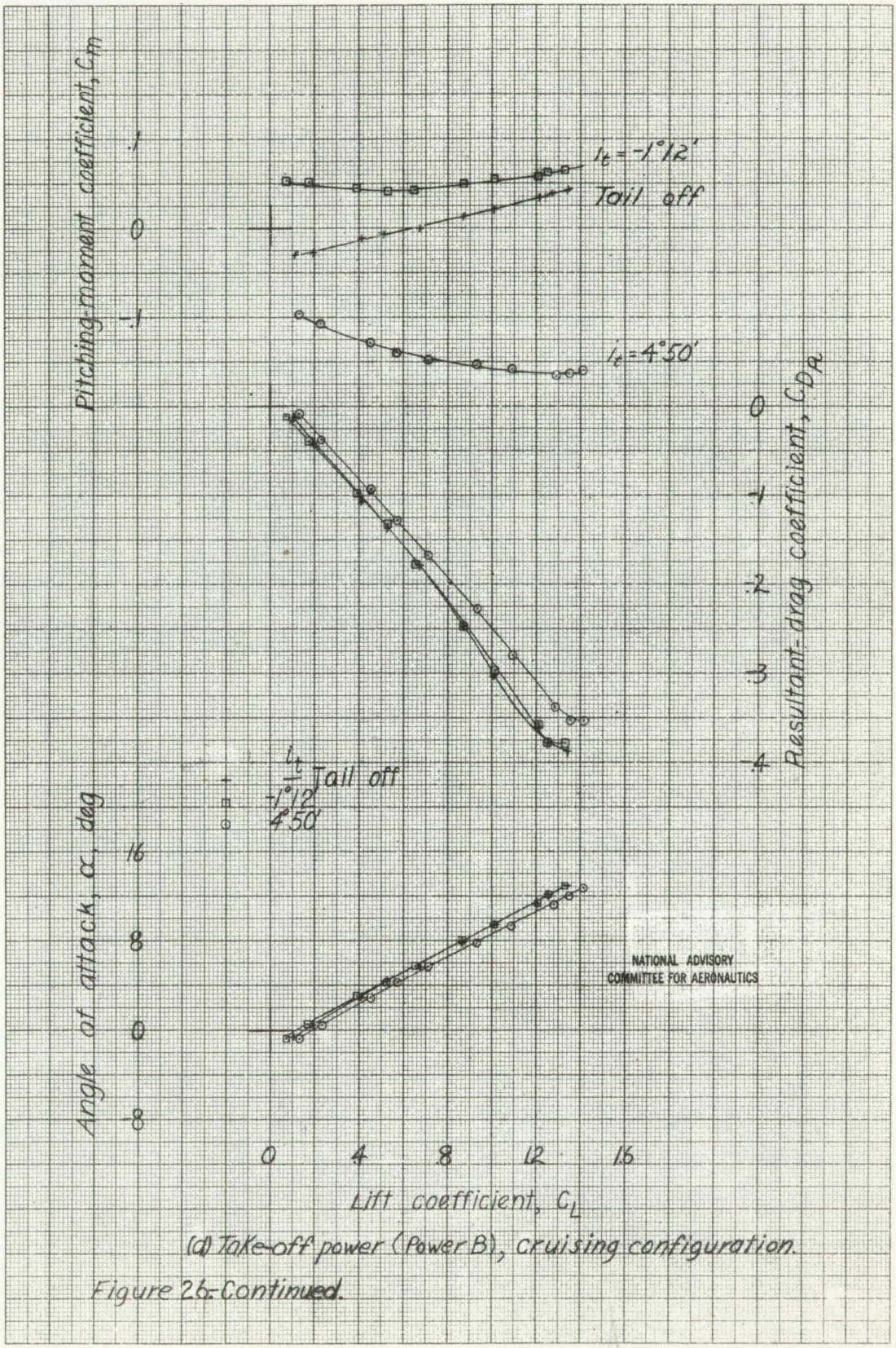

(d) Take-off power (Power B), cruising configuration.

Figure 26.- Continued.

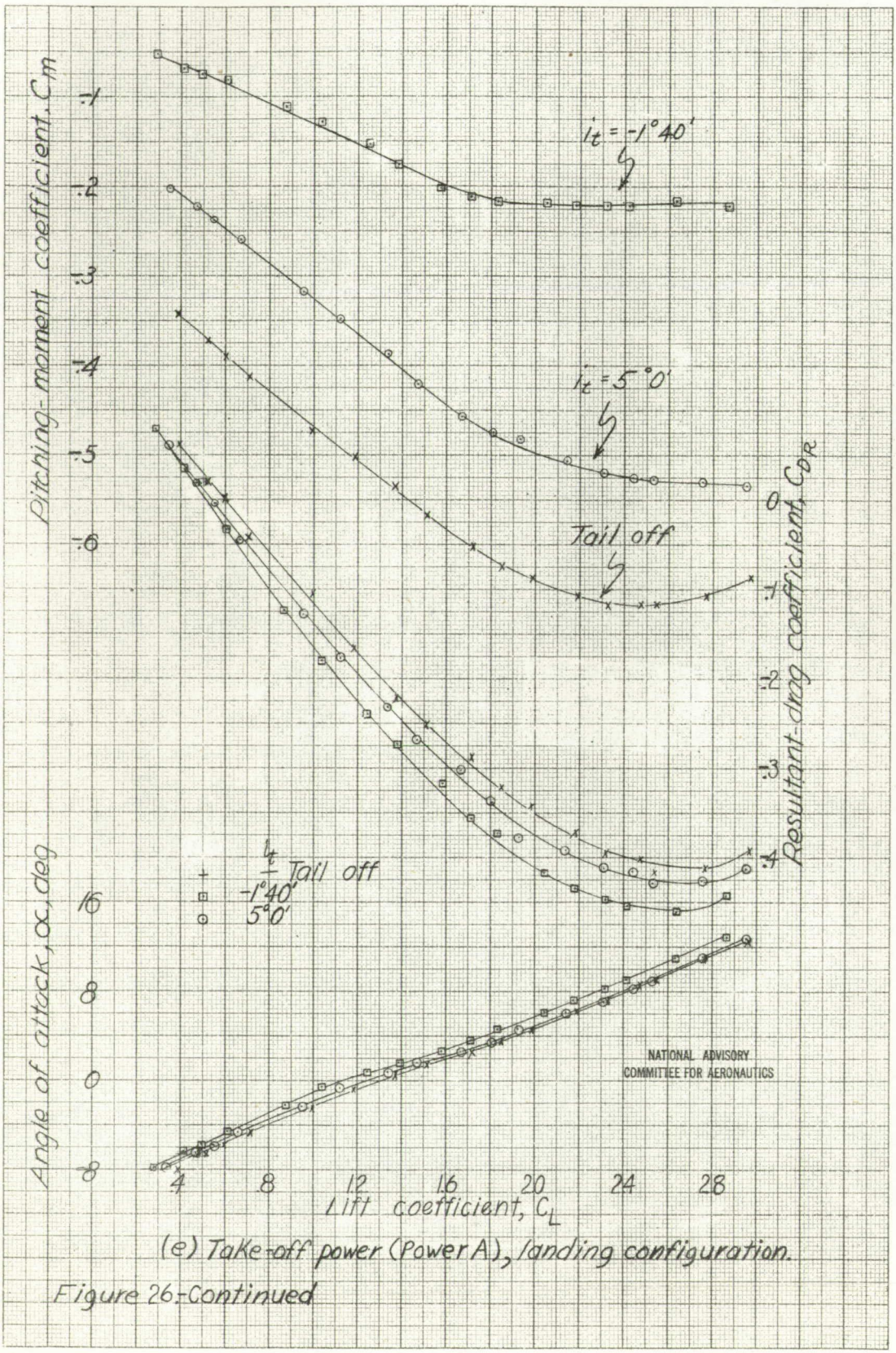

(e) Take-off power (Power A), landing configuration.

Figure 26.-Continued

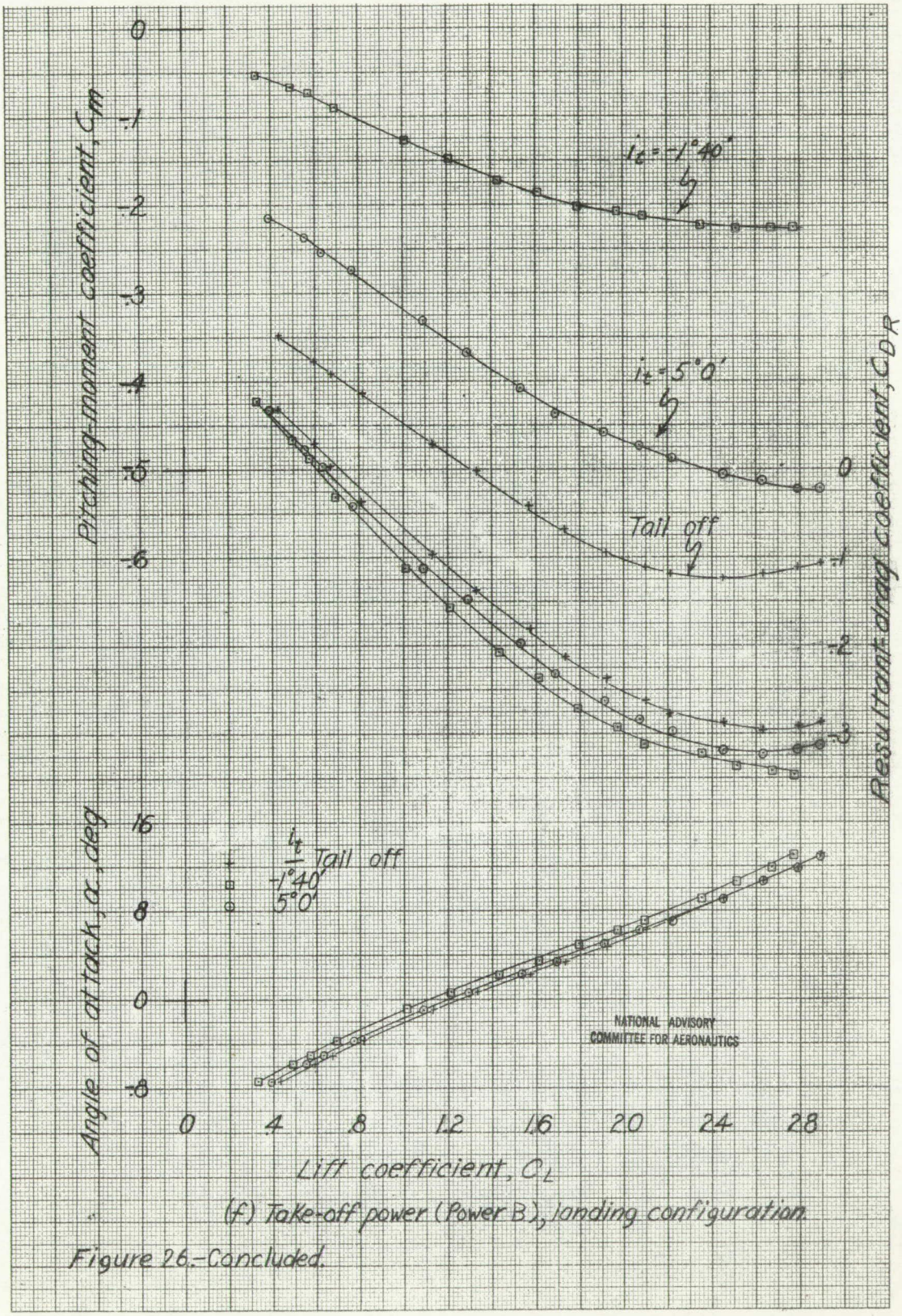

(f) Take-off power (Power B), landing configuration.

Figure 26.- Concluded.

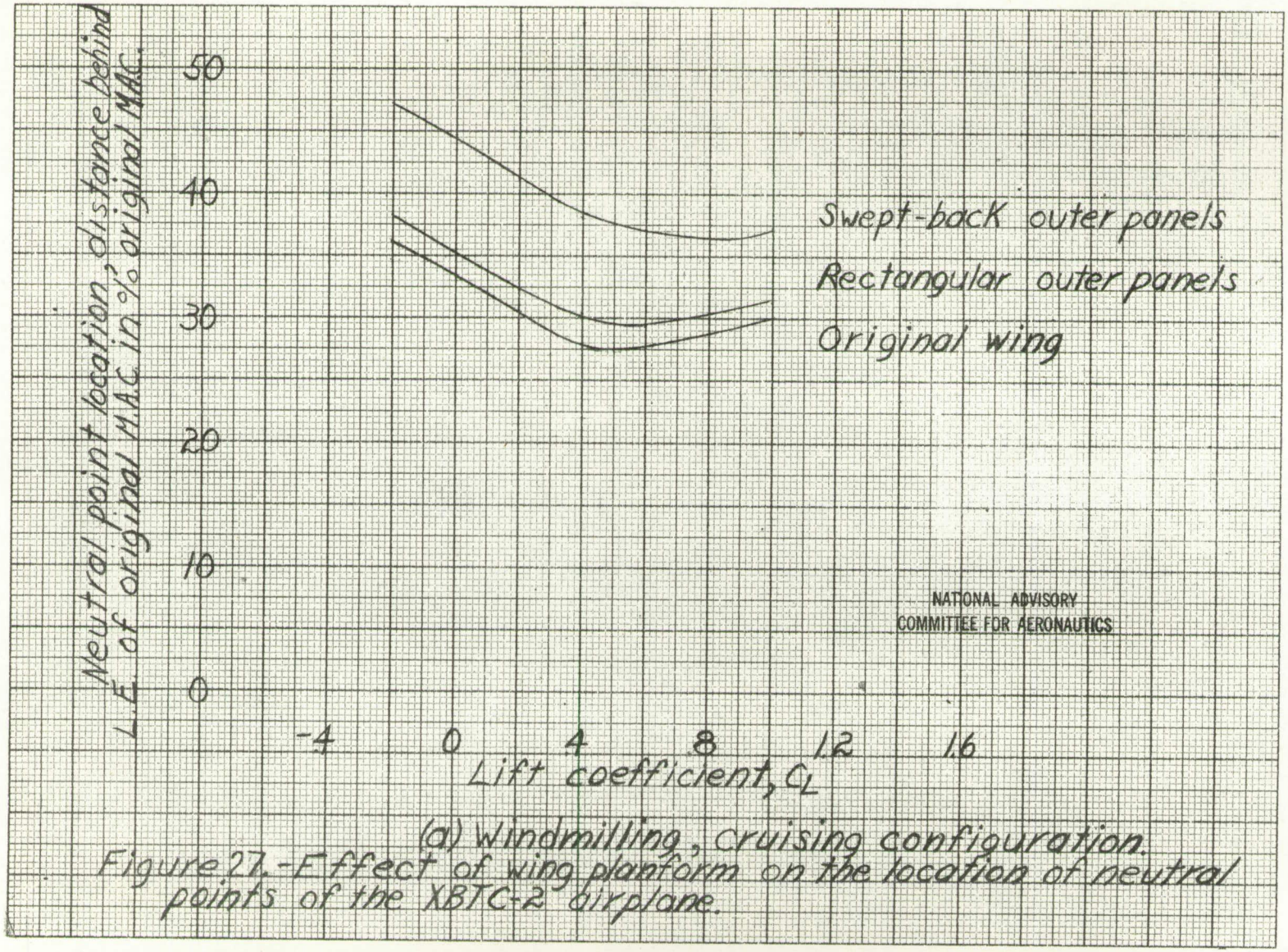

(a) Windmilling, cruising configuration.

Figure 27.- Effect of wing planform on the location of neutral points of the XBTC-2 airplane.

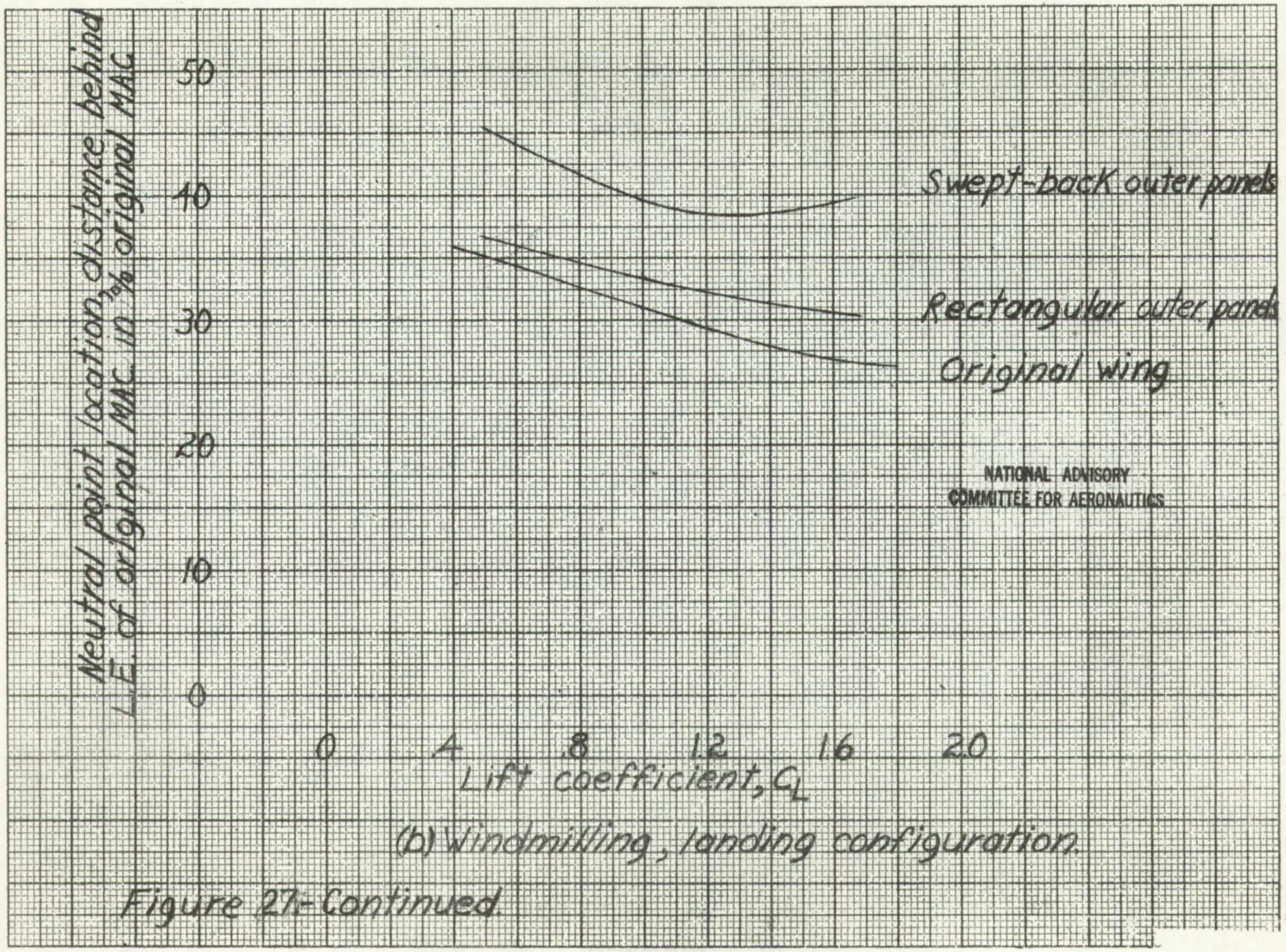

(b) Windmilling, landing configuration.

Figure 27.- Continued.

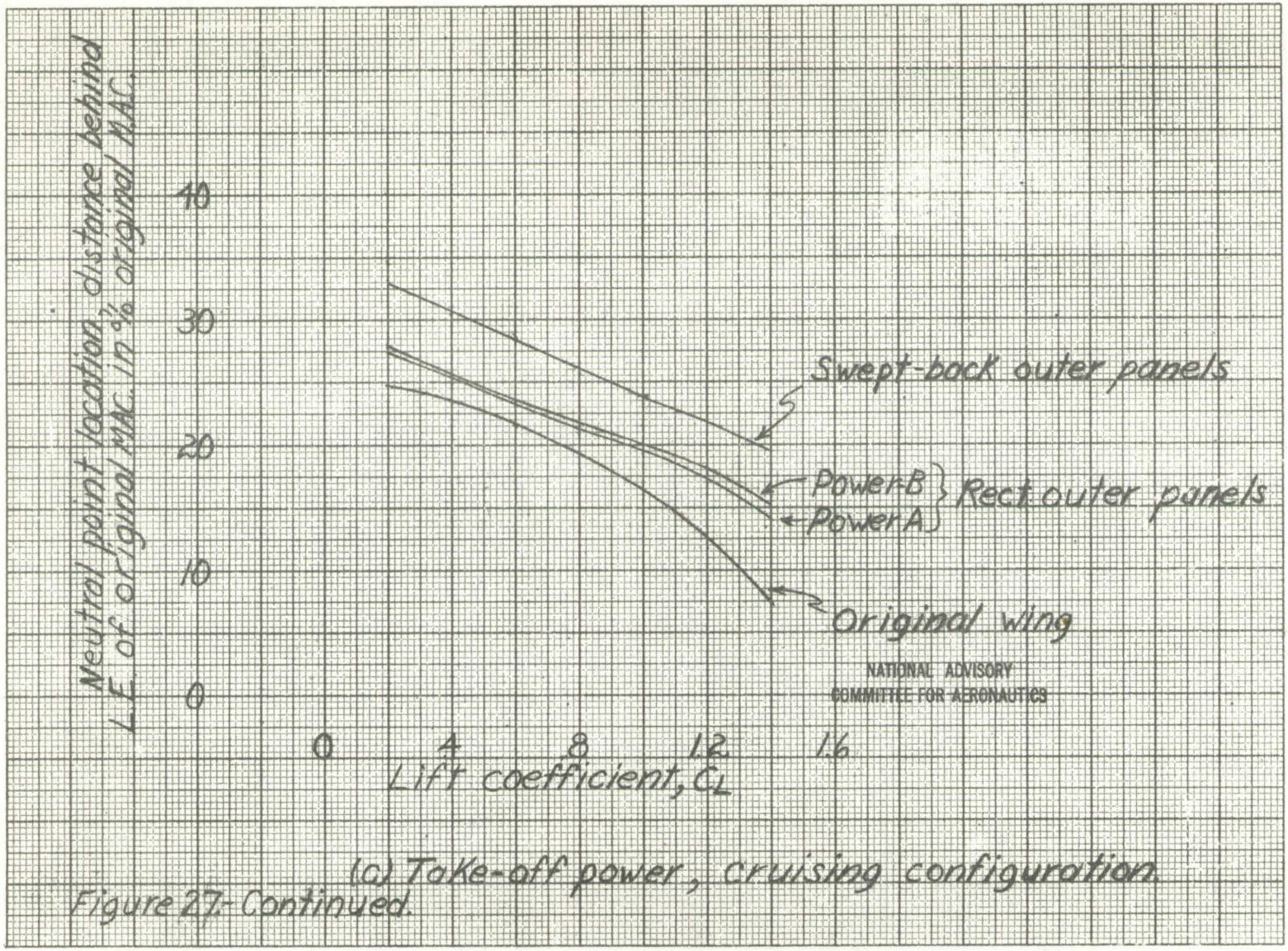

(c) Take-off power, cruising configuration.

Figure 27.- Continued.

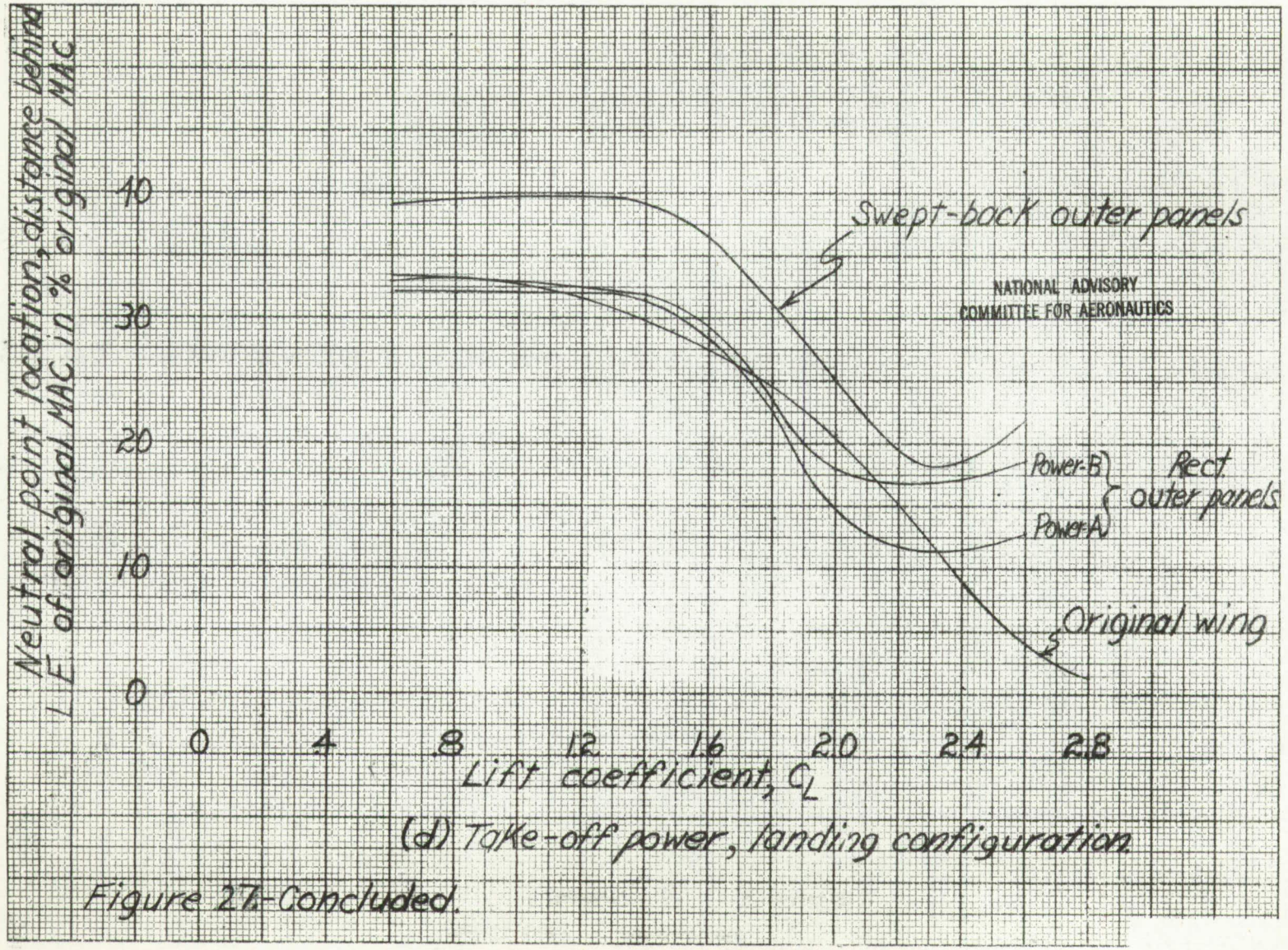

(d) Take-off power, landing configuration.

Figure 27.- Concluded.

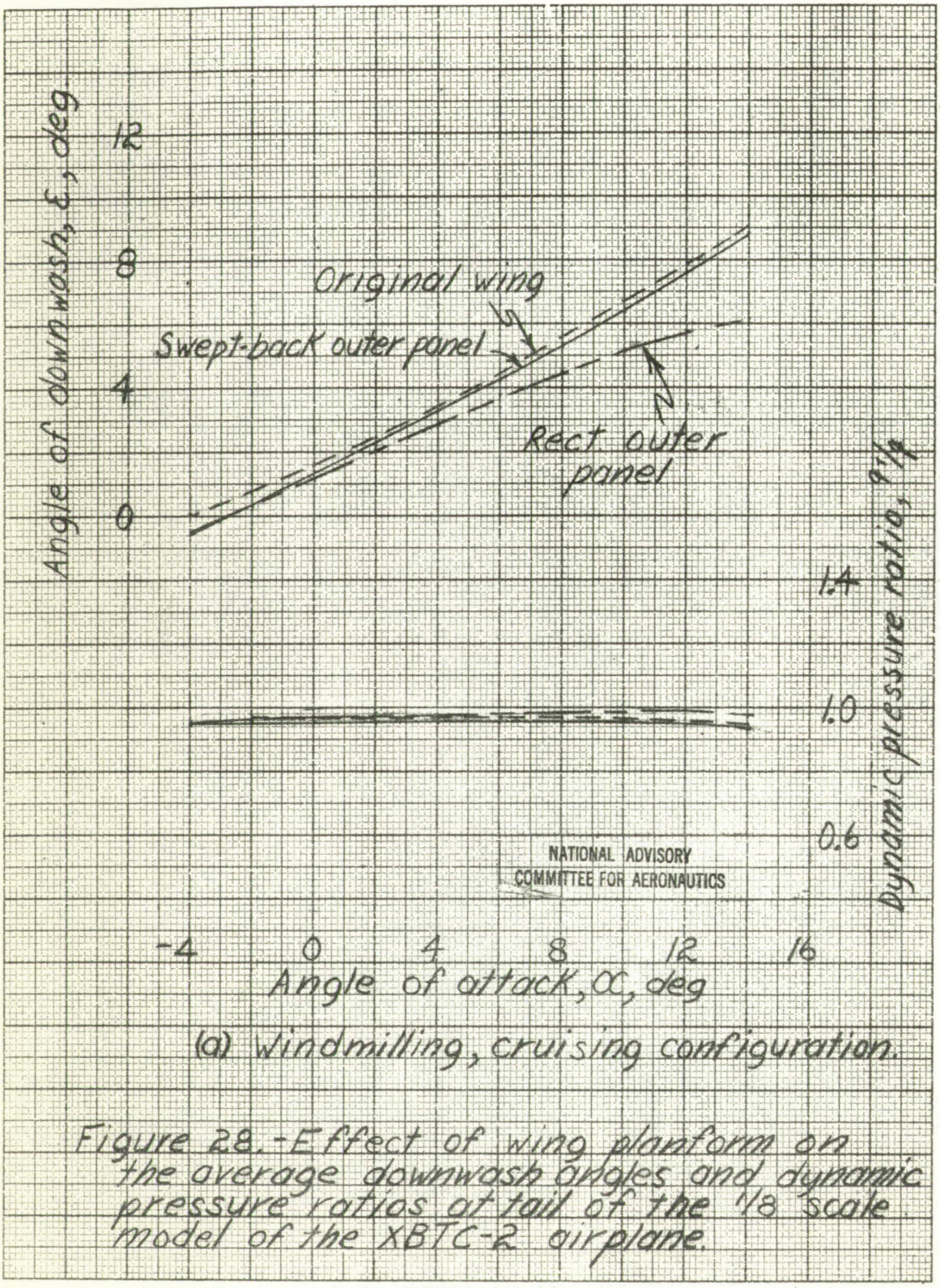

(a) Windmilling, cruising configuration.

Figure 28.- Effect of wing planform on the average downwash angles and dynamic pressure ratios at tail of the 1/8 scale model of the XBTC-2 airplane.

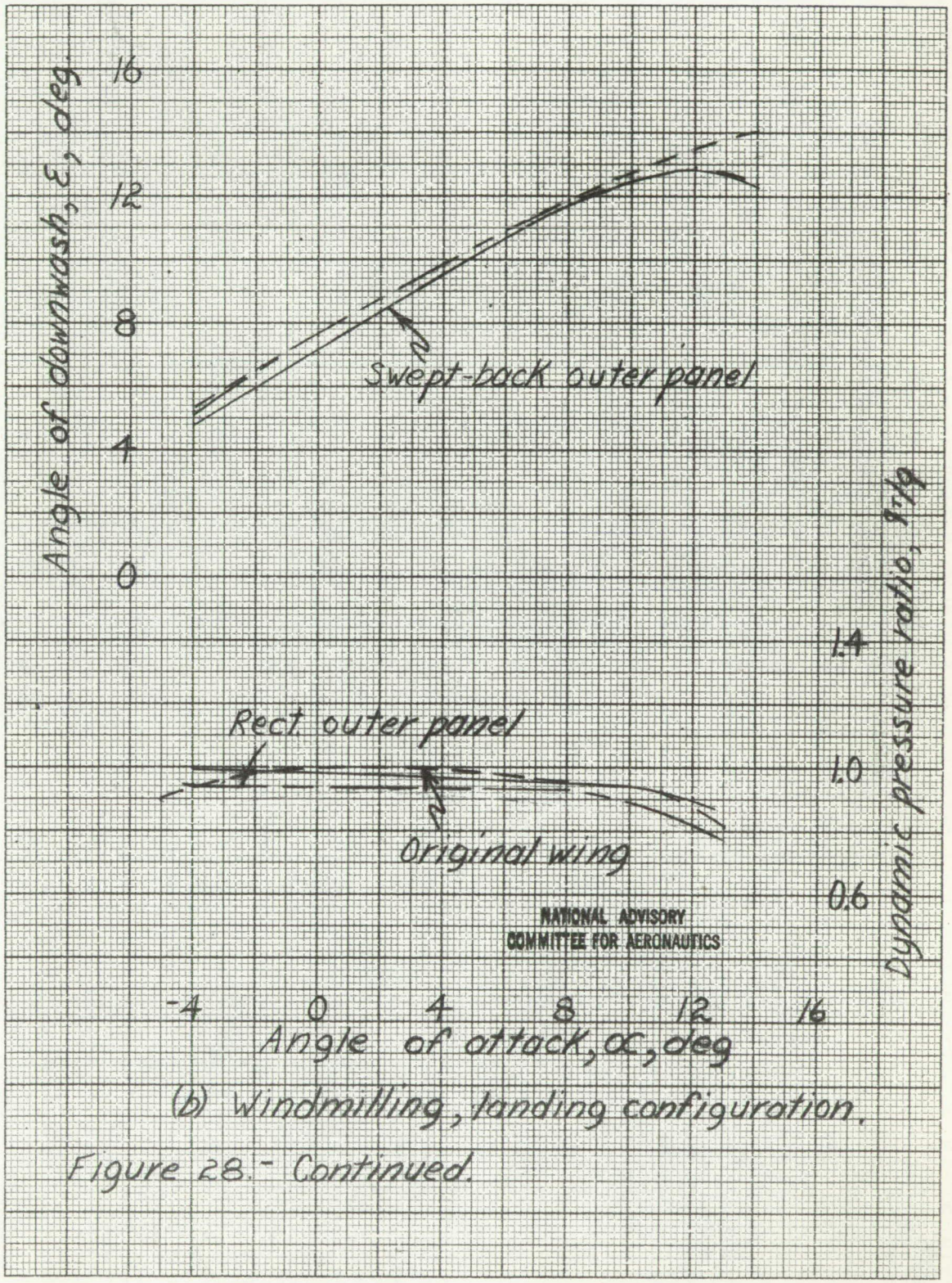

(b) Windmilling, landing configuration.

Figure 28.- Continued.

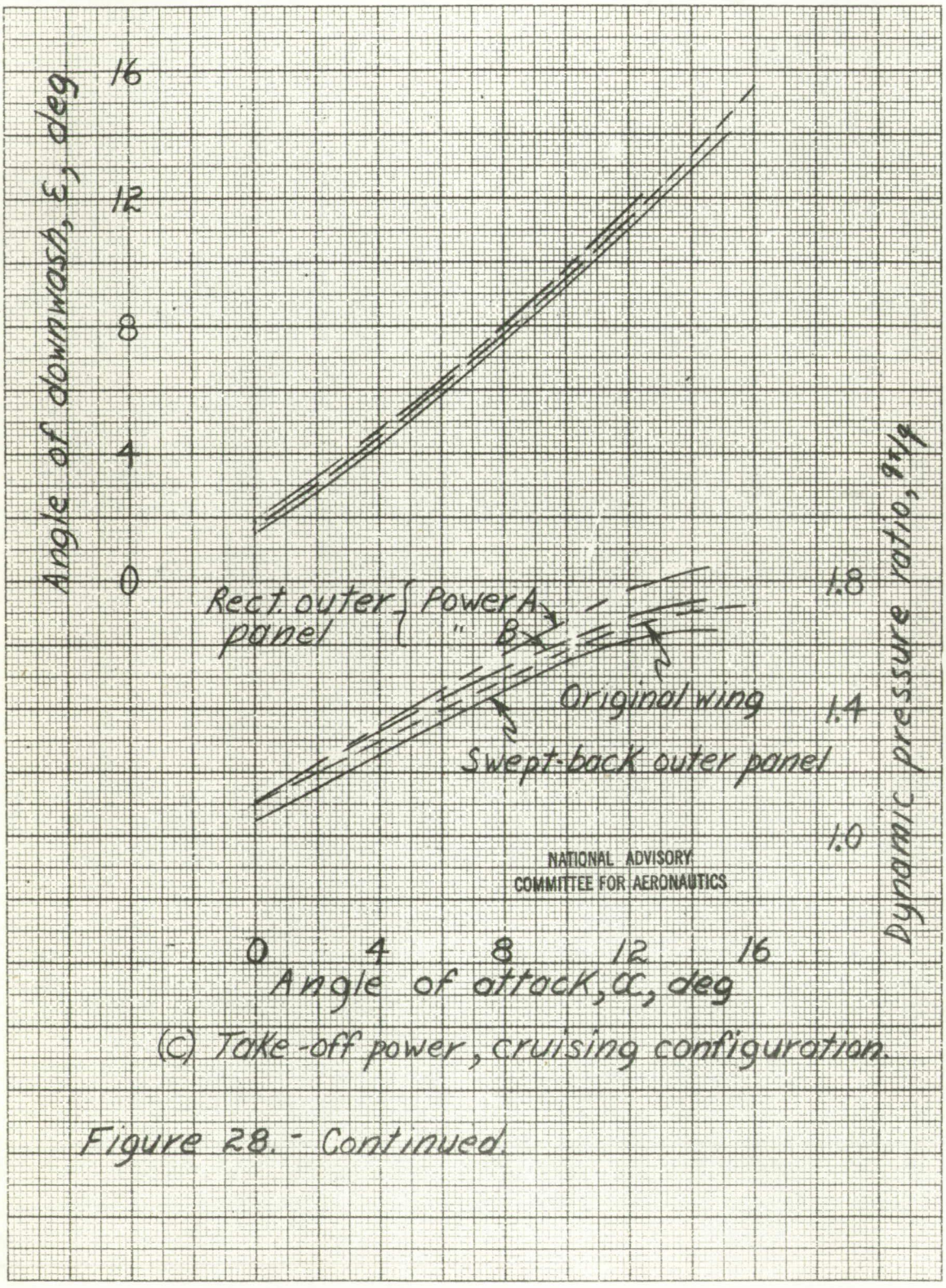

(c) Take-off power, cruising configuration.

Figure 28.- Continued.

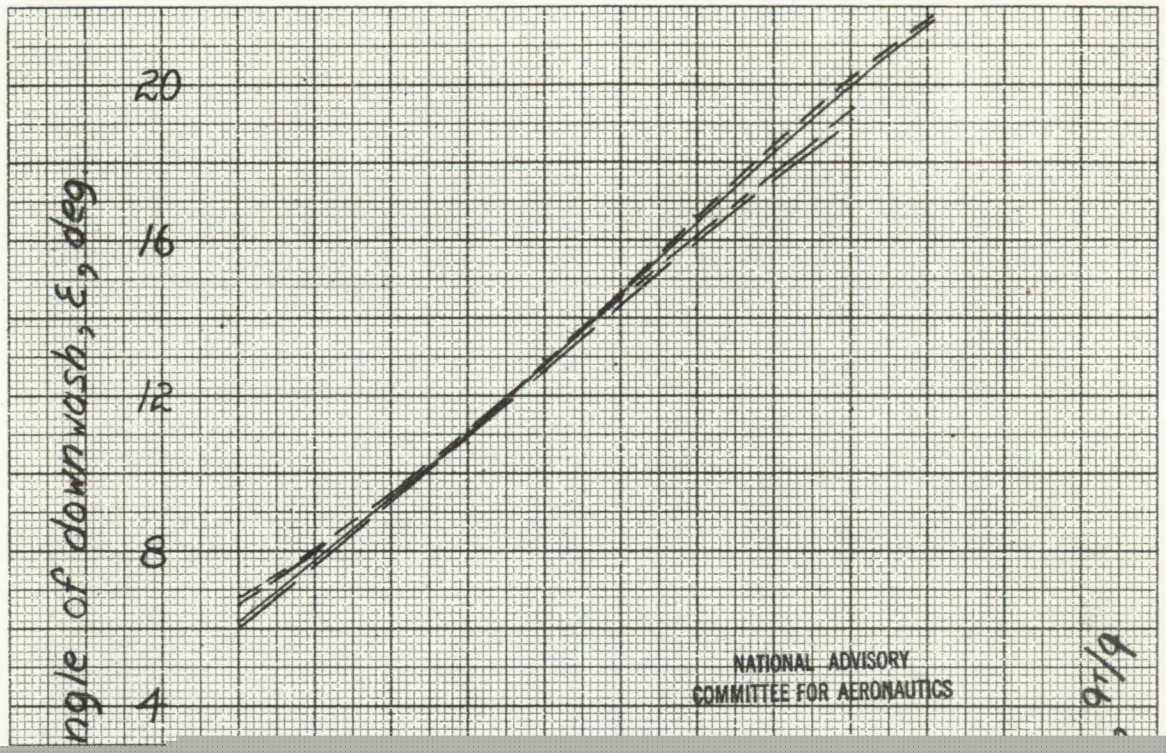
20
16
12
8
4
ngle of downwash, ε, deg.
NATIONAL ADVISORY
COMMITTEE FOR AERONAUTICS
q1/q

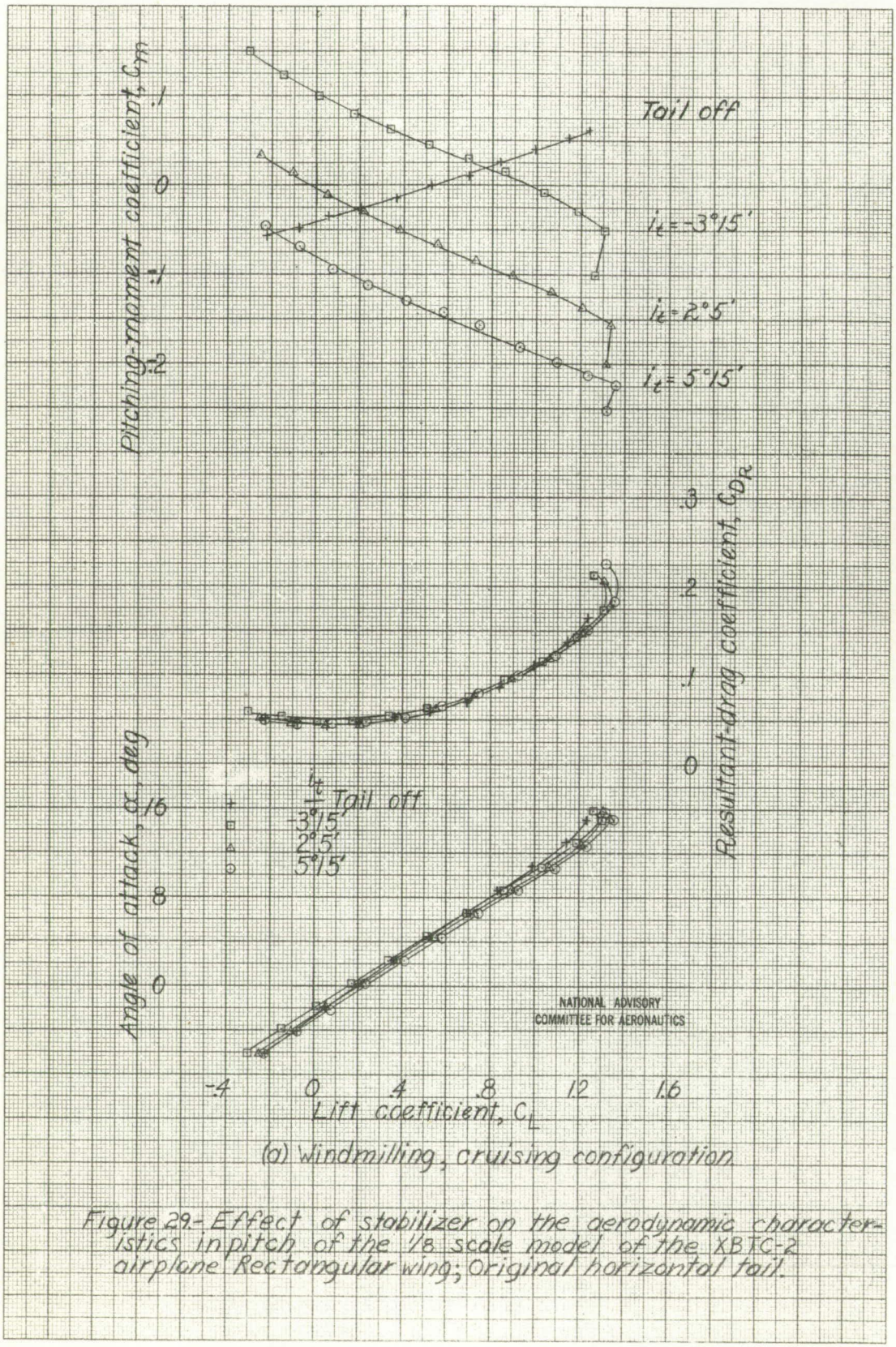

(a) Windmilling, cruising configuration.

Figure 29.- Effect of stabilizer on the aerodynamic characteristics in pitch of the 1/8 scale model of the XBTC-2 airplane. Rectangular wing; original horizontal tail.

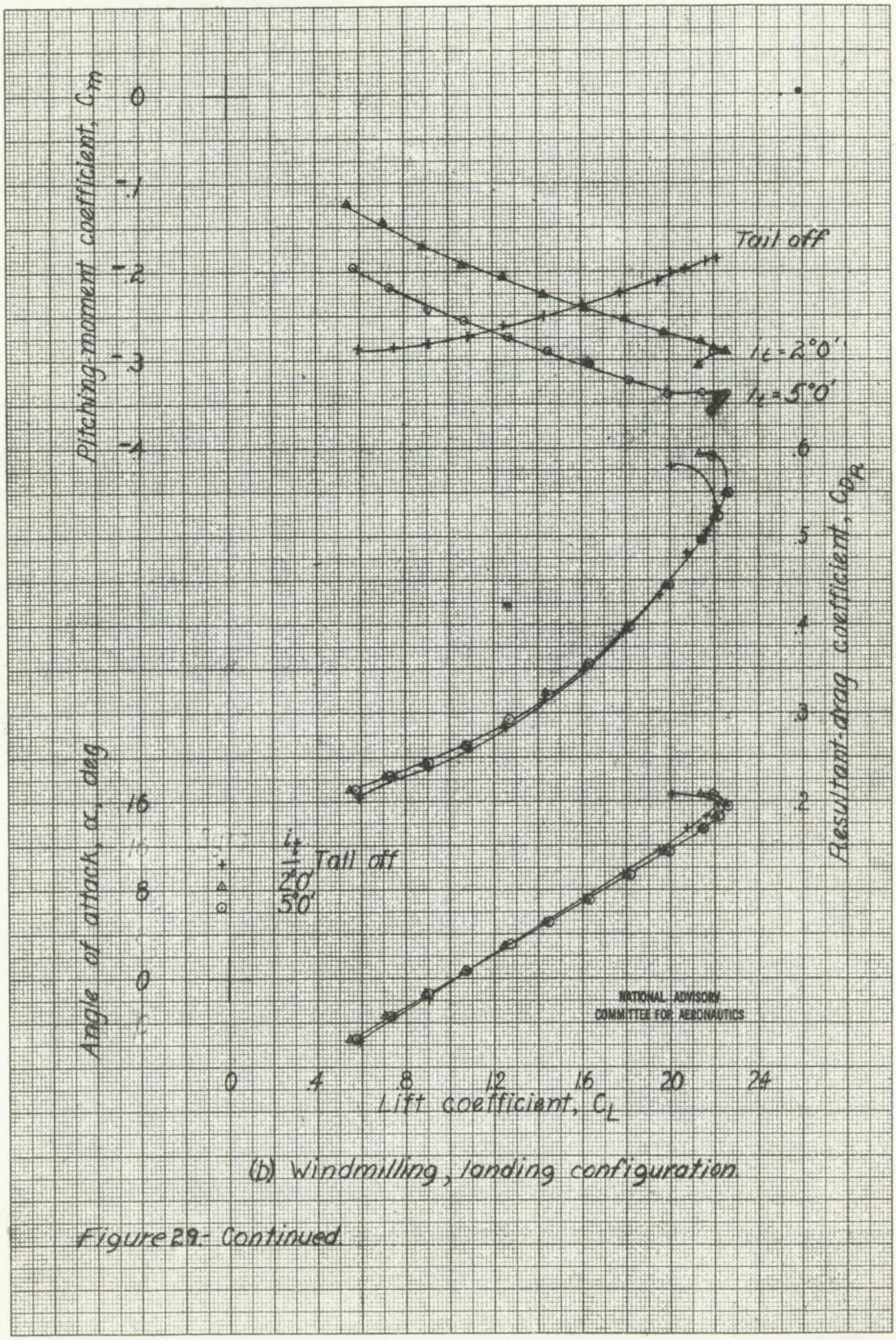

(b) Windmilling, landing configuration.

Figure 29.- Continued.

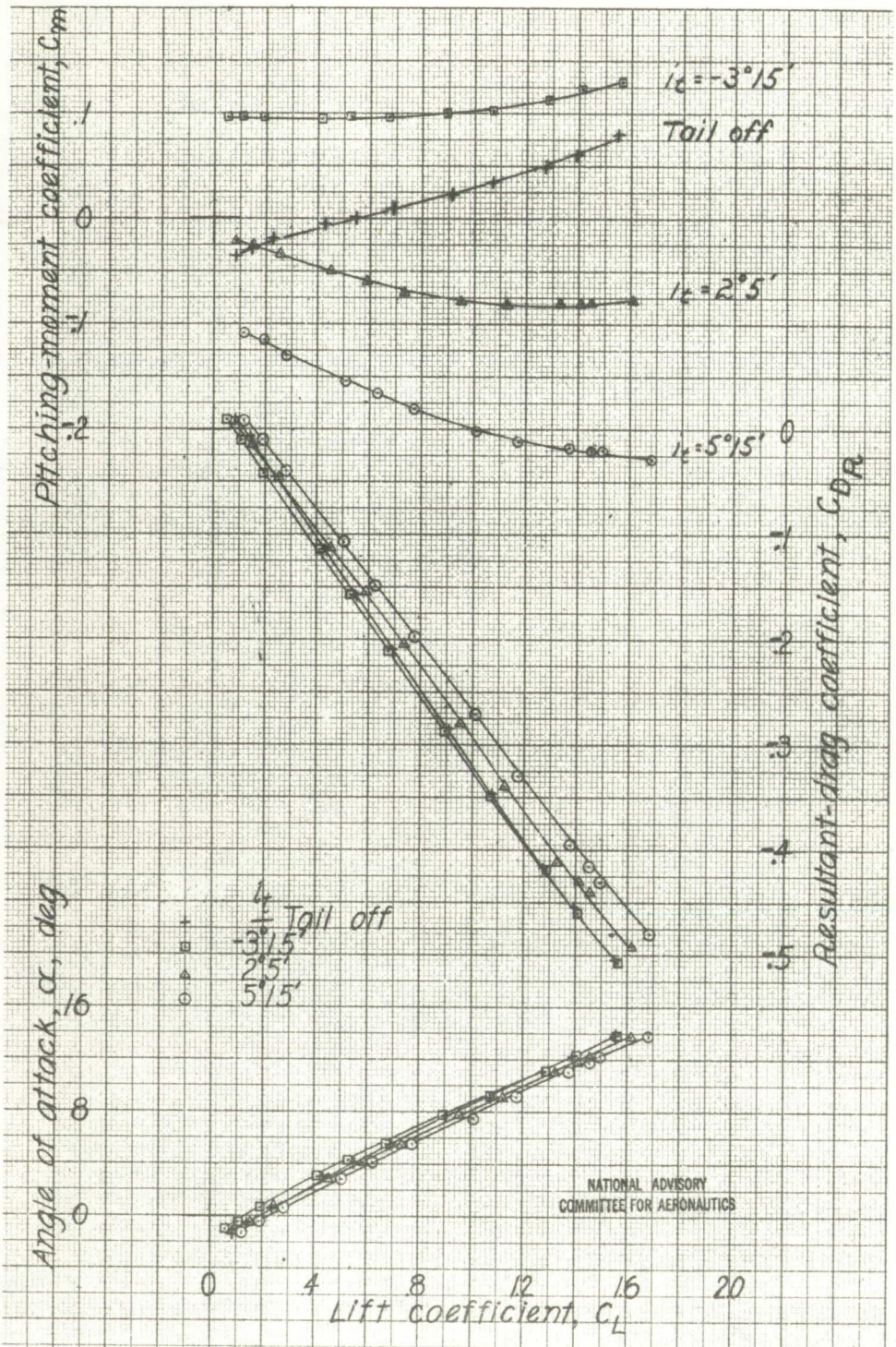

(c) Take-off power, cruising configuration.

Figure 29.- Continued.

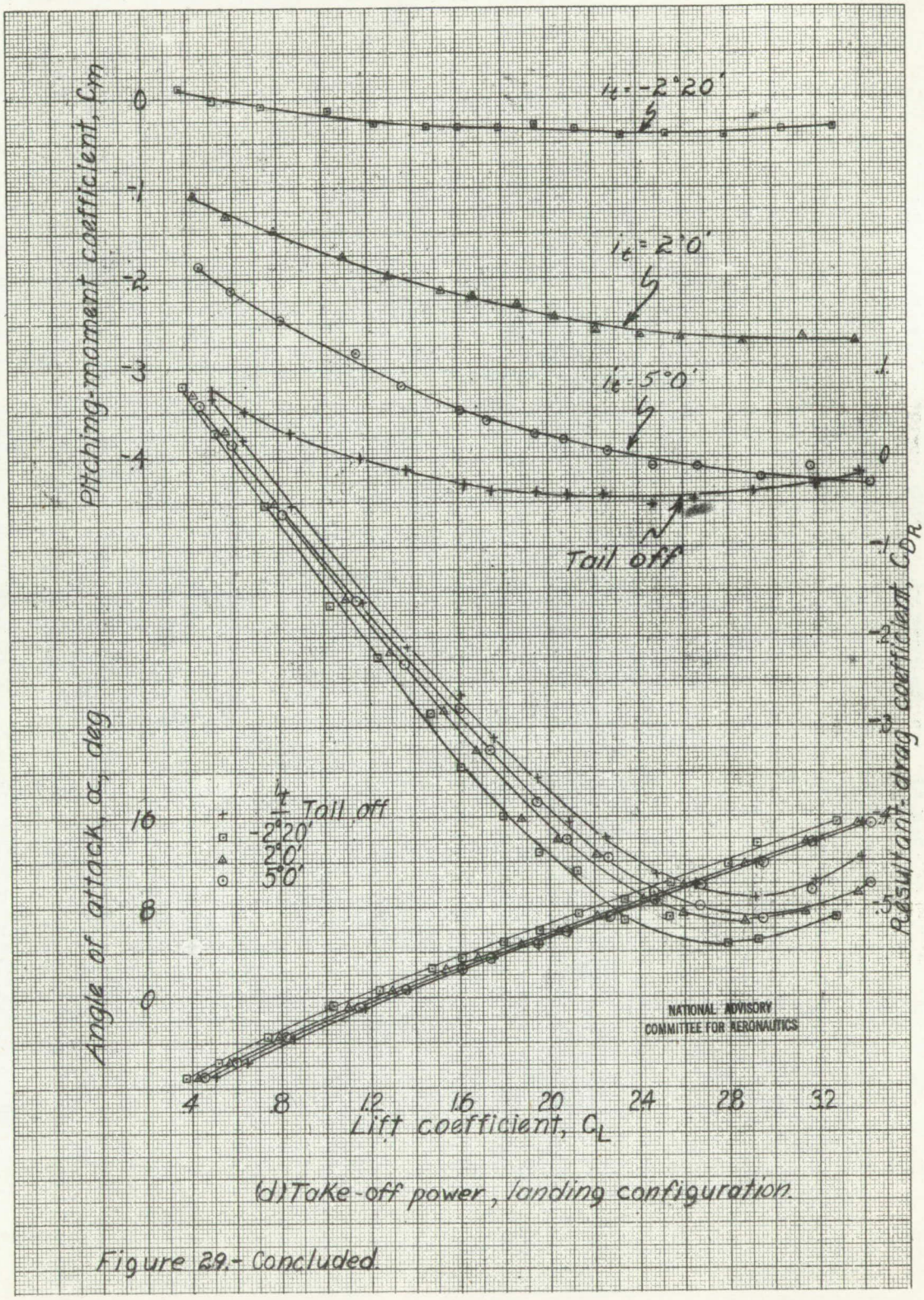

(d) Take-off power, landing configuration.

Figure 29.- Concluded.

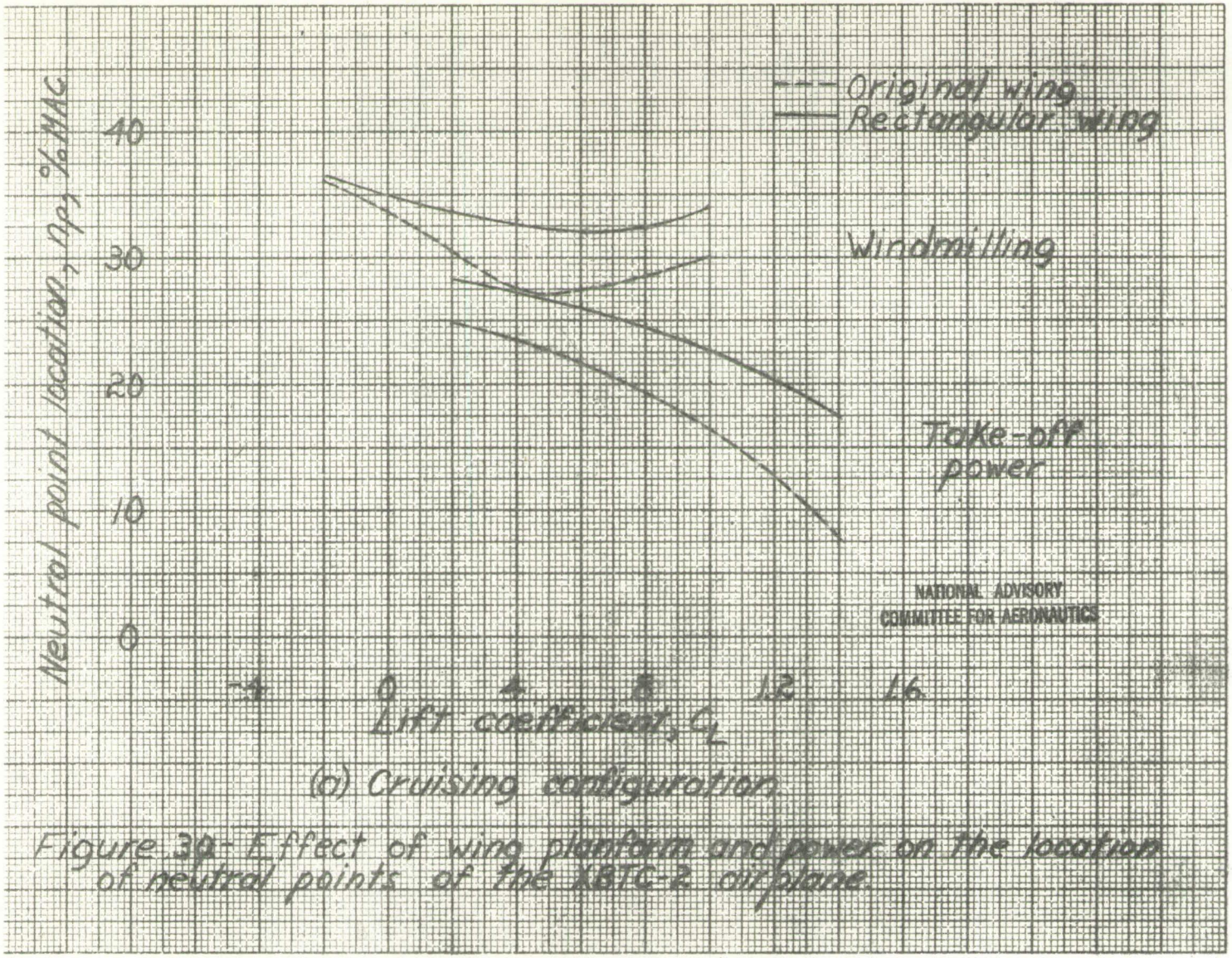

(a) Cruising configuration.

Figure 39.- Effect of wing planform and power on the location of neutral points of the XBTC-2 airplane.

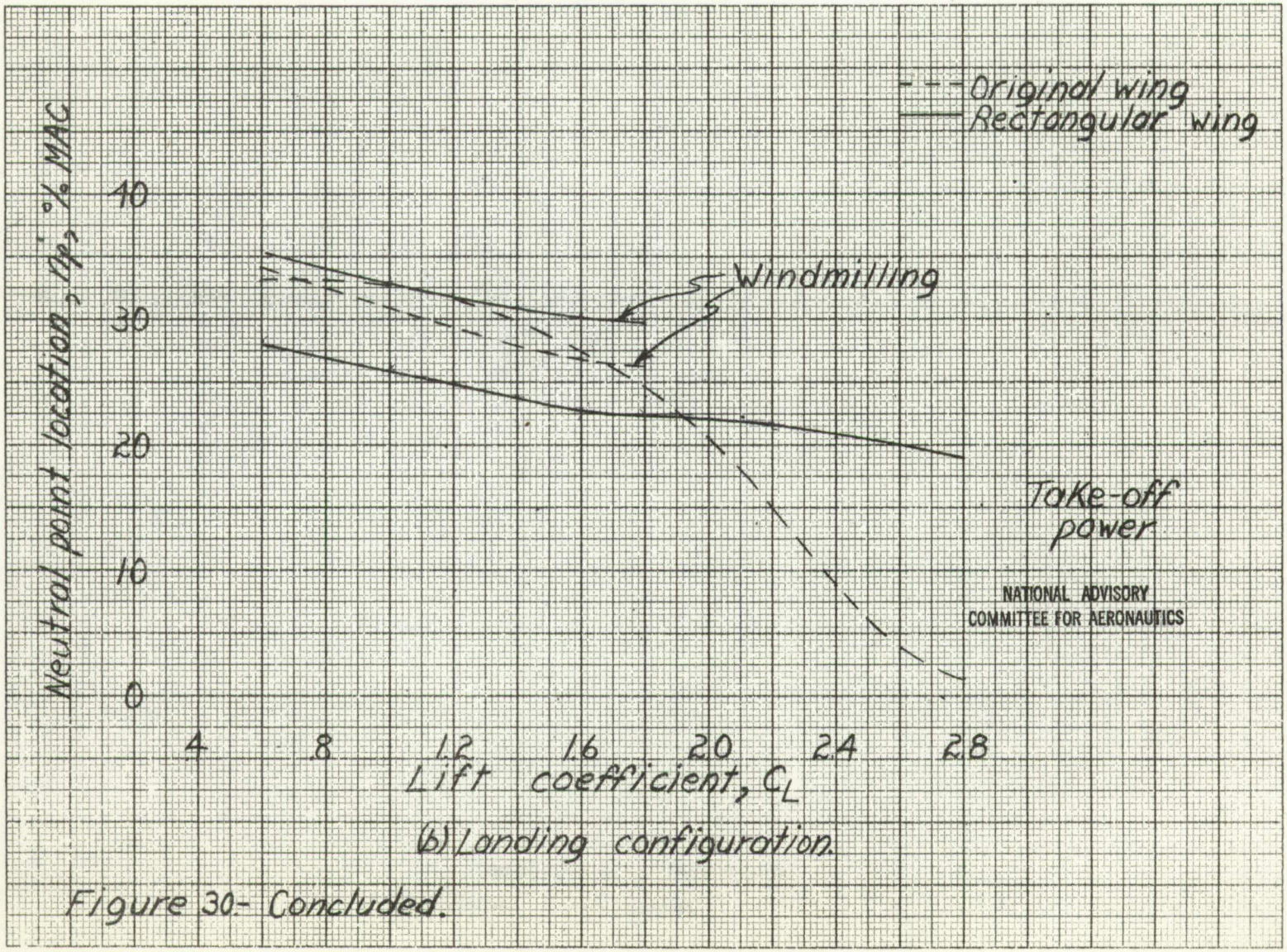

(b) Landing configuration.

Figure 30.- Concluded.

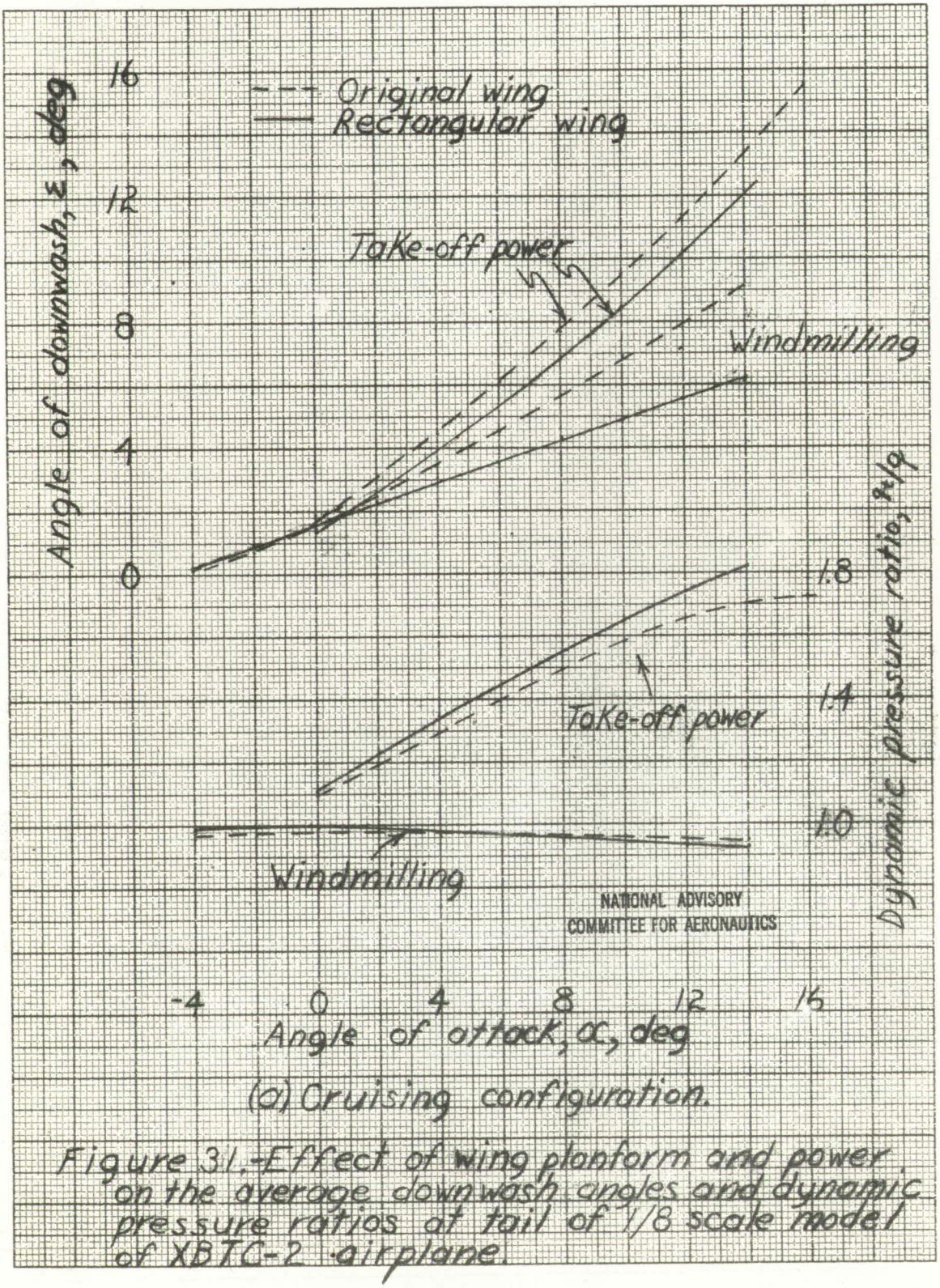

(a) Cruising configuration.

Figure 31.-Effect of wing planform and power on the average downwash angles and dynamic pressure ratios at tail of 1/8 scale model of XBTC-2 airplane.

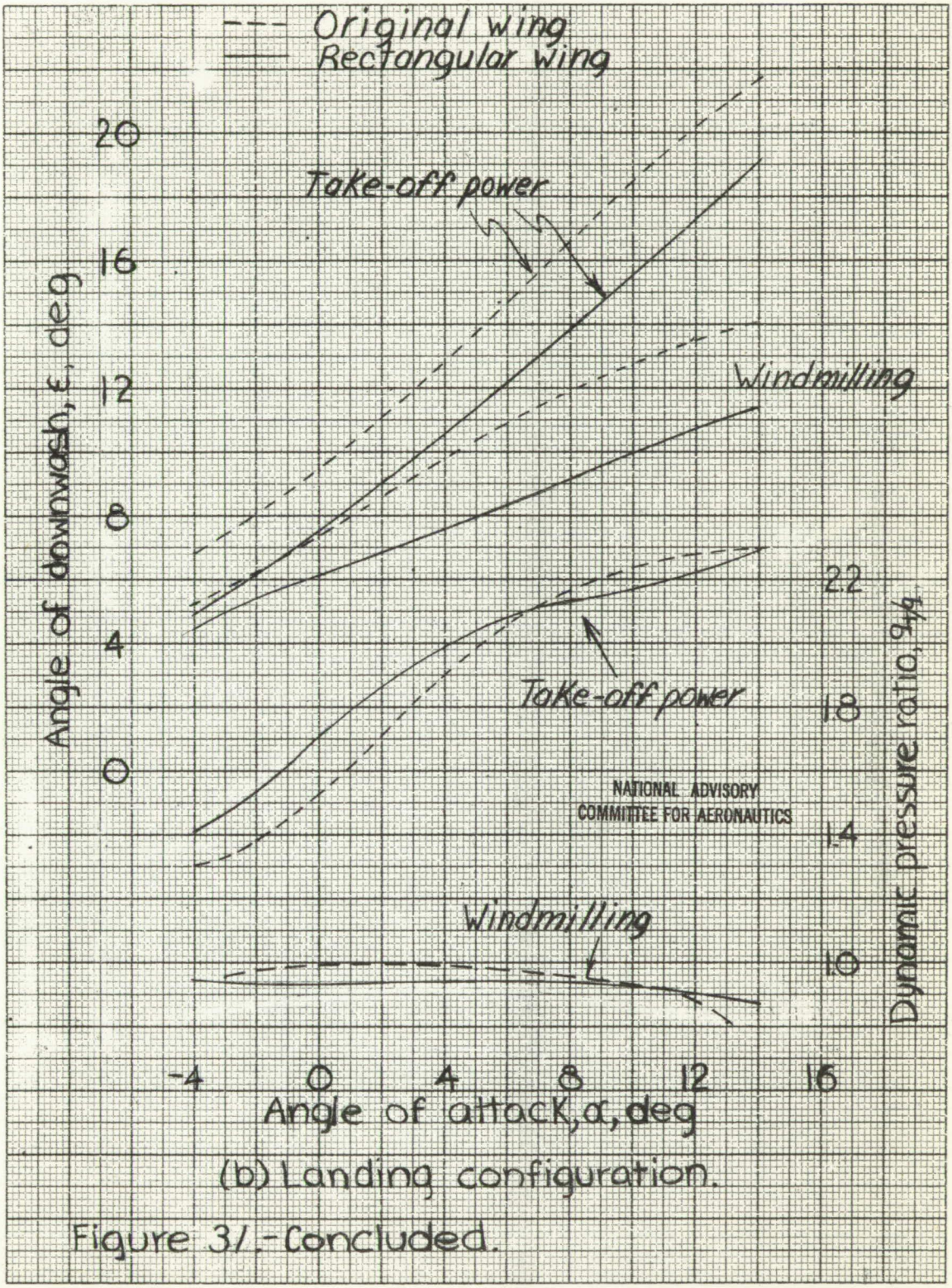

(b) Landing configuration.

Figure 31.- Concluded.

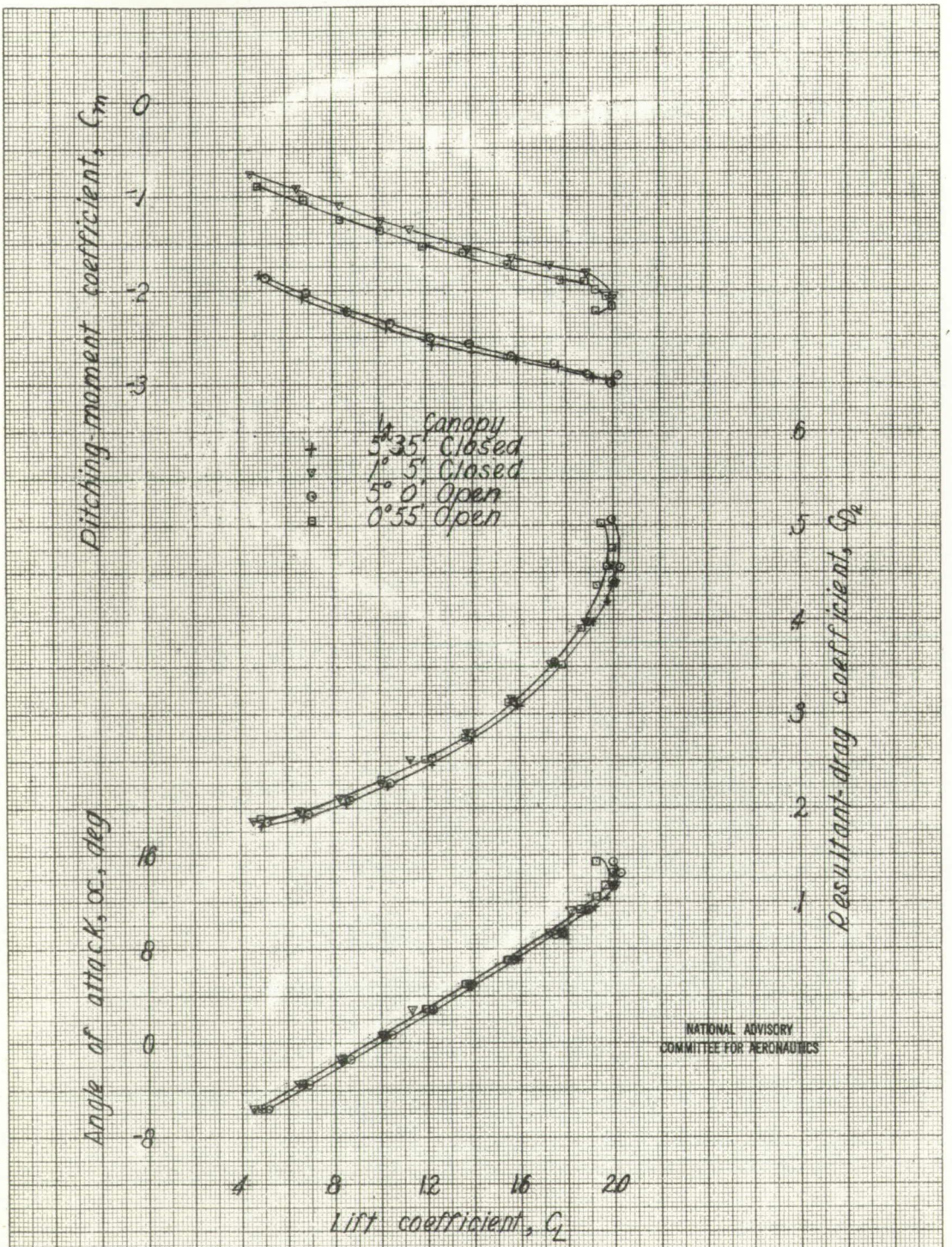

(a) Windmilling.

Figure 32. - Effect of opening the canopy on the aerodynamic characteristics in pitch of the 1/8-scale model of the XBTC-2 airplane. Landing configuration, Original H. T.,

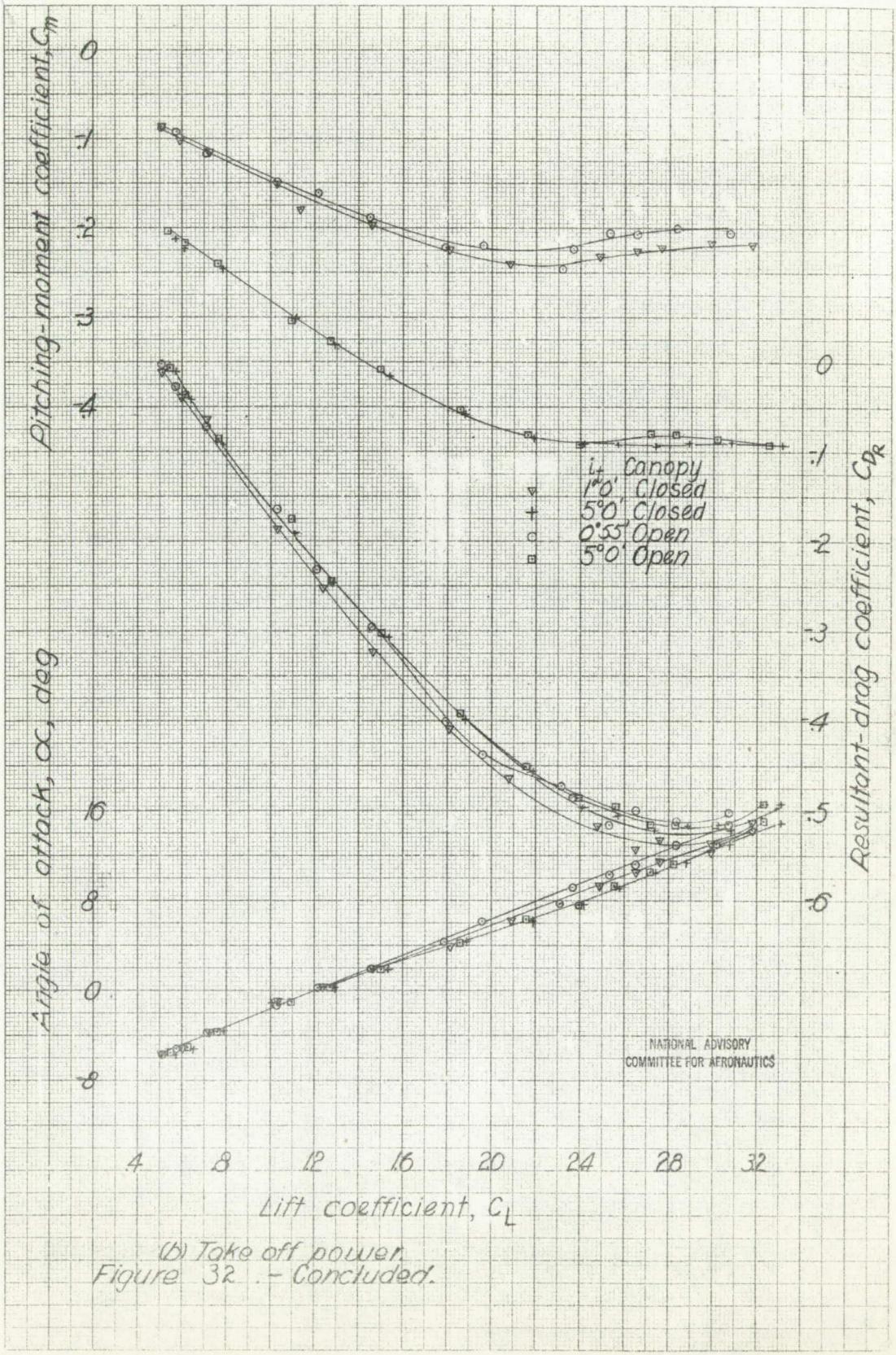

(b) Take off power.

Figure 32 .- Concluded.

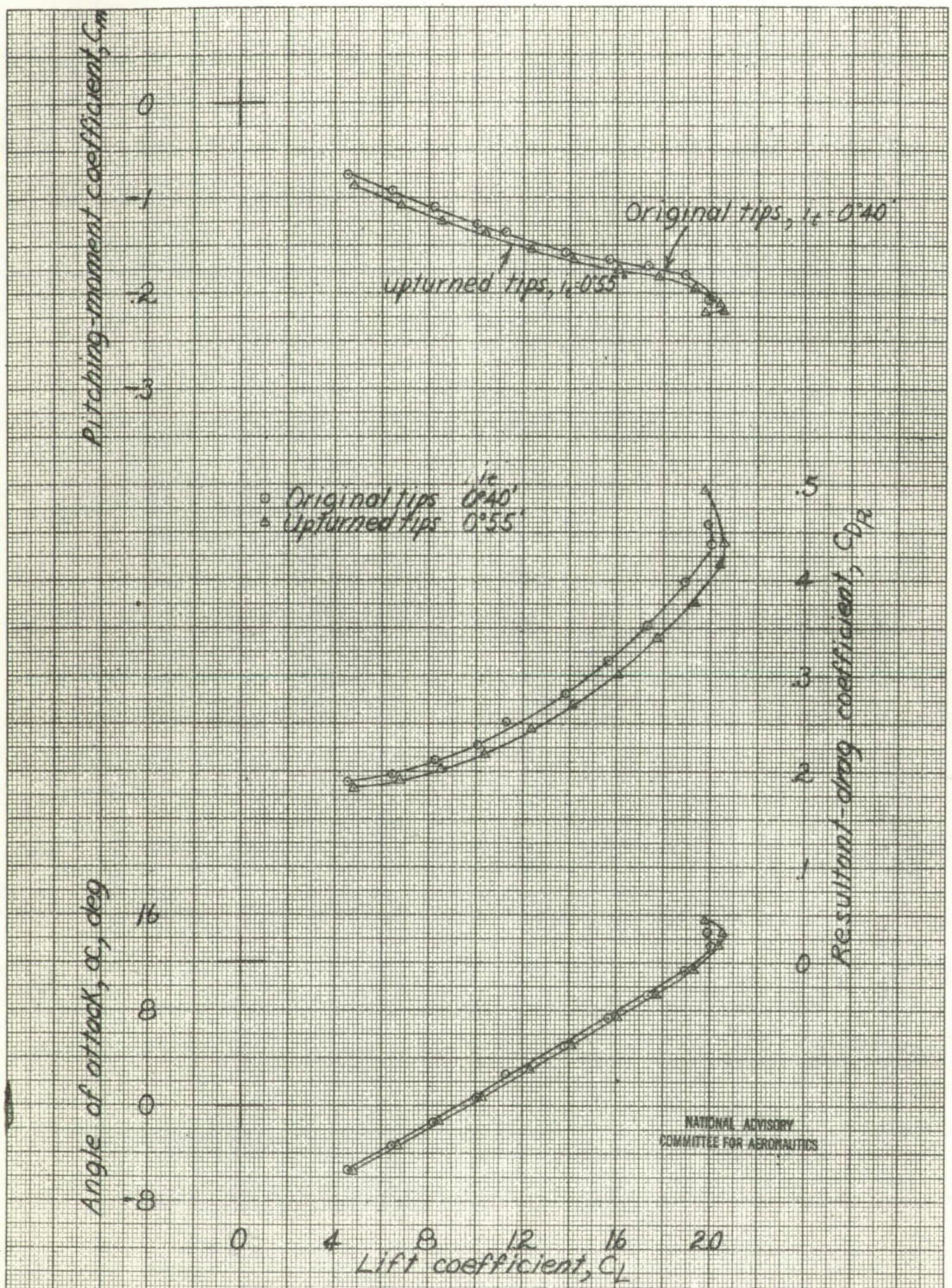

Figure 33- Effect of upturned wing tips on the aerodynamic characteristics in pitch on the 1/8 scale model of the XBTC-2 airplane. Landing configuration; windmilling.

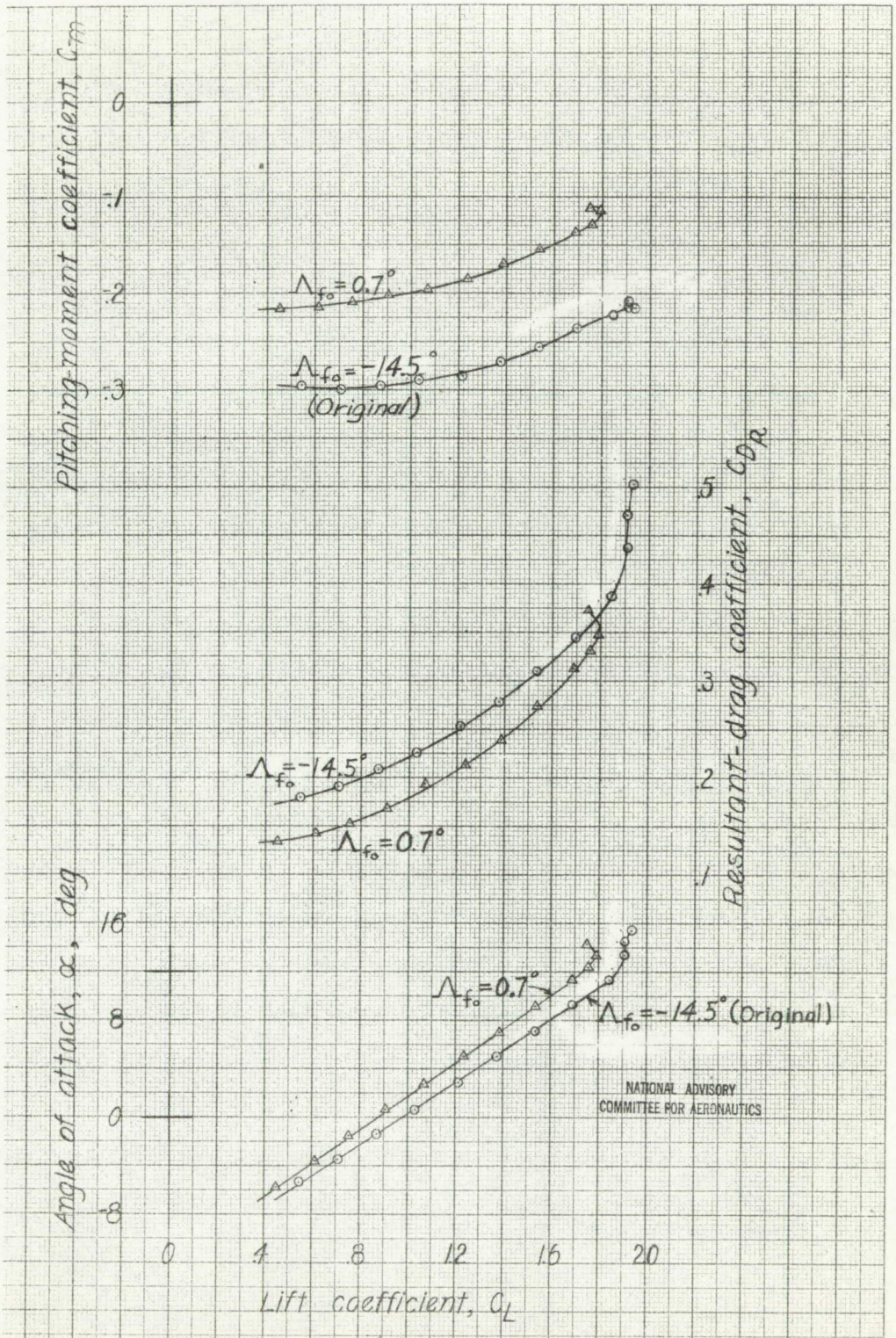

(a) Propeller windmilling.

Figure 34.- Effect of skewing the outboard flaps on the aerodynamic characteristics in pitch of the 1/8 scale model of the XBTC-2 airplane. Landing configuration; Tail off. Inboard slot open

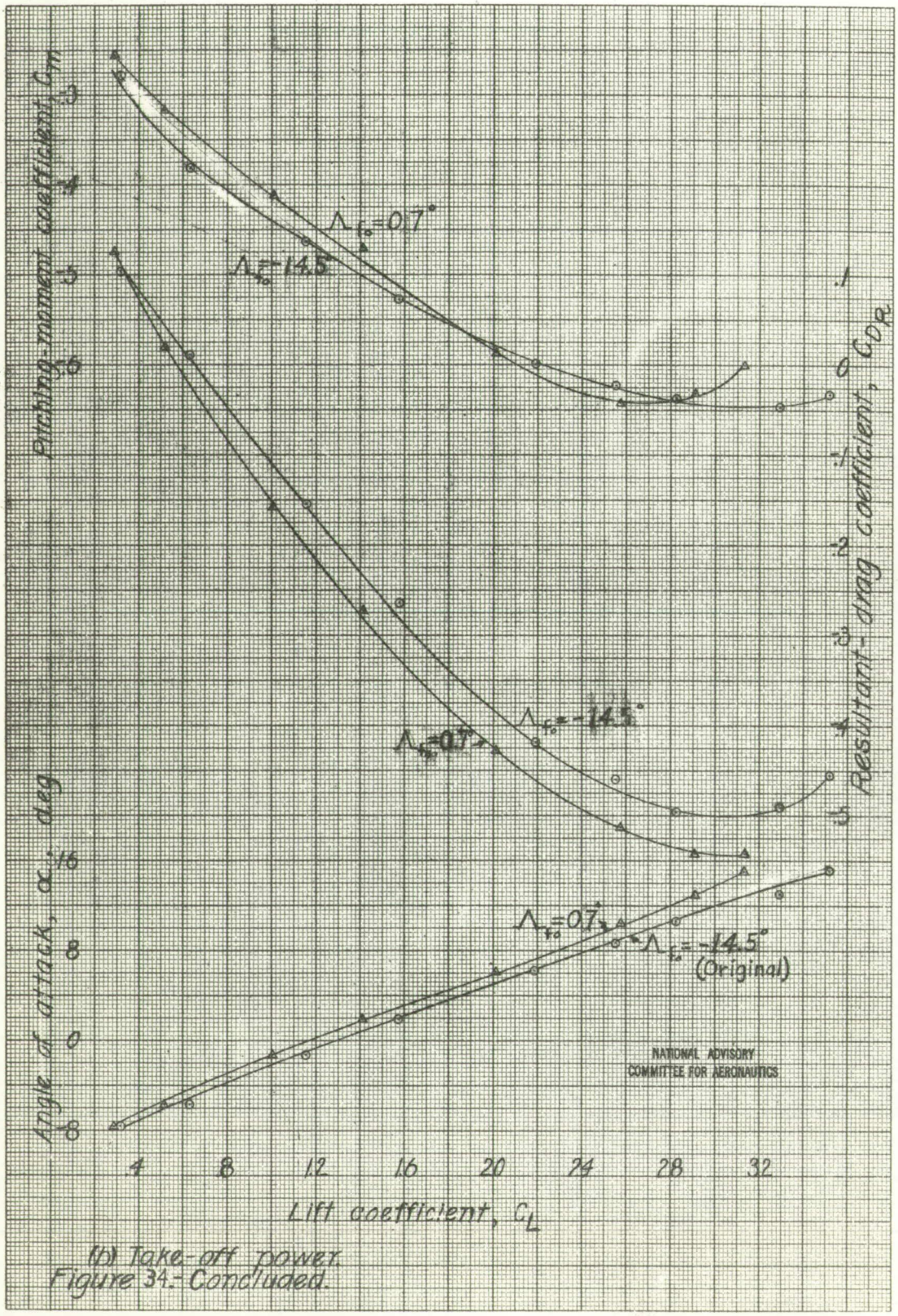

(b) Take-off power.

Figure 34.- Concluded.

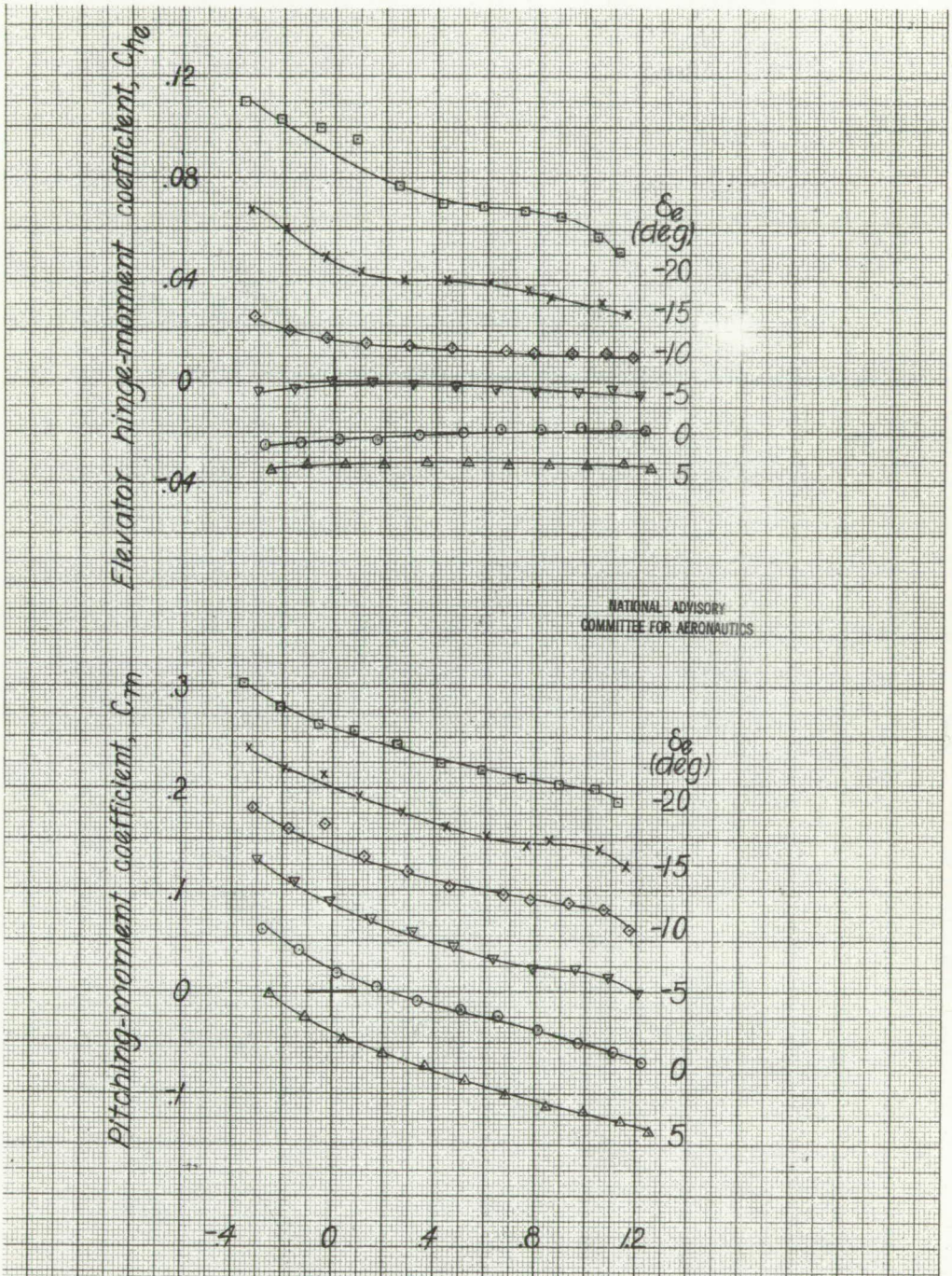

(a) Cruising configuration.

Figure 35.-Effect of elevator deflection on the aerodynamic characteristics in pitch of the 1/8 scale model of the XBTC-2 airplane. Windmilling; Original H.T. configuration; $i_t = +1°$

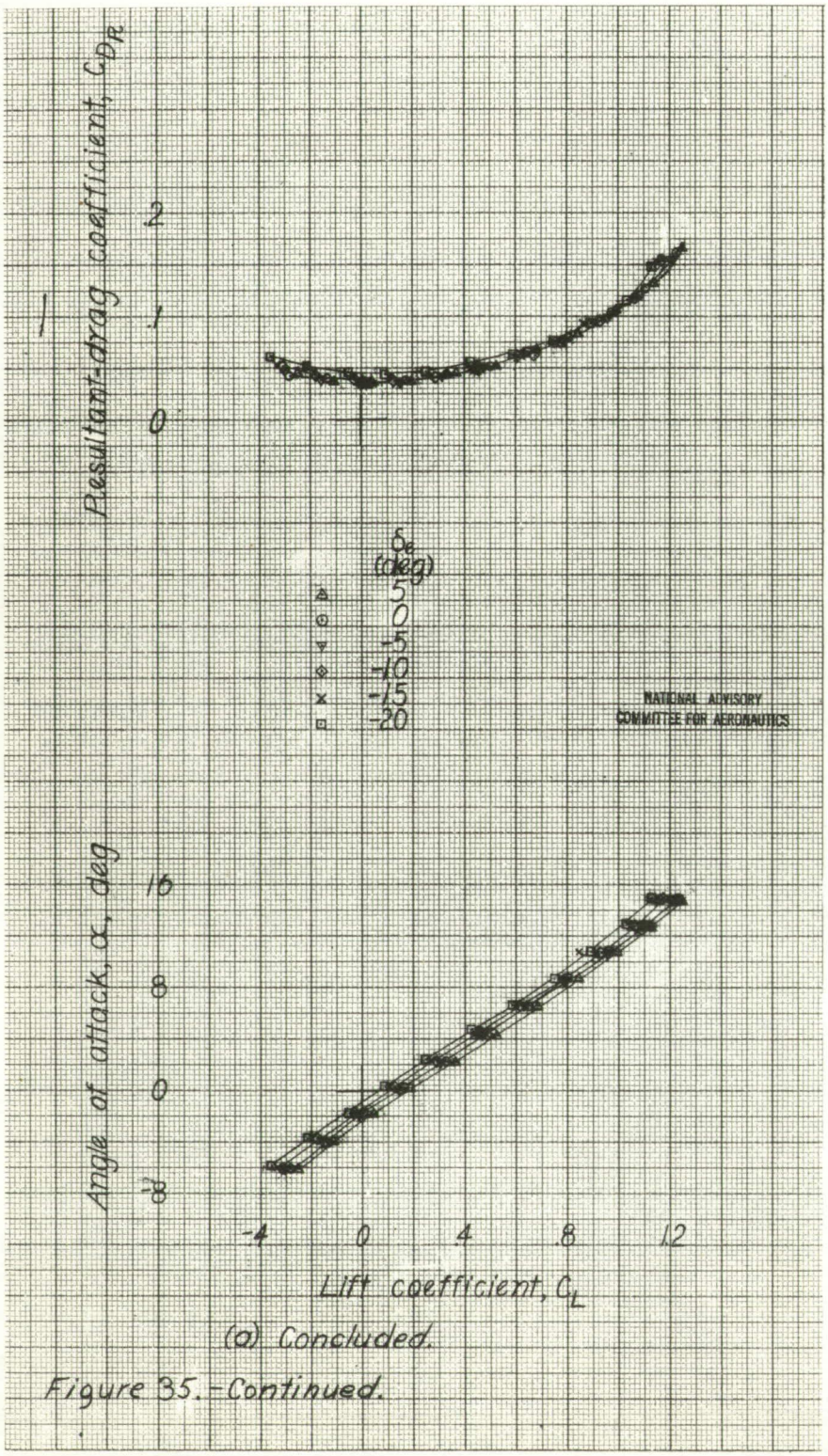

(a) Concluded.

Figure 35.- Continued.

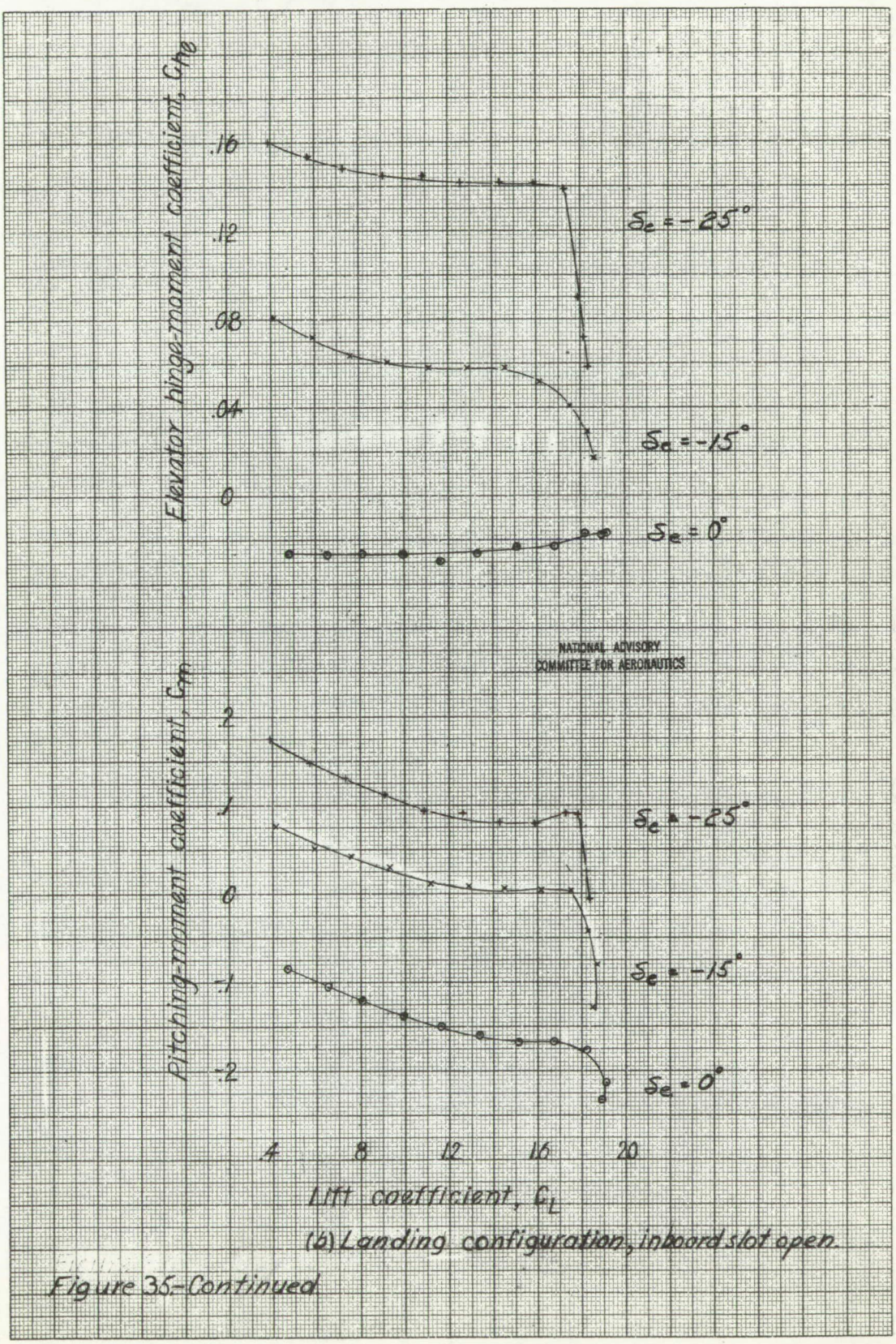

(b) Landing configuration, inboard slot open.

Figure 35.-Continued

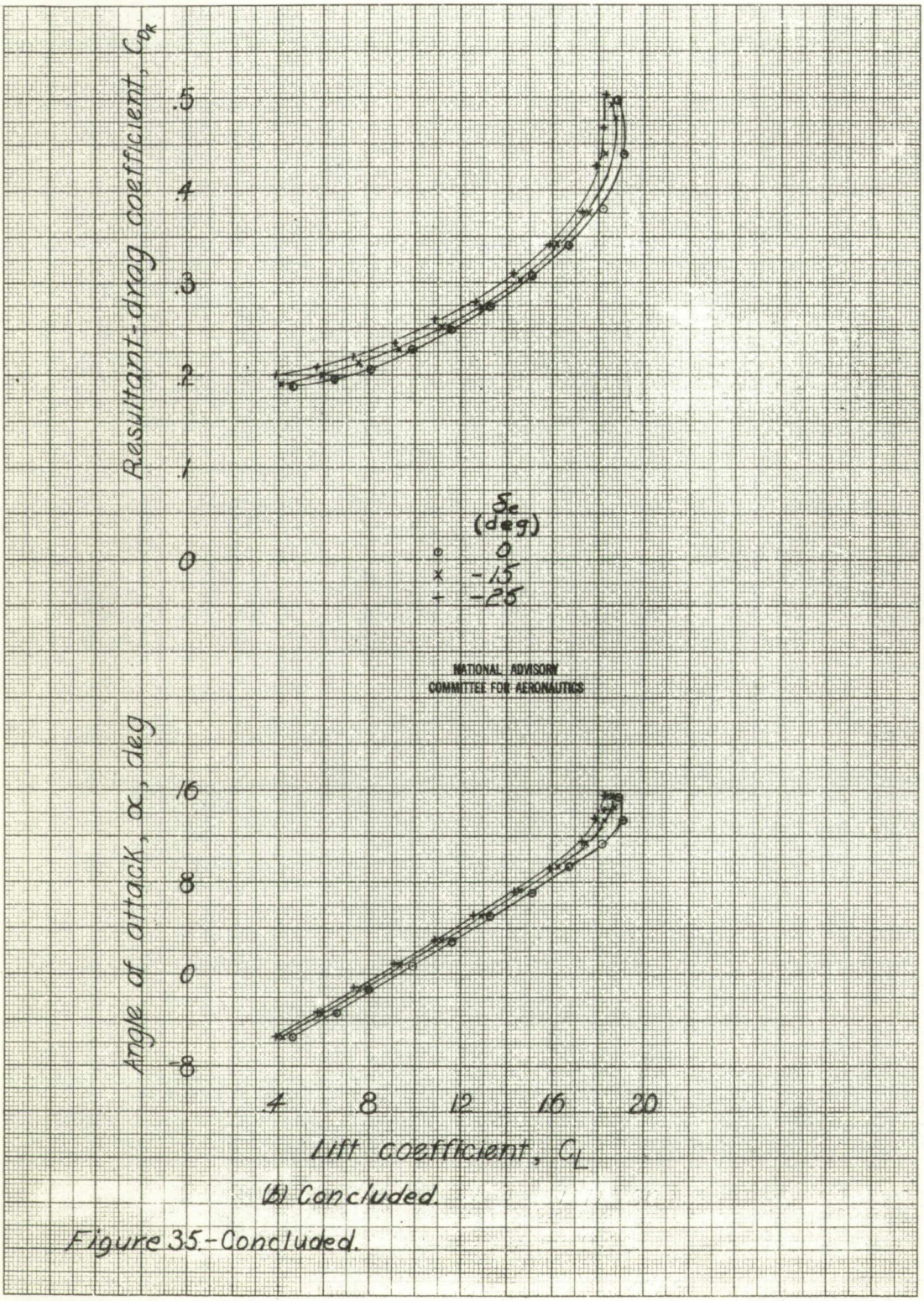

(b) Concluded.

Figure 35.- Concluded.

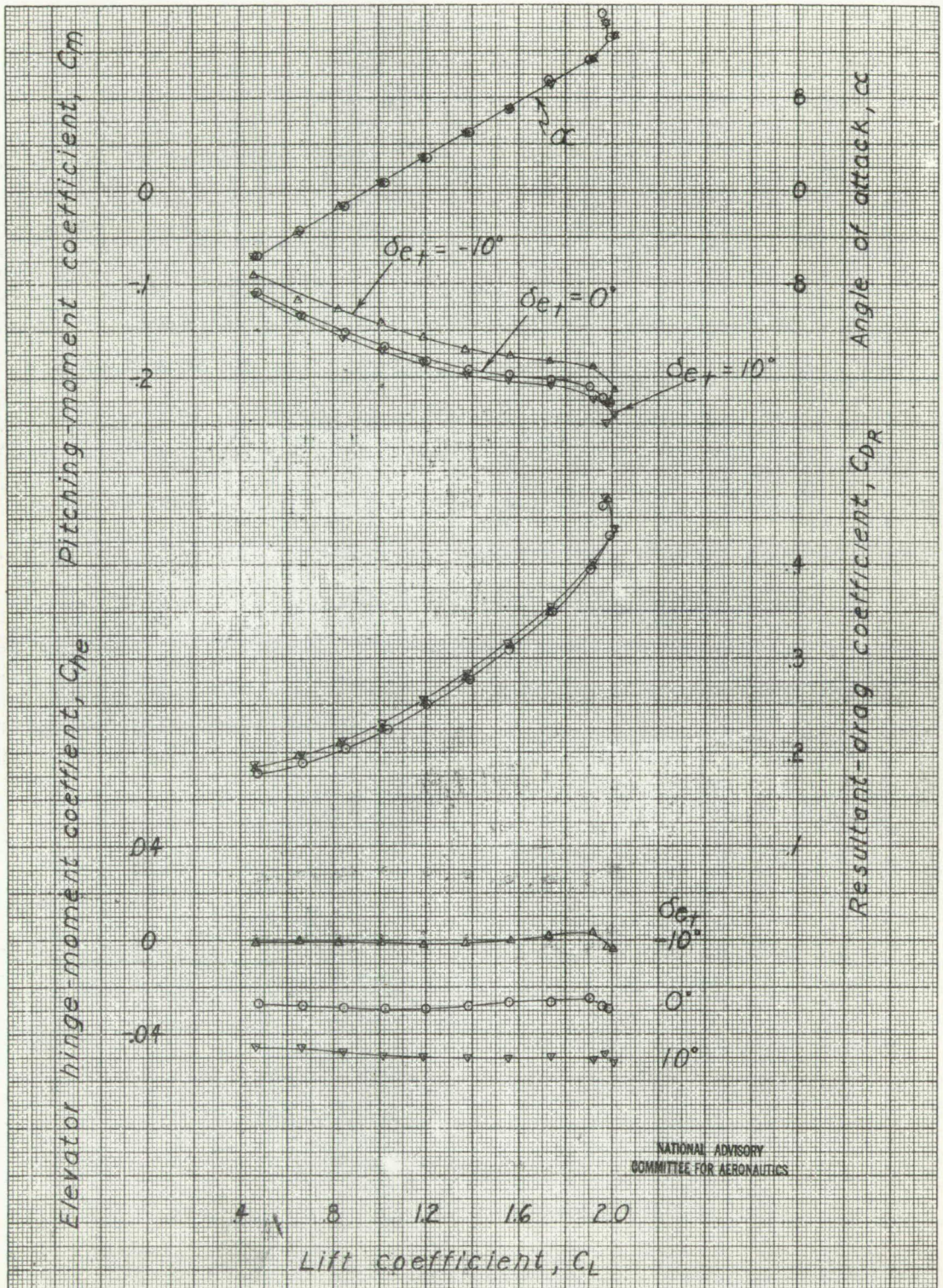

Figure 36.- Effect of elevator tab deflection on the aerodynamic characteristics in pitch of the 1/8 scale model of the XBTC-2 airplane. Landing configuration; Inboard slot open; Original horizontal tail; Windmilling. $i_t \approx 1°$

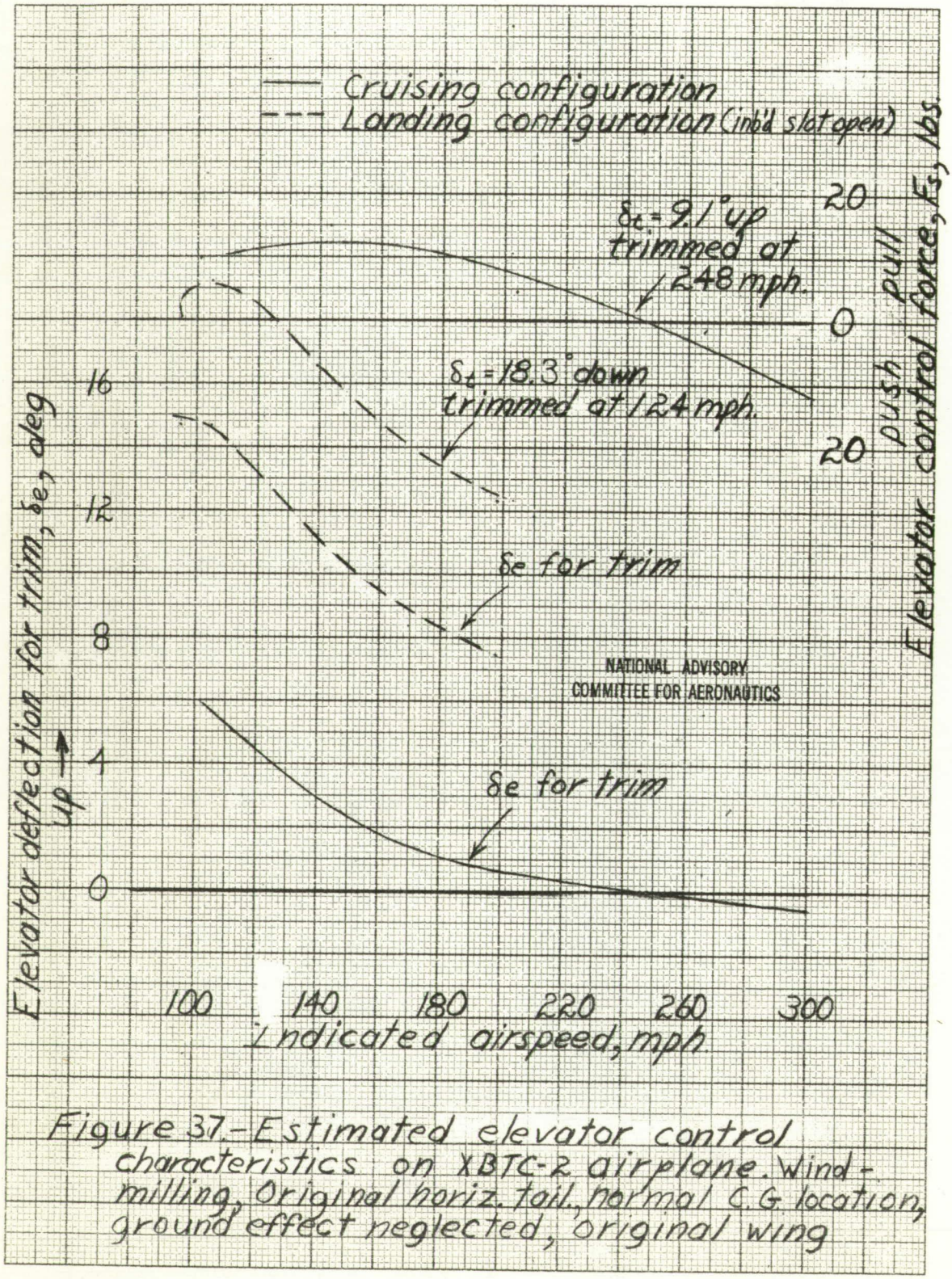

Figure 37.- Estimated elevator control characteristics on XBTC-2 airplane. Windmilling, original horiz. tail, normal C.G. location, ground effect neglected, original wing

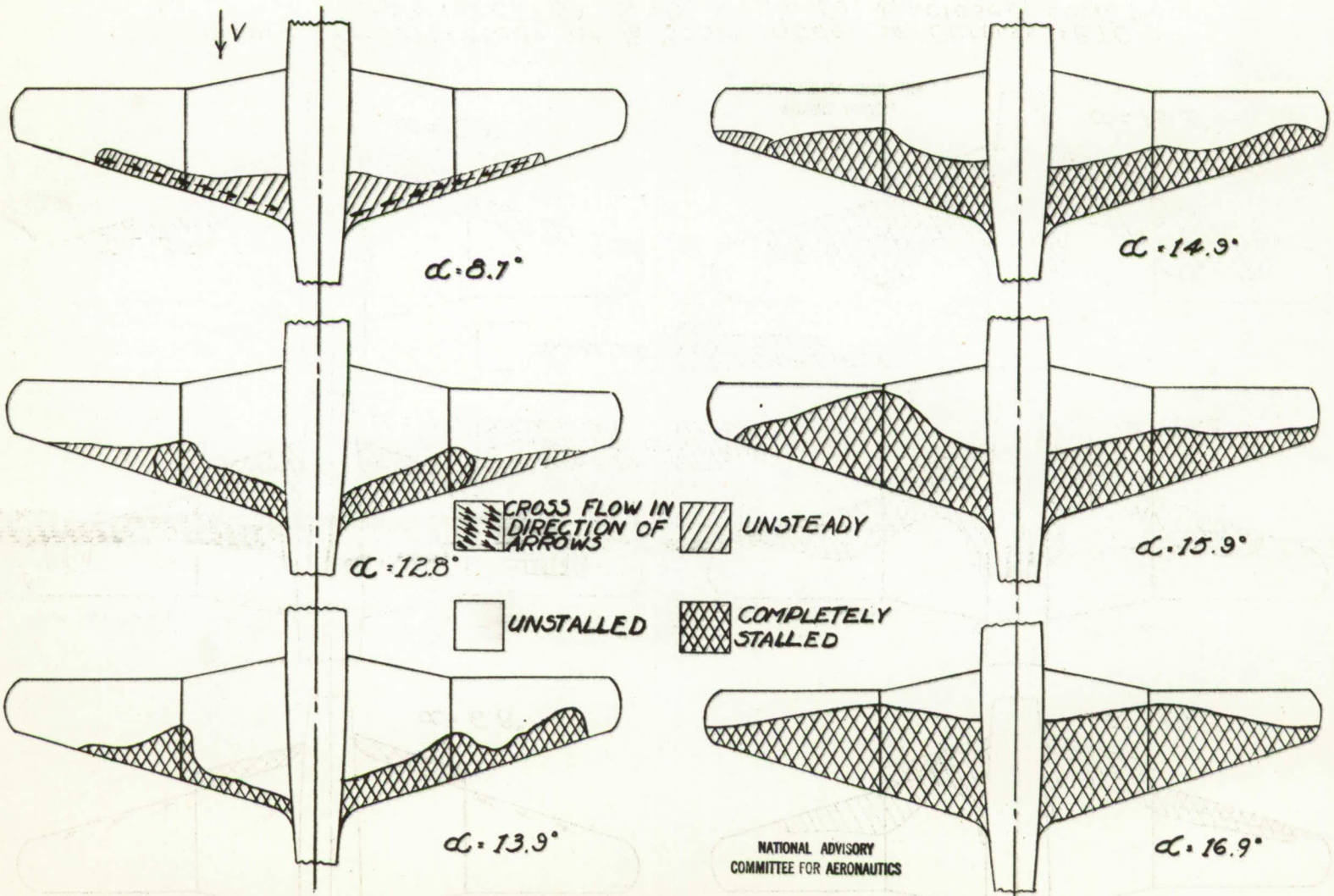

Figure 38.- Tuft study of 1/8 scale model of Curtiss XBTC-2 airplane. $\delta_{f_i} = 0$; $\delta_{f_o} = 0$; s_i = closed; s_o = closed; cowl flap closed; L.G. up, windmilling.

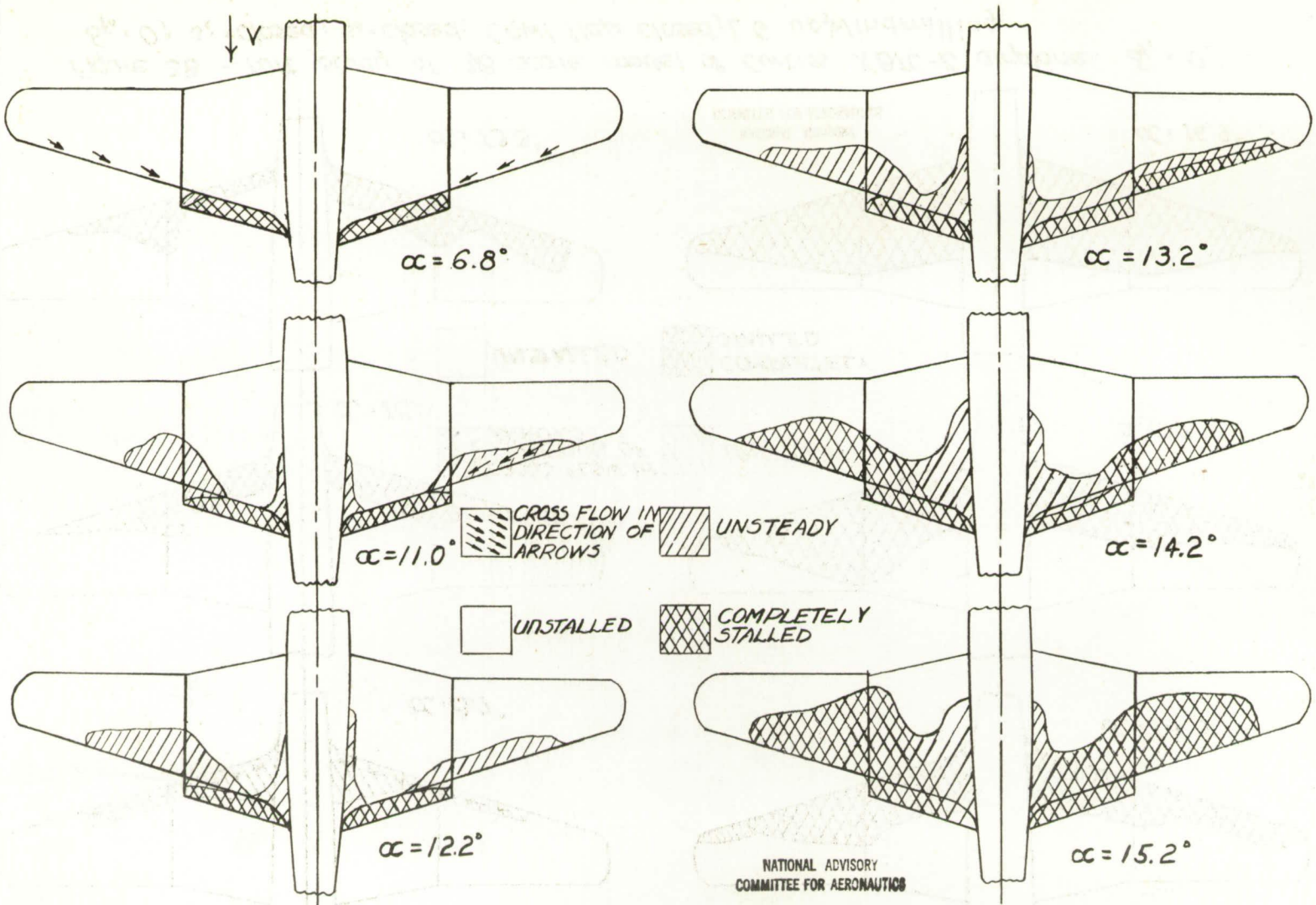

Figure 39.- Tutt study of 1/8 scale model of Curtiss XBTC-2 airplane. $\delta_{f_i} = 50$; $\delta_{f_o} = 0$; s_i = closed; s_o = closed; cowl flap closed, L.G. up. Windmilling

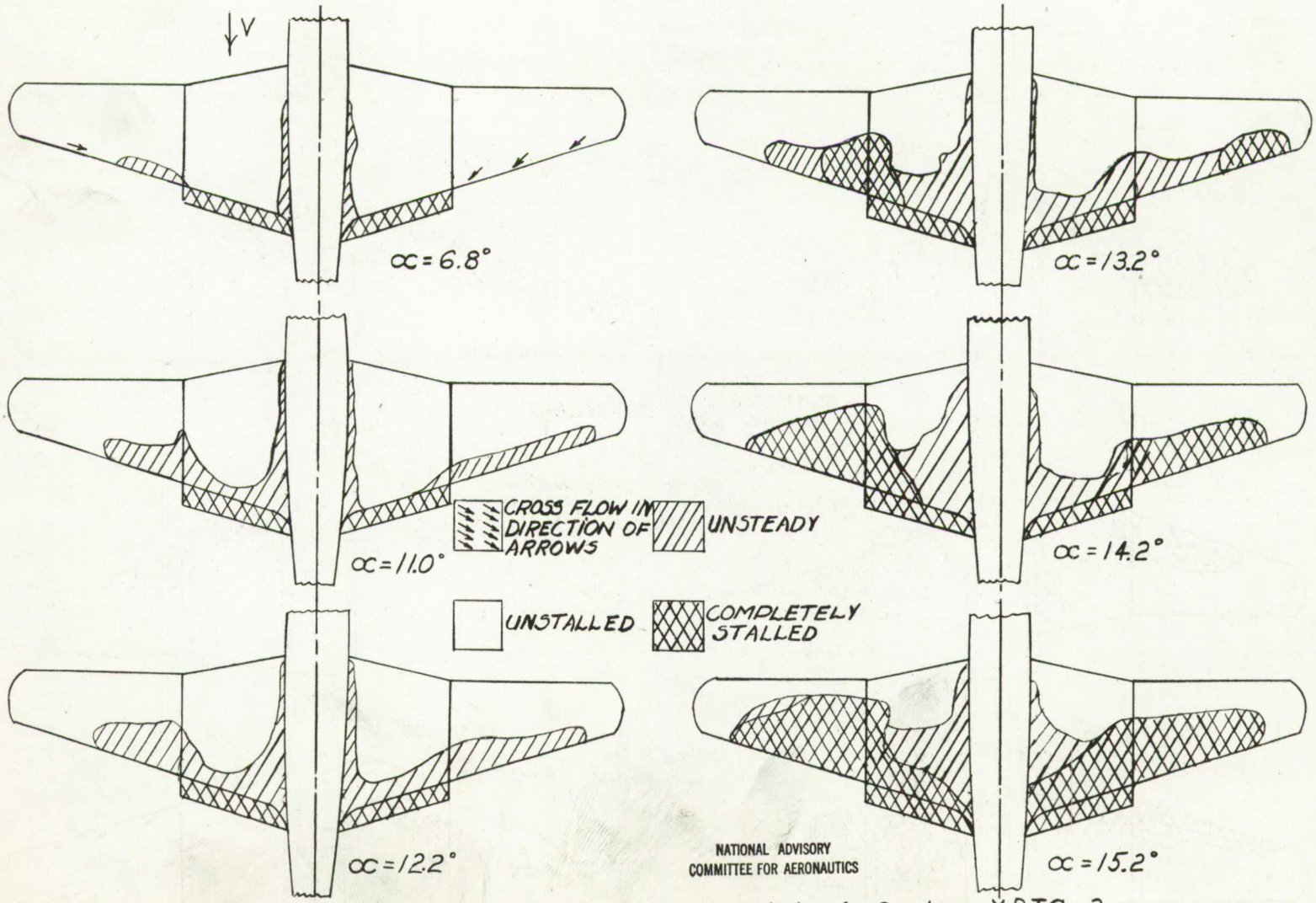

Figure 40.- Tuft study of the 1/8 scale model of Curtiss XBTC-2 airplane. $\delta_{t_i} = 50$; $\delta_{t_o} = 0$; s_i = closed; s_o = closed; cowl flap closed; L.G. down. Windmilling

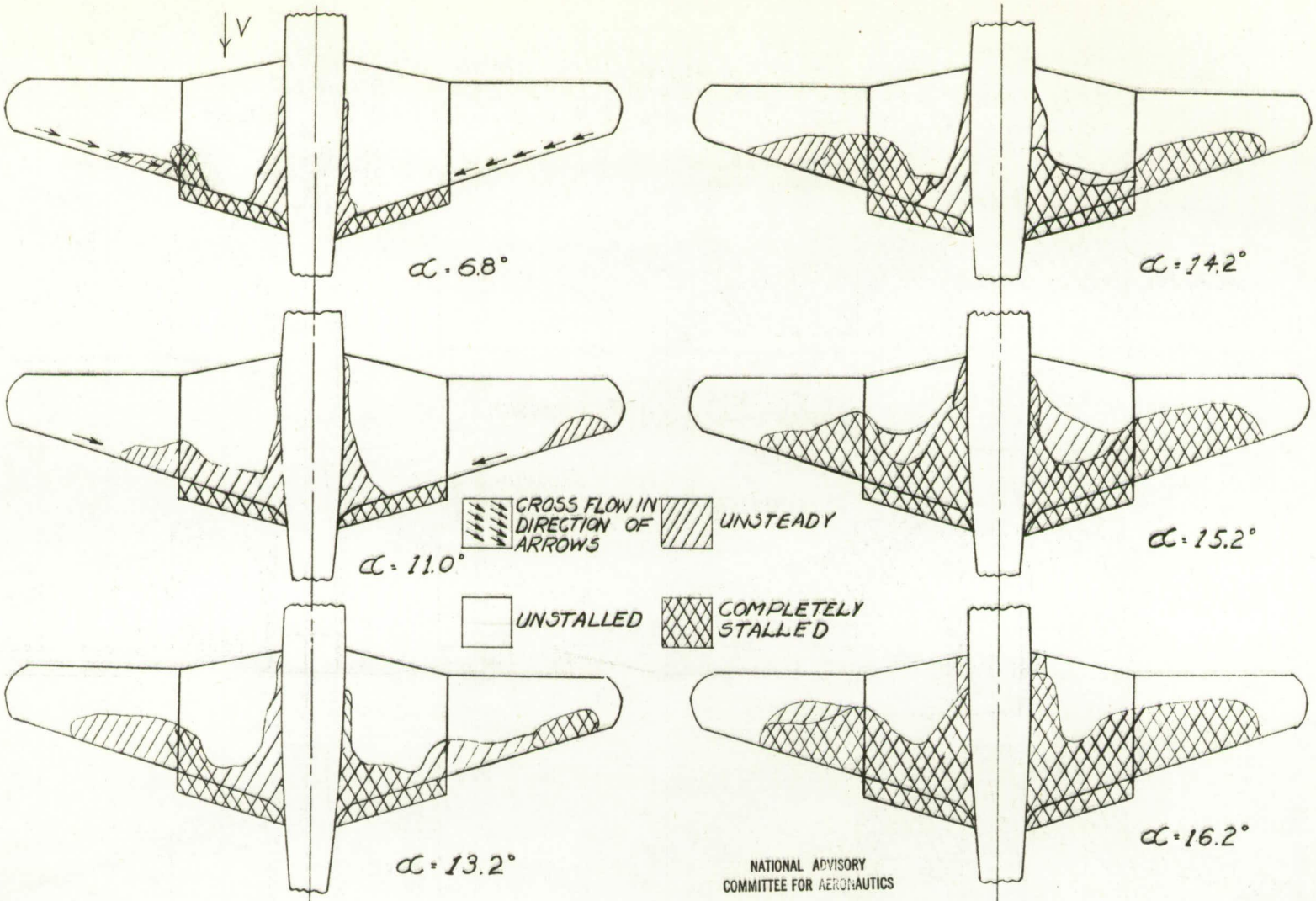

Figure 41.- Tuft study of 1/8 scale model of Curtiss XBTC-2 airplane. $\delta_{f_i} = 50$; $\delta_{f_o} = 0$; S_i = closed; S_o = closed, Cowl flap open; L.G. down. Windmilling.

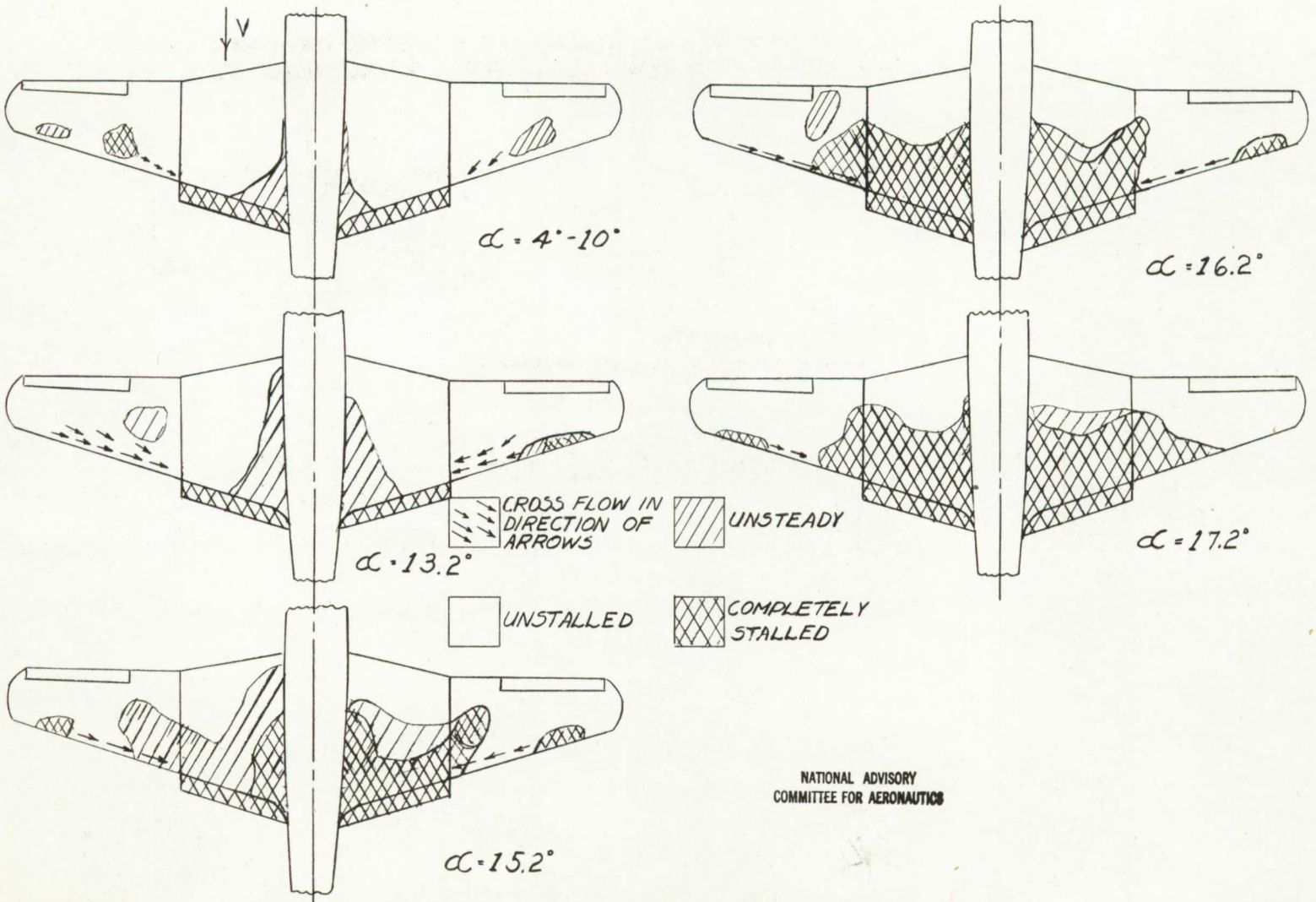

Figure 42 .- Tuft study of 1/8 scale model of Curtiss XBTC-2 airplane. $\delta_{f_i} = 50$; $\delta_f = 0$; s_i = closed; s_o = open; Cowl flap open; L.G. down. Windmilling

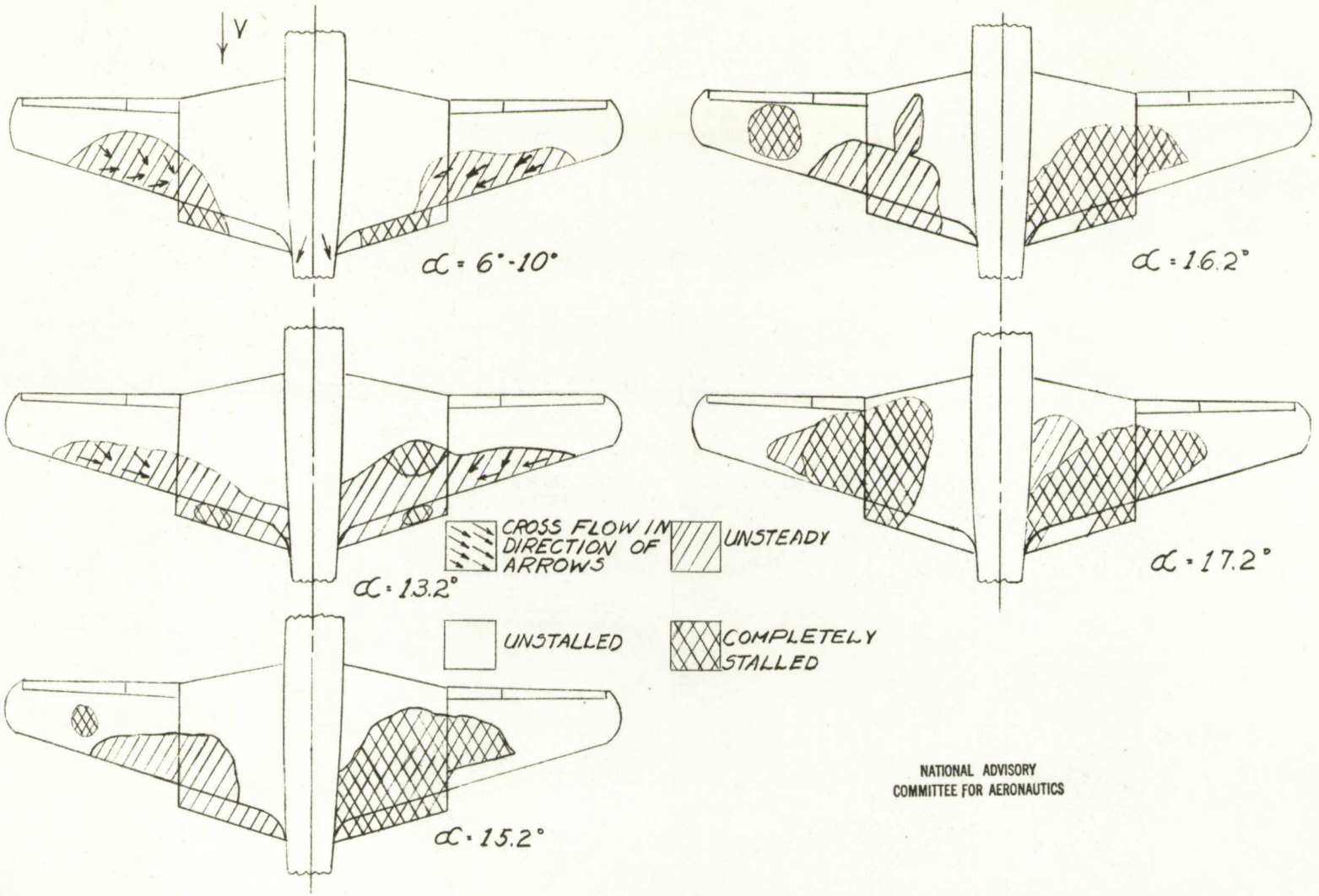

Figure 43.- Tuft study of 1/8 scale of model of Curtiss XBTC-2 airplane. $\delta_{f_i} = 50$ $\delta_{f_o} = 0$; s_i = open; s_o = open.; Cowl flap open; L.G. down. Windmilling

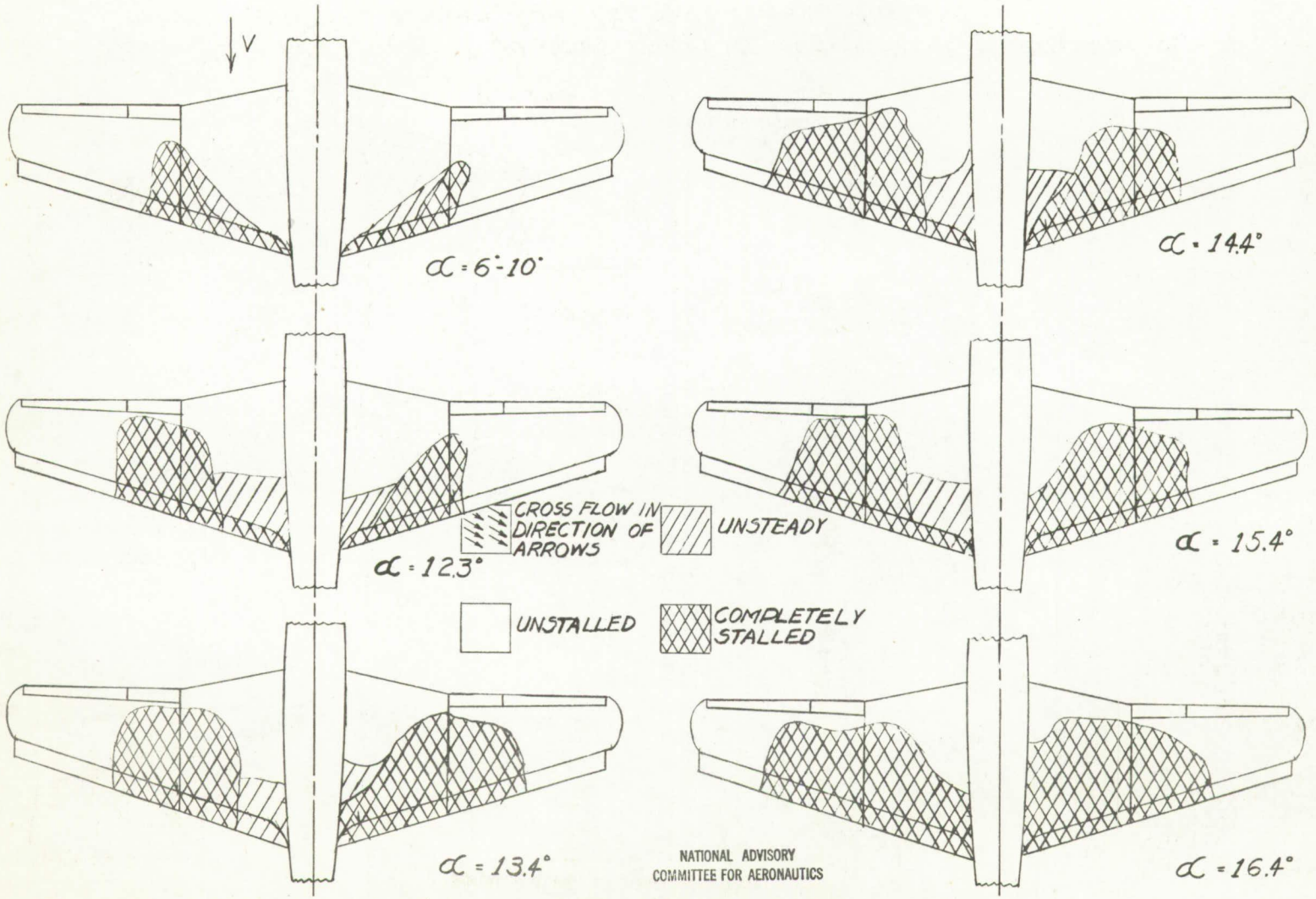

Figure 44 .- Tuft study of 1/8 scale model of Curtiss XBTC-2 airplane. $\delta_{f_i} = 50$; $\delta_{f_o} = 50$; s_i = open; s_o = open; Cowl flap open; L.G. down. Windmilling.

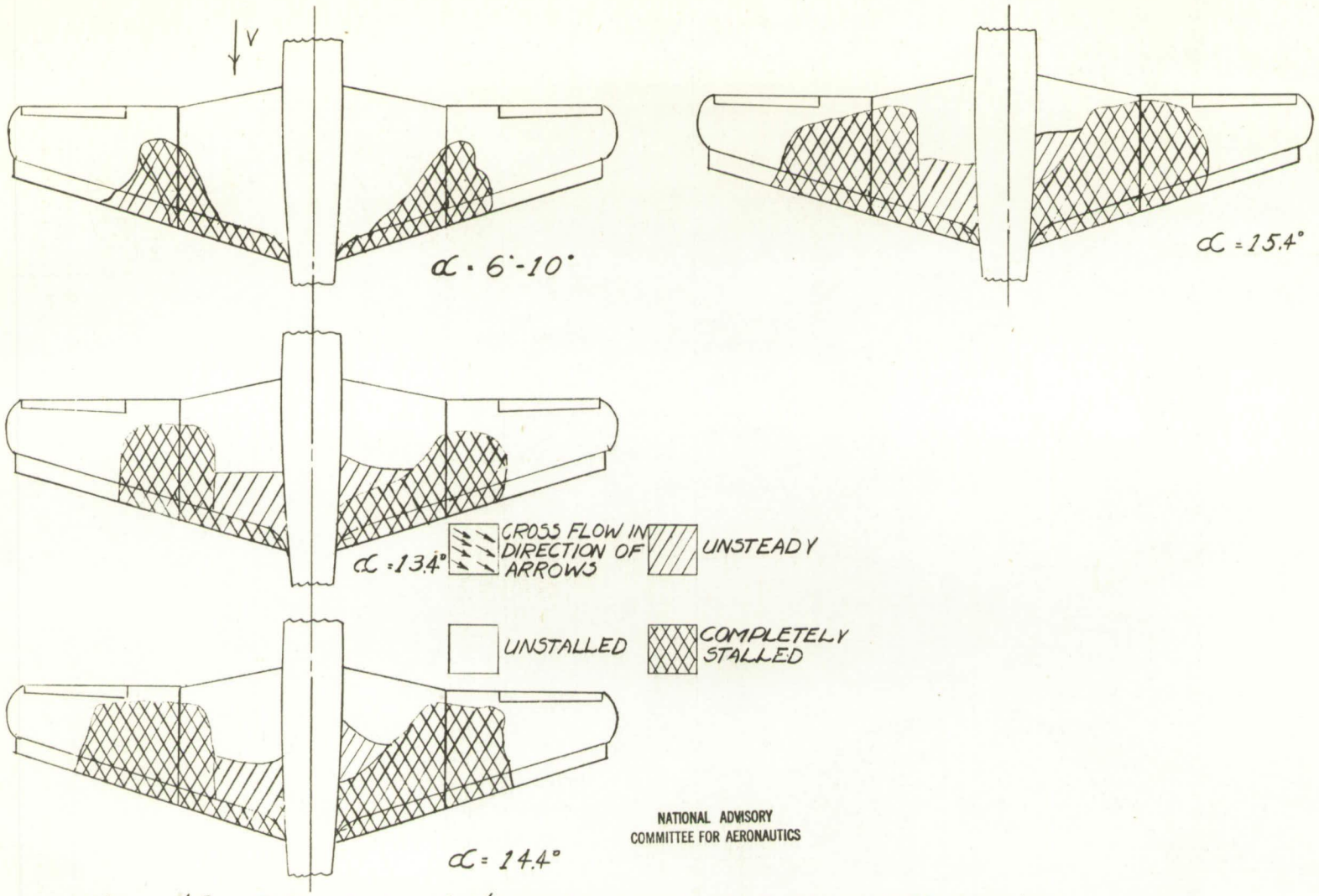

Figure 45. - Tuft study of 1/8 scale model of Curtiss XBTC-2 airplane. $\delta_{f_i} = 50$; $\delta_{f_o} = 50$; s_i = closed; s_o = open; Cowl flap open L.G. down. Windmilling.

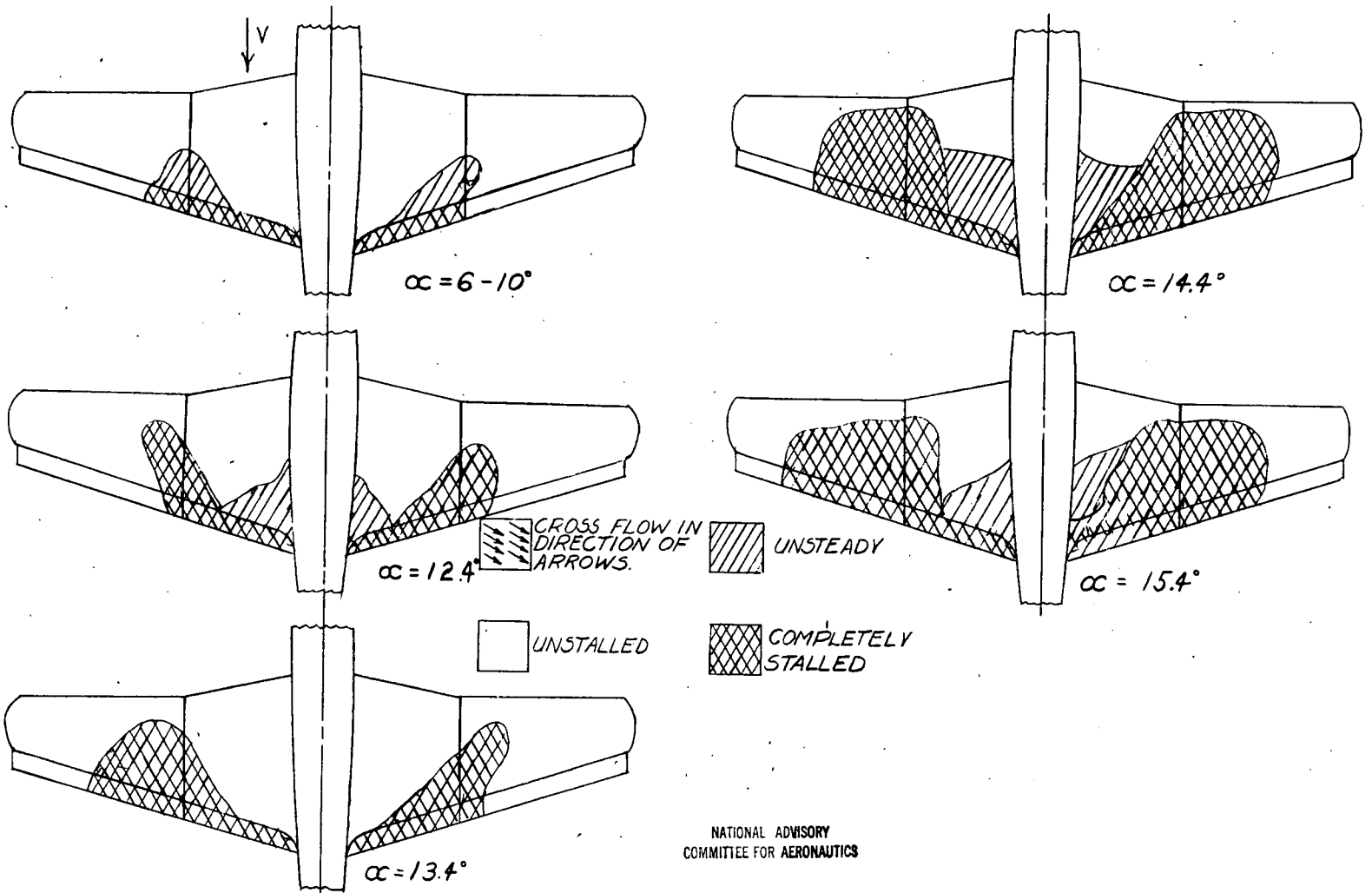

Figure 46.- Tuft study of 1/8 scale model of Curtiss XBTC-2 airplane. $\delta_f = 50$; $\delta_f = 50$; s_i = closed; s_o = closed cowl flap open; L.G. down. Windmilling.

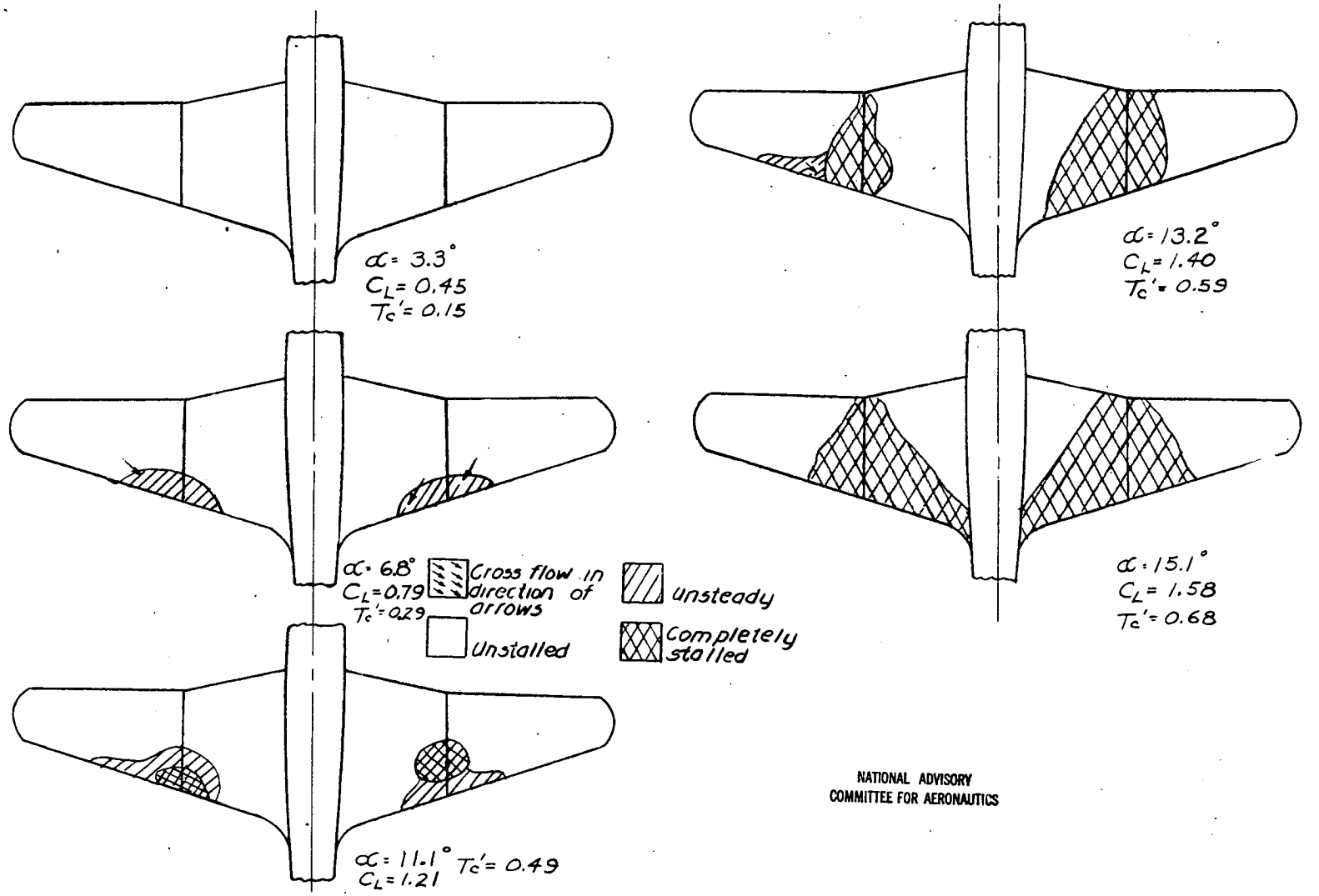

Figure 47.- Tuft study of 1/8-scale model of Curtiss XBTC-2 airplane $\delta_{f_i} = 0$, $\delta_{f_o} = 0$; s_i = closed, s_o = closed; cowl flap closed; L.G. up; Take-off power.

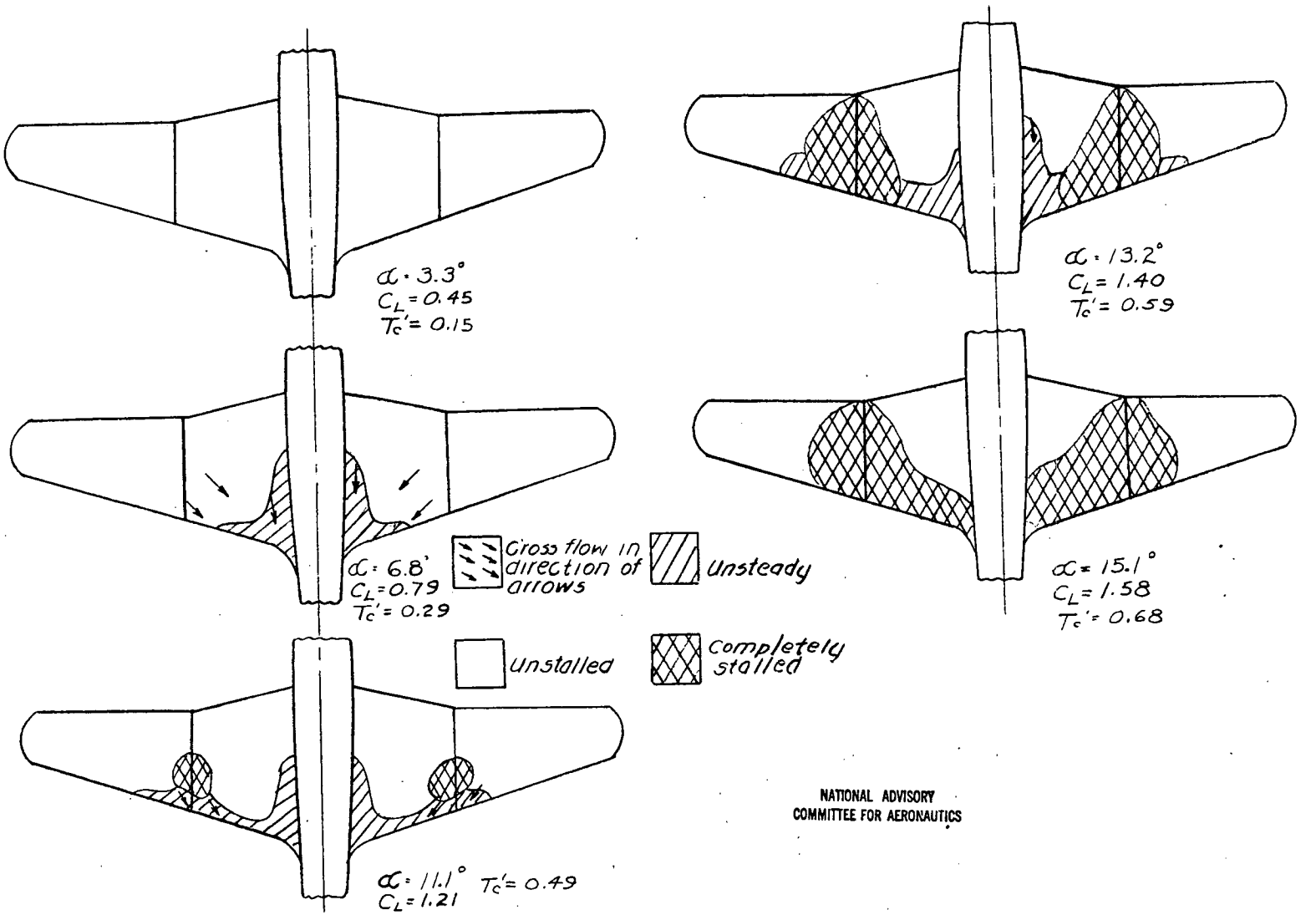

Figure 48.- Tuft study of 1/8-scale model of Curtiss XBTC-2 airplane. $\delta_{f_i} = 0$, $\delta_{f_o} = 0$; s_i: closed, s_o: closed; Cowl flap open; L.G. up; Take-off power.

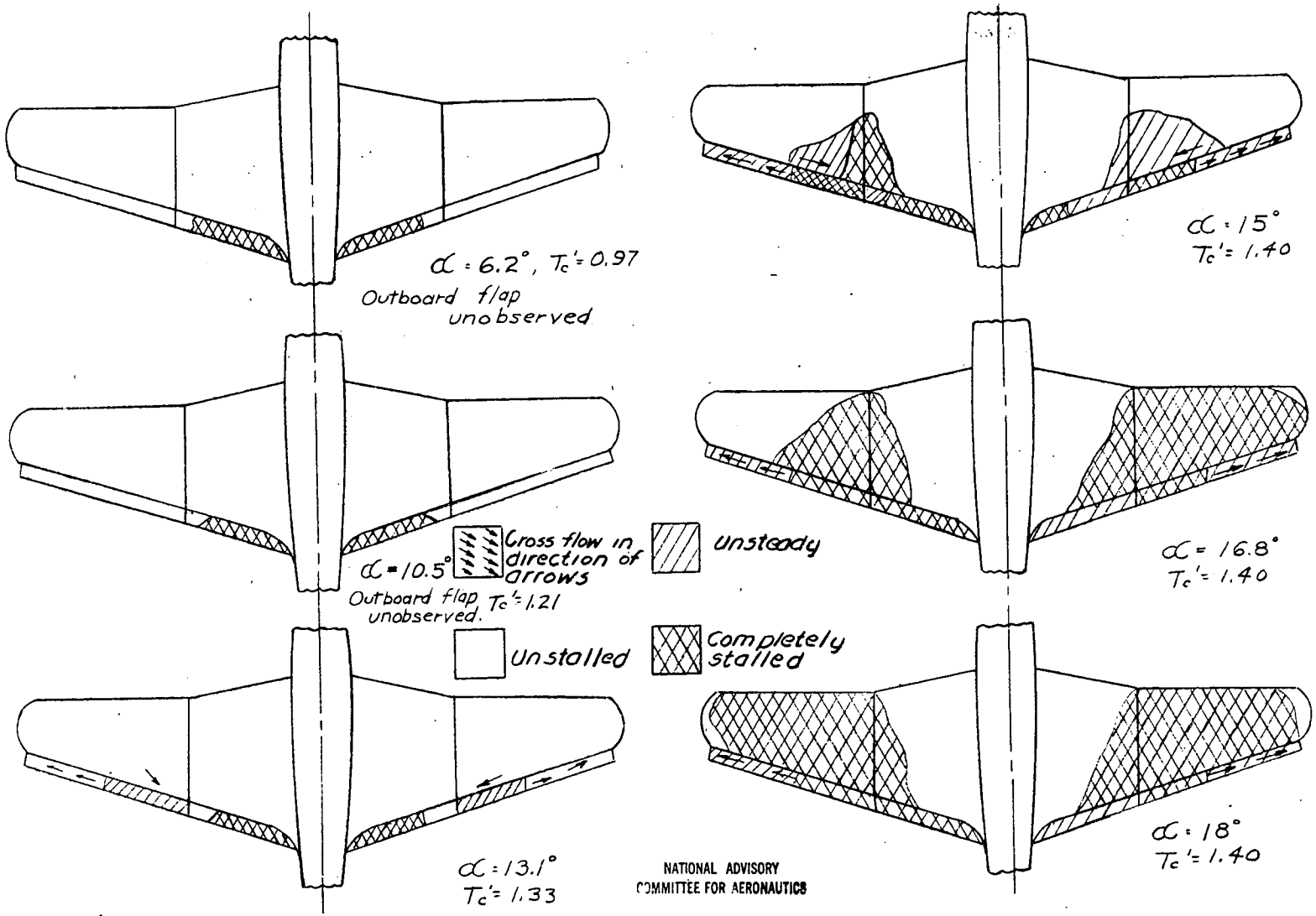

Figure. 49.- Tuft study of 1/8 scale model of Curtiss XBTC-2 airplane. δ_{f_i} = 50, δ_{f_o} = 50; S_i = closed, S_o = closed; Cowl flap open; L.G. down; Take-off power.

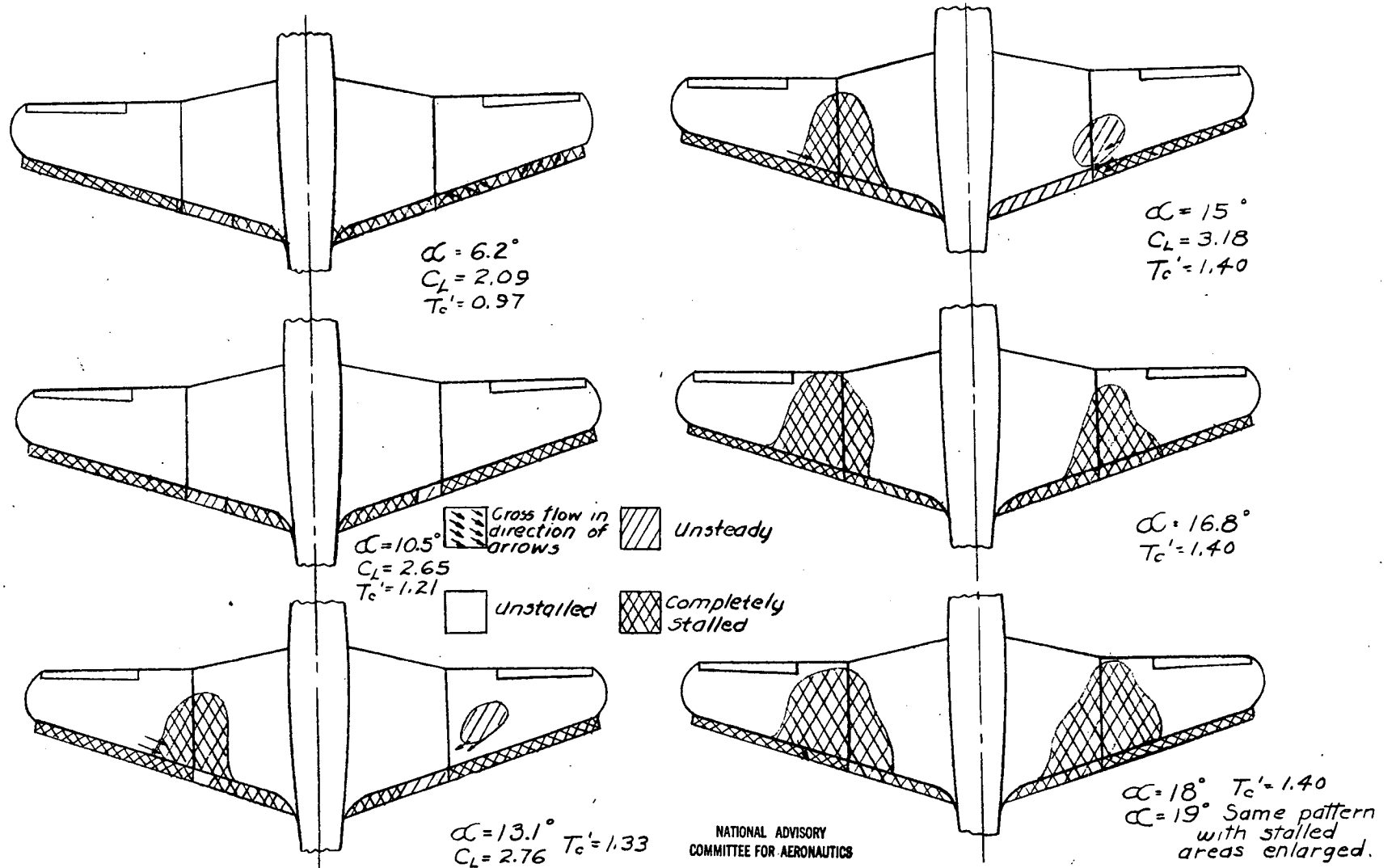

Figure 50. - Tuft study of 1/8-scale model of Curtiss XBTC-2 airplane. δ_{f_i} = 50, δ_{f_o} = 50; s_i = closed, s_o = open; Cowl flap open; L.G. down. Take-off power.

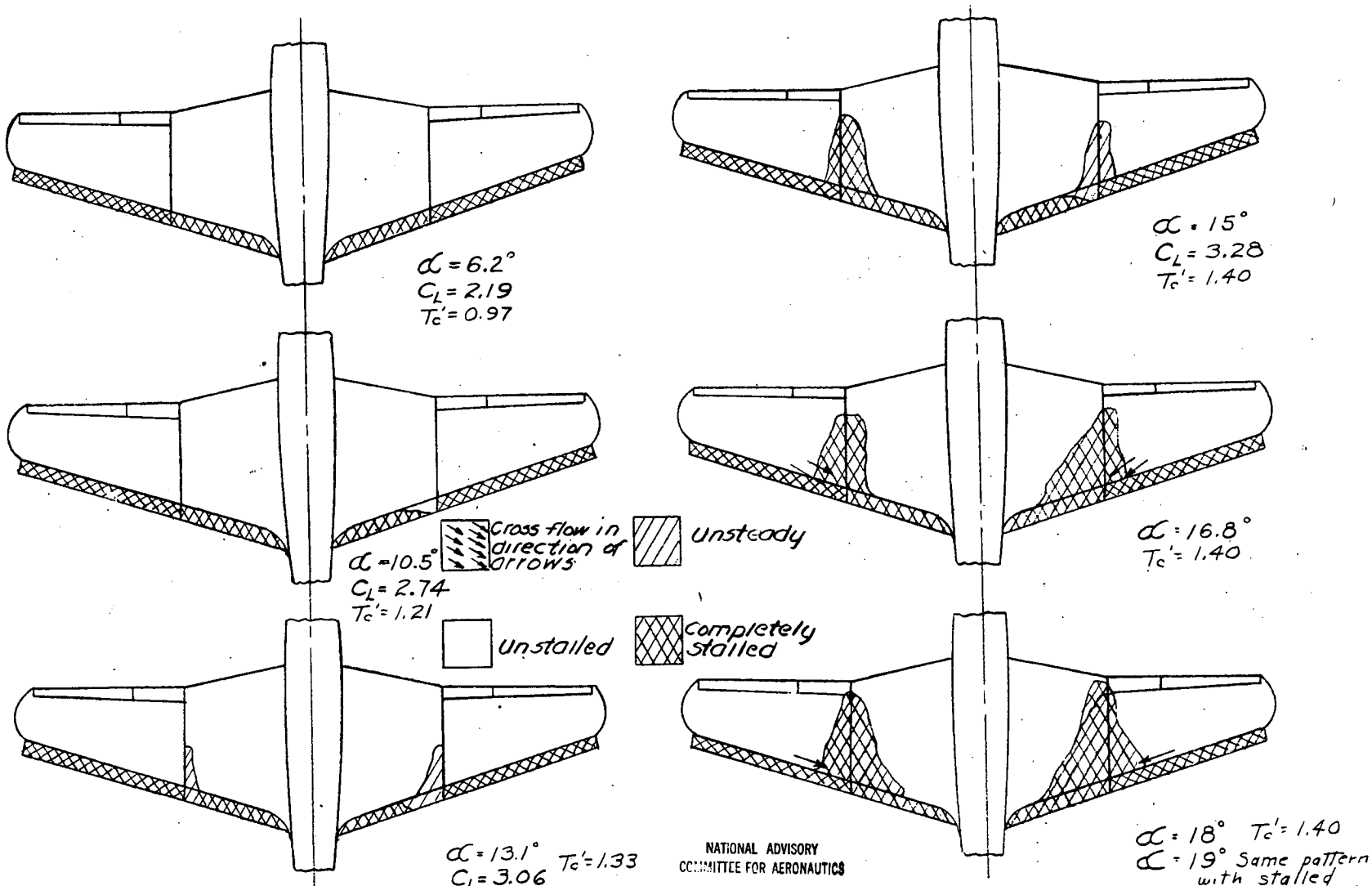

Figure 51.- Tuft study of 1/8 scale model of Curtiss XBTC-2 airplane δ_{f_i} = 50, δ_{f_o} = 50; s_i = open, s_o = open; Cowl flap open; L.G. down; Take-off power.

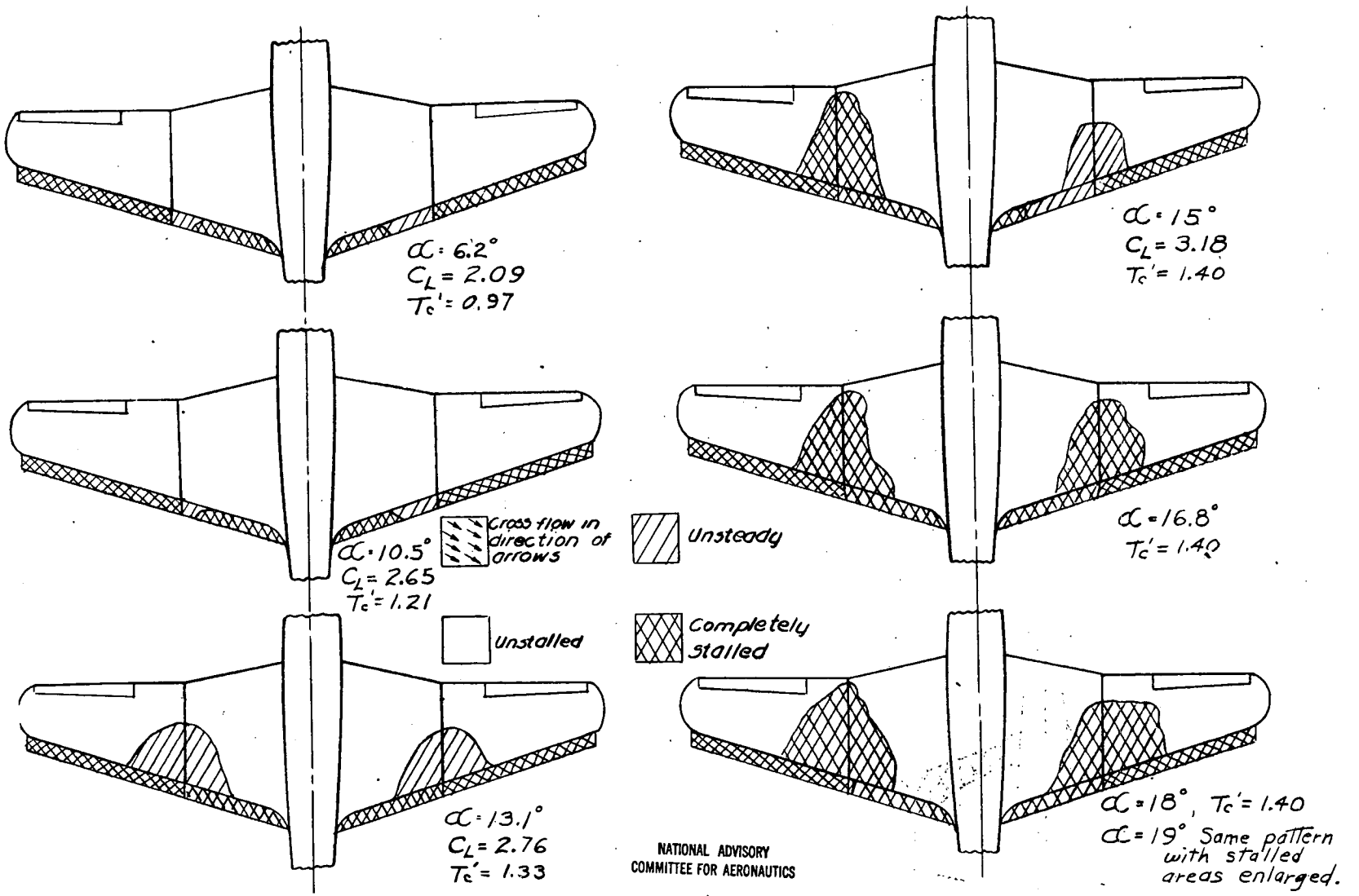

Figure 52.-Tuft study of 1/8 scale model of Curtiss XBTC-2 airplane. δ_{f_i} = 50, δ_{f_o} = 50; s_i = closed, s_o = open; cowl flap open; L.G up; Take-off power.

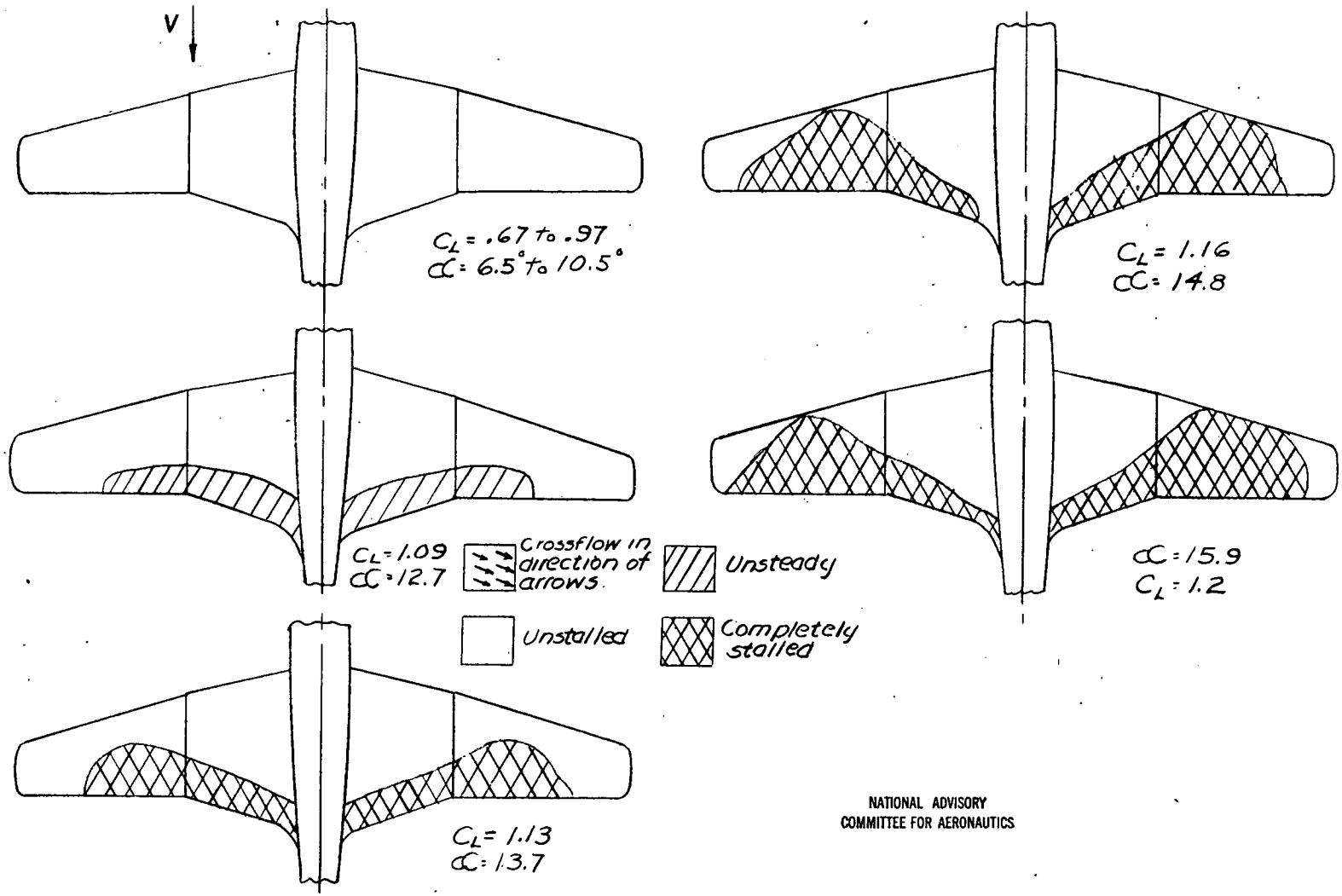

Figure 53.-Tuft study of 1/8-scale model of Curtiss XBTC-2 airplane. $\delta_{f_i} = 0$, $\delta_{f_o} = 0$; s_i = closed, s_o = closed; Cowl flap closed; L.G. up; windmilling. Swept-back outboard panel.

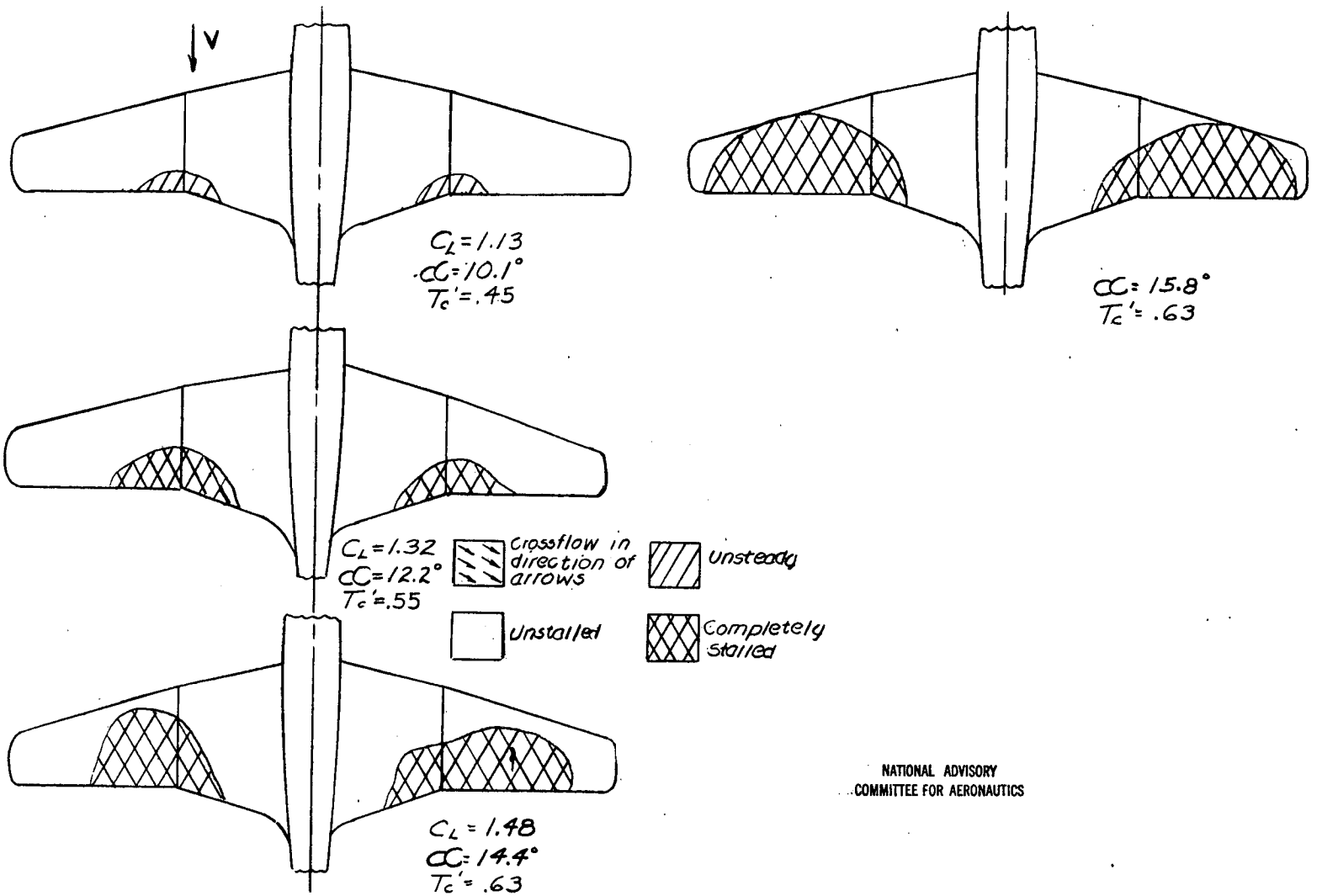

NATIONAL ADVISORY
COMMITTEE FOR AERONAUTICS

Figure 54.-Tuft study of 1/8-scale model of Curtiss XBTC-2 airplane. $\delta_{f_i} = 0$, $\delta_{f_o} = 0$; s_i = closed, s_o = closed; Cowl flap closed; L.G. up; Take-off power. Swept-back outboard panel.

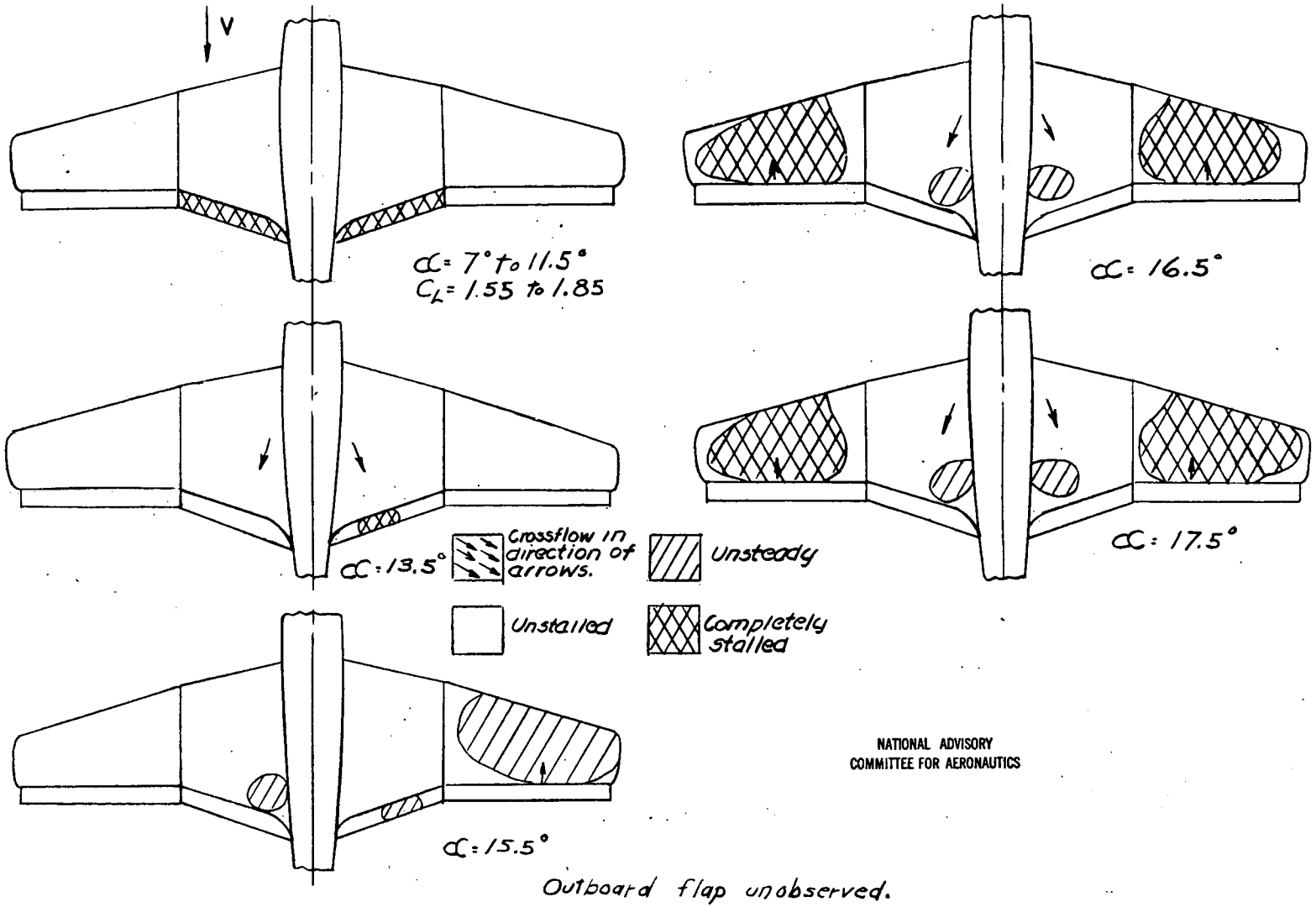

Figure 55.-Tuft study of 1/8 scale model of Curtiss XBTC-2 airplane. $\delta_f = 50$, $\delta_{f_o} = 50$; s_i = closed, s_o = closed; Cowl flap open; L.G. down; Windmilling. Swept-back outboard panel.

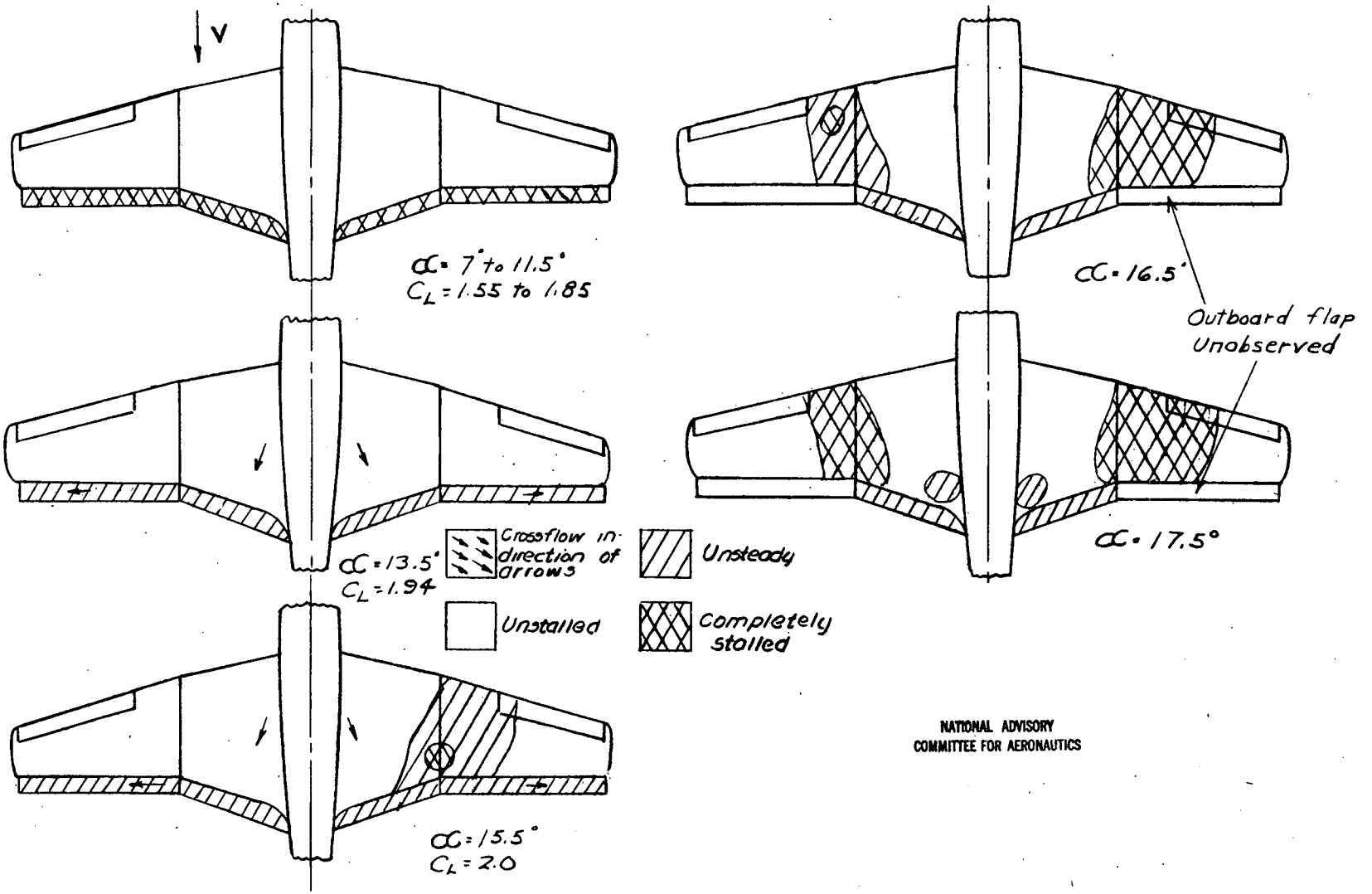

Figure 56.- Tuft study of 1/8 scale model of Curtiss XBTC-2 airplane. δ_i = 50, δ_o = 50; s_i = closed, s_o = open; Cowl flap open; L.G. down; Windmilling. Swept-back outboard panel.

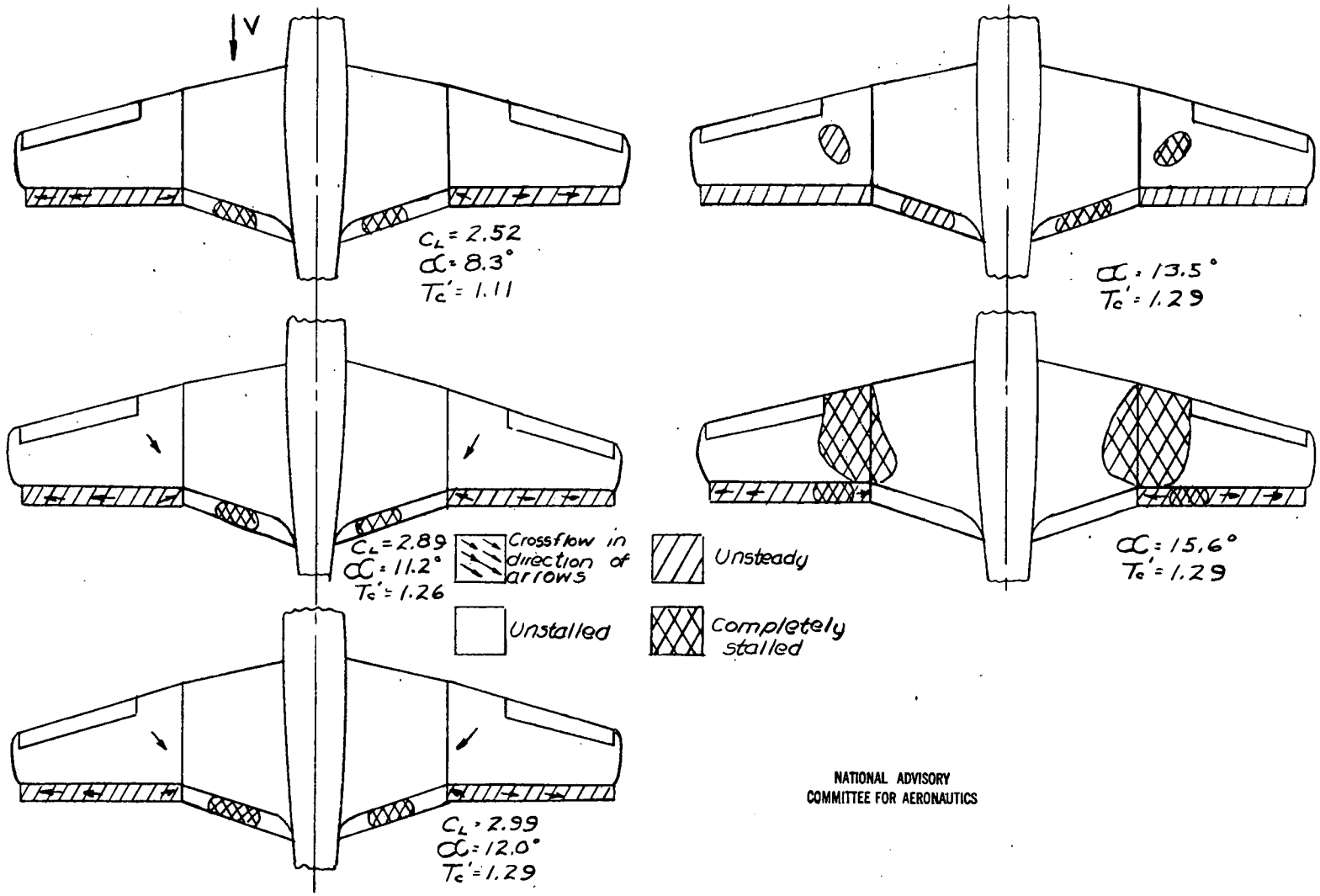

Figure 57.- Tuft study of 1/8 scale model of Curtiss XBTC-2 airplane. δ_i = 50, δ_{fo} = 50; s_i = closed, s_o = open; Cowl flap open; L.G. down; Take off power. Swept-back outboard panel.

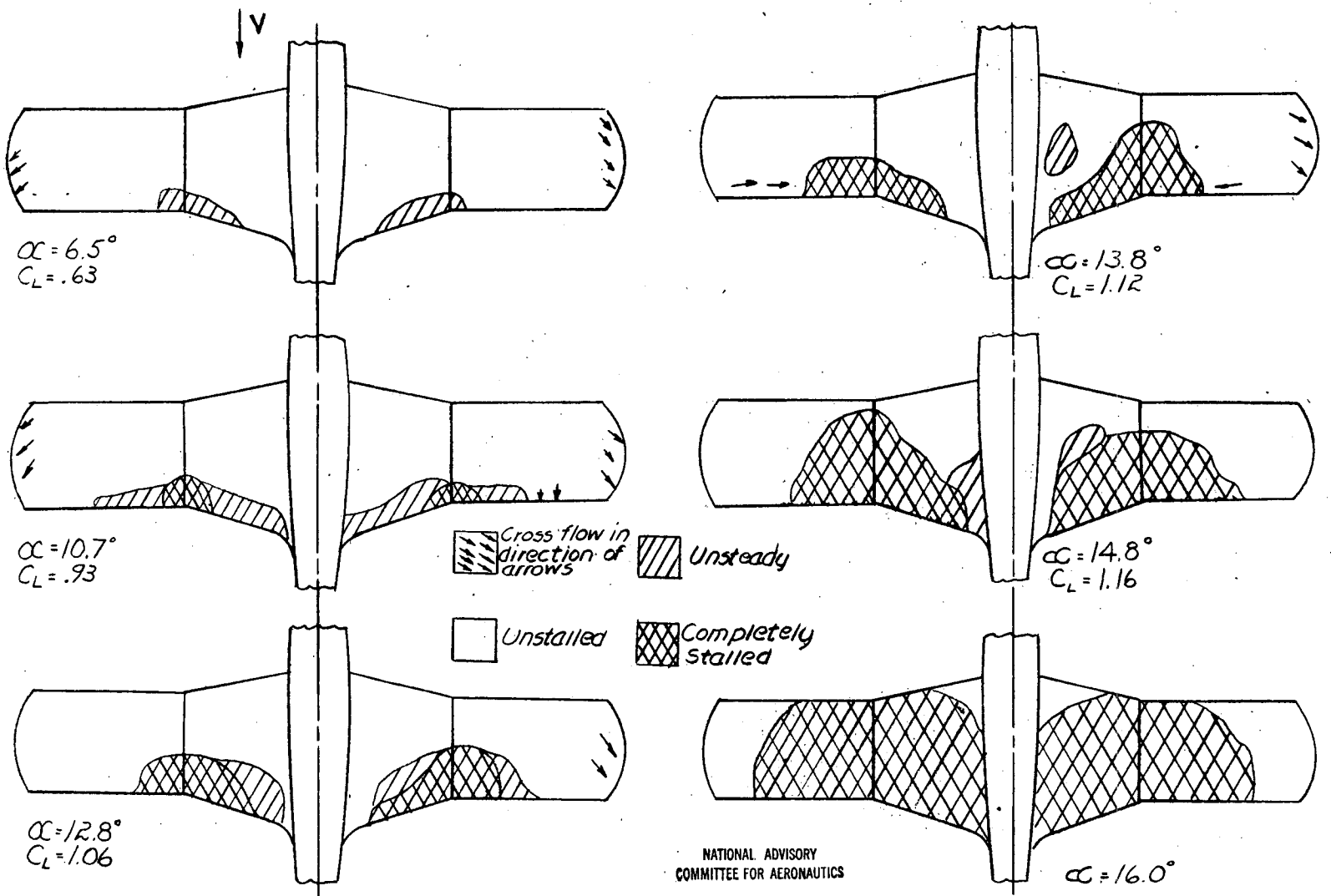

Figure 58.-Tuft study of ⅛-scale model of Curtiss XBTC-2 airplane. $\delta_{fi} = 0$, $\delta_{fo} = 0$; s_i = closed, s_o = closed; Cowl flap closed; L.G. up; Windmilling. Rectangular outboard panel.

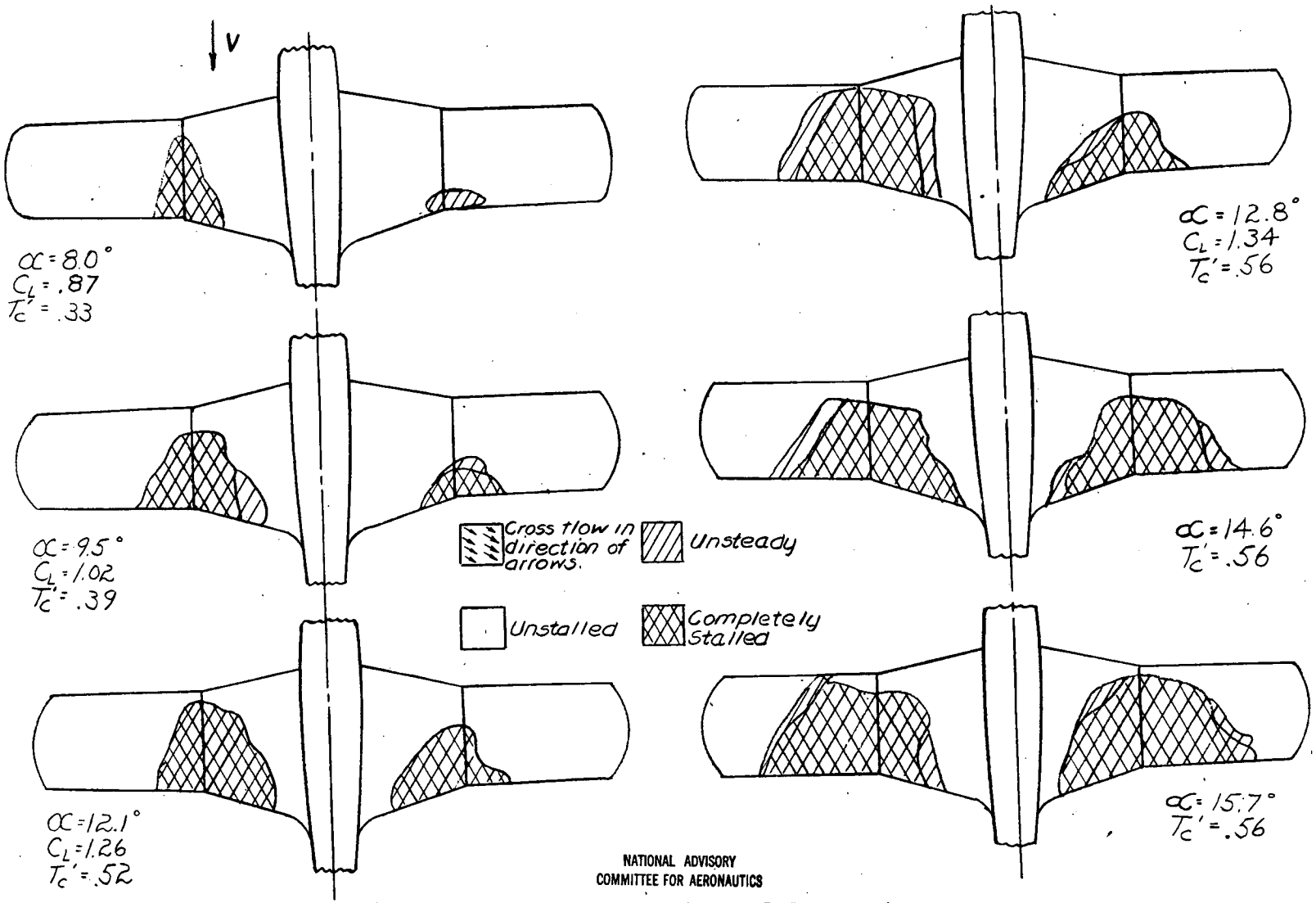

Figure 59.- Tuft study of 1/8 scale model of Curtiss XBTC-2 airplane. δ_f = closed, δ_f = closed; s_i = closed, s_o = closed. Cowl flap closed; L.G. up; Take-off power. Rectangular outboard panel

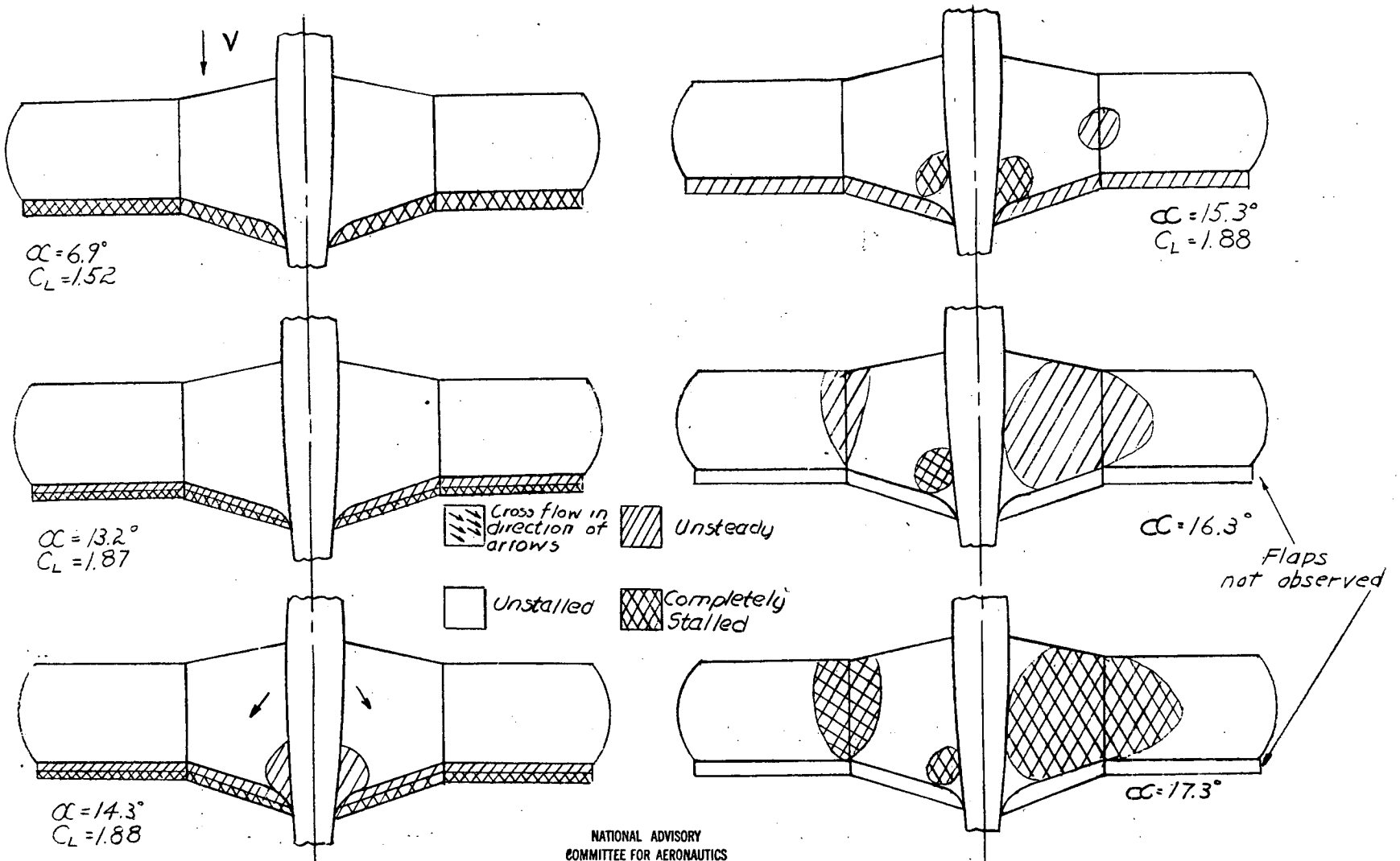

NATIONAL ADVISORY
COMMITTEE FOR AERONAUTICS

Figure 60.-Tuft study of 1/8-scale model of Curtiss XBTC-2 airplane. $\delta_{f_i} = 50$, $\delta_{f_o} = 50$; s_i = closed, s_o = closed; Cowl flap open; L.G. down; Windmilling. Rectangular outboard panel.

1,010

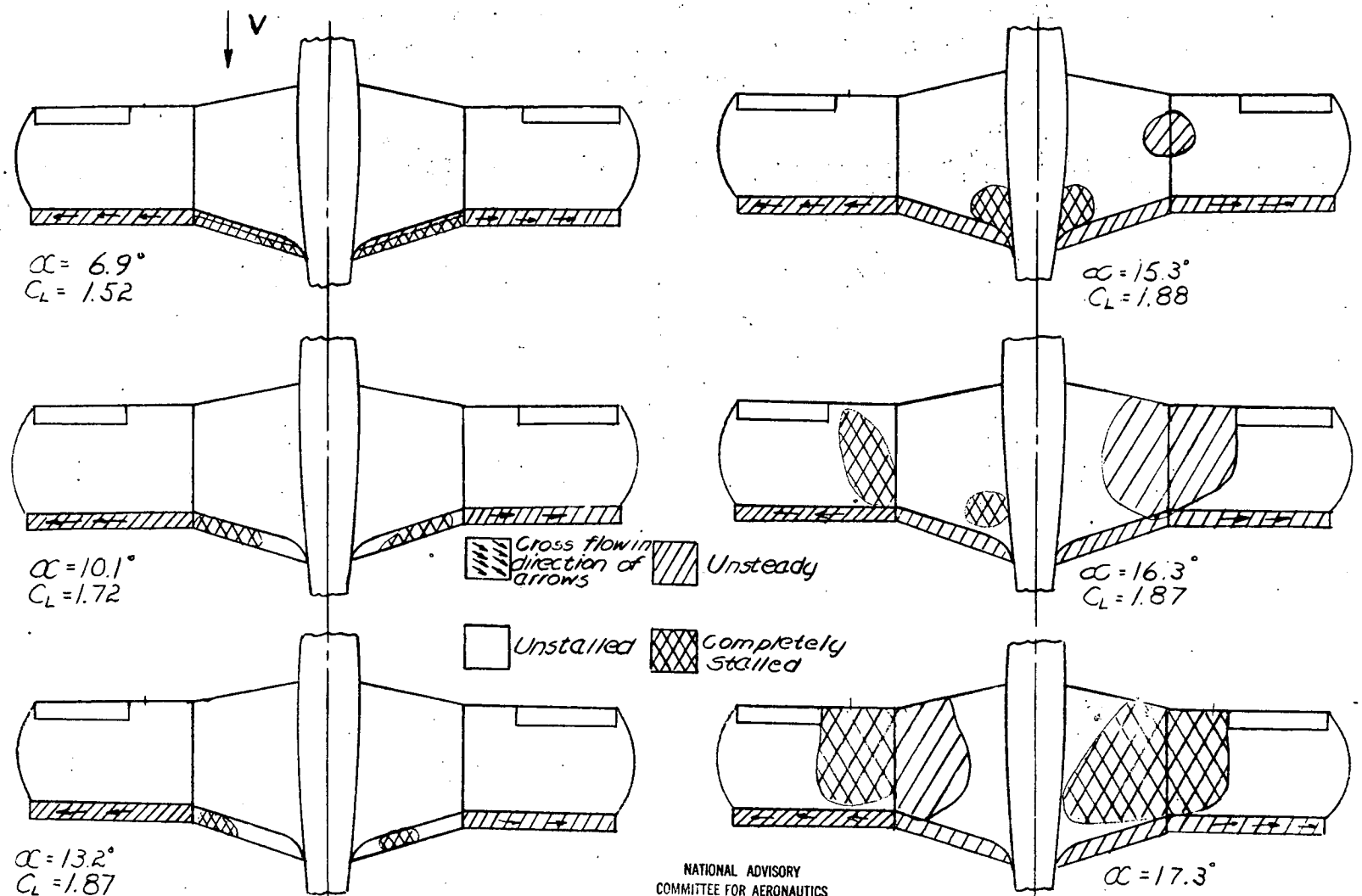

Figure 61.-Tuft studies of 1/8-scale model of Curtiss XBTC-2 airplane. δ_f = 50, δ_{f_o} = 50; s_i = closed, s_o = open; Cowl flap open; L.G. down; Windmilling. Rectangular outboard panel.

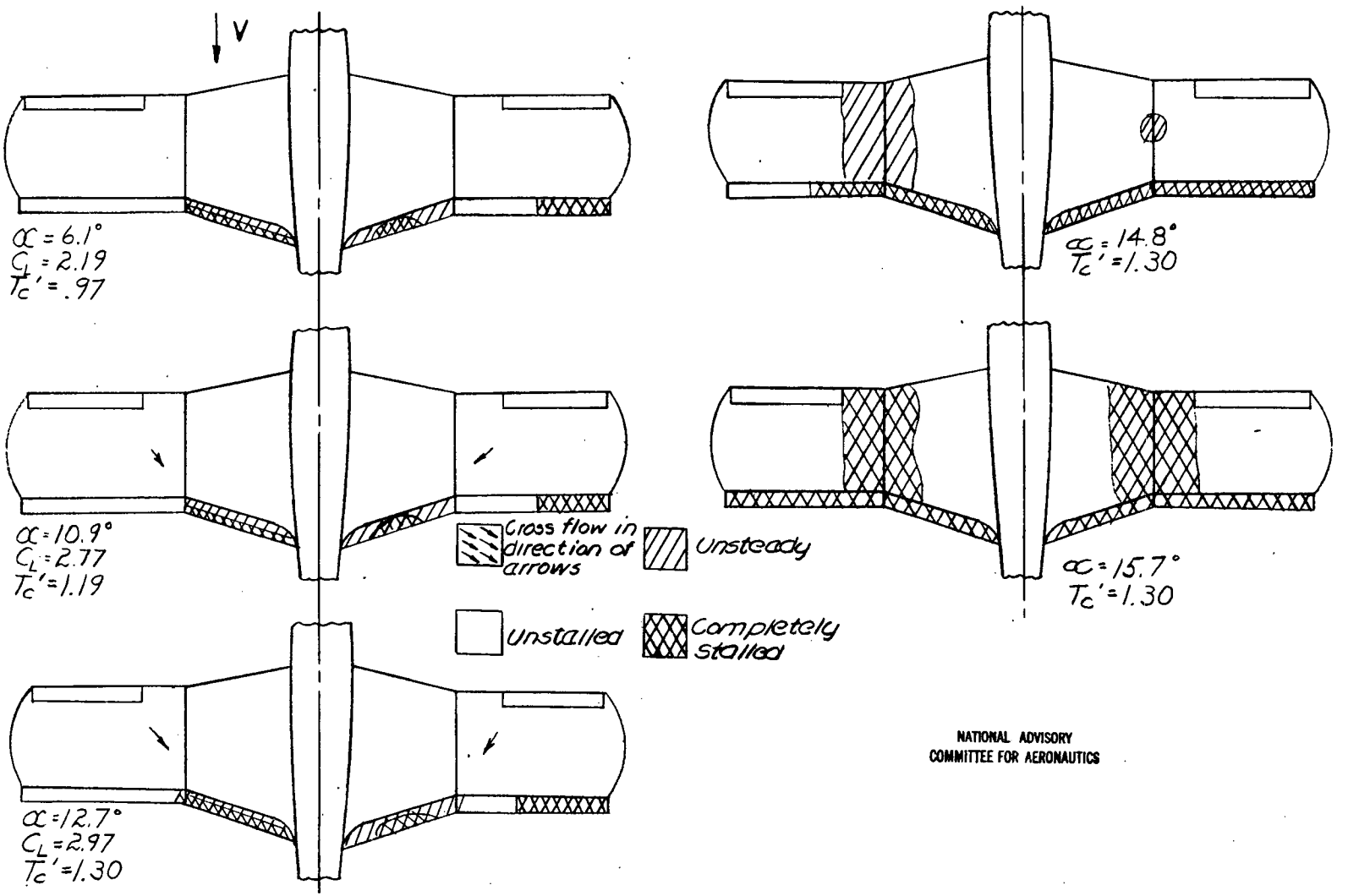

Figure 62-Tuft study of 1/8-scale model of Curtiss XBTC-2 airplane. δ_{f_i} = 50, δ_{f_o} = 50; s_i = closed, s_o = open; Cowl flap open; L.G. down; Take-off power. Rectangular outboard panel.

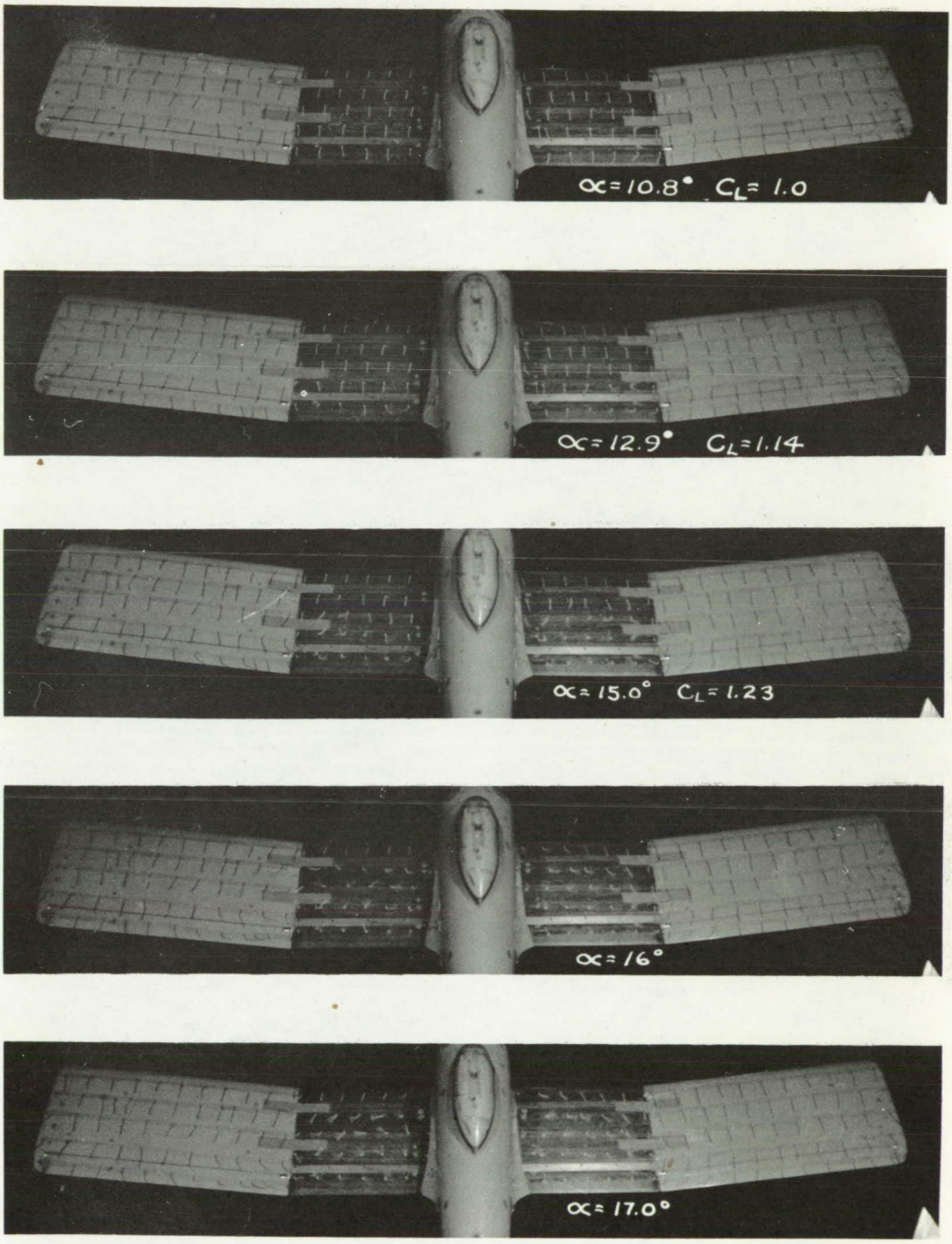

Figure 63.- Tuft study of $\frac{1}{8}$-scale model of Curtiss XBTC-2 airplane with rectangular wing, $\delta_{f_i} = 0$, $\delta_{f_o} = 0$; slats closed; cowl flaps closed; L.G. up; windmilling.

Root incidence 1.5°
Break section incidence 1.5°
Tip incidence -0.4°

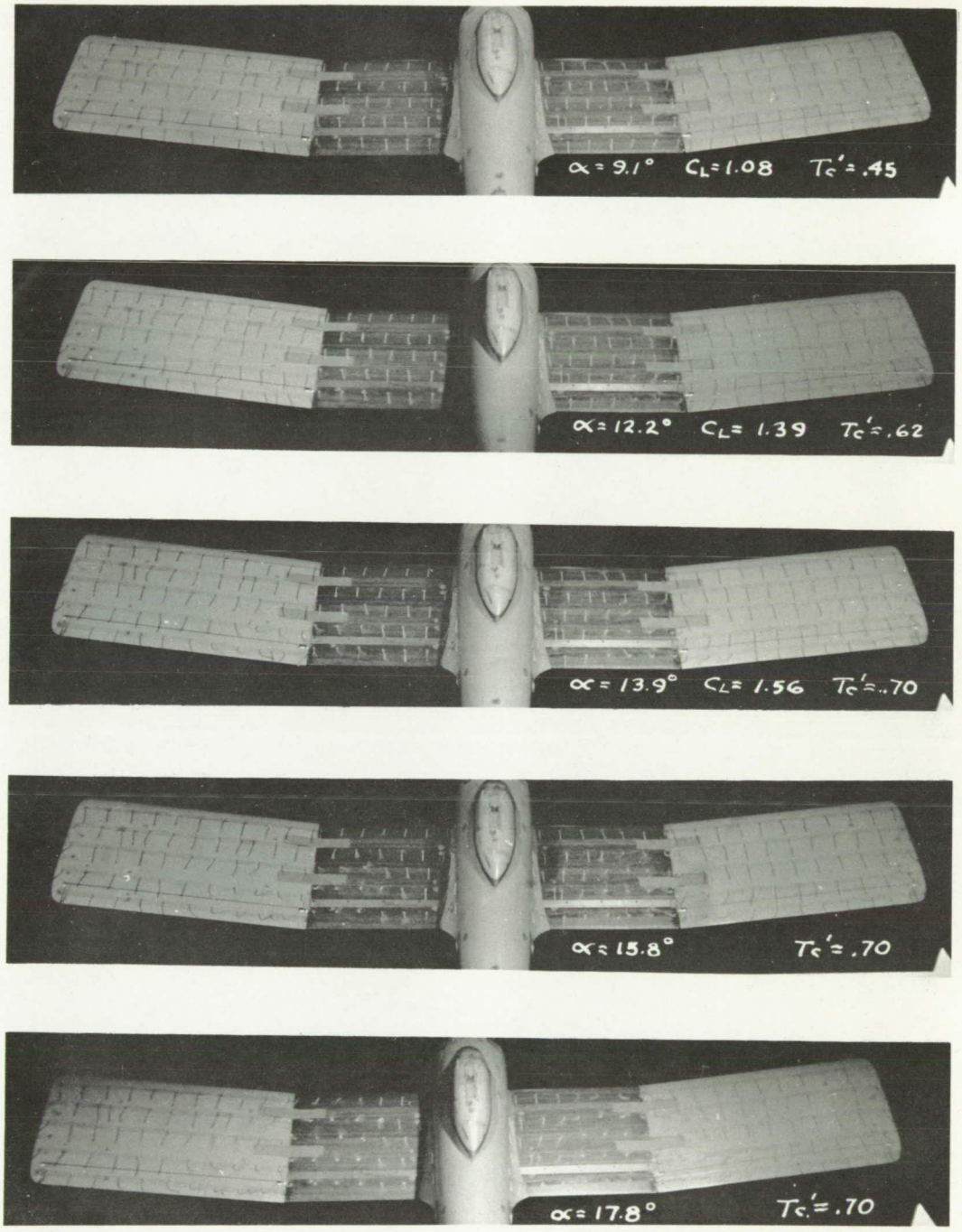

Figure 64.- Tuft study of $\frac{1}{8}$-scale model of Curtiss XBTC-2 airplane with rectangular wing; $\delta_{f_i} = 0$, $\delta_{f_o} = 0$; slats closed; cowl flaps closed; L.G. up; take-off power.

Root incidence 1.5°
Break section incidence 1.5°
Tip incidence -0.4°

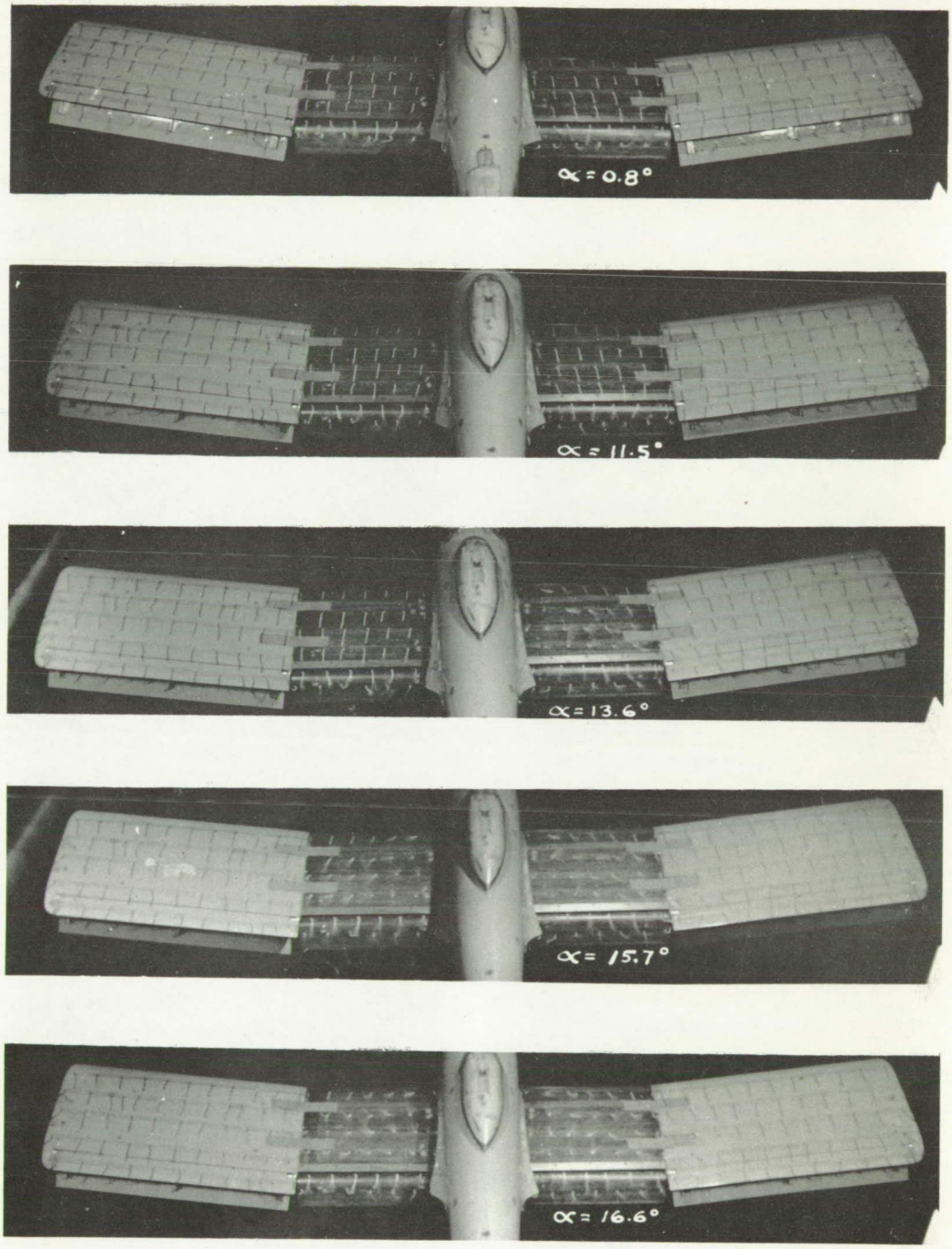

Figure 65.- Tuft study of $\frac{1}{8}$-scale model of Curtiss XBTC-2 airplane with rectangular wing; $\delta_{f_i} = 50^\circ$, $\delta_{f_o} = 50^\circ$; slats closed; cowl flaps open; L.G. up; windmilling.

Root incidence 1.5°
Break section incidence 1.5°
Tip incidence -0.4°

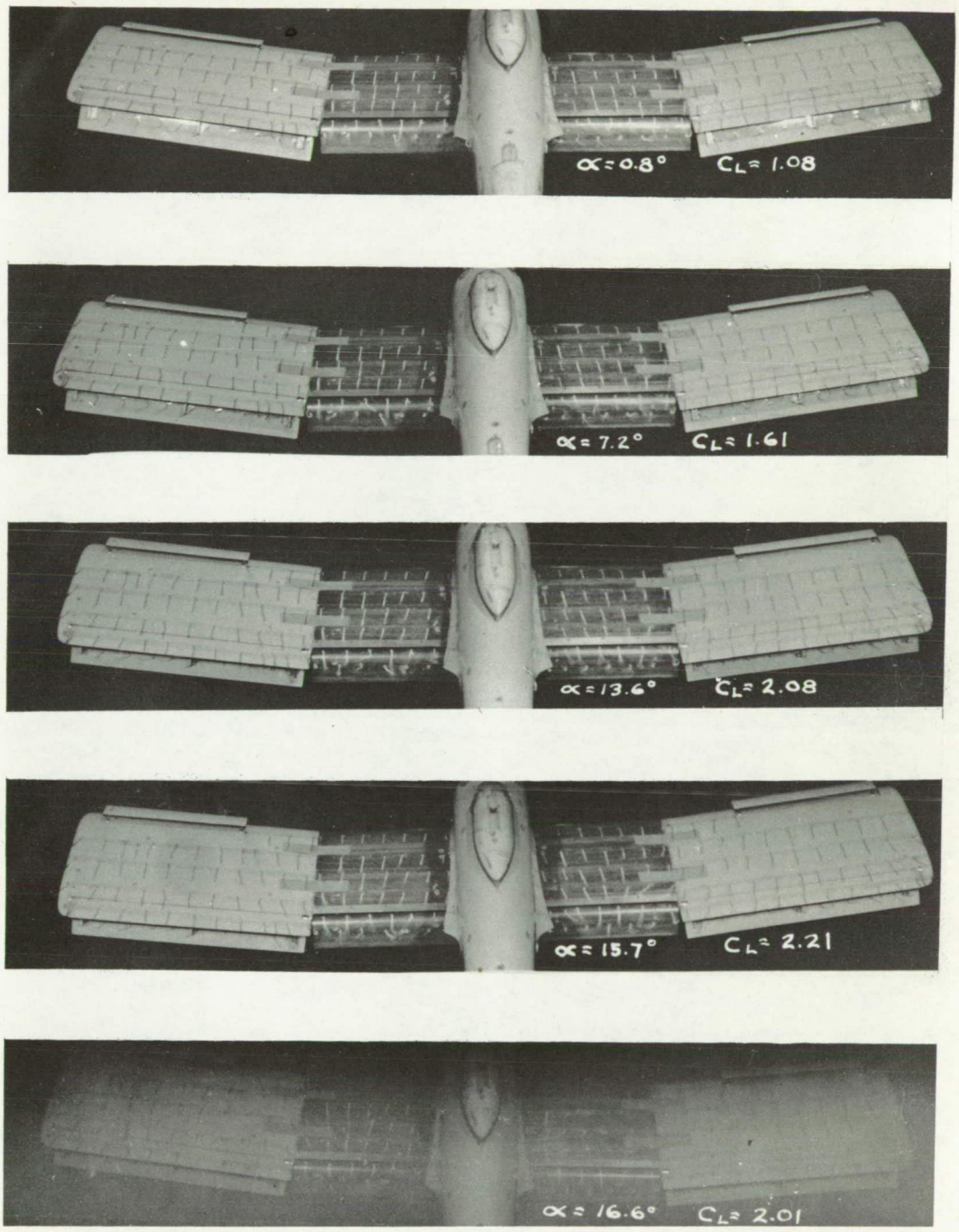

Figure 66.- Tuft study of $\frac{1}{8}$-scale model of Curtiss XBTC-2 airplane with rectangular wing; $\delta_{f_i} = 50^\circ$, $\delta_{f_o} = 50^\circ$; slats open; cowl flaps open; L.G. up; windmilling.

Root incidence 1.5°
Break section incidence 1.5°
Tip incidence -0.4°

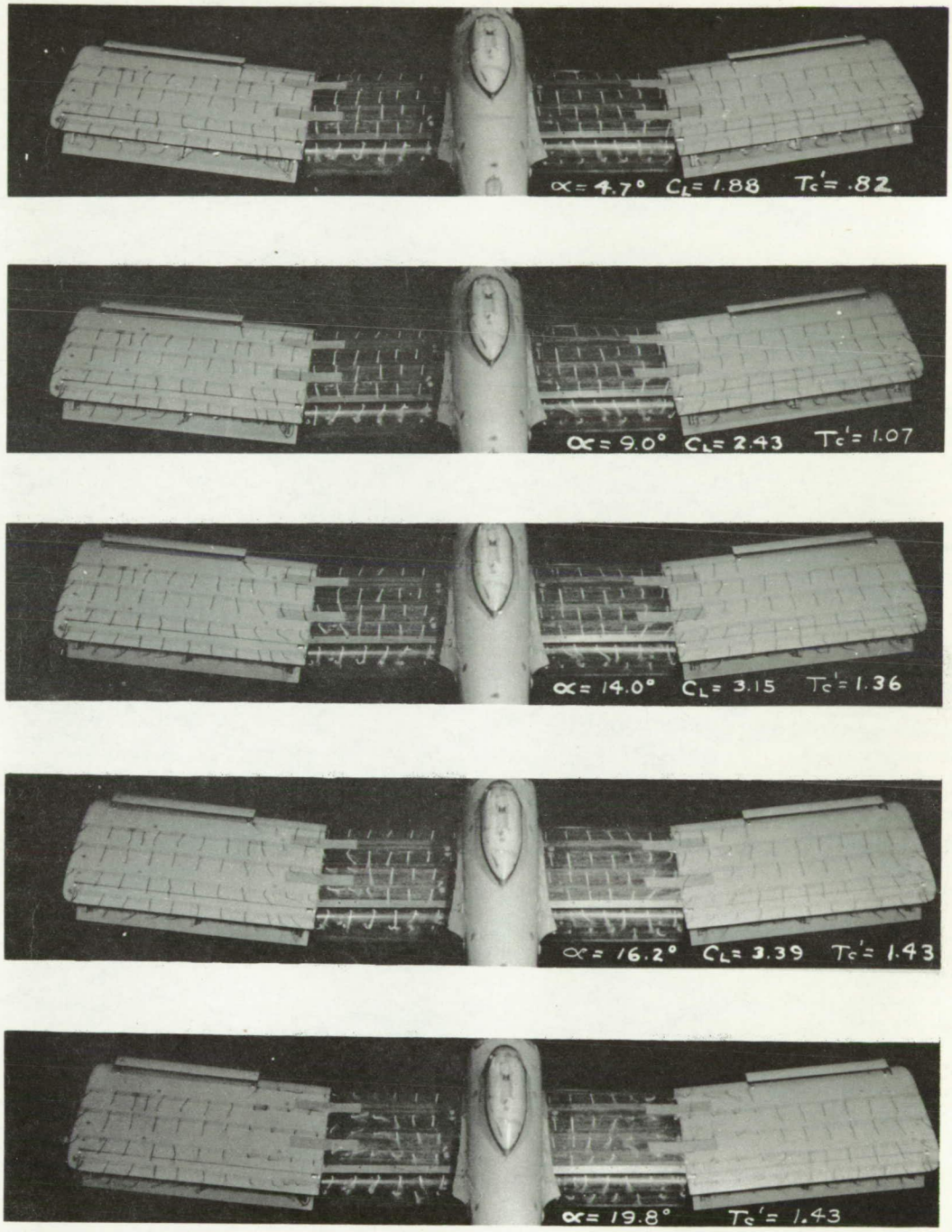

Figure 67.- Tuft study of $\frac{1}{8}$-scale model of Curtiss XBTC-2 airplane with rectangular wing; $\delta_{f_i} = 50^\circ$, $\delta_{f_o} = 50^\circ$; slats open; cowl flaps open; L.G. up; take-off power.

Root incidence 1.5°
Break section incidence 1.5°
Tip incidence -0.4°

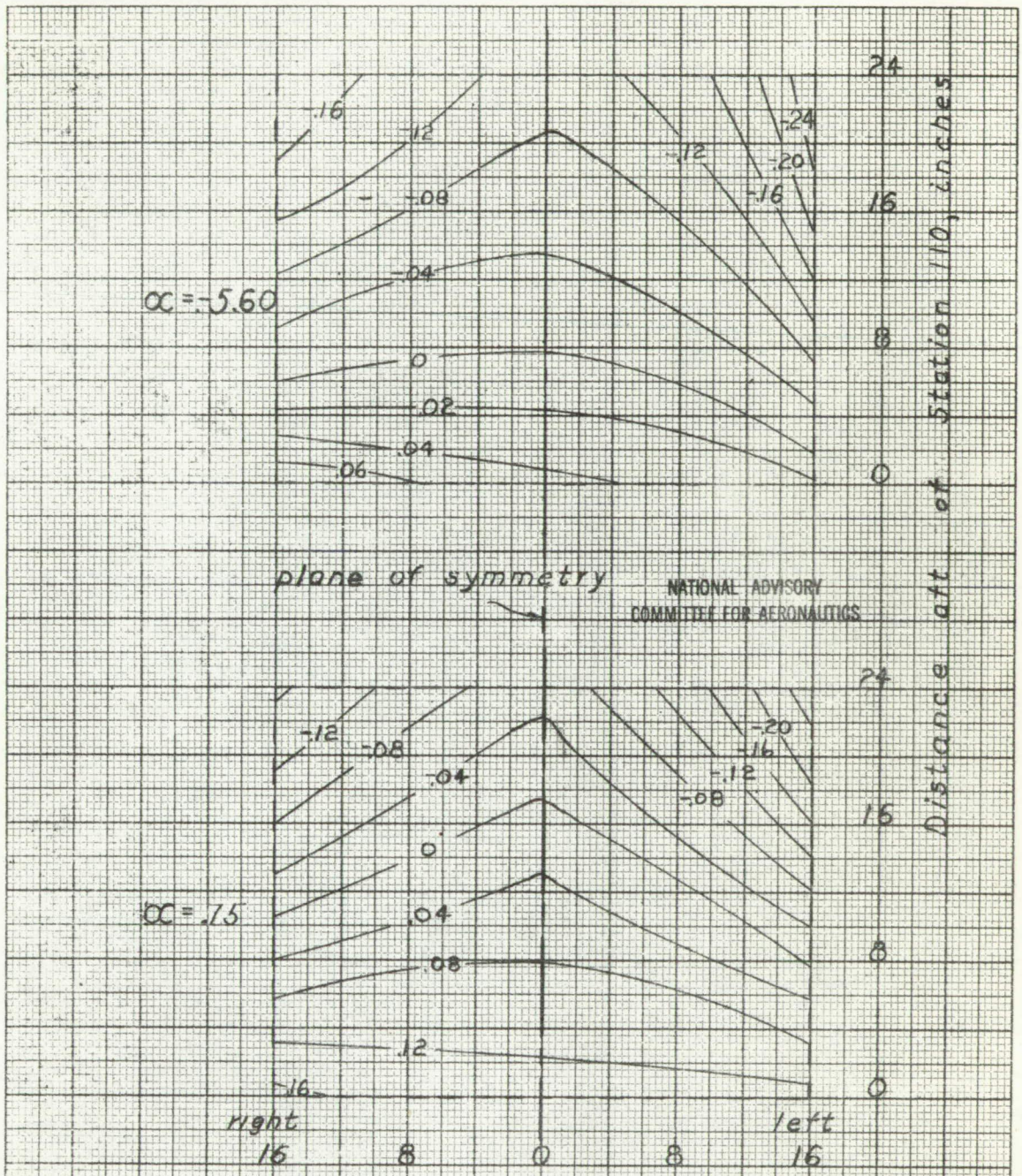

Figure 68 - Contours of pressure coefficients, P_l, over location of oil cooler flap for Curtiss XBTC-2 airplane. Landing configuration, windmilling propeller.

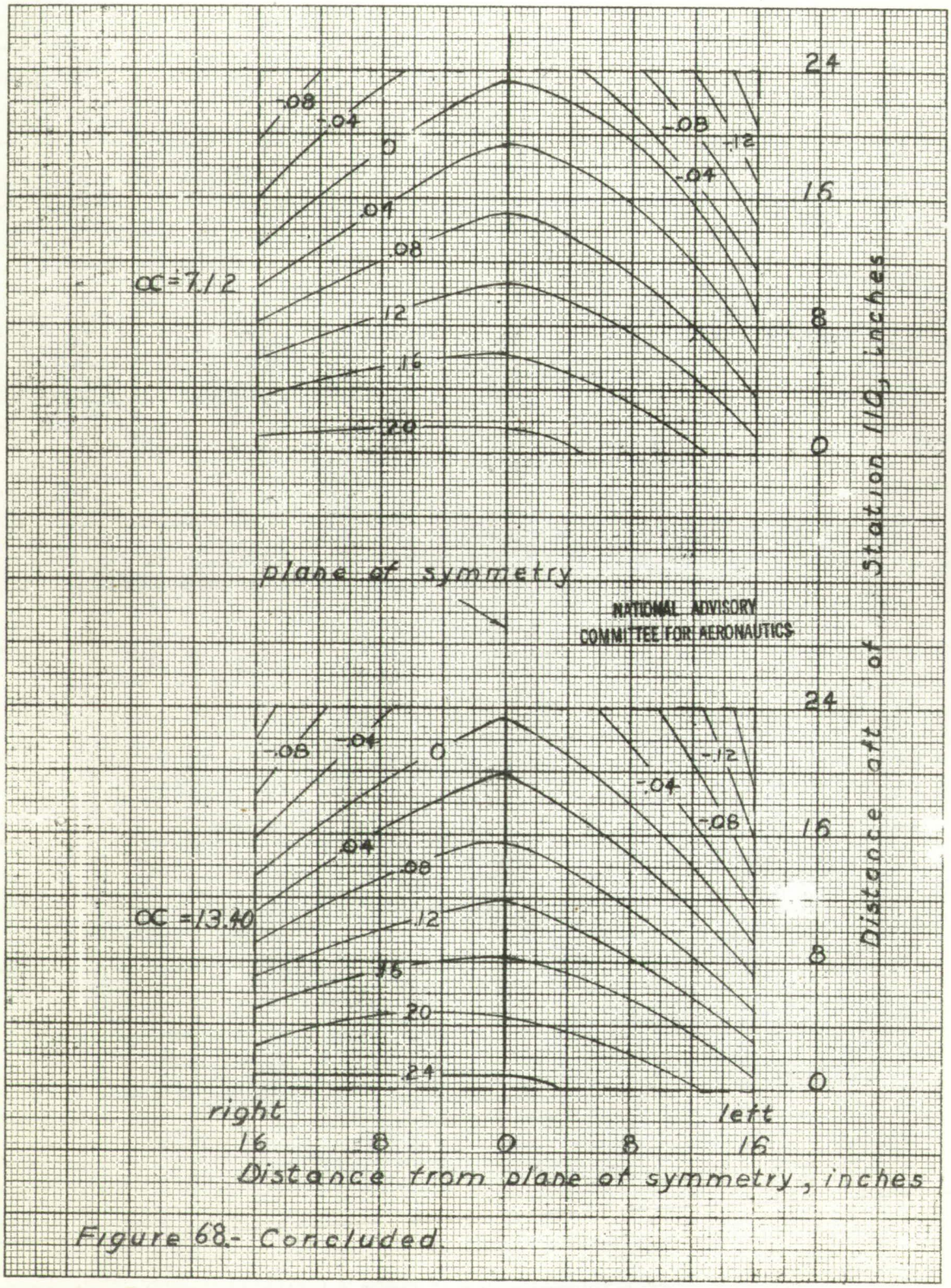

Figure 68.- Concluded.